

# **Dynamics of the Plasma Membrane Transporter GLUT4**

**Silke Morris (née Machauer)**

**BSc, MSc**

Thesis submitted in fulfilment of the requirements for the Degree of  
Doctor of Philosophy

April 2020

Institute of Molecular, Cell and Systems Biology

College of Medical, Veterinary and Life Sciences

University of Glasgow

## Abstract

Glucose homeostasis in the human body is maintained by hormones of the pancreas, mostly glucagon and insulin. Insulin is secreted when blood glucose levels are high and triggers a signalling cascade that results in glucose uptake via the glucose transporter GLUT4 in peripheral tissues.

GLUT4 is the only glucose transporter that responds to insulin stimulation and it slowly recycles between intracellular storage compartments and the plasma membrane. In the basal state, the majority of GLUT4 is intracellularly localised. Insulin stimulation results in movement (“translocation”) of GLUT4 from these intracellular stores to the plasma membrane. The signalling cascade from insulin binding to its receptor to translocation of GLUT4 is comparatively well understood. Less is known about the dynamics of GLUT4 within the plasma membrane itself. Advances in light microscopy techniques, such as Total Internal Reflection Fluorescence and super-resolution microscopy, have allowed new insights into the events in the membrane. It has recently been proposed that GLUT4 is located in plasma membrane clusters and that another effect of insulin is the dispersal of these GLUT4 clusters.

The main objective of this work was to develop a microscopy-based assay to visualise and quantify these clusters and to investigate the molecular mechanisms behind clustering and dispersal of the glucose transporter in response to insulin. The majority of this work has been carried out in 3T3 L1 adipocytes, a widely used cell model for the study of GLUT4. However, this cell line is difficult to maintain, and its genetic manipulation is very challenging. For this reason, we investigated HeLa cells as a suitable substitute cell model for preliminary screenings.

Using Total Internal Reflection Fluorescence Microscopy and Spatial Intensity Distribution Analysis, we gained new insight into the dynamics of plasma membrane GLUT4 in both 3T3 L1 adipocytes and HeLa cells. We found that the transporter forms an oligomer of high order in the plasma membrane in both cell types. Further, we compared the dynamics of GLUT4 mobilisation in response to insulin and found similar results. Based on these findings, we carried out an siRNA knock-down screening to determine proteins involved in intracellular

GLUT4 trafficking and found that GOSR1 and Ykt6 are promising targets for further examination.

Single molecule localisation microscopy allowed us to accomplish our aim to assay GLUT4 clustering and dispersal. Using dSTORM and Ripley's K-function, as well as Bayesian cluster analysis methods, we showed that GLUT4 is indeed located in clusters in the plasma membrane and that insulin stimulation leads to its dispersal. We found that treatment with Galectin-3, a drug that inhibits glucose uptake, impedes the dispersal. Building upon previous research in our group that identified EFR3a as a membrane-localised protein involved in glucose uptake, we knocked-down EFR3a in 3T3 L1 adipocytes and found that this also disrupts GLUT4 dispersal, which we hypothesise could be a potential drug target for type 2 diabetes.

Taken together, the findings presented in this thesis suggest HeLa cells as a suitable cell model for initial assessments of research questions related to GLUT4 trafficking. Furthermore, a robust assay to measure GLUT4 dispersal was established.

## Table of Contents

Abstract .....	2
List of Tables .....	8
List of Figures .....	9
Acknowledgements .....	11
Author's Declaration .....	13
Abbreviations .....	14
Chapter 1 Introduction .....	18
1.1 Glucose Homeostasis .....	18
1.2 Diabetes Mellitus .....	20
1.3 Glucose Transporters .....	21
1.3.1 Glucose Transporter 4 .....	23
1.4 The GLUT4 Storage Compartment .....	25
1.4.1 Endocytosis of GLUT4 .....	30
1.4.2 Other Components and Biogenesis of GSVs .....	30
1.5 Insulin Signalling .....	33
1.5.1 The APS Pathway .....	34
1.5.2 The PI3K Pathway .....	34
1.6 GLUT4 Trafficking Proteins .....	36
1.6.1 Rab Proteins .....	36
1.6.2 SNARE and SM Proteins .....	38
1.6.2.1 The SNARE Complex .....	38
1.6.2.2 VAMPs .....	39
1.6.2.3 SM Proteins .....	40
1.6.3 Translocation of GSVs Along Filaments and Microtubules .....	41
1.7 GLUT4 in the Plasma Membrane .....	42
1.7.1 GSVs in the TIRF Zone .....	45
1.7.2 GLUT4 Clustering in Response to Insulin .....	46
1.7.3 Tethering and Fusion of GSVs with the Plasma Membrane .....	46
1.7.4 GLUT4 Clustering and Dispersal .....	49
1.7.5 Single Molecule Imaging of GLUT4 in the Plasma Membrane .....	50
1.7.6 Possible Mechanisms of GLUT4 Clustering .....	52
1.7.7 EFR3 and its Potential Role in GLUT4 Dispersal .....	53
1.8 Working Hypothesis and Aims of this Study .....	54
Chapter 2 General Materials and Methods .....	57
2.1 Materials .....	57
2.1.1 Reagents and Enzymes .....	57
2.1.2 Buffers and Solutions .....	60
2.1.3 Antibodies .....	62

2.1.3.1	Primary Antibodies .....	62
2.1.3.2	Secondary Antibodies for Western Blotting .....	63
2.1.3.3	Secondary Antibodies for Immunofluorescence .....	63
2.1.4	Plasmids and siRNA .....	64
2.1.5	Mammalian Cell Lines .....	65
2.1.6	Materials .....	65
2.2	Methods .....	65
2.2.1	Cell Culture Methods .....	65
2.2.1.1	Growth and Maintenance of HeLa and HEK Cells .....	66
2.2.1.2	Growth and Maintenance of 3T3 L1 Cells .....	66
2.2.1.3	Differentiation of 3T3 L1 Cells .....	66
2.2.1.4	Freezing and Resurrecting Cells .....	67
2.2.1.5	Cleaning and Seeding on Cover Glasses .....	67
2.2.1.6	Transfection .....	67
2.2.1.7	siRNA Electroporation of 3T3 L1 Adipocytes .....	68
2.2.2	IF Staining .....	68
2.2.2.1	IF Staining for Permeabilised Cells .....	68
2.2.2.2	IF Surface Staining for Confocal Microscopy .....	69
2.2.2.3	IF Surface Staining for dSTORM .....	69
2.2.3	Lentivirus .....	70
2.2.3.1	Lentivirus Production .....	70
2.2.3.2	Lentiviral Infection .....	70
2.2.3.3	Generation of a Stable Cell Line Using Lentivirus. ....	70
2.2.4	Molecular Biology Methods .....	71
2.2.4.1	Transformation .....	71
2.2.4.2	Plasmid DNA Purification .....	71
2.2.4.3	Agarose Gel Electrophoresis .....	72
2.2.4.4	Restriction Endonuclease Digest .....	72
2.2.4.5	Cloning .....	72
2.2.5	Gel Electrophoresis and Western Blotting .....	73
2.2.5.1	Cell Lysates .....	73
2.2.5.2	SDS-PAGE .....	73
2.2.5.3	Immunoblotting .....	73
2.2.6	BN-PAGE .....	74
2.2.6.1	BN-PAGE Sample Preparation .....	74
2.2.6.2	BN-PAGE .....	75
2.2.6.3	BN-PAGE Immunoblotting .....	76
2.2.7	Microscopy .....	76
2.2.7.1	Confocal Microscopy .....	76

2.2.7.2	TIRF Microscopy .....	76
2.2.7.3	dSTORM .....	77
2.2.8	Image Analysis .....	77
2.2.8.1	HA/GLUT4 Ratio .....	77
2.2.8.2	Spatial Intensity Distribution Analysis .....	77
2.2.8.3	Colocalisation Analysis .....	77
2.2.8.4	dSTORM Analysis .....	78
2.2.9	Statistical Analysis.....	78
Chapter 3	Comparison of HeLa Cells and 3T3 L1 Adipocytes Using TIRFM .....	79
3.1	Introduction .....	79
3.1.1	Principles of Fluorescence Microscopy .....	79
3.1.2	Principles of Total Internal Reflection Fluorescence Microscopy....	81
3.1.3	The Built In-House TIRFM System .....	84
3.1.4	Hypothesis and Aims .....	85
3.2	Results .....	86
3.2.1	HA-GLUT4-GFP Expression in HeLa Cells and 3T3 L1 Adipocytes ....	86
3.2.2	Fluorescence Intensity in the TIRF Zone .....	88
3.2.3	Mobile and Static Vesicles in the TIRF Zone .....	92
3.3	Discussion .....	95
Chapter 4	The Oligomeric State of GLUT4 in the Plasma Membrane .....	99
4.1	Introduction .....	99
4.1.1	Oligomerisation of Proteins .....	99
4.1.2	Spatial Intensity Distribution Analysis .....	100
4.1.3	Hypothesis and Aims .....	101
4.2	Results .....	102
4.2.1	Construction of a HA-GLUT4-eGFP Lentiviral Plasmid .....	102
4.2.2	Production and Testing of Lentivirus .....	105
4.2.3	Generation of a 3T3 L1 Cell Line Expressing HA-GLUT4-eGFP .....	107
4.2.4	Validation of the Method - Oligomeric State of the M <sub>1</sub> Muscarinic Receptor.....	109
4.2.5	Oligomeric State of GLUT4 as by SpIDA .....	111
4.2.6	Oligomeric State of GLUT4 as by BN-PAGE .....	114
4.3	Discussion .....	115
Chapter 5	Clustering and Dispersal of GLUT4 in the Plasma Membrane .....	120
5.1	Introduction .....	120
5.1.1	Super Resolution Microscopy.....	120
5.1.2	Stochastic Optical Reconstruction Microscopy .....	122
5.1.3	Cluster Analysis .....	125
5.1.3.1	Ripley's K Function Analysis.....	126

5.1.3.2	Bayesian Cluster Analysis .....	127
5.1.4	Hypothesis and Aims .....	127
5.2	Results .....	128
5.2.1	Insulin Regulates GLUT4 Dispersal .....	128
5.2.2	Galectin-3 Inhibits GLUT4 Clustering .....	134
5.2.3	EFR3a Knock-Down in 3T3 L1 Adipocytes .....	138
5.2.4	EFR3a Controls Insulin Regulated GLUT4 Dispersal .....	140
5.3	Discussion .....	142
Chapter 6	SNARE Proteins Regulating Intracellular GLUT4 Trafficking .....	146
6.1	Introduction .....	146
6.1.1	The ERGIC is Involved in the GSC formation in Human Cells .....	146
6.1.2	SNAREs Involved in Intracellular Trafficking .....	147
6.1.3	Hypothesis and Aims .....	149
6.2	Results .....	150
6.2.1	GLUT4 Colocalisation .....	150
6.2.1.1	GLUT4 Colocalisation with the ERGIC .....	150
6.2.1.2	GLUT4 Colocalisation with the ER .....	152
6.2.1.3	GLUT4 Colocalisation with the Golgi .....	154
6.2.2	Total GLUT4 Levels after SNARE Knock-Down .....	155
6.2.3	Intracellular GLUT4 Distribution After SNARE Knock-Down .....	156
6.3	Discussion .....	158
Chapter 7	Discussion .....	163
7.1	Summary of Results .....	163
7.2	Results in the Context of Existing Literature .....	165
7.3	Future Directions .....	166
7.3.1	GLUT4 Clustering and EFR3a .....	166
7.3.2	HeLa Cells as Model for GLUT4 Trafficking .....	168
7.4	Conclusions .....	169
Chapter 8	Appendices .....	170
	List of References .....	173

## List of Tables

Table 1.1 Studies on GLUT4 in the Plasma Membrane .....	44
Table 2.1 Reagents and Enzymes .....	57
Table 2.2 Buffers and Solutions .....	60
Table 2.3 Primary Antibodies .....	62
Table 2.4 Secondary Antibodies for Western Blotting .....	63
Table 2.5 Secondary Antibodies for Immunofluorescence.....	63
Table 2.6 Plasmids .....	64
Table 2.7 siRNAs .....	64
Table 2.8 Mammalian Cell Lines.....	65
Table 2.9 Materials.....	65
Table 2.10 SDS-PAGE Gel Components .....	73
Table 2.11 BN-PAGE Gel Components .....	75



## List of Figures

Figure 1.1 Regulation of Blood Glucose Levels through the Pancreas. ....	19
Figure 1.2 Structure of the Membrane Protein GLUT4. ....	23
Figure 1.3 Model of Dynamic Exchange and Static Retention of GLUT4. ....	28
Figure 1.4 Schematic of the APS Pathway .....	34
Figure 1.5 Schematic of the PI3K Pathway. ....	35
Figure 1.6 Formation of the SNARE Complex and Vesicle Fusion.....	39
Figure 1.7 Fusion of GSV with the Plasma Membrane .....	49
Figure 1.8 Clustering and Dispersal of GLUT4 in Response to Insulin. ....	55
Figure 1.9 Schematic of the Working Hypothesis Involving EFR3a and PI4P. ....	55
Figure 3.1 Schematic of an Epifluorescence Widefield Microscope .....	80
Figure 3.2 Principle of TIR .....	81
Figure 3.3 Widefield vs Confocal vs TIRF .....	83
Figure 3.4 TIR Alignment Mask .....	84
Figure 3.5 HA Surface Staining of HA-GLUT4-GFP HeLa Cells in Response to Insulin .....	87
Figure 3.6 HA Surface Staining of HA-GLUT4-GFP 3T3 L1 Adipocytes in Response to Insulin.....	88
Figure 3.7 Time Course of Insulin Stimulated HeLa Cells in TIRFM.....	89
Figure 3.8 Normalised Fluorescence Intensity in HeLa Cells in TIRFM.....	89
Figure 3.9 Time Course of Insulin Stimulated 3T3 L1 Adipocytes in TIRFM .....	91
Figure 3.10 Normalised Fluorescence Intensity in 3T3 L1 Adipocytes in TIRFM ..	91
Figure 3.11 Static and Mobile GLUT4 Vesicles in 3T3 L1 Adipocytes.....	94
Figure 3.12 Static and Mobile GLUT4 Vesicles in HeLa Cells .....	95
Figure 4.1 The Quantal Brightness $\epsilon$ Depends on the Oligomeric State of the Protein. ....	101
Figure 4.2 Maps of pCDH-CMV-MCS-EF1-Puro and pcDNA3.1 HA-GLUT4-eGFP...	102
Figure 4.3 pCDH-CMV-MCS-EF1-Puro Digested with BamHI and NotI.....	103
Figure 4.4 pcDNA3.1 HA-GLUT4-eGFP Digested with BamHI and NotI .....	104
Figure 4.5 pCDH HA-GLUT4-eGFP Clones .....	105
Figure 4.6 HeLa Cells Infected with HA-GLUT4-eGFP Lentivirus .....	106
Figure 4.7 Kill Curve of 3T3 L1 Cells Treated with Puromycin.....	107
Figure 4.8 3T3 L1 Adipocytes Stably Expressing HA-GLUT4-eGFP .....	108
Figure 4.9 Oligomeric State of the $M_1$ Muscarinic Receptor.....	110
Figure 4.10 Oligomeric State of GLUT4 in HeLa Cells.....	111
Figure 4.11 Oligomeric State of GLUT4 in 3T3 L1 Adipocytes .....	113
Figure 4.12 BN-PAGE of 3T3 L1 Lysates .....	114
Figure 5.1 Principle of Resolution.....	120
Figure 5.2 Principle of STORM and other SMLM Techniques.....	123
Figure 5.3 Principle of Photoswitching .....	124
Figure 5.4 STORM Images of Surface GLUT4 in Basal and Insulin Stimulated 3T3 L1 Adipocytes .....	128
Figure 5.5 STORM Localisation Density in Basal and Insulin Stimulated 3T3 L1 Adipocytes.....	129
Figure 5.6 Bayesian Cluster Analysis of Basal and Insulin Stimulated 3T3 L1 Adipocytes.....	132
Figure 5.7 Ripley's K-Function Analysis of Basal and Insulin Stimulated 3T3 L1 Adipocytes.....	133
Figure 5.8 HA-Surface Staining in Galectin-3 Treated 3T3 L1 Adipocytes .....	136
Figure 5.9 Ripley's K-Function Analysis of Galectin-3 Treated Basal and Insulin Stimulated 3T3 L1 Adipocytes .....	137

Figure 5.10 EFR3a Knock-Down in 3T3 L1 Adipocytes .....	139
Figure 5.11 Ripley's K-Function Analysis of EFR3a Knock-Down Basal and Insulin Stimulated 3T3 L1 Adipocytes .....	141
Figure 6.1 Model of Intracellular GLUT4 Trafficking in Human Cells .....	147
Figure 6.2 Intracellular Localisation of ERGIC-related SNARE proteins.....	148
Figure 6.3 ERGIC and DAPI Staining of HA-GLUT4-GFP HeLa Cells (negative control) .....	150
Figure 6.4 GLUT4/ERGIC Colocalisation.....	151
Figure 6.5 ER and DAPI Staining of HA-GLUT4-GFP HeLa Cells (negative control) .....	153
Figure 6.6 GLUT4/ER Colocalisation .....	153
Figure 6.7 Golgi and DAPI Staining of HA-GLUT4-GFP HeLa Cells (negative control) .....	154
Figure 6.8 GLUT4/Golgi Colocalisation.....	155
Figure 6.9 Total GLUT4 Levels after siRNA Knock-Down.....	156
Figure 6.10 Intracellular GLUT4 Distribution .....	157
Figure 8.1 Full GAPDH Blot from Figure 5.10.....	171
Figure 8.2 Full EFR3a Blot from Figure 5.10.....	171
Figure 8.3 Full GLUT4 Blot from Figure 5.10 .....	171
Figure 8.4 Full Stx16 Blot from Figure 5.10 .....	172
Figure 8.5 Full SNAP23 Blot from Figure 5.10 .....	172

## Acknowledgements

This work could not have been completed without the help of many amazing people. First and foremost, I would like to thank my Doktorvater, Gwyn, who has been the most amazing supervisor. Thank you so much, Gwyn, for always leaving your door open and for always being there when I needed you. For listening and helping when experiments didn't work and for your infectious excitement when we got a great result. Working with you was fantastic and I have learned so much thanks to you.

I would like to thank the University of Glasgow for funding my research with a Lord Kelvin Adam Smith scholarship and also for supporting me through two periods of maternity leave.

All members, past and present, of Lab241, particularly my fellow PhD students Kamilla, Shaun, Peter, Mohammed, Rachel, Fatmah, and Anna, as well as our amazing lab tech Laura. You are a wonderful bunch and I loved seeing your faces every day in the lab. Thank you for always being there for a chat, for helping out with experiments, and for providing me with vegan sweets when I was a very hungry pregnant PhD student.

Light microscopy, as beautiful as it is, needs to be carried out in dark, windowless rooms and I'm grateful to the smart people who kept me company and shared their knowledge and expertise with me. Niall Geoghegan, who built the TIRF microscope and showed me how to use it. John Pediani and Richard Ward for helping me with SpIDA. Alison Dun, the lovely manager at the Edinburgh Super-Resolution Imaging Consortium who I'm so happy to now call my friend and Colin Rickman, who always managed to fix the instrument when nobody else could. Sebastian van de Linde, the dSTORM god, who was always eager to hear about my results using his method and for helping me with the analysis. Lucy Miller and Marco Laub, my fantastic summer students who spent many hours imaging for me, and Peter Bowman for helping me with the stats. Afroditi Chatzi who explained the dark arts of BN-PAGE to me and to Kostas Tokatlidis for letting me borrow his lab equipment.

Mama und Papa, danke, dass ihr mich auf meinem Weg immer unterstützt und an mich geglaubt habt. Diabetes habe ich leider nicht geheilt, aber zumindest sind wir jetzt einen Schritt weiter.

I would like to thank my wonderful children, Logan and Eva. You didn't exactly help getting this thesis written, but you reminded me that life is not all about work and even though I loved being in the lab, at least most of the time, I also loved the time I got to spend going on adventures with you.

Last but certainly not least, I would like to thank my Hasi-husband. Thank you for always being there for me, for keeping my imposter syndrome at bay and for admiring the pretty pictures I took on various microscopes. Thank you for not only being there for me as my husband, but also as a fellow scientist. I love you!

## **Author's Declaration**

I declare that the work presented in this thesis is my own, unless otherwise cited or acknowledged. It is entirely of my own composition and has not, in whole or in part, been submitted for any other degree.

Silke Morris (née Machauer)

## Abbreviations

2YT	2 Yeast Tryptone
AMPK	AMP-activated protein kinase
AP	Adaptor Protein
APS	Adaptor protein with Pleckstrin homology and Src homology 2 domains
APS	Ammonium Persulfate
AS160	Akt Substrate of 160 kDa
ATP	Adenosine Triphosphate
BMI	Body Mass Index
BN-PAGE	Blue Native Polyacrylamide Gel Electrophoresis
BRET	Bioluminescence Resonance Energy Transfer
BSA	Bovine Serum Albumin
CAP	c-CBL-Associated Protein
CHO	Chinese Hamster Ovary
CLSM	Confocal Laser Scanning Microscopy
DAPI	4',6-Diamidino-20-Phenylindole
DMEM	Dulbecco's Modified Eagle's Medium
DMSO	Dimethyl Sulfoxide
dSTORM	Direct Stochastic Optical Reconstruction Microscopy
DTT	Dithiothreitol
DV	Docked Vesicle
<i>E. coli</i>	<i>Escherichia coli</i>
ECL	Enhanced Chemiluminescence
EDTA	Ethylenediaminetetraacetic acid
eGFP	Enhanced Green Fluorescent Protein
EGTA	Ethylene glycol-bis(2-aminoethylether)- <i>N,N,N',N'</i> -tetraacetic acid
ER	Endoplasmic Reticulum
ERGIC	ER-to-Golgi Intermediate Compartment
FCS	Foetal Calf Serum
FKBP	FK506 Binding Protein 12
FPALM	Fluorescence Photoactivation Localisation Microscopy
FRB	FKBP Rapamycin Binding protein

FRET	Fluorescence Resonance Energy Transfer
GAP	GTPase-Activating Protein
GFP	Green Fluorescent Protein
GGA	Golgi-localized, gamma-ear containing, ADP-ribosylation factor binding
GLUT	Glucose Transporter
GLUT4/G4	Glucose Transporter 4
Gly	Glycine in PBS
GPCR	G-Protein Coupled Receptor
GSC	GLUT4 Storage Compartment
GSV	GLUT4 Storage Vesicle
HA	Haemagglutinin
HDM	High Density Microsome
HEPES	4-(2-hydroxyethyl)-1-piperazineethanesulfonic acid
HES	HEPES-EDTA-Sucrose
HMIT	H <sup>+</sup> -coupled Myo-Inositol Transporter
HRP	Horseradish Peroxidase
IB	Immunoblotting
IBMX	3-isobutyl-1-methylxanthine
IF	Immunofluorescence
IRAP	Insulin-Responsive Aminopeptidase
IRS	Insulin Receptor Substrate
ISC	Intersystem Crossing
LDM	Low Density Microsome
LRP1	Lipoprotein Receptor related Protein 1
LSB	Laemmli Sample Buffer
M6PR	Mannose-6-Phosphate Receptor
MEA	Mercaptoethylamine
MEU	Monomeric Equivalent Unit
MOI	Multiplicity of Infection
mTORC2	mTOR Complex 2
MV	Moving Vesicle
NA	Numerical Aperture
NAPA	N-ethylmaleimide-sensitive factor Attachment Protein Alpha

NCS	Newborn Calf Serum
PAGE	Polyacrylamide Gel Electrophoresis
PAO	Phenylarsine Oxide
PBS	Phosphate Buffered Saline
PBST	Phosphate Buffered Saline with Tween
PDK1	Phosphoinositide-Dependent Kinase 1
PFA	Paraformaldehyde
PI	Phosphoinositide
PI3K	Phosphoinositide 3-Kinase
PI4KIII $\alpha$	Phosphatidylinositol 4-Kinase type III $\alpha$
PI4P	Phosphatidylinositol 4-Phosphate
PIK	Phosphoinositide Kinase
PIP3	Phosphoinositide-3,4,5-triphosphate
PKB	Protein Kinase B
PLD	Phospholipase D1
PSF	Point Spread Function
ROI	Region of Interest
SD	Standard Deviation
SDS	Sodium Dodecyl Sulfate
SE	Standard Error
SIM	Structured Illumination Microscopy
SM	Sec1/Munc18
SMLM	Single Molecule Localisation Microscopy
SNAP	Soluble NSF Attachment Protein
SNAP	Synaptosome-Associated Protein
SNARE	Soluble <i>N</i> -ethylmaleimide sensitive fusion protein Attachment protein Receptor
SOC	Super Optimal Broth with Catabolite repression
SORL1	Sortilin-related Receptor
SpIDA	Spatial Intensity Distribution Analysis
STED	Stimulated Emission Depletion
STORM	Stochastic Optical Reconstruction Microscopy
TAE	Tris-Acetate EDTA
TfR	Transferrin Receptor
TGN	Trans-Golgi Network



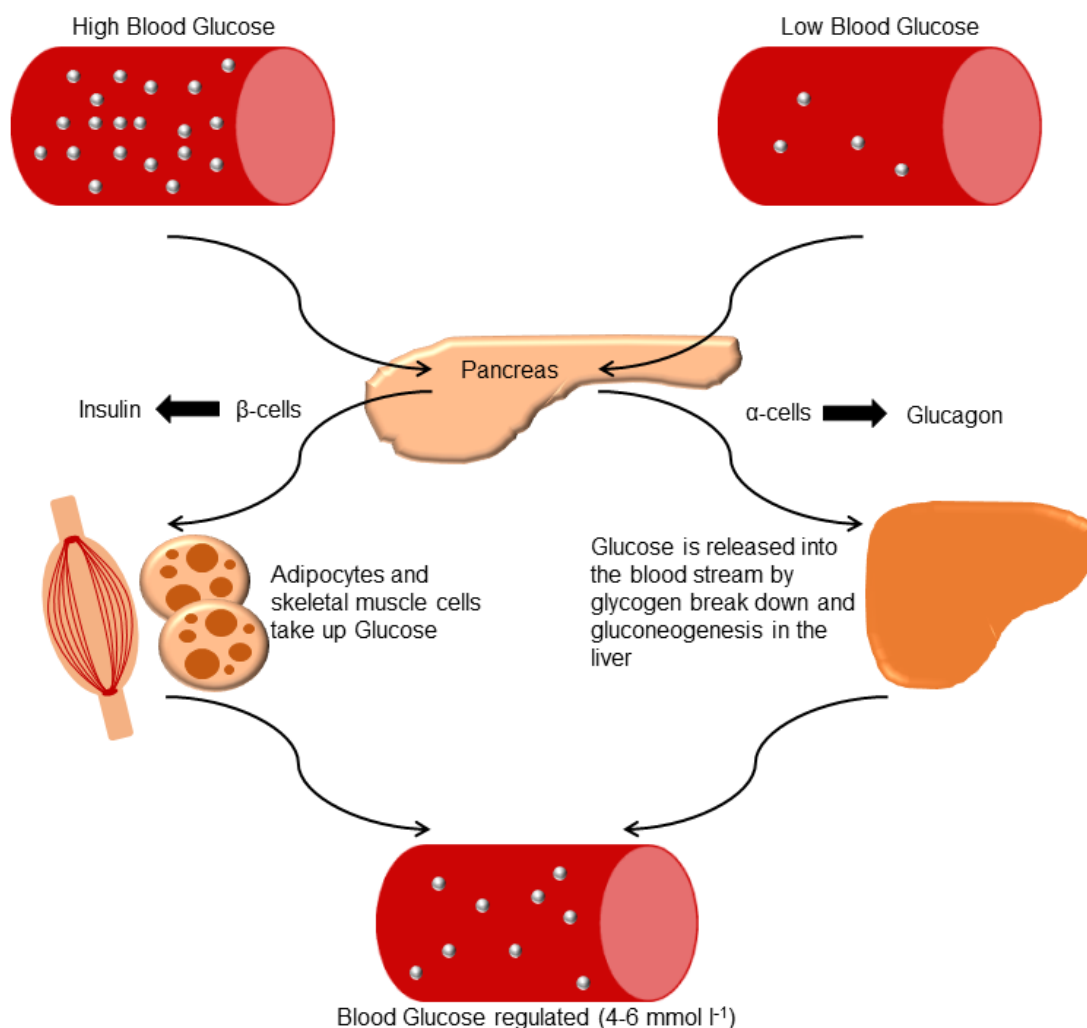
TIR	Total Internal Reflection
TIRF	Total Internal Reflection Fluorescence
TIRFM	Total Internal Reflection Fluorescence Microscopy
t-SNARE	Target-SNARE
VAMP	Vesicle-Associated Membrane Protein
v-SNARE	Vesicle-SNARE

# Chapter 1 Introduction

## 1.1 Glucose Homeostasis

Carbohydrates are sugars and their polymers, polysaccharides. The most basic carbohydrates are monosaccharides and glucose is the most common monosaccharide. Glucose is our bodies main energy supplier. Its energy is released by an oxidative process called cell respiration, in which it is enzymatically broken down. Glycolysis and the citric acid cycle are the first two steps of cell respiration, in which each molecule of glucose is broken down to two molecules of pyruvate. Pyruvate is then converted to coenzyme A, which undergoes the citric acid cycle where  $\text{CO}_2$  is released. Some steps of glycolysis and citric acid cycle are redox reactions, in which electrons and protons are transferred onto substrates which are then fed into the electron transport chain, which ultimately ends in oxidative phosphorylation and the production of adenosine triphosphate (ATP). Glucose is produced by plants through photosynthesis, a reaction that converts  $\text{CO}_2$  and  $\text{H}_2\text{O}$  to Glucose and  $\text{O}_2$  using light energy. But animals also produce glucose from pyruvate and oxaloacetate, products of the amino acid metabolism during a process called gluconeogenesis, which takes place mostly in the liver and in the kidney (Campbell & Reece, 2006; Nelson & Cox, 2017).

In healthy individuals blood glucose levels are controlled by the pancreas and are typically maintained at a level around  $4\text{-}6 \text{ mmol l}^{-1}$  (Nelson & Cox, 2017; Perley & Kipnis, 1967). The pancreas contains endocrine cells,  $\alpha$ -,  $\beta$ -, and  $\delta$ -cells, which are located within the islets of Langerhans. When blood glucose levels are low during hypoglycaemia due to lack of food and continuing oxidation of glucose by the brain and other tissues,  $\alpha$ -cells secrete glucagon which in turn facilitates the hydrolysis of glycogen to glucose in the liver, but glucose is also newly synthesised during gluconeogenesis as previously mentioned. In fact, the liver can produce up to 500 g of glucose during this process every day. After a meal, when blood glucose levels rise, pancreatic  $\beta$ -cells secrete insulin, thus allowing glucose transport into the liver, muscle, and adipose tissue, where it is converted to glycogen (liver and muscle) and triacylglycerols (adipose tissue) (Nelson & Cox, 2017).



**Figure 1.1 Regulation of Blood Glucose Levels through the Pancreas.**

Blood glucose levels are regulated by the  $\alpha$ - and  $\beta$ -cells of the pancreas. In case of hypoglycaemia  $\alpha$ -cells secrete glucagon, which initiates breakdown of glycogen in the liver to glucose. During hyperglycaemia  $\beta$ -cells release insulin, which stimulates fat and skeletal muscle cells to take up glucose from the blood stream.

Figure 1.1 schematically shows glucose homeostasis as regulated by the pancreas.  $\delta$ -cells secrete somatostatin, which regulates the secretion of both glucagon and insulin (Gerich, 1981).

The vast majority of insulin-stimulated glucose-uptake (~90 %) occurs in skeletal muscle tissue (Kraegen et al., 1985). The remaining less than 10 % that is cleared by adipose tissue is, however, not to be neglected. Adipose tissue is in fact significant for insulin sensitivity, as insulin-resistant individuals show decreased expression of Glucose Transporter 4 (GLUT4) in adipocytes, but not in muscle (Shepherd & Kahn, 1999). Abel et al. confirmed this by adipose selective knock-down of GLUT4 in mice and found that this led to whole-body insulin-resistance and glucose intolerance (Abel et al., 2001). Therefore, while liver and muscle

take up most of the blood glucose, adipocytes play an important role in overall glucose homeostasis and communicate with liver and muscle in this regard.

## 1.2 Diabetes Mellitus

Diabetes is one of the most prevalent diseases worldwide, with currently about 422 million adults affected. This number has nearly quadrupled since 1980, whilst the age-standardised frequency has almost doubled from 4.7 % in 1980 to 8.5 % in 2014 and is expected to rise even further (Mathers & Loncar, 2006; Tareque et al., 2016). This increase has been especially steep during the last ten years in low- and middle-income countries. In the UK, it is estimated that 4.5 million people currently live with diabetes (Diabetes UK, 2016). Diabetes not only affects patients' personal lives but also has a huge impact on health-care systems and indirectly on the global economy. It is estimated that in the UK, about 10 % of the NHS budget is spent on diabetes care, which accounts for approximately £9.8bn for direct costs and £13.9bn for indirect costs. This figure is suspected to rise to a total cost of £39.8bn or 17 % of the NHS budget in 2035/2036 (Hex et al., 2012; Seuring et al., 2015).

Diabetes mellitus is a metabolic disorder, which is mainly characterised by chronic hyperglycaemia. Insulin plays an important role in the development of diabetes, because the release of insulin from the pancreatic  $\beta$ -cells is disturbed or even completely inhibited. This results in elevated blood glucose levels and the inability of cells to effectively take up glucose. Depending on the underlying mechanisms, there are different types of diabetes.

Type I diabetes is an autoimmune disease, in which the immune system produces antibodies against pancreatic  $\beta$ -cells, which leads to  $\beta$ -cell destruction, inflammation and consequently the immediate need for external insulin substitution. Therefore, this form of diabetes is also referred to as insulin-dependent diabetes. An estimated 10 % of people with diabetes suffers from this type. The onset is typically early on in life, where the terms juvenile and childhood-onset diabetes are derived from and it is not yet curable or preventable (Atkinson et al., 2014; Diabetes UK, 2016; Knip et al., 2005).

Type 2 diabetes, or non-insulin-dependent diabetes, is far more common (90 % of people with diabetes) and is primarily characterised by insulin resistance, hyper-insulinaemia. Insulin resistance is caused by a disturbance in insulin signalling, which results in the cell requiring increased amounts of insulin to take up the glucose from the blood stream. The body reacts with increased insulin production, which eventually leads to an impairment of the pancreas and other organs. This in turn will lead to pancreatic  $\beta$ -cell failure. Different from type 1 diabetes, the development of type 2 is largely due to poor life-style choices, such as little to no exercise and the consumption of food and drinks high in fat and sugar, which can lead to overweight or obesity (Diabetes UK, 2016). 60 % of type 2 diabetics are classified as obese, although there is also a genetic component to the development of the disease. However, changes to a more active and healthier lifestyle have been shown to be effective in prevention or even reversal of type 2 diabetes (Chatterjee et al., 2017). Formerly also known as adult-onset diabetes, type 2 diabetes was long thought to be only present in adults, but since the first reported cases of type 2 diabetes in children in 2000, more and more children and adolescents are becoming affected (Ehtisham et al., 2000).

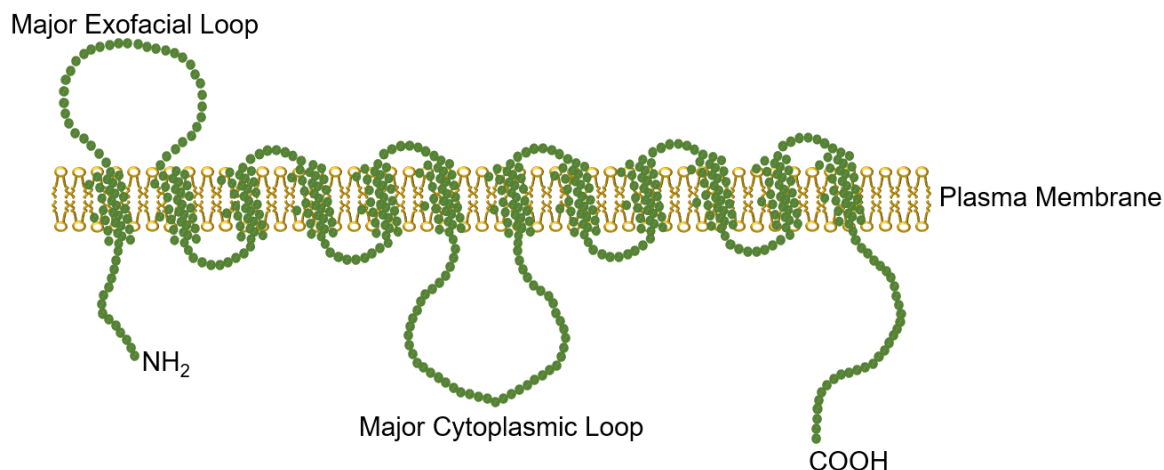
Where lifestyle changes and weight loss are not enough to control blood glucose levels in type 2 diabetics, medication can be given to treat the symptoms of the disease. Metformin is usually the first drug that is prescribed in this case (Maruthur et al., 2016). It works by inhibiting gluconeogenesis in the liver and increasing insulin sensitivity, thus making glucose uptake more efficient. Other drugs such as sulfonylureas and meglitinides stimulate the pancreas to increase insulin production. Eventually, with the progression of type 2 diabetes, external administration of insulin will be necessary (Maruthur et al., 2016; Tareque et al., 2016). All those medications have in common that they only treat the symptoms of the disease; a cure for type 2 diabetes is yet to be found and relies on a better understanding of glucose uptake in healthy individuals as well as type 2 diabetics.

### **1.3 Glucose Transporters**

Glucose and other hexoses are transported from the blood stream into cells by glucose transporters (GLUTs). They are facilitative transporters that transport glucose and other hexoses through aqueous pores along a concentration gradient

into the cell. Although structurally very similar, GLUTs differ in their kinetic properties, substrate specificity, as well as their tissue and intracellular distribution (Kahn, 1992). GLUT1 was the first transporter to be characterised (Mueckler et al., 1985) and is mostly expressed in erythrocytes, the brain, and the placenta. GLUT2 has a high  $K_m$  for glucose, allowing rapid glucose flux into the cell or out of the cell, such as after gluconeogenesis (Gould et al., 1991). Another transporter that is highly expressed in the brain is GLUT3. Because the energy demand in this tissue is relatively constant, the GLUTs in the brain are constitutively targeted to the plasma membrane (Duelli & Kuschinsky, 2001). In contrast, muscle tissue for example does not require a constant supply of energy, but its demand increases sharply during exercise. Muscle tissue therefore requires a more specialised glucose uptake system and GLUTs that can respond quickly to sudden changes in energy demand (Shepherd & Kahn, 1999). GLUT4 is found mostly in muscle and fat. It is located intracellularly and translocates to the plasma membrane in response to insulin stimulation, or, in the case of skeletal muscle, in response to muscle contraction, which is a unique behaviour and not exhibited by the other GLUTs (Bryant et al., 2002). In muscle tissue, this feature is responsible for the quick response during exercise. GLUT4 translocation in skeletal muscle cells is related to the release of  $Ca^{2+}$ , which is thought to activate other signalling molecules. Muscle contraction also results in the activation of AMP-activated protein kinase (AMPK), which is thought to decrease the rate of GLUT4 endocytosis and enhances GLUT4 regulation (Richter & Hargreaves, 2013).

Currently, 13 different GLUTs are known (GLUT1-12 and HMIT (H<sup>+</sup>-coupled myo-inositol transporter)). They are integral membrane proteins that are each unique in their kinetic properties and function, and are expressed in different tissues (S. Huang & Czech, 2007; Wood & Trayhurn, 2003). Mueckler *et al.* were the first who described the membrane topology of the transporter GLUT1, which is similar in all GLUTs: the proteins consist of 12 amphiphilic transmembrane helices that are embedded in the plasma membrane as well as an exofacial and a cytoplasmic loop. These domains are arranged in such a way that hydrophobic parts are facing the plasma membrane, while hydrophilic parts are forming the pore. Both, the C- and the N-terminus are located on the cytosolic side of the membrane as depicted in Figure 1.2 (Mueckler et al., 1985).



**Figure 1.2 Structure of the Membrane Protein GLUT4.**

GLUT4 spans the plasma membrane 12 times and exhibits an exofacial as well as a cytoplasmic loop. Both, the N- and the C-terminal region are on the cytoplasmic side. All 13 GLUTs have a similar structure, the specificity of GLUT4 is thought to lie in the unique N- and C-terminus (Bryant et al., 2002; S. Huang & Czech, 2007).

The 13 types of GLUTs are divided into three sub-classes based on homologies in their primary structure: class I (GLUT1-4) contains glucose transporters, class II (GLUTs 5, 7, 9, 11) are fructose transporters, and the remaining GLUTs as well as HMIT belong to class III, they are yet to be defined in more detail (Bryant et al., 2002; Wood & Trayhurn, 2003).

### 1.3.1 Glucose Transporter 4

In 1980 the two independent groups of Cushman and Kono were the first to report that insulin-stimulated glucose transport was the result of translocation of pre-existing glucose transporters from intracellular storage sites to the plasma membrane. They observed this effect in isolated rat adipocytes (Cushman & Wardzala, 1980) and in cell fractions respectively (Suzuki & Kono, 1980). We now know that the glucose transport systems they described are in fact GLUT4 containing vesicles and that this behaviour is specific for the GLUT4 isoform.

Glucose transporter 4 was first identified by James *et al.* in 1988, when they identified a protein of a molecular mass of  $M_r = 43,000$  that was expressed only in adipose, skeletal muscle, and heart tissue. Furthermore, they found that the subcellular distribution of this protein responded to insulin stimulation by increasing the concentration of the protein in the plasma membrane while decreasing the concentration in low density microsomes (James et al., 1988). Kayano *et al.* isolated the mRNA of this protein and published the result in the

same year (Kayano et al., 1988). James *et al.* characterised it further by molecular cloning of a cDNA isolated from rat adipocyte and heart libraries, which shared 65 % of its nucleotide sequence with GLUT1; back then known as HepG2 glucose transporter. The protein encoded by this sequence exhibited an almost identical hydropathy plot and tertiary structure to GLUT1. Moreover, the protein could be found in insulin responsive tissues and in 3T3 L1 adipocytes, but not in fibroblasts. Interestingly, it showed translocation to the plasma membrane in response to insulin. They concluded that the sequence they had cloned belonged to a highly insulin-sensitive glucose transporter (James et al., 1989). This transporter is today known as GLUT4.

Around the same time, other groups from all over the world reported that they had isolated cDNA clones encoding GLUT4 in insulin responsive tissues from rats and humans (Charron et al., 1989; Fukumoto et al., 1989), other groups found that 3T3 L1 cells expressed GLUT4 after differentiation into adipocytes, but not as fibroblasts (de Herreros & Birnbaum, 1989; Kaestner et al., 1989).

GLUT4 displays the same structure as other GLUTs shown in Figure 1.2, but has distinct sequences specifically in its NH<sub>2</sub>- and COOH-termini. The COOH-terminal domain contains an acidic motif as well as a double leucine that regulate the intracellular distribution of GLUT4. Mutation of the acidic region results in accumulation of GLUT4 at the plasma membrane (Shewan et al., 2000), while the dileucine is crucial for endocytosis and retention (Corvera et al., 1994). The NH<sub>2</sub>-terminus contains an F<sub>5</sub>QQI motif that interacts with adaptor proteins (APs) AP1 and AP2, which are important for endosomal sorting (Bernhardt et al., 2009). Furthermore, mutation of a phenylalanine in the NH<sub>2</sub>-terminus leads to constitutive targeting of GLUT4 to the plasma membrane (Piper et al., 1993).

While other GLUTs are mostly found in the plasma membrane of tissues that have consistent energy and therefore glucose requirements (e.g. GLUT1 and 3 in the brain) or act as a glucose sensor (GLUT2 in pancreatic  $\beta$ -cells), GLUT4 is mostly found in cardiomyocytes, skeletal muscle and adipose tissue and it is the only one of the 13 glucose transporters that responds to insulin and other stimuli, such as exercise (in muscle tissue), with increased translocation to the membrane; This makes sense because glucose requirements vary in these tissues. Muscle cells need to adapt quickly to physical activity and adipocytes



are responsible for post-prandial glucose uptake, so need to respond to insulin stimulation when blood glucose levels rise after a meal. Consequently, these cell types require a glucose transport system that can be regulated by the current glucose concentration in the blood through insulin.

If this mechanism is defective, it contributes to insulin resistance and ultimately type 2 diabetes (Garvey et al., 1988; Maianu et al., 2001; Sinha et al., 1991), which is why GLUT4 and its associated signalling pathways are particularly interesting as potential drug targets.

## 1.4 The GLUT4 Storage Compartment

In the absence of stimuli, GLUT4 is mostly located in tubulo-vesicular structures within the cell and only a small percentage is at the cell surface (Dawson et al., 2001; Piper et al., 1991; Slot et al., 1991). Slot *et al.* investigated the intracellular distribution of GLUT4 in rat adipose tissue of basal and insulin-stimulated animals by immunolocalization and electron microscopy. Under basal conditions, they found that the majority of GLUT4 is located in small vesicles (60 - 100 nm) as well as tubulo-vesicular structures near the Golgi and only 1 % of total GLUT4 is in the plasma membrane. This increased to 40 % after insulin stimulation, which was not exclusive to certain regions of the membrane but universally distributed (Slot et al., 1991). Herman *et al.* confirmed the existence of these unusually small vesicles that are exclusive to GLUT4 by density gradient centrifugation (Herman et al., 1994). Using subcellular fractionation of 3T3 L1 adipocytes, Livingstone *et al.* found a compartment that was separate from the endosomal system; 60 % of total GLUT4 did not colocalise with its marker the transferrin-receptor (TfR) the way other membrane proteins such as GLUT1 do. They concluded that there is another intracellular compartment of GLUT4 that does not participate in the cycling with the plasma membrane and eluded that this may be essential for the insulin responsiveness of GLUT4 (Livingstone et al., 1996). In a review, Rea and James named this the GLUT4 storage compartment (GSC) and the small vesicles that had previously been described received the term GLUT4 storage vesicles (GSVs) (Rea & James, 1997).

Because GLUT4 does only colocalise with furin, a *Trans*-Golgi network (TGN) marker, in the presence of the TfR, the Golgi was not considered to be this

second compartment (Karylowski et al., 2004). However, the Golgi does seem to play a role in insulin regulated GLUT4 trafficking. When adipocytes are incubated at 19 °C, a temperature where trafficking out of the TGN is inhibited, there is no insulin response. This finding suggests that the TGN precedes the sorting of GLUT4 into insulin sensitive vesicles (Robinson & James, 1992). It is thought that Syntaxins 6 and 16 are involved in this sorting step (Perera et al., 2003; Proctor et al., 2006; Shewan et al., 2003).

Subcellular fractionation of cell lysates can resolve five different fractions: the cytosol, mitochondria and nuclei, the plasma membrane, high density and low density microsomes (HDM and LDM) (I. A. Simpson et al., 1983). GLUT4 can be found mostly in the HDM, LDM, and the plasma membrane fractions. Insulin stimulation leads to a 10-fold increase of GLUT4 in the plasma membrane fraction (Piper et al., 1991), which mirrors the results of the previously discussed experiments by Slot *et al.* Using vesicle immunoadsorption and iodixanol equilibrium sedimentation analysis together with the transferrin-horseradish peroxidase-3,3'-diaminobenzidine-mediated endosomal ablation technique, Hashiramoto and James managed to resolve the LDM fraction of 3T3 L1 adipocytes further. They found two separate GLUT4 containing peaks in the fractions they collected. One peak was rich in markers of endosomes and the TGN, the other peak had a higher GLUT4 concentration and was very responsive to insulin stimulation. They concluded that with this peak they had found another vesicular population of GLUT4 that is probably derived from the endosomal cycle (Hashiramoto & James, 2000). The question remained whether GSVs are part of the known recycling pathways or if they represent a new GLUT4 specific organelle.

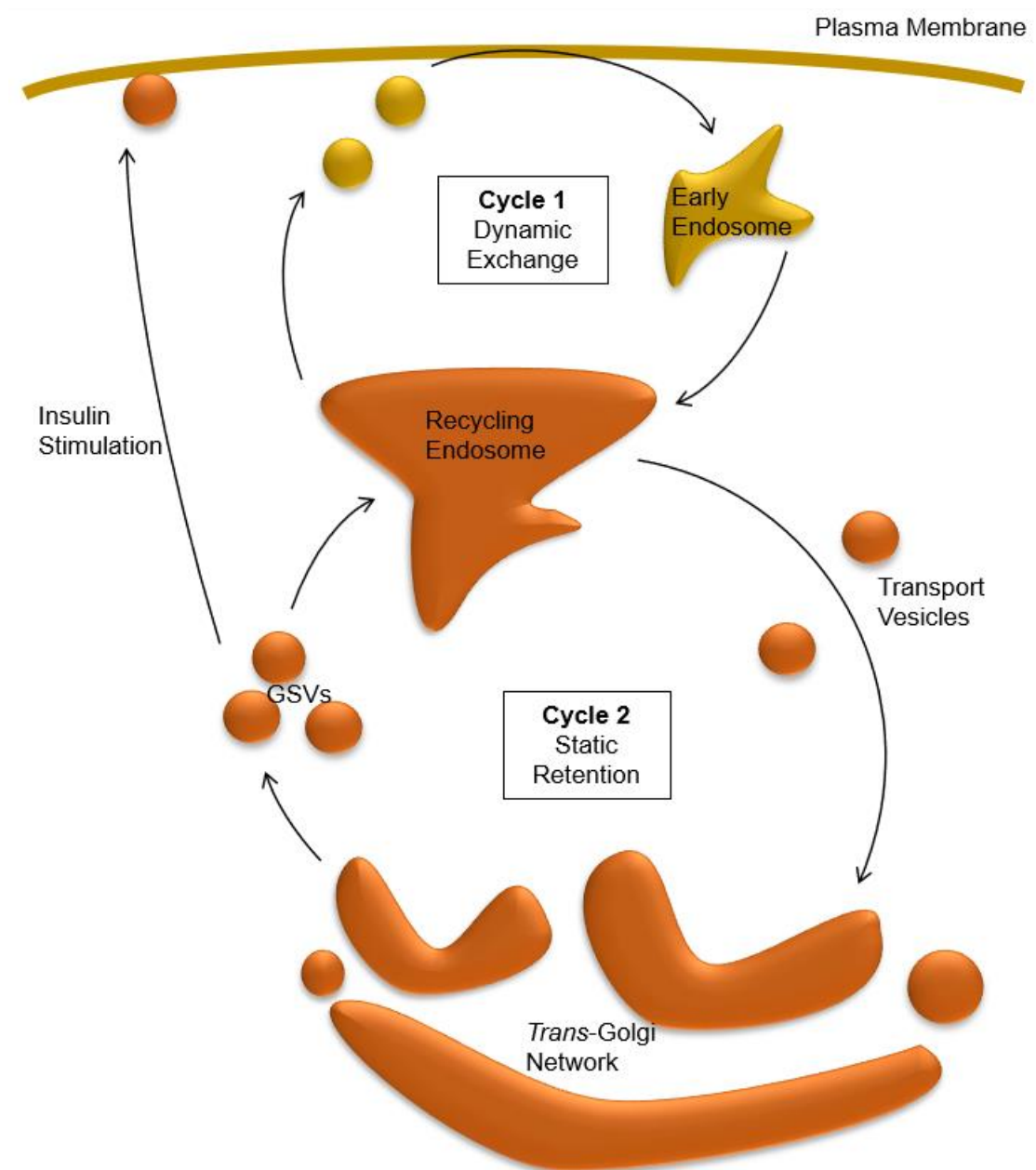
The translocation of GLUT4 to the cell surface happens quickly and reaches its maximum after about 10-15 minutes in 3T3 L1 adipocytes (Brewer et al., 2014; Govers et al., 2004). To facilitate this rapid response to insulin, GLUT4 must be either selectively retained in intracellular storage compartments until insulin triggers its release (static retention model), or it is constantly recycling between intracellular organelles and the plasma membrane and insulin stimulation leads to an increase of exocytosis and/or a decrease of endocytosis (dynamic exchange model) (Govers et al., 2004; Karylowski et al., 2004; O. J. Martin et al., 2006).

Mathematical modelling showed that either model is likely to be comprised of four or five pools: two intracellular compartments and two or three at the plasma membrane, with occluded pools that act as intermediates in endo- and/or exocytosis (Holman et al., 1994). Only a model with multiple intracellular pools accounts for the fast initial insulin response and subsequent slow recycling of plasma membrane GLUT4, therefore excluding a simple 2-pool model. The modelling results also showed that insulin must have a greater effect on GLUT4 exocytosis than endocytosis, because changing the latter does not result in a response as fast as it is observed experimentally (Holman et al., 1994).

It has been shown that the majority of total GLUT4 is not recycling via the plasma membrane in the basal state and that increasing insulin concentration increases the number of GLUT4 molecules participating in this pathway (Govers et al., 2004). However, even at maximal insulin concentration only 70 % of total GLUT4 is recycling with the plasma membrane. The static retention model argues that the proportion of GLUT4 that is not involved in recycling is therefore stored in a static intracellular compartment (Coster et al., 2004). Single molecule tracking in basal and insulin stimulated 3T3 L1 adipocytes supported this model, as GLUT4 molecules showed a significant increase in mobility in the presence of insulin (Fujita et al., 2010).

In the basal state, the equilibrium of GLUT4 between the GSC and the endosomal compartment is reached much quicker ( $t_{1/2} = 20$  min) than with the plasma membrane ( $t_{1/2} = 230$  min) (Karyłowski et al., 2004). This means a GSV is about 5 times more likely to fuse with an endosome than with the plasma membrane. The movement between the two compartments has been suggested to be part of a dynamic retention system of GLUT4 in the absence of insulin. Insulin stimulation then leads to an increase in the exocytosis rate, even under physiological insulin concentrations. Different from GLUT4 exocytosis, this cycling does not require intact microtubules, as it is not affected by nocodazole treatment (Karyłowski et al., 2004; O. J. Martin et al., 2006). The rapid cycling between the intracellular GLUT4 containing compartments supports the dynamic exchange model.

Interestingly, the cell culture conditions also influence the size of the cycling GLUT4 pool in the basal state. Replating the cells for microscopy, which is a common practice, was shown to increase the percentage of cycling GLUT4 from 22 % in confluent cells to 80 % in replated cells (Muretta et al., 2008). This illustrates further the complexity of the process and shows how different experimental procedures can have a significant effect on results.



**Figure 1.3 Model of Dynamic Exchange and Static Retention of GLUT4.**

GLUT4 is thought to be recycled within two different cycles. Cycle 1 comprises the endosomal system, while cycle 2 comprises the static retention model, where GLUT4 continuously cycles between the recycling endosome and the *Trans-Golgi* network until insulin stimulation leads to rapid translocation of GSVs to the plasma membrane (Bryant et al., 2002).

Currently, it is believed that in fact both models are valid and GLUT4 is indeed found in two different intracellular recycling pathways. (Bryant et al., 2002). Using flow cytometry, Muretta *et al.* developed an assay that allowed them to analyse large numbers of cells, in contrast to microscopy-based experiments. They found that under basal conditions the majority of GLUT4 is retained statically within the cell and insulin controls the population that is actively cycling through the plasma membrane through quantal release; i.e. the amount of GLUT4 in the actively cycling pool is proportional to the concentration of insulin. When insulin is withdrawn, GLUT4 returns to the static compartment very slowly. Only after 12 hours post insulin, the static GLUT4 pool has returned to its original size. However, GLUT4 is cleared from the plasma membrane in a much faster manner by adjusting the endo- and exocytosis rates accordingly, suggesting that GLUT4 remains within this cycling pool until it has fully returned to the intracellular static pool. Under physiological conditions this might mean that the mode of GLUT4 cycling depends on the fluctuation of serum insulin. When insulin levels are fluctuating rapidly, the dynamic exchange model applies, and in the case of slow insulin level fluctuation, such as in basal versus stimulated model cell culture systems, the static retention model is valid (Muretta et al., 2008).

Figure 1.3 shows the model of the two cycling pathways that are thought to be comprising both the static retention and the dynamic exchange model previously described, which was first thought of as early as 1996 by Martin *et al.* (S. Martin et al., 1996). After synthesis and post-translational modifications in the Golgi network, GLUT4 is packaged into GSVs, which upon insulin stimulation rapidly translocate to and fuse with the plasma membrane. In the absence of insulin GLUT4 enters the endosomal system, but it is selectively held back in favour of other membrane proteins, such as TfR, and only a small portion of GLUT4 recycles between the plasma membrane and the endosomes, while the majority is in a second cycle between transport vesicles, the TGN, and newly formed GSVs, ready for translocation in the event of insulin stimulation. This second cycle is unique to insulin-responsive cells and forms during the early stages of 3T3 L1 differentiation into adipocytes, even before GLUT4 is expressed in these cells (Bryant et al., 2002; El-Jack et al., 1999)

### 1.4.1 Endocytosis of GLUT4

Clathrin, a protein that is involved in the formation of coated vesicles and endocytosis (Pearse, 1976), appears to be involved in the intracellular retention of GLUT4. GLUT4 is present in clathrin-coated vesicles derived from both, the plasma membrane and the TGN (Robinson et al., 1992). About 5 % of total GLUT4 is in clathrin-coated vesicles at the plasma membrane, which is noteworthy, and it is hypothesised that insulin has an effect on the coating and uncoating of GSVs with clathrin, thus regulating their endocytosis (Chakrabarti et al., 1994). It has also been shown that the GTPase dynamin is involved in the endocytosis of GLUT4, since expression of dynamin decreases the GLUT4 levels in the plasma membrane. In contrast, maximal expression of a GTPase-negative mutant form of dynamin leads to the majority of GLUT4 being located in the plasma membrane and insulin has no further effect (Al-hasani et al., 1998).

Blot and McGraw found that GLUT4 can be internalised by two different mechanisms: a cholesterol- and an AP2-dependent pathway. Under basal conditions a cholesterol-dependent pathway is favoured. Insulin-stimulation results in preferred GLUT4 uptake by the AP2-dependent mechanism. The latter involves the FQQI motif and is less rapid than basal GLUT4 endocytosis (Blot & McGraw, 2006).

By determining the half-time for internalisation of labelled surface GLUT4, the endocytosis rate of the transporter could be calculated. It was found that insulin has a small effect on GLUT4 endocytosis. The endocytosis rate constant is about 30 % slower after insulin stimulation compared to the basal state. The main effect of insulin however, is on the exocytosis rate (J. Yang & Holman, 1993).

### 1.4.2 Other Components and Biogenesis of GSVs

In undifferentiated 3T3 L1 adipocytes exogenous GLUT4 does not translocate to the plasma membrane in response to insulin. Instead, it enters the lysosomal pathway and degrades quickly (Haney et al., 1991; Shi & Kandror, 2005). GSVs begin to form between day 2 and 3 of differentiation (El-Jack et al., 1999; Shi et al., 2008). After this point, increased insulin-responsiveness and insulin-stimulated glucose uptake can be observed. Moreover, exogenous GLUT4 is now

stable and can be found within small vesicles that do not sediment after centrifugation at  $16,000 \times g$ : the GSVs. At the same time the concentration of the membrane protein sortilin increases dramatically (Lin et al., 1997; N. J. Morris et al., 1998; Shi & Kandror, 2005). This discovery led to the hypothesis that sortilin is in fact involved in the biogenesis of GSVs. Indeed, overexpression of sortilin in 3T3 L1 adipocytes leads to increased GSV formation.

Correspondingly, knock-down of sortilin results in a decrease of total GLUT4 expression, insulin-stimulated glucose-uptake and formation of GSVs (Shi & Kandror, 2005). Interestingly, if undifferentiated 3T3 L1 fibroblasts are transfected with both GLUT4 and sortilin, they form GSVs and become insulin-responsive. These findings suggest that sortilin is in fact not only necessary but also sufficient for the biogenesis of GSVs (Kandror, 2018; Shi & Kandror, 2005).

After GLUT4 itself, the insulin-responsive aminopeptidase (IRAP) is probably the most significant component of GSVs (Kupriyanova et al., 2002; Shi et al., 2008). It was discovered in traditional protein sequencing studies and was found to colocalise with GLUT4 almost completely (Kandror & Pilch, 1994; Mastick et al., 1994). It is expressed in the same tissues as GLUT4, namely fat and skeletal muscle, but it was also found in other tissues and cells that do not express GLUT4 (Albiston et al., 2001; Nikolaou et al., 2014). IRAP is a zinc-dependent membrane aminopeptidase, which features large extracellular and cytoplasmic domains and spans the membrane once (Rogi et al., 1996). Interestingly, the intracellular domain features two dileucine motives, like the C-terminus of GLUT4, which may be involved in trafficking of the protein similar to the glucose transporter (Keller et al., 1995). Chinese Hamster Ovary (CHO) cells express IRAP, but not GLUT4. Johnson *et al.* expressed a fusion protein of C-terminal IRAP and N-terminal TfR in this cell line and found that the chimera recycled slowly through the endosomal compartment to the plasma membrane. Insulin stimulation increased this 2-3-fold (Johnson et al., 1998). The chimera expressed in undifferentiated 3T3 L1 fibroblasts behaves the same way (Lampson et al., 2000). The fact that IRAP and GLUT4 are so similar in their localisation and their response to insulin makes IRAP a popular protein for the study of GSVs (Stenkula et al., 2010). It is debated whether IRAP and GLUT4 physically interact with each other. The two proteins do not co-precipitate, eliminating the possibility of a strong interaction (Keller, 2003). However, experiments with a yeast two-

hybrid system showed that there is an interaction between the luminal domain of IRAP and the first luminal loop of GLUT4 (Shi et al., 2008), although it has now been suggested that this is via a retromer that binds to GLUT4 and IRAP (Pan et al., 2017; Z. Yang et al., 2016). When IRAP is knocked down in 3T3 L1 adipocytes, intracellular GLUT4 retention under basal conditions is not as effective, while membrane trafficking of other proteins, such as TfR, is not affected (Jordens et al., 2010). Determination of the exocytosis rate constants revealed that it is in fact the exocytosis rate that is elevated after IRAP knock-down. Using the endosome ablation assay, it could be shown that IRAP knock-down specifically leads to an increased amount of GLUT4 within endosomes, which led to the conclusion that IRAP plays a crucial role in the sorting of GLUT4 into GSVs. On the other hand, knock-down of GLUT4 does not alter the intracellular distribution of IRAP, suggesting that IRAP traffics independently of GLUT4 (Jordens et al., 2010).

Low density lipoprotein receptor-related protein 1 (LRP1) is a large (~500 kDa) protein, also known as  $\alpha_2$ -macroglobulin receptor (Corvera et al., 1989). Crosslinking experiments have shown a direct interaction between the luminal domains of LRP1 with GLUT4, IRAP, and sortilin. It also binds AS160, a protein that is part of the insulin signalling pathway (see 1.5 Insulin Signalling) Knock-down of the protein inhibits the formation of fully functional GSVs, which means it must play a role in the biogenesis of the vesicles (Brewer et al., 2014; Jedrychowski et al., 2010).

GLUT4, IRAP, sortilin, and LRP1 are thought to interact with each other via their luminal domains and form an oligomeric complex. Golgi-localized, gamma-ear containing, ADP-ribosylation factor binding (GGA) proteins then recognise the DXXLL sequence of sortilin and enable the sorting into GSVs. All four proteins contain amino acid sequences that are known to bind clathrin APs, which then facilitate budding off the donor membrane (Kandror & Pilch, 2011).

Other proteins that are associated with GSVs and show significant colocalisation with GLUT4 in microscopy images are TfR (Davis et al., 1986), mannose-6-phosphate receptor (M6PR) (Oka et al., 1984), syntaxins 6 (Perera et al., 2003) and 16 (Proctor et al., 2006), and Vti1a (Kandror & Pilch, 2011). These proteins, particularly TfR and M6PR have long been known to translocate to the cell



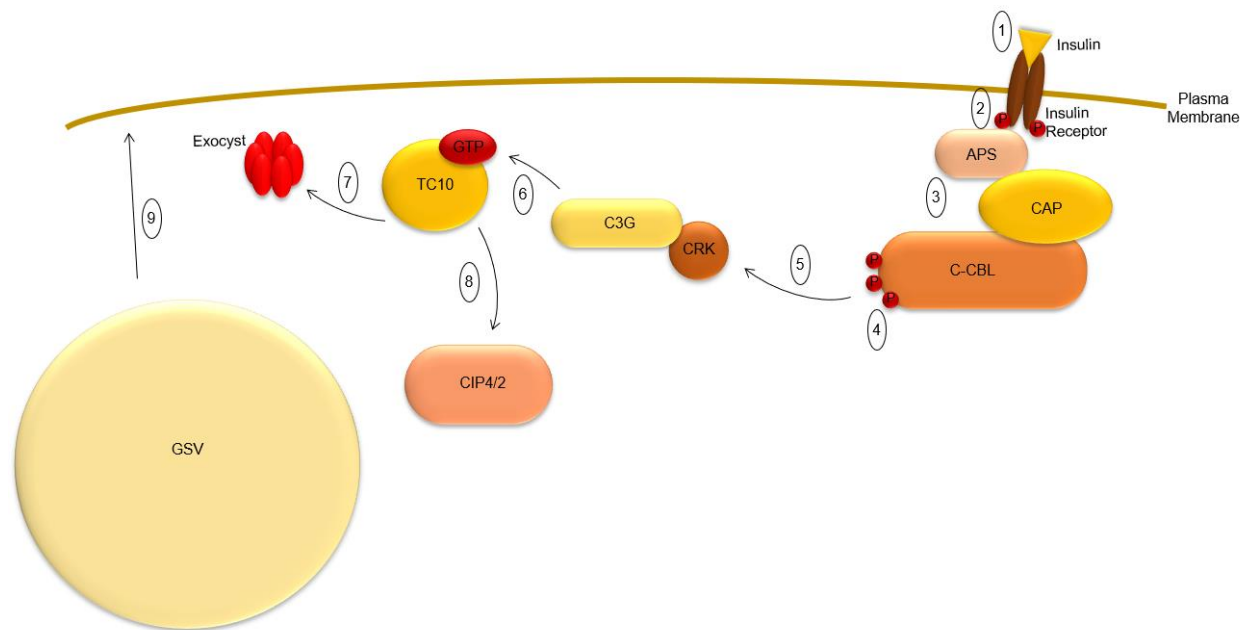
surface in response to insulin stimulation (Kandror & Pilch, 1996). About 50 % of total TfR and 10 - 15 % of total M6PR is associated with GSVs in adipocytes. It was hypothesised that they recycle in GSVs to fulfil general nutritional requirements of the cell during insulin stimulation (Kandror & Pilch, 1996). More recently it has been suggested that these proteins are not actively sorted into GSVs but rather end up there “by chance” because they share the same donor membrane (recycling endosome and/or TGN) (Kandror & Pilch, 2011).

## 1.5 Insulin Signalling

Since this work has been mostly carried out in adipocytes, the following section will concentrate on insulin signalling leading to GLUT4 translocation and omit the signalling pathways that are mediated by muscle contraction.

The insulin receptor is located in the plasma membrane and consists of two subunits  $\alpha$  and  $\beta$ . The  $\alpha$  domain is located extracellularly and binds insulin, while the intracellular  $\beta$  domain has tyrosine kinase activity. When insulin binds to the  $\alpha$  subunit of the receptor, this leads to autophosphorylation of a tyrosine residue in the  $\beta$  subunit (Kasuga et al., 1982; Shia & Pilch, 1983). Autophosphorylation initiates two different signalling cascades: the adaptor protein with pleckstrin homology and Src homology 2 domains (APSH) pathway and the phosphoinositide 3-kinase (PI3K) pathway.

### 1.5.1 The APS Pathway



**Figure 1.4 Schematic of the APS Pathway**

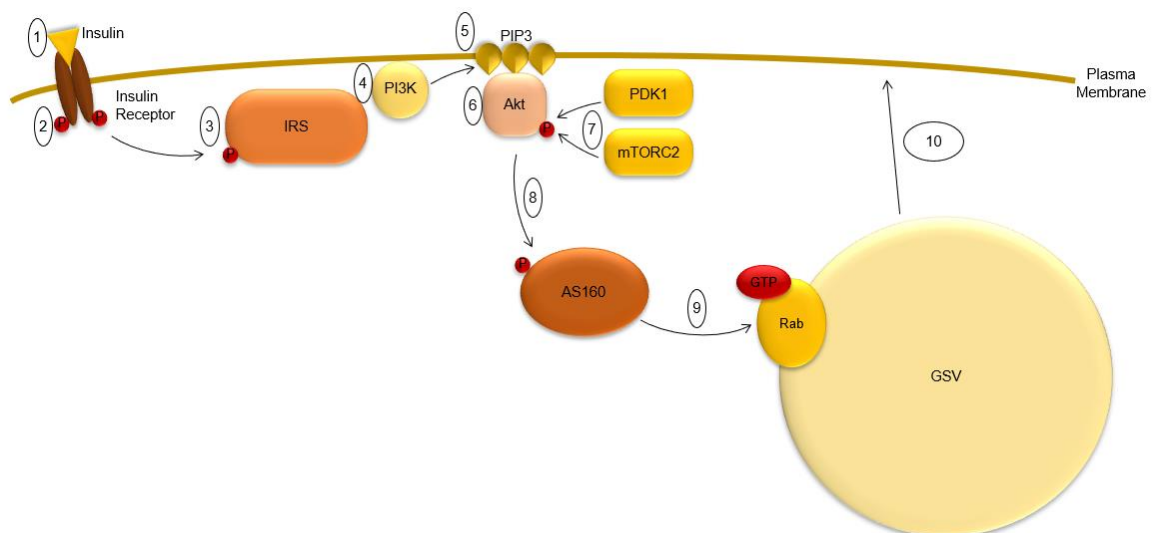
(1) Insulin binds to its receptor (2) Autophosphorylation of the insulin receptor (3) Recruitment of APS, CAP, and c-CBL (4) Phosphorylation of c-CBL (5) Recruitment of C3G and CRK (6) Activation of TC10 (7) Interaction with exocyst subunit (enabling exocytosis) (8) Interaction with CIP4/2 (inhibiting GSV retention) (9) GSV translocation and exocytosis. (Saltiel & Kahn, 2001)

Autophosphorylation of the insulin receptor leads to the recruitment of APS, the proto-oncogene c-CBL and c-CBL-associated protein (CAP). C-CBL is then phosphorylated on three different tyrosines by the insulin receptor (Liu et al., 2002). Activated c-CBL recruits a complex of CRK and C3G (Ribon et al., 1996) which in turn leads to the activation of the GTPase TC10. The active form of TC10 interacts with CIP4/2, which is involved in GSV retention (Chang et al., 2002). It also interacts with EXO70, a subunit of the exocyst, which plays a role in the exocytosis of vesicles (Leto & Saltiel, 2012).

### 1.5.2 The PI3K Pathway

The second pathway initiated by binding of insulin to its receptor is the PI3K pathway. Autophosphorylation of the insulin receptor is followed by phosphorylation of several insulin receptor substrates (IRS). IRS1 and IRS2 are the most common IRS in fat cells (White, 2002). IRS do not have any inherent enzymatic activity, but enable the recruitment of other proteins, such as PI3K, to the membrane (Sun et al., 1991). The PI3K family consists of various structurally related enzymes that are divided into four subgroups based on the

structure of their catalytic subunits and substrate specificity (Leevers et al., 1999). The activation of PI3K has multiple consequences that are not yet all known. An obvious effect is the phosphorylation of phosphoinositides (PIs), which generates PI-3,4,5-triphosphate (PIP3) (Saltiel & Kahn, 2001). The serine/threonine kinase Akt, also known as protein kinase B (PKB) is downstream off PI3K and is an important regulator of glucose uptake (Kohn et al., 1996). It binds to PIP3 at the plasma membrane via the pleckstrin homology domain at its N-terminus and is phosphorylated by phosphoinositide-dependent kinase 1 (PDK1) and mTOR complex2 (mTORC2) (Stephens et al., 1998). The Rab GTPase-activating protein (GAP) AS160 (Akt substrate of 160 kDa) is one of the many substrates of phosphorylated Akt (Kane et al., 2002). Rab proteins are GTPases that are associated with membrane trafficking, they switch between an active form (GTP loaded) and an inactive form (GDP loaded) (Zerial & McBride, 2001). Phosphorylation of AS160 inhibits its GAP activity, which activates the GSV associated Rab proteins and allows translocation of GSVs to the plasma membrane (Manning & Toker, 2007; Zeigerer et al., 2002). This process is likely linked to the fact that AS160 is associated with IRAP in the membrane of GSVs in the basal state but separates after insulin stimulation.



**Figure 1.5 Schematic of the PI3K Pathway.**

(1) Insulin binds to its receptor (2) Autophosphorylation of the insulin receptor (3) Phosphorylation of several insulin receptor substrates (4) Activation of PI3K (5) Production of PIP3 in the plasma membrane (6) Recruitment of Akt to the plasma membrane (7) Phosphorylation of Akt by PDK1 and mTORC2 (8) Phosphorylation of AS160 (9) Activation of GSV associated Rab proteins (10) Translocation of GSVs to the plasma membrane (Bryant et al., 2002; Saltiel & Kahn, 2001; Shepherd & Kahn, 1999).

Knock-down of AS160 in adipocytes indeed leads to GLUT4 translocation even under basal conditions (Larance et al., 2005) and overexpression of a dominant-negative mutated form of AS160 in which each of the phosphorylation sites are mutated, hinders GLUT4 translocation (Sano et al., 2003). The signalling pathways associated with insulin-mediated GLUT4 translocation to the plasma membrane are not yet fully resolved and are far more complex than outlined in this chapter (Bryant et al., 2002; S. Huang & Czech, 2007; Tavaré et al., 2001). Figure 1.5 shows a simplified representation as described here.

Funaki *et al.* found that the PI-binding peptide (PBP10) can induce GLUT4 translocation to the plasma membrane but does not affect glucose uptake, indicating that insulin stimulation has these two different effects. Pre-treatment of 3T3 L1 adipocytes with PBP10 before insulin stimulation showed that the insulin response was faster than without PBP10 pre-treatment. Thus, activation of GLUT4 for glucose uptake by insulin must happen while the transporter is already in the membrane. Both, the translocation and activation of GLUT4 involve PI3K (Funaki et al., 2004).

## 1.6 GLUT4 Trafficking Proteins

The cargo of GSVs was discussed in chapter 1.4.2, but there are other proteins associated with GSVs that enable translocation and fusion with membranes.

### 1.6.1 Rab Proteins

Rab proteins are monomeric small GTPases that are involved in most, if not all steps of intracellular vesicle transport. They play an important role in the tethering/docking and fusion of vesicles with acceptor membranes but are also implicated in the budding off donor membranes and transport along the cytoskeleton. Their intracellular location is very specific and different Rab proteins are linked to different organelles. Some Rab proteins even show cell- or tissue-specificity (Zerial & McBride, 2001). Subcellular membrane fractionation and immunopurification studies have revealed a number of Rab proteins that are associated with the GSC or GSVs, among them are Rab2A, Rab3A, Rab8A, Rab10, Rab11, and Rab14 (Koumanov et al., 2015; Larance et al., 2005; Mîinea et al., 2005).

Rab10 is thought to be the key Rab protein for GSV translocation (Sadacca et al., 2013; Sano et al., 2007). It is a downstream target of AS160, which has a Rab GAP domain. Rab GAPs interact with Rabs and trigger their GTPase activity, thus increasing the proportion of inactive GDP-bound Rab proteins (Zerial & McBride, 2001). In the basal state, AS160 is active, which leads to the inactivation of the associated Rab and consequently retention of GSVs (Kane et al., 2002).

Expression of mutated Rab10 that lacks the ability to hydrolyse GTP to GDP, leads to increased levels of GLUT4 in the plasma membrane. Knock-down inhibits insulin-induced translocation (Sano et al., 2007).

Using total internal reflection fluorescence (TIRF) microscopy (TIRFM), Chen *et al.* developed an assay that allowed them to link the different Rabs to specific steps in insulin-mediated GLUT4 trafficking. They visualised GSVs in the TIRF zone using mCherry-tagged GLUT4 and determined the colocalisation with GFP-tagged Rabs. In the basal state Rab4A, Rab4B, Rab14, and Rab8A colocalised with GLUT4 to a high degree. Interestingly, Rab10 showed only little colocalisation under basal conditions (Yu Chen et al., 2012). To distinguish between GSVs close to the membrane and fusing GSVs, they tagged IRAP with the pH-sensitive fluorescent protein pHluorin. Within the acidic environment of the GSVs the fluorescence of pHluorin is quenched. Upon fusing with the membrane, the protein comes into contact with the neutral pH of the medium, which turns on fluorescence (Yu Chen & Lippincott-Schwartz, 2015; Jiang et al., 2008). After insulin stimulation >90 % of the fusion events they observed colocalised with Rab10, while Rab4A and Rab4B did not. This result led to the hypothesis that Rab10 is a mediator of GSV fusion, while Rab4A and Rab4B are involved in GLUT4 recycling with the early endosome. Rab14 showed moderate association with fusing vesicles but little overlap with Rab10. Further investigation revealed that Rab14 is indeed present in endosomal vesicles and thus probably associated with the recycling of GSVs within the endosomal cycle (Yu Chen et al., 2012). Rab10 in its active GTP-form was also found to be associated with the exocyst subunits Exoc6 and Exoc6b (Sano et al., 2015).

In a study investigating GTP loading of Rabs in response to insulin in primary rat adipocytes, Rab3A was found to play a role in GLUT4 translocation. Rab3A is inhibited by Noc2 and insulin-mediated loading of Rab3 with GTP disrupts this

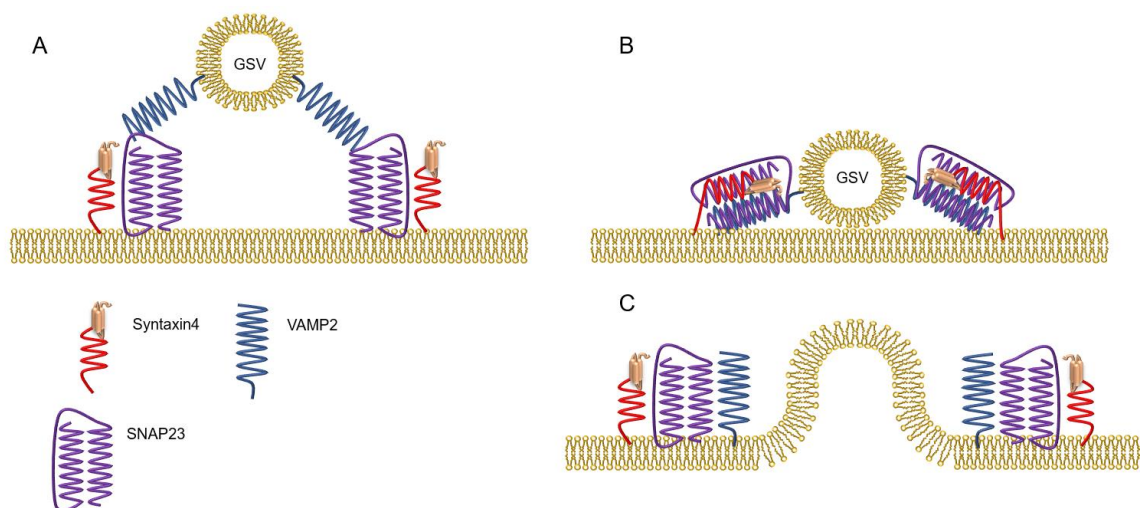
complex, allowing translocation of GSVs to the plasma membrane (Koumanov et al., 2015). The number of Rabs colocalising with GSVs may be even higher, as GSV trafficking is comprised of many different steps, that may be regulated by different Rabs.

## 1.6.2 SNARE and SM Proteins

Most membranes in eukaryotic cells consist of phospholipid bilayers. Water molecules arrange themselves around the hydrophilic head groups and are difficult to separate, which makes two membranes repel each other. To overcome this hydration repulsion and enable fusion, it requires the membranes to be in very close proximity to each other. This is mediated by SNARE (soluble *N*-ethylmaleimide sensitive fusion protein attachment protein receptor) proteins. This family consists of syntaxins, vesicle-associated membrane proteins (VAMPs), and synaptosome-associated proteins (SNAPs) (Malsam et al., 2008). SNAP25 is not to be confused with soluble NSF attachment proteins (SNAPs) also termed *N*-ethylmaleimide-sensitive factor Attachment Protein Alpha (NAPA), which recruit NSF to the membrane

### 1.6.2.1 The SNARE Complex

SNAREs are anchored to their membrane via their C-terminus or in the case of SNAPs by palmitoylation and can be divided into two groups, depending on their location: v-(vesicle)-SNAREs and t-(target)-SNAREs (Malsam et al., 2008). They contain a ~60 amino acid sequence made up of heptads, the SNARE motif (Laidlaw et al., 2017). When a v- and a t-SNARE come into close proximity to each other they form the SNARE complex, a tight alpha helical bundle consisting of four helices, one each from VAMP and syntaxin, two from SNAP. The side chains of the amino acids in the SNARE domains interact with each other and form hydrophobic layers (Sutton et al., 1998). The formation of a SNARE complex from these components is energetically favourable, as this occurs spontaneously *in vitro*. These experiments have also shown that SNARE complexes are not only necessary but also sufficient for vesicle fusion with a target membrane (Weber et al., 1998). The SNARE hypothesis postulates that the specificity of fusion events is derived from the pairing of a v-SNARE with its cognate t-SNARE (Söllner, Bennett, et al., 1993; Söllner, Whiteheart, et al., 1993).



**Figure 1.6 Formation of the SNARE Complex and Vesicle Fusion**

A: GSV containing the v-SNARE VAMP2 approaches the plasma membrane with embedded t-SNAREs syntaxin4 and SNAP23 B: SNAREs form the SNARE complex and zipper up, bringing the vesicle and plasma membrane into close proximity to each other C: Vesicle fusion and disassembly of the complex using energy provided by ATPase (Y. A. Chen & Scheller, 2001).

The zipping up of the complex is thought to provide the energy that brings the two membranes close together, overcoming hydration repulsion, and thus allowing fusion. Figure 1.6 demonstrates this process.

The key t-SNAREs involved in GSV fusion with the plasma membrane are syntaxin4 and SNAP23. Knock-down of either of these proteins results in inhibition of vesicle tethering to the membrane. Knock-down of the v-SNARE VAMP2 on the other hand does not interfere with the tethering process but inhibits vesicle fusion (Kawaguchi et al., 2010; Kioumourtzoglou, Sadler, et al., 2014).

Other SNAREs are involved in intracellular GSV trafficking, which will be expanded on in more detail in Chapter 6.

### 1.6.2.2 VAMPs

VAMPs 2, 3, 4, 5, 7, and 8 are all expressed in 3T3 L1 fibroblasts, but they are selectively up-regulated during differentiation into adipocytes, which indicates a role in insulin-sensitivity (Larance et al., 2005; Sadler et al., 2014; Volchuk et al., 1995). Levels of VAMP 2, 3, and 4 increase significantly, while VAMPs 5, 7, and 8 remain unchanged. Subcellular fractionation showed that VAMPs 2, 5, and 8 are present in both GSVs and recycling endosomes, while VAMPs 3,4, and 7 are

mostly found in recycling endosomes. Insulin stimulation leads to an increase of VAMP2 and 3 in the plasma membrane, suggesting that these two VAMPs are present in GSVs and are involved in GSV fusion with the plasma membrane (Cheatham et al., 1996; Sadler et al., 2014). It is thought that VAMP2 is the v-SNARE that mediates membrane fusion, since depletion of the protein inhibits GLUT4 translocation and glucose uptake (Bryant & Gould, 2011). On the other hand, *in vitro* experiments have shown that all VAMPs can form SNARE complexes with syntaxin4 and SNAP23 (Sadler et al., 2014). Suggesting that VAMPs can be redundant, it was found that when inhibiting GSV fusion by disruption of the VAMPs 2, 3, and 8, insulin sensitivity could be restored by either of these VAMPs (Zhao et al., 2009).

Contradictory, other studies found that VAMP2 depletion alone can impair GSV translocation (L. B. Martin et al., 1998) and, more specifically, fusion (Kawaguchi et al., 2010). Moreover, while both, VAMP2 and VAMP3 translocate to the plasma membrane in response to insulin, VAMP2 is more abundant in GSVs and it also co-precipitates with syntaxin4 in immunoprecipitation experiments, while VAMP3 does not (Sadler et al., 2014). These studies indicate, that VAMP2 plays a major role in GLUT4 exocytosis.

### 1.6.2.3 SM Proteins

Sec1/Munc18 (SM) proteins are known to control the assembly of SNARE complexes (Toonen & Verhage, 2003). Adipocytes express two Munc18 homologues: Munc18b and c, while Munc18a is neuronal specific and not found in fat cells (Tellam et al., 1995). While Munc18a and b have been shown to bind to syntaxins 1A, 2, and 3 in *in vitro* binding assays, only Munc18c binds to syntaxin4. In addition, both proteins translocate to the plasma membrane from intracellular membranes in response to insulin in 3T3 L1 adipocytes, as assessed by subcellular fractionation (Tellam et al., 1997). Munc18c is an arch-shaped protein that can bind to the regulatory domain H<sub>abc</sub> of syntaxin4. The H<sub>abc</sub> domain binds to the SNARE motif of the syntaxin, which inhibits SNARE complex assembly. The arch-shape of the SM protein holds the syntaxin in this closed conformation (Bracher & Weissenhorn, 2002). The relationship between SNAREs and SM proteins is however more complicated than this, as there are different



modes of interaction, which can in fact enable fusion of vesicles with target membranes (Laidlaw et al., 2017).

Using the microscopy-based proximity ligation assay, Kioumourtzoglou *et al.* found that insulin does indeed facilitate the formation of SNARE complexes containing syntaxin4, SNAP23, VAMP2, as well as the SM protein Munc18c in 3T3 L1 adipocytes. Tyrosin phosphorylation of Munc18c on Tyr<sub>521</sub> allows SNARE complex assembly *in vitro* and this residue is also a direct target of the insulin receptor (Jewell et al., 2011; Schmelzle et al., 2006). This data has led to the hypothesis that phosphorylation of Munc18c in response to an insulin stimulus enables SNARE complex formation and thus allows GSV fusion with the membrane (Kioumourtzoglou, Gould, et al., 2014).

### 1.6.3 Translocation of GSVs Along Filaments and Microtubules

Using high-speed microscopy, Patki *et al.* were the first to live image individual cells expressing GLUT4-GFP under the influence of insulin. Within six minutes of insulin stimulation, individual GSVs can be observed to translocate from the perinuclear region of 3T3 L1 adipocytes towards the plasma membrane with a speed of 0.180 to 0.707  $\mu\text{m s}^{-1}$ . This movement is enabled by the interaction with both, actin and the microtubulin network, since disruption of either inhibits translocation as well as intracellular compartmentalisation (Patki et al., 2001). When treated with nocodazole, a potent drug that disrupts microtubulin filaments, 3T3 L1 adipocytes do not show the typical distribution of GLUT4 in the basal state that includes concentration around the nucleus. Instead, GLUT4 is homogenously distributed in the cytoplasm (J. Huang et al., 2005; Karylowski et al., 2004). Another effect of the drug is diminished glucose uptake in response to insulin. Similarly, the addition of the actin-depolymerising toxin Lat-A stops all movement of GLUT4 within 3T3 L1 adipocytes, resulting in accumulation of the transporter in the juxtannuclear region and also inhibits glucose uptake. On the base of their findings, Patki *et al.* hypothesised that actin enables the interaction of GSVs with microtubules, thus allowing GSV translocation, and that insulin stimulation supports this interaction (Patki et al., 2001). This and other studies found that microtubules are necessary for insulin induced GSV translocation (J. Huang et al., 2005; Karylowski et al., 2004; Molero et al., 2001). The entire process, however, is clearly not regulated by microtubules

alone. Stabilisation of microtubules has no increasing effect on GSV translocation in the absence of insulin (Molero et al., 2001).

In fact, microtubules at the membrane appear to be involved in GSV fusion itself and not only transport to the membrane as microtubule density near the plasma membrane increases with insulin stimulation and fusion events colocalise with microtubules. This colocalisation is not due to previous transport of the GSV along microtubules (Dawicki-McKenna et al., 2012).

Studying isolated rat adipocytes via TIRFM, Lizunov *et al.* found that GSVs are indeed moving rapidly along microtubules close to the plasma membrane, but this movement is decelerated significantly after addition of insulin when GSVs are tethered to the membrane in preparation for fusion (Lizunov et al., 2005). These results illustrate the important role that the cytoskeleton plays in the insulin-induced translocation of GSVs. Particularly microtubules are involved in GSV trafficking near the membrane, how exactly insulin stimulation inhibits these movements remains to be discovered.

## 1.7 GLUT4 in the Plasma Membrane

While GLUT4 signalling pathways have been studied extensively since the discovery of the transporter, its dynamics within the plasma membrane have been mostly neglected, which has been due to the lack of a suitable experimental setup to study exocytosed GLUT4. Classical biochemical approaches do not or only partially allow differentiation between intracellular and plasma membrane GLUT4. The discovery of the green fluorescent protein (GFP) and the ability to express it in living organisms opened up new ways for the study of all kinds of proteins (C. Martin et al., 1994; Shimomura et al., 1962). Enhanced GFP (eGFP) is a variant of GFP (Cormack et al., 1996). Two years after GFP had first been expressed in *Escherichia coli* (*E.coli*) by Martin *et al.* (C. Martin et al., 1994), Dobson *et al.* used the back then revolutionary technology to express the fusion protein GLUT4-GFP in CHO cells, thus allowing visualisation of GLUT4 in single cells. For the first time, GLUT4 translocation to the plasma membrane upon insulin stimulation was observed (Dobson et al., 1996). Shortly afterwards the same group managed to express their construct in 3T3 L1 adipocytes (Powell et al., 1999).

By inserting a haemagglutinin (HA) tag into the first exofacial loop of GLUT4-GFP and visualise this by non-permeable immunofluorescent surface staining, it was furthermore possible to distinguish between intracellular GLUT4 and GLUT4 that had been inserted into the plasma membrane (Dawson et al., 2001), making HA-GLUT4-GFP the most commonly used genetically modified variant of GLUT4. Engineering of GLUT4-GFP and later HA-GLUT4-GFP lay the foundation for most of the work that involves GLUT4 and fluorescence microscopy.

The development of light microscopy techniques such as TIRFM and super-resolution microscopy allowed to characterise GLUT4 in the plasma membrane. This field is still very young and the key studies that will be described in more detail in this section are summarised in Table 1.1.

**Table 1.1 Studies on GLUT4 in the Plasma Membrane**

Studies used Total Reflection Fluorescence Microscopy (TIRFM), Fluorescence Photoactivation Localisation Microscopy (FPALM), and direct Stochastic Optical Reconstruction Microscopy (dSTORM)

Study	Microscopy Method and Main Probe	Cell System	Key findings
Li <i>et al.</i> 2004	TIRFM GLUT4-EGFP	3T3 L1 adipocytes	Movement of GLUT4 in the membrane is restricted
Lizunov <i>et al.</i> 2005	TIRFM HA-GLUT4-GFP	Rat adipocytes	Insulin induces vesicle tethering to the membrane
Huang <i>et al.</i> 2007	TIRFM GLUT4-EGFP	3T3 L1 adipocytes	GLUT4 colocalises with clathrin in the membrane
Bai <i>et al.</i> 2007	TIRFM GLUT4-EGFP	3T3 L1 adipocytes	Insulin regulates the fusion of GSVs with the membrane
Jiang <i>et al.</i> 2008	TIRFM TDimer2-IRAP-pHluorin	3T3 L1 adipocytes	Some fusion events are of the kiss-and-run type
Stenkula <i>et al.</i> 2010	TIRFM IRAP-pHluorin	Rat adipocytes	Insulin induces dispersal of GLUT4 in the membrane
Xu <i>et al.</i> 2011	TIRFM VAMP2-pHluorin	3T3 L1 adipocytes	Insulin stimulation decreases the number of kiss-and-run events
Lizunov, Lee <i>et al.</i> 2013	TIRFM HA-GLUT4-GFP	Human adipocytes	Insulin resistance in humans results in impaired GSV tethering
Lizunov, Stenkula <i>et al.</i> 2013	FPALM HA-GLUT4-EOS	Rat adipocytes	Further characterisation of GLUT4 clusters. Eliminating some possible clustering mechanisms, such as clathrin
Gao <i>et al.</i> 2017	dSTORM HA-GLUT4-GFP	3T3 L1 adipocytes	Insulin-induced dispersal of GLUT4 is impaired in insulin-resistance

### 1.7.1 GSVs in the TIRF Zone

TIRFM has been a valuable tool in the study of GLUT4 near the plasma membrane. The evanescent wave that is formed when the laser beam is totally reflected off the glass coverslip illuminates only the plasma membrane and a thin layer of cytosol adjacent to the coverslip, allowing the examination of fluorescent labelled proteins less than 100 nm away from the membrane while fluorescence of intracellularly located proteins does not disturb the image (Axelrod, 2001a; Mattheyses et al., 2010). The principles of TIRFM are described in more detail in Chapter 3.

Li *et al.* were the first to employ TIRFM to track single GSVs near the plasma membrane and study their mobility and dynamics. Another characteristic of the evanescent wave generated in TIRFM is that it is exponentially decreasing with the distance from the coverslip (Axelrod, 2001a). This means that a GSV containing GFP-tagged GLUT4 can be seen approaching by its increasing fluorescence (C. H. Li et al., 2004). Li *et al.* used this attribute to study the vertical movement of GSVs. They found that most GSVs move up and down in the TIRF zone repeatedly, which indicates that they are not docked to the plasma membrane. Laterally, GSVs moved in a constrained or caged fashion, usually not more than 100 nm away from their initial site, indicating some sort of tethering (C. H. Li et al., 2004).

Under basal conditions, GSVs can be seen moving near the plasma membrane in the manner previously described. A lot of this movement is along trajectories that are likely related to the microtubule network. One study found that insulin stimulation reduced this movement by a factor of 8, which is due to the immobilisation of GSVs to the membrane. Immobilised vesicles also “wriggle” to a lesser degree in the presence of insulin than they do in the basal state (Lizunov et al., 2005).

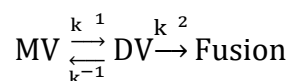
With TIRF microscopy, it was possible to investigate processes happening directly at the plasma membrane in response to an insulin stimulus. Specifically, the docking and fusion of GSVs could be examined more closely and differences between the basal and insulin stimulated state could be observed on a much more resolved level.

### 1.7.2 GLUT4 Clustering in Response to Insulin

In their first TIRFM experiments, Lizunov *et al.* noticed that insulin stimulation leads to immobilisation of GLUT4 in the plasma membrane. While the distribution is relatively homogenous in the basal state, insulin stimulation results in accumulation of glucose transporters in specific areas of the membrane (Lizunov *et al.*, 2005). This immobilisation could be due to two reasons: Tethering of GSVs in these regions prior to fusion as suggested by Lizunov *et al.* or the movement of GLUT4 into relatively static regions within the plasma membrane. Clathrin has been shown to localise to mostly immobile domains within the plasma membrane (Bellve *et al.*, 2006) and GLUT4 indeed colocalises with these static patches after insulin stimulation but to a much lesser degree in the basal state (S. Huang *et al.*, 2007). Contradicting this finding, more recent data using surface staining has revealed that most of the GLUT4 that colocalises with clathrin is found in close proximity to the membrane but is not actually exocytosed. Instead, clathrin is probably involved in the endocytosis of existing GLUT4 clusters (Stenkula *et al.*, 2010).

### 1.7.3 Tethering and Fusion of GSVs with the Plasma Membrane

The single steps that happen at the plasma membrane are thought to be reversible docking and fusion of the vesicle (Bai *et al.*, 2007). When imaging GLUT4-GFP expressing adipocytes in TIRF, a docking event is characterised by a fluorescent spot, the GSV, approaching the membrane and then remaining static for a defined period. After docking the fluorescence can disperse in the field of view, which signifies fusion of the vesicle. In other cases, the fluorescence decreases again, meaning that the vesicle has undocked. Bai *et al.* described this behaviour with the following reaction scheme:



According to this scheme, moving vesicles (MV) are mobile fluorescent GSVs within the TIRF zone. They dock to the membrane with the docking rate  $k^1$  and become docked vesicles (DV). From this state they can either undergo fusion with the fusion rate  $k^2$  or they undock again with the undocking rate  $k^{-1}$ . Kinetic analysis of these steps revealed that insulin increases the fusion rate by

approximately 8-fold, but the docking rate only about 2-fold. The time the vesicles remained in the docked state, the mean dwell time, decreased by about 30 %. The docking step appears to be regulated by PI3K, since treatment with the PI3K inhibitor Wortmannin reduces the docking rate significantly. In conclusion, insulin stimulates mainly the fusion of vesicles with the membrane and there may be an insulin-regulated priming step after docking that prepares the GSVs for fusion (Bai et al., 2007).

Fusion of other GSV specific proteins such as IRAP and VAMP2 with the pH sensitive fluorescent protein pHluorin offered the opportunity to witness fusion events of GSVs with the membrane based on the protein's fluorescent properties (Ashby et al., 2004). If fused with the C-terminus of IRAP or VAMP2, pHluorin is located inside the GSV where the pH is acidic. Fusion of the GSV with the plasma membrane exposes the protein to the neutral pH of the extracellular culture medium, which activates fluorescence (Yu Chen & Lippincott-Schwartz, 2015; Jiang et al., 2008). Using pHluorin tagged GSV proteins is a very elegant way to visualise fusion. Fusion events are much easier to witness by a sudden increase in fluorescence than by simply observing a spreading of fluorescence as Bai *et al.* did. It is also less ambiguous whether a vesicle is indeed fused with the membrane or only docked to it.

Jiang *et al.* used the unique properties of IRAP-pHluorin and engineered the fusion protein further by adding the red fluorescent protein Tdimer2 to its N-terminus. With the help of this construct and dual-colour TIRFM they could observe the docking and fusion of GSVs in real time and reported that some of the fusion events were of the “kiss-and-run” type, meaning that the vesicles fused briefly with the membrane to be endocytosed again shortly after. According to their observations, 15 % of fusion events in the basal state were of the kiss-and-run type. By expressing a mutated form of AS160 in adipocytes, the four times phosphorylated AS160-4P, they found out that this leads to the inhibition of insulin stimulated GSV docking, indicating that AS160 is crucial for the docking, but not the fusion of GSVs (Jiang et al., 2008).

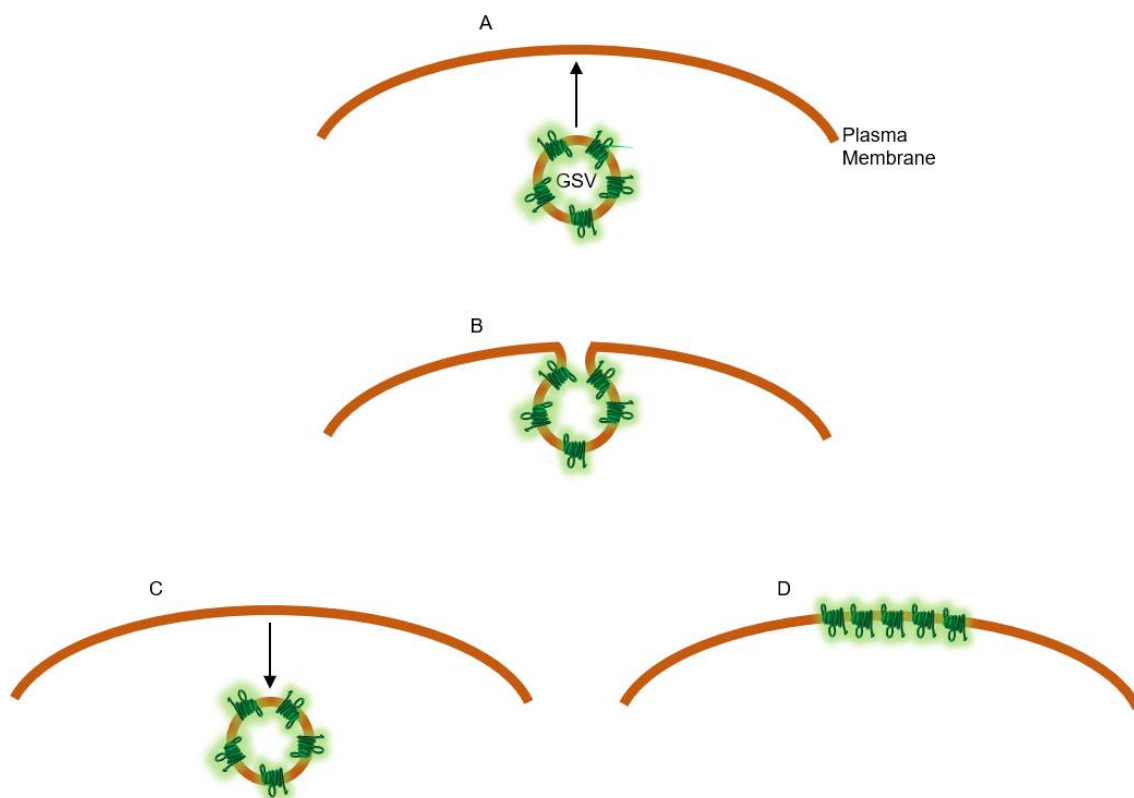
Using a similar probe, VAMP2-pHluorin, Xu *et al.* also reported kiss-and-run events. In contrast to the findings of Jiang *et al.*, with almost 40 % of fusion events they found them to be very common in unstimulated cells. This number

dropped to about 5 % after insulin stimulation. Disruption of the phospholipase D1 (PLD) increased the number of kiss-and-run events in both the basal and the insulin-stimulated state. In another experiment they quantified fusion events further by determining the duration between docking and fusion. This fusion pore duration was significantly shorter in insulin stimulated cells than in basal cells. They concluded that insulin must lower the energy barrier for full fusion after vesicle pore formation, possibly in correlation with PLD. Thus, insulin not only regulates GSV translocation to the plasma membrane, but it also appears to have a direct effect at the fusion pore itself (Y. Xu et al., 2011).

Figure 1.7 shows the process of vesicle fusion schematically. When the GSV approaches the plasma membrane (A) it can dock, and a fusion pore opens up (B). From here, there are two possibilities: the fusion pore can either close again and the vesicle undocks in a kiss-and-run like fashion (C), this is more likely in the basal state. During insulin stimulation the likelihood of the vesicle fusing entirely is increased, allowing dispersal of GLUT4 in the membrane (D).

Defective tethering of GSVs has been linked to type 2 diabetes (Lizunov, Lee, et al., 2013). Human adipocytes from subjects with varying systemic insulin sensitivity and body mass index (BMI) were transfected with fluorescently tagged GLUT4 and observed via TIRFM in the basal state and after insulin stimulation. Interestingly, cells from all subjects behaved the same under basal conditions, whether they were derived from lean, obese, insulin-sensitive, or insulin-resistant subjects. GSVs all translocated, tethered, and fused in the same manner, indicating that the machinery that is required for basal GSV trafficking is not affected by either BMI or insulin-sensitivity. Insulin-stimulated GLUT4 translocation, however, was significantly impaired in insulin-resistant subjects. Surface staining of GLUT4 revealed that there was less total GLUT4 present in the plasma membrane after insulin stimulation at low systemic insulin-sensitivity. This is due to fewer fusion events as a result of impaired vesicle tethering. BMI alone did not have such drastic effect (Lizunov, Lee, et al., 2013).





**Figure 1.7 Fusion of GSV with the Plasma Membrane**

A: A GSV is approaching the membrane. B: Docking of the vesicle and opening of the fusion pore. C: Retreat of the GSV in a kiss-and-run like fashion D: Full vesicle fusion with the membrane

### 1.7.4 GLUT4 Clustering and Dispersal

Although insulin has been shown to regulate many steps from GLUT4 recycling to translocation to the membrane, it is now thought that it has a major effect on the distribution of GLUT4 in the plasma membrane itself. Stenkula *et al.* delivered evidence for this when they reported that in the basal state GLUT4 can be mostly found in clusters, whereas insulin stimulation leads to a much more dispersed distribution of the transporter. Importantly, this is not an artefact of fixation or labelling. What exactly mediates the formation of clusters and their dispersal remains unknown, but it has been shown that they are associated with neither caveola, nor clathrin (Stenkula *et al.*, 2010). The latter however is involved in the endocytosis of pre-existing clusters particularly in the basal state. In terms of exocytosis, Stenkula *et al.* described two different modes: fusion-with-retention (previously referred to as kiss-and-run) and fusion-with-release. In the basal state 95 % of all fusion events were attributed to the fusion-with-retention type. Insulin stimulation then not only increased the overall fusion rate from 0.03 events/ $\mu\text{m}^2/\text{min}$  in the basal state to

0.15 events/ $\mu\text{m}^2/\text{min}$  after only 2 minutes, but it also led to a 60-fold increase of fusion-with-release events, while only having a very small effect on the number of fusion-with-retention events. This indicates that fusion-with-retention events form clusters of GLUT4 in the plasma membrane. The group developed a mathematical model that assumes that insulin only affects the dispersal of GLUT4 and assumes GLUT4 to be relatively constant in all other GLUT4 containing compartments in response to insulin. Remarkably, this model fits experimental data of number of fusion events over time very well. Based on their observations, Stenkula *et al.* proposed a new mode of insulin-regulated glucose uptake. In unstimulated cells GLUT4 is mostly found in clusters which can be readily re-endocytosed. Insulin-stimulation leads to a dispersal of these clusters and monomeric GLUT4 takes up glucose more efficiently (Stenkula *et al.*, 2010).

### **1.7.5 Single Molecule Imaging of GLUT4 in the Plasma Membrane**

Single molecule imaging had been used in the past to describe the trafficking kinetics of GLUT4 inside the cell (Fujita *et al.*, 2010; Hatakeyama & Kanzaki, 2011), but not to investigate the dynamics of GLUT4 in the plasma membrane.

Single molecule localisation microscopy (SMLM) is a form of light microscopy in which super-resolution is achieved by localising single molecules based on the centre of a fluorescent tag's point-spread function (Betzig *et al.*, 2006; Hess *et al.*, 2006; van de Linde, Löschberger, *et al.*, 2011). In short, structures of interest are labelled either externally with a fluorescently tagged antibody, or internally fused to a fluorescent protein. This fluorophore has the ability to switch between the dark and the light state, which results in blinking when excited. Blinking means that not all fluorophores are "switched on" at the same time, which makes it possible to detect single molecules in different frames (for a more detailed explanation refer to Chapter 5). Two SMLM techniques have been applied to address the clustering and dispersal of GLUT4: Fluorescence Photoactivation Localisation Microscopy (FPALM) (Lizunov, Stenkula, *et al.*, 2013) and Direct Stochastic Optical Reconstruction Microscopy (dSTORM) (Gao *et al.*, 2017).

In order to characterise the nature of GLUT4 clusters further, the same group that first reported them developed a GLUT4 variant tagged with a photoswitchable fluorophore: HA-GLUT4-EOS. This allowed the tracking of single GLUT4 molecules in live cells. Using the probe in FPALM, they found three different types of GLUT4 movement in the plasma membrane: directed motion, free lateral diffusion, and constrained diffusion within clusters. In the basal state, almost half of all trajectories were of the constrained diffusion type, this decreased to 27 % after insulin stimulation, while more than 70 % were freely diffusing in the membrane. This process is not ATP-dependent. Single molecules can enter and leave the clusters, but formation of new clusters from freely diffusing molecules was not observed. Interestingly, the rate at which single GLUT4 molecules leave clusters more than doubles with insulin stimulation. When imaging adipocytes expressing HA-GLUT4-EOS as well as IRAP-pHluorin, it becomes clear that cluster formation happens upon fusion of GSVs with the plasma membrane as the previously described fusion-with-retention events. The retention and subsequent cluster formation is specific for GLUT4, as IRAP diffuses after exocytosis and is not retained (Lizunov, Stenkula, et al., 2013).

Recently, dSTORM has been deployed to confirm the formation of GLUT4 clusters and their dispersal upon insulin stimulation in 3T3 L1 adipocytes (Gao et al., 2017). Compared to the basal state, insulin stimulated cells show more clusters, which is due to the higher GLUT4 concentration. However, the degree of clustering is clearly reduced, and the transporters tend to a more dispersed distribution. The cluster size itself is unchanged, but the proportion of GLUT4 molecules in small clusters is increased. This data strongly supports the hypothesis that insulin induces dispersal of GLUT4 in the cell membrane of adipocytes. When insulin-resistance is induced by incubation with insulin overnight, both insulin-resistant basal and insulin-resistant insulin-stimulated cells show a more clustered pattern. This is a ground-breaking revelation, as it indicates that GLUT4 cluster formation and dispersal is involved in the development of insulin-resistance and therefore diabetes.

The clustering appears to be linked to the N-terminal F<sup>5</sup>QQI motif of GLUT4, indicating that this region is involved in the maintenance of GLUT4 clusters.

Cells expressing a mutant of this motif exhibit less clustering than the wild-type, while size and shape of the clusters remains unaltered. (Gao et al., 2017).

To my knowledge, Lizunov *et al.* and Gao *et al.* are the only research groups that have investigated the clustering and dispersal of GLUT4 via SMLM. Both their studies deliver compelling evidence that insulin-sensitivity of adipocytes relies on the ability of GLUT4 to form clusters and disperse in the plasma membrane. The question remains how clusters are formed and maintained in the absence of insulin on a molecular basis.

### 1.7.6 Possible Mechanisms of GLUT4 Clustering

GLUT4 clusters appear to be elongated rather than round and have a diameter of approximately 90-170 nm, which does not change in the presence of insulin. The elongated shape of the clusters suggests that they are not maintained by cross-linked structures. Solid-phase domains can be excluded as a reason, as this would not allow mobility of single GLUT4 molecules within them, which is, however, the case. Nor are they dependent on lipid rafts, as disruption of cholesterol does not alter the cluster shape or size (Lizunov, Stenkula, et al., 2013). Contradicting this conclusion, Gao *et al.* find that disruption of cholesterol does indeed lead to loss of clusters. This could be explained by the higher methyl- $\beta$ -cyclodextrin concentration they used or by the fact that they conducted this experiment in cells expressing the mutated form of the F<sup>5</sup>QQI motif (Gao et al., 2017). This needs to be addressed further, however the lipid raft theory itself is heavily disputed amongst scientists (Shaw, 2006). It is likely that GLUT4 clusters form in the GSVs before fusion with the membrane and components retaining GLUT4 inside the clusters are present in GSVs but not necessarily at the plasma membrane. The elongated shape of the clusters could therefore also be explained by fusion of tubular-vesicular GSVs (Lizunov, Stenkula, et al., 2013).

The picket fence model was originally proposed to explain why the diffusion velocity is much slower in biological membranes than in artificial phospholipid bilayers. According to this model, membranes are compartmentalised, and regions are separated from each other by molecular “picket fences”. The pickets in these fences are proteins anchored to the actin cytoskeleton (Fujiwara et al.,

2002). It is conceivable that the clustering of GLUT4 is based on its confinement within a molecular picket fence, however, the disruption of actin structures does not lead to a change in cluster features (Lizunov, Stenkula, et al., 2013). This means that the fence around GLUT4 clusters must be maintained independently of the actin cytoskeleton. The idea of a protein structure corralling GLUT4 in the basal state is nevertheless plausible. The fact that IRAP can diffuse from newly formed clusters, but GLUT4 cannot (Lizunov, Stenkula, et al., 2013), excludes the classical picket-fence hypothesis, since this would not allow for diffusion of any proteins. Stenkula *et al.* instead proposed a slightly altered protein-specific confinement model. It is possible that GLUT4, but not IRAP, interacts directly with a component of the molecular picket-fence.

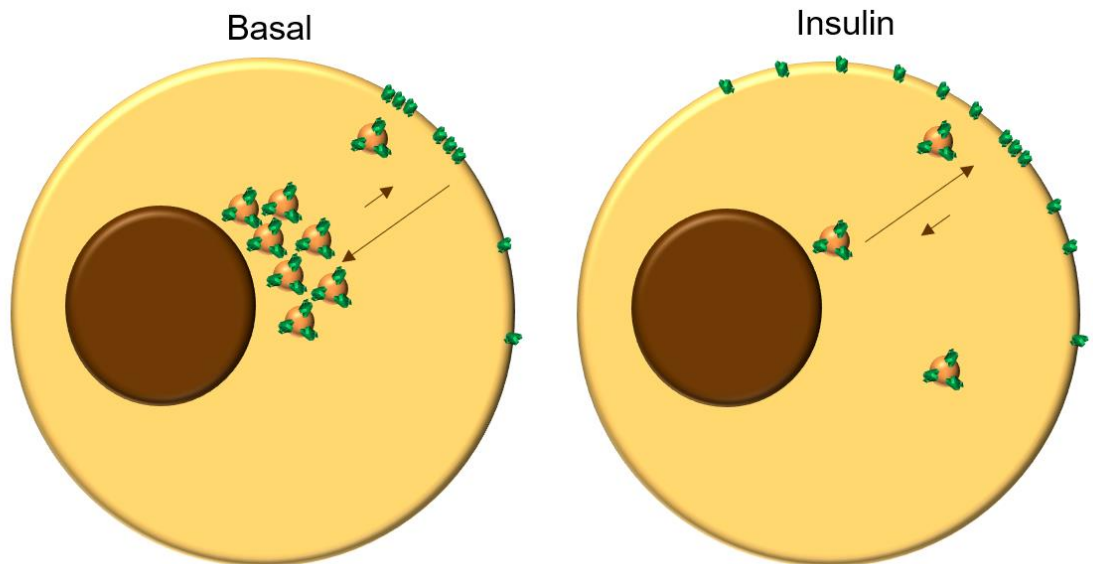
### 1.7.7 EFR3 and its Potential Role in GLUT4 Dispersal

A genetic screen of the yeast *Saccharomyces cerevisiae* has revealed a potential role of the protein EFR3 in the dynamics of GLUT4 in the plasma membrane (Wieczorke et al., 2003). EFR3 is a highly conserved membrane protein that has been shown to be involved in the formation of Stt4 phosphoinositide kinase (PIK) clusters in yeast. It binds to Ypp1, which binds to Stt4. This complex is held at the plasma membrane via palmitoylation of the N-terminus of EFR3 (Baird et al., 2008; Wu et al., 2014). The mammalian homologues of Ypp1 and Stt4, are TTC7 and phosphatidylinositol 4-kinase type III  $\alpha$  (PI4KIII $\alpha$ ) respectively (Nakatsu et al., 2012). In mammalian cells, another protein, FAM126A, is part of the PI4KIII $\alpha$  complex (Baskin et al., 2016). Phosphatidylinositols are glycerophospholipids that contain a *myo*-inositol head group, which can be phosphorylated or dephosphorylated at the 3', 4', and/or 5' hydroxyl group, allowing for diversity in signalling pathways (Falkenburger et al., 2010). When phosphorylated, phosphatidylinositols are referred to as phosphoinositides (PIs). The location of each PI is specific to a cellular membrane and their principal role is to interact with proteins that have a function in the respective membrane (Tan & Brill, 2014). PI3K for example can be found in the late endosome and plays an important role in insulin signalling as has been discussed in chapter 1.5. PI4K is predominantly found in the TGN but it is also part of GSVs (DeVecchio & Pilch, 1991) It catalyses the conversion of PI to phosphatidylinositol 4-phosphate (PI4P) and generates pools of this in the plasma membrane (Tan & Brill, 2014).

Recent studies in our laboratory have revealed that the homolog EFR3a plays a role in glucose uptake in 3T3 L1 adipocytes. It is localised at the plasma membrane and has a regulating effect on GLUT4. Overexpression of EFR3a leads to increased GLUT4 translocation and glucose uptake, which is probably due to its association with PI4KIII $\alpha$ . Inhibition of PI4KIII $\alpha$  with phenylarsine oxide (PAO) inhibits glucose uptake, indicating that PI4P is involved in the process. The subcellular localisation of PI4KIII $\alpha$  does not change in response to insulin, however, knock-down of PI4KIII $\alpha$  in 3T3 L1 adipocytes leads to a significant decrease in insulin-stimulated glucose uptake, indicating that insulin signalling leads to the activation of PI4KIII $\alpha$  and thus enabling glucose uptake via GLUT4 (Laidlaw, 2018).

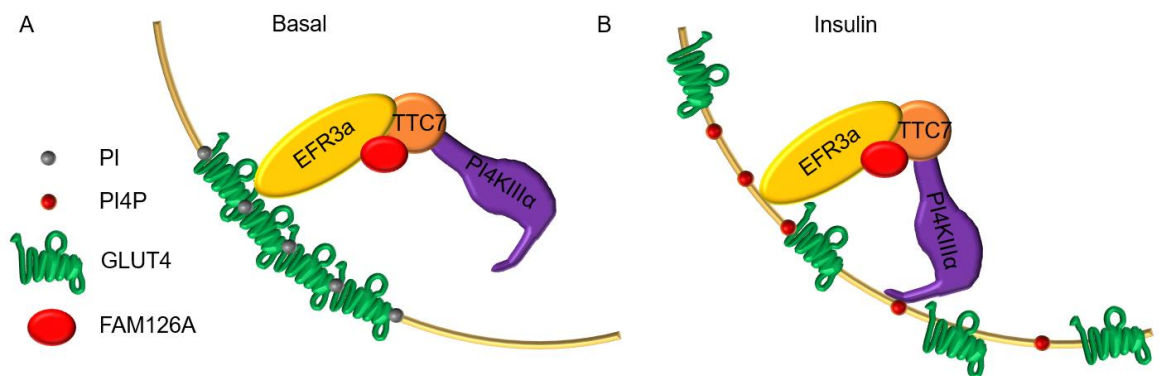
## 1.8 Working Hypothesis and Aims of this Study

Since the discovery of GLUT4 and its association with type 2 diabetes, research in the field has come a long way. Numerous effects insulin has on the glucose transporter and its associated signalling pathway have been found and analysed and the malfunction of either of them may or may not be involved in the development of the disease. There is still no cure for type 2 diabetes and therapies and medication mostly target the symptoms but not the underlying cause. During the previous years it has become clear that insulin has a considerable effect on GLUT4 translocation and specifically on its dynamics in the plasma membrane. In the basal state, GLUT4 can be found in clusters which can be readily endocytosed, which was observed as so-called kiss-and-run events. Insulin stimulation then leads to dispersal of the transporter and this is thought to facilitate glucose uptake. The exact mechanisms of these clustering and dispersal processes remain unclear but could provide a valuable drug target for the treatment of type 2 diabetes.



**Figure 1.8 Clustering and Dispersal of GLUT4 in Response to Insulin.**

In the basal state the majority of GSVs is located in the perinuclear region and GLUT4 in the plasma membrane is mostly clustered. Insulin stimulation leads to increased translocation of GSVs to the plasma membrane and dispersal of GLUT4.



**Figure 1.9 Schematic of the Working Hypothesis Involving EFR3a and PI4P.**

A: In the basal state PI4KIII $\alpha$  is inactive and GLUT4 is corralled in clusters by PI. B: Activation of PI4KIII $\alpha$  by mobilisation of EFR3a, TTC7, and FAM126A after insulin stimulation leads to phosphorylation of PI at the 4' position, resulting in the generation of PI4P. This releases GLUT4 clusters and allows dispersal of the transporter.

Based on the research that has been described in the previous sections, we have developed a working hypothesis that is illustrated in Figure 1.8 and Figure 1.9. A small percentage of GLUT4 is located in the plasma membrane under basal conditions. Those molecules can be found in clusters, which enable the transporter to be easily re-endocytosed and undergo recycling with the endosomal system. We propose that these clusters are maintained by lipid domains in the plasma membrane containing unphosphorylated PI. The binding of insulin to its receptor leads to a signalling cascade that eventually results in

the translocation of GSVs to the plasma membrane and an increase in fusion events. We believe that insulin also has an effect on the EFR3 machinery by activating PI4KIII $\alpha$ . This results in the phosphorylation of PI in the plasma membrane to PI4P, which loses the ability to coral GLUT4 clusters. Consequently, GLUT4 disperses from its clusters, which not only prevents re-endocytosis but also allows efficient glucose uptake.

The main objective of this work was to develop a microscopy-based assay to observe and quantify the clustering and dispersal of GLUT4 and to shed light on its molecular mechanisms. This will be further discussed in Chapter 4 and Chapter 5. The majority of experiments have been carried out in 3T3 L1 adipocytes, which can be challenging to work with. For this reason, the human HeLa cell line, expressing HA-GLUT4-GFP has been studied and compared to 3T3 L1 adipocytes to determine whether it could be used as a suitable cell model that is easier to work with. For this study TIRFM has been used, which is discussed in Chapter 3. Based on the results of this chapter, a different angle of GLUT4 signalling in human cells has been illuminated by focusing on SNARE proteins facilitating GLUT4 transport between the endoplasmic reticulum (ER), the Golgi, and the ER-to-Golgi intermediate compartment (ERGIC). This is discussed in Chapter 6.



## Chapter 2 General Materials and Methods

### 2.1 Materials

#### 2.1.1 Reagents and Enzymes

Table 2.1 Reagents and Enzymes

Reagent/Enzyme	Supplier	Catalogue Number
Acetic Acid	VWR Chemicals (Leicestershire, UK)	20104.334
Acetone	VWR Chemicals (Leicestershire, UK)	20066.330
Acrylamide	BDH (Dubai, UAE)	442993Y
30 % Acrylamide Mix	Severn Biotech (Worcestershire, UK)	20-2100-10
Agar	Formedium (Norfolk, UK)	A6A02
Agarose	Invitrogen (Paisley, UK)	16500
6-aminocaproic acid	Sigma-Aldrich (Dorset, UK)	A2504
Ammonium Persulfate (APS)	ThermoFisher Scientific (Leicestershire, UK)	A/6160/60
Ampicillin	Sigma-Aldrich (Dorset, UK)	A0166
$\beta$ -mercaptoethanol	Sigma-Aldrich (Dorset, UK)	M6250
Bisacrylamide	Sigma-Aldrich (Dorset, UK)	146072
Bis-tris	Sigma-Aldrich (Dorset, UK)	B9754
Blasticidin	Sigma-Aldrich (Dorset, UK)	15205
BN-PAGE marker	GE Healthcare BioSciences (Chalfont, UK)	17044501
Bovine Serum Albumin (BSA)	ThermoFisher Scientific (Leicestershire, UK)	BP9702
Bromophenol blue	Sigma-Aldrich (Dorset, UK)	B8026
BSA	Promega (Southampton, UK)	R396E
CaCl <sub>2</sub>	BDH (Dubai, UAE)	275844L
Collagenase Type I	Worthington Biochemical Corporation (Lakewood, USA)	4197
Coomassie Brilliant Blue G-250	Serva (Heidelberg, Germany)	35050
Cysteamine	Sigma-Aldrich (Dorset, UK)	30070
Cytochalasin B	Sigma-Aldrich (Dorset, UK)	C6762
[3H]Deoxy-D-Glucose	Perkin Elmer (Massachusetts, USA)	NET328A001MC
4',6-diamidino-20-phenylindole (DAPI)	Sigma-Aldrich (Dorset, UK)	D9542
Dexamethasone	Sigma-Aldrich (Dorset, UK)	D4902
Digitonin	Calbiochem (San Diego, USA)	300411
Dimethyl Sulfoxide (DMSO)	ThermoFisher Scientific (Leicestershire, UK)	D/4120/PB08
Dithiothreitol (DTT)	Melford Laboratories (Suffolk, UK)	3483-12-3

Reagent/Enzyme	Supplier	Catalogue Number
DNA Marker 1kb	Promega (Southampton, UK)	G571A
DNA 6x sample buffer	Promega (Southampton, UK)	G1881
Donkey Serum	Sigma-Aldrich (Dorset, UK)	D9663
Doxycycline	Sigma-Aldrich (Dorset, UK)	D1822
Dulbecco's Modified Eagle's Medium (DMEM)	Gibco (Paisley, UK)	41965-039
Dulbecco's Phosphate Buffered Saline (DPBS)	Gibco (Paisley, UK)	14190-094
Enhanced Chemiluminescence (ECL) Western Blotting Substrate	ThermoFisher Scientific (Leicestershire, UK)	32106
Ethanol	VWR Chemicals (Leicestershire, UK)	20821.330
Ethylenediaminetetraacetic acid (EDTA)	Sigma-Aldrich (Dorset, UK)	E4884
Ethylene glycol-bis(2-aminoethylether)-N,N,N',N'-tetraacetic acid (EGTA)	Sigma-Aldrich (Dorset, UK)	E4378
Foetal Calf Serum (FCS)	Gibco (Paisley, UK)	10500-064
Galectin 3	R&D Systems (Minneapolis, USA)	1197-GA
Gelatin from cold water fish	Sigma-Aldrich (Dorset, UK)	G7765
Glucose	ThermoFisher Scientific (Leicestershire, UK)	G/0500/53
Glycerol	ThermoFisher Scientific (Leicestershire, UK)	G/0650/17
Glycine	ThermoFisher Scientific (Leicestershire, UK)	G/0800/60
Goat Serum	Sigma-Aldrich (Dorset, UK)	G9023
HCl	ThermoFisher Scientific (Leicestershire, UK)	H/1200/PB17
4-(2-hydroxyethyl)-1-piperazineethanesulfonic acid (HEPES)	VWR Chemicals (Leicestershire, UK)	441485H
Hygromycin	Sigma-Aldrich (Dorset, UK)	H3274
Insulin	Sigma-Aldrich (Dorset, UK)	I5523
3-isobutyl-1-methylxanthine (IBMX)	Sigma-Aldrich (Dorset, UK)	I5879
Isopropanol	Riedel-de Haën (Seelze, Germany)	24137
Kanamycin	Sigma-Aldrich (Dorset, UK)	60615
KCl	VWR Chemicals (Leicestershire, UK)	26764.260
KH <sub>2</sub> PO <sub>4</sub>	ThermoFisher Scientific (Leicestershire, UK)	P/4800/53
Lentiviral Packaging Kit pPACKH1	System Biosciences (Palo Alto, USA)	LV510A-1

Reagent/Enzyme	Supplier	Catalogue Number
Lenti-X GoStix	Clontech (Mountain View, USA)	631244
L-Glutamine	Sigma-Aldrich (Dorset, UK)	G7513
Ligase Buffer	Invitrogen (Paisley, UK)	P/N Y 90001
Lipofectamine 2000	Invitrogen (Paisley, UK)	11668-022
Maxiprep Kit	Quiagen (Crawley, UK)	12163
Methanol	ThermoFisher Scientific (Leicestershire, UK)	M/4000/PC17
MgCl <sub>2</sub>	VWR Chemicals (Leicestershire, UK)	25108.260
MgSO <sub>4</sub>	BDH (Dubai, UAE)	1015144
Milk Powder	Marvel (London, UK)	n.a.
Miniprep Kit	Promega (Southampton, UK)	A1330
Mounting Medium	Ibidi (Martinsried, Germany)	50001
Immu-Mount	ThermoFisher Scientific (Leicestershire, UK)	9990402
Mycoplasma Detection Kit	Minerva Biolabs (Berlin, Germany)	11-1100
Na <sub>2</sub> HPO <sub>4</sub>	VWR Chemicals (Leicestershire, UK)	102494C
NaCl	Merck (Darmstadt, Germany)	1.06404
NaH <sub>2</sub> PO <sub>4</sub>	Merck (Darmstadt, Germany)	1.06345
NaOH	ThermoFisher Scientific (Leicestershire, UK)	S/4920/60
Newborn Calf Serum (NCS)	Gibco (Paisley, UK)	16010-159
NH <sub>4</sub> Cl	Fisons (Loughborough, UK)	A/3920
One Shot® Stbl3™ Chemically Competent <i>E. coli</i>	ThermoFisher Scientific (Leicestershire, UK)	C737303
Opti-MEM	Gibco (Paisley, UK)	31985-062
Paraformaldehyde (PFA)	Sigma-Aldrich (Dorset, UK)	P6148
Penicillin/Streptomycin	Gibco (Paisley, UK)	15140122
Pirenzepine	Tocris Bioscience (Abingdon, UK)	1071
Polybrene	Sigma-Aldrich (Dorset, UK)	TR-1003
Ponceau S	Sigma-Aldrich (Dorset, UK)	P3504
Protease Inhibitor Tablet	ThermoFisher Scientific (Leicestershire, UK)	A32965
Protein Marker	Bio-Rad Laboratories (Hertfordshire, UK)	161-0373
PureFection Transfection Reagent	System Biosciences (Palo Alto, USA)	LV750A
Puromycin	Sigma-Aldrich (Dorset, UK)	P8833
Restriction Endonuclease BamHI	New England Biolabs (Massachusetts, USA)	R3136
Restriction Endonuclease NotI	New England Biolabs (Massachusetts, USA)	R3189
Shrimp alkaline phosphatase	New England Biolabs (Massachusetts, USA)	M0371

Reagent/Enzyme	Supplier	Catalogue Number
Sodium dodecyl sulfate (SDS)	VWR Chemicals (Leicestershire, UK)	442444H
Sodium Pyruvate	Gibco (Paisley, UK)	11360070
Sucrose	Sigma-Aldrich (Dorset, UK)	S9378
SYBR™ Safe DNA Gel Stain	Invitrogen (Paisley, UK)	S33102
T4 DNA Ligase	Invitrogen (Paisley, UK)	15224-017
Temed	Sigma-Aldrich (Dorset, UK)	T9281
Tricine	Sigma-Aldrich (Dorset, UK)	T0377
Tris Base	ThermoFisher Scientific (Leicestershire, UK)	BP152-1
Tris acetate	Sigma-Aldrich (Dorset, UK)	T1258
Triton X-100	Sigma-Aldrich (Dorset, UK)	T9284
Troglitazone	Tocris Bioscience (Abingdon, UK)	3114
Trypan Blue	Sigma-Aldrich (Dorset, UK)	T6146
Trypsin-EDTA (0.05 %)	Gibco (Paisley, UK)	25300054
Tryptone	Formedium (Norfolk, UK)	TRP02
Tween-20	Sigma-Aldrich (Dorset, UK)	P7949
Twinsil®	Picodent (Wipperfürth, Germany)	1300 1000
Virapower	Invitrogen (Paisley, UK)	A11145
Virkon Rely+On	Lanxess (Köln, Germany)	12358662
Wizard® SV Gel and PCR Clean-Up System	Promega (Southampton, UK)	A9281
Yeast Extract	Sigma-Aldrich (Dorset, UK)	M6250

### 2.1.2 Buffers and Solutions

If not stated otherwise, all buffers and solutions were made up in demineralised water. If necessary, pH was adjusted using HCl or NaOH.

**Table 2.2 Buffers and Solutions**

Buffer	Components
2 Yeast Tryptone (2YT) Medium	1.6 % (w/v) Tryptone 1 % (w/v) Yeast extract 0.5 % (w/v) NaCl (2 % (w/v) Agar for plates)
Blue Native Polyacrylamide Gel Electrophoresis (BN-PAGE) Acrylamide Solution	48 % Acrylamide 1.5 % Bisacrylamide
BN-PAGE Anode Buffer	50 mM BisTris/HCl pH 7.0
BN-PAGE Cathode Buffer	50 mM Tricine 15 mM BisTris/HCl pH 7.0 0.02 % (w/v) Coomassie Blue G-250
BN-PAGE Cathode Buffer (colourless)	50 mM Tricine 15 mM BisTris/HCl pH 7.0

Buffer	Components
BN-PAGE Destain Solution	25 % (v/v) Methanol 10 % (v/v) Acetic Acid
BN-PAGE Gel Buffer	100 mM BisTris/HCl pH 7.0 1 M 6-aminocaproic acid
BN-PAGE 10x Sample Buffer	5 % (w/v) Coomassie Brilliant Blue G-250 0.5 M 6-aminocaproic acid 100 mM BisTris/HCl pH 7.0
Glycine in PBS (Gly)	20 mM Glycine In PBS
HEPES-EDTA-Sucrose (HES) Buffer	250 mM Sucrose 20 mM HEPES 1 mM EDTA pH 7.4
Immunofluorescence (IF) Buffer	0.2 % (w/v) Fish skin gelatin 0.1 % (v/v) Goat serum In PBS
Laemmli Sample Buffer (LSB)	100 mM Tris/HCl pH6.8 4 % (w/v) SDS 20 % (v/v) Glycerol 0.2 % (w/v) bromophenol blue 10 % $\beta$ -mercaptoethanol
Lysis Buffer	50 mM HEPES pH 7.2 100 mM KCl 5 mM NaCl 1 mM MgCl <sub>2</sub> 0.5 mM EGTA 1 mM EDTA 0.1 % (v/v) Triton X-100 Complete protease inhibitor (1 tablet per 50 ml)
Mercaptoethylamine (MEA) Buffer	10 mM Cysteamine In PBS pH 7.4
Phosphate Buffered Saline (PBS)	170 mM NaCl 3.4 mM KCl 10 mM Na <sub>2</sub> HPO <sub>4</sub> 1.8 mM KH <sub>2</sub> PO <sub>4</sub> pH 7.2
Phosphate Buffered Saline with Tween (PBST)	170 mM NaCl 3.4 mM KCl 10 mM Na <sub>2</sub> HPO <sub>4</sub> 1.8 mM KH <sub>2</sub> PO <sub>4</sub> 0.1 % Tween-20 pH 7.2
Permeabilisation Buffer	0.1 % Triton X-100 In PBS
PFA solution	3 % (w/v) PFA 1 mM CaCl <sub>2</sub> 1 mM MgCl <sub>2</sub> In PBS

Buffer	Components
Ponceau S	0.2 % Ponceau S 1 % (v/v) acetic acid
SDS-Polyacrylamide Gel Electrophoresis (PAGE) Running Buffer	25 mM Tris 192 mM Glycine 0.1 % (w/v) SDS
SDS-PAGE Transfer Buffer	25 mM Tris 192 mM Glycine 20 % (v/v) Ethanol
Semi-Dry Transfer Buffer	9.6 mM Tris 7.8 mM Glycine 0.26 mM SDS 20 % Methanol
Super Optimal broth with Catabolite repression (SOC) medium	2 % (w/v) Tryptone 0.5 % (w/v) Yeast extract 0.05 % (w/v) NaCl 0.02 % (w/v) KCl 2 mM MgCl <sub>2</sub> 8 mM Glucose pH 7.0
Tris-acetate EDTA (TAE) Buffer	40 mM Tris acetate 1 mM EDTA
Quenching Buffer	50 mM NH <sub>4</sub> Cl In PBS

## 2.1.3 Antibodies

### 2.1.3.1 Primary Antibodies

Primary antibodies were used for immunoblotting (IB) and IF.

**Table 2.3 Primary Antibodies**

Antigen	Details	Working Dilution	Supplier
EFR3a	Rabbit polyclonal	IB 1:250	Sigma-Aldrich (HPA023092)
ID3	Mouse monoclonal Cell Culture Supernatant	IF 1:2	Gift from Neil Bulleid
ERGIC-53/p58	Rabbit Polyclonal	IF 1:200	Sigma Aldrich (E1031)
GAPDH	Mouse monoclonal	IB 1:10,000	Applied Biosystems (AM4300)
GLUT4	Rabbit polyclonal	IB 1:1000	AbCam (ab654)
GM130	Mouse Monoclonal	IF 1:200	BD Biosciences (610823)
HA	Mouse Monoclonal	IF 1:500	Covance Research Products (MMS 101P)

Antigen	Details	Working Dilution	Supplier
HA	Mouse Monoclonal	IF/dSTORM 20 $\mu\text{g}\cdot\text{ml}^{-1}$	Invitrogen (26183-A647)
IRAP	Mouse Polyclonal	IB 1:1000	Cell Signalling (3808)
SNAP23	Rabbit Polyclonal	IB 1:1000	Synaptic Systems (111202)
Syntaxin 5	Rabbit Polyclonal	IB 1:1000	Synaptic Systems (110053)
Syntaxin 6	Mouse Monoclonal	IB 1:1000	BD Biosciences (610635)
Syntaxin 16	Rabbit Polyclonal	IB 1:1000	Synaptic Systems (110162)

### 2.1.3.2 Secondary Antibodies for Western Blotting

Table 2.4 Secondary Antibodies for Western Blotting

Antigen	Details	Working Dilution	Supplier
Mouse IgG	Donkey IRDye 680LT	1:10,000	LI-COR Biosciences (926 68022)
Rabbit IgG	Donkey IRDye 800CW	1:10,000	LI-COR Biosciences (925 32213)
Rabbit IgG	Donkey Horseradish peroxidase (HRP) linked	1:3000	GE Healthcare (RPN1004)

### 2.1.3.3 Secondary Antibodies for Immunofluorescence

Table 2.5 Secondary Antibodies for Immunofluorescence

Antigen	Details	Working Dilution	Supplier
Mouse IgG	Goat Alexa Fluor 647	1:500	Invitrogen (A21235)
Mouse IgG	Goat Alexa Fluor 568	1:500	Invitrogen (A11004)
Rabbit IgG	Goat Alexa Fluor 568	1:500	Invitrogen (A11011)

## 2.1.4 Plasmids and siRNA

Table 2.6 Plasmids

Plasmid	Details	Supplier
Synthetic HA-GLUT4-eGFP	Synthetic plasmid Vector: pcDNA3.1(+) Cloning Site BamHI-EcoRI Ampicillin Resistance	Genscript, custom-made
pCDH-CMV-MCS-EF1-Puro	Cloning and Expression Lentiviral Vector	System Biosciences (CD510)

All siRNAs were purchased from ThermoFisher Scientific

Table 2.7 siRNAs

siRNA - Target	Catalogue Number
BET1	s20092 s20093
BET1L	s226724 s226725
EFR3a	s94605
GOSR1	s18278 s18279
GOSR2	s18383 s18384
SEC22A	s25658 s25659
SEC22B	s18347 s18348
SEC22C	s17398 s17399
Syntaxin 5	s13598 s13599
Syntaxin 6	s19958 s19959
Syntaxin 16	s16528 s16529
Ykt6	s20936 s80937



## 2.1.5 Mammalian Cell Lines

Table 2.8 Mammalian Cell Lines

Cell Line	Source
3T3 L1	American Tissue Culture Collection (ATCC)
HeLa	American Tissue Culture Collection (ATCC)
HA-GLUT4-GFP 3T3	Previously generated in our laboratory
HA-GLUT4-GFP HeLa	Previously generated in our laboratory
HEK293TN	American Tissue Culture Collection (ATCC)
M1mEGFP T-Rex 293 cells	Provided by Richard Ward

## 2.1.6 Materials

Table 2.9 Materials

Material	Supplier
3 mm filter paper	ThermoFisher Scientific (Leicestershire, UK)
96 well plates with glass bottom	Mat Tek (Ashland, USA)
Cavity Microscope Slides	Agar Scientific (Stansted, UK)
Cell Culture Dishes and Flasks (for HeLa and HEK293TN)	Corning (Maine, USA)
Cell Culture Dishes and Flasks (for 3T3 L1)	Falcon by Corning (Maine, USA)
Chamber Slides	Ibidi (Martinsried, Germany)
Electroporation cuvettes	Bio-Rad Laboratories (Hertfordshire, UK)
Glass cover slips for confocal microscopy (13 mm)	VWR Chemicals (Leicestershire, UK)
High performance glass cover slips for dSTORM (18 mm)	Marienfeld-Superior (Lauda-Königshofen, Germany)
Microscope Slides	VWR Chemicals (Leicestershire, UK)
Needles	BD Biosciences (Oxford, UK)
Nitrocellulose transfer membrane, 0.2 µm pore size	Pall Life Sciences (Portsmouth, UK)
Syringe filters	Sartorius (Göttingen, Germany)
Syringes	BD Biosciences (Oxford, UK)
µ-dishes	Ibidi (Martinsried, Germany)

## 2.2 Methods

### 2.2.1 Cell Culture Methods

Cell culture was carried out in laminar airflow cabinets under sterile conditions. Testing for mycoplasma contamination was carried out for all cell lines at regular intervals.

### 2.2.1.1 Growth and Maintenance of HeLa and HEK Cells

HeLa, HEK293TN, and M1mEGFP T-Rex 293 cells were routinely cultured on Corning tissue culture flasks and dishes in a 5 % CO<sub>2</sub> humidified incubator at 37 °C. HeLa cells were cultured in DMEM containing 10 % FCS and 1 % L-Glutamine. HEK293TN cells were cultured in DMEM containing 10 % FCS, 1 % L-Glutamine and 1 % sodium pyruvate. M1mEGFP T-Rex 293 cells were cultured in DMEM containing 10 % FCS, 1 % Penicillin/Streptomycin, 10 µg·ml<sup>-1</sup> blasticidin, and 200 µg·ml<sup>-1</sup> hygromycin. Medium was changed every second day and cells were passaged when they reached approximately 70 % confluency. Passaging was undertaken by washing the cells with DPBS and detaching them off the plastic surface with trypsin-EDTA. If cells had to be counted for subsequent experiments, this was done using a haemocytometer and trypan blue solution.

### 2.2.1.2 Growth and Maintenance of 3T3 L1 Cells

3T3 L1 cells were routinely cultured on Falcon tissue culture flasks and dishes in a 10 % CO<sub>2</sub> humidified incubator at 37 °C. Fibroblasts were cultured in DMEM containing 10 % NCS. Medium was changed every second day and cells were passaged when they reached approximately 70 % confluency. Passaging was undertaken by washing the cells with DPBS and detaching them off the plastic surface with trypsin-EDTA.

### 2.2.1.3 Differentiation of 3T3 L1 Cells

3T3 L1 fibroblasts were differentiated into adipocytes 2 days post-confluency, referred to as “day 0”, using differentiation medium. Day 0 differentiation medium consisted of DMEM supplemented with 10 % FCS, 250 µM IBMX, 170 nM insulin, 0.25 µM dexamethasone, and 5 µM troglitazone. After three days, this was replaced with Day 3 differentiation medium, which consisted of DMEM supplemented with 10 % FCS, 170 nM insulin, and 5 µM troglitazone. After day 6 post differentiation the medium was replaced with DMEM with 10 %FCS, which was then replaced every second day until day 8-12 post differentiation. If cells were used for electroporation, day 0 medium contained 680 nM insulin and day 3 medium did not contain insulin (Miller, 2006).

#### **2.2.1.4 Freezing and Resurrecting Cells**

To ensure the maintenance of stocks of all cell lines, cells were frozen down regularly. For this, they were grown in flasks until 70 % confluence, washed with DPBS and detached with trypsin-EDTA. The cell suspension was centrifuged, and the resulting cell pellet washed with DPBS and resuspended in freezing medium consisting of FCS with 10 % DMSO. Aliquots were immediately transferred into a cryogenic freezing container and kept at -80 °C overnight before long term storage in liquid nitrogen.

Fresh cells were resurrected by thawing an aliquot rapidly at 37 °C and transferred into prewarmed cell culture medium. Medium was changed after 24 h when the cells had attached to remove DMSO.

#### **2.2.1.5 Cleaning and Seeding on Cover Glasses**

Cells that were to be stained and examined by either confocal microscopy or dSTORM were seeded onto cover glasses. Prior to this cover glasses were sterilised by dipping them in 100 % ethanol and dried in a safety cabinet under UV light.

For dSTORM an extensive cleaning protocol of the cover glasses was carried out. Cover glasses were submerged in the following solutions under constant sonication in an ultrasound bath for 90 seconds each: 0.1 M NaOH, 0.1 % Virkon, deionised water 3x, 100 % ethanol, 100 % acetone, deionised water. After this the cover glasses were dipped in 100 % ethanol to sterilise and left to dry under UV light in a safety cabinet for a minimum of 1 h.

#### **2.2.1.6 Transfection**

Transfection of HeLa cells was carried out using Lipofectamine 2000 according to the manufacturer's instructions. For transfection with plasmid DNA, cells were plated on cover glasses in a 12 well tissue culture plate. 4 µg of plasmid DNA per well was used and diluted in 100 µl Opti-MEM, 4 µl Lipofectamine was used per reaction and also diluted in 100 µl Opti-MEM. Diluted DNA and Lipofectamine were combined and incubated at room temperature for 5 min before being

added to the cells. After transfection, cells were incubated for 1-3 days before further analysis.

For transfection with siRNA, HA-GLUT4-GFP HeLa cells were cultured on 96 well tissue culture plates with glass bottom. The day prior to transfection 9000 cells per well were plated. Per well 1.5 pmol of siRNA and 0.5  $\mu$ l Lipofectamine were used and diluted in Opti-MEM prior to transfection. Lipofectamine was incubated in Opti-MEM for 7 min and the combined Lipofectamine and siRNA were incubated for 20 min before being added to the cells. Cells were incubated with the Lipofectamine and siRNA in serum-free DMEM for 4 h before adding 30 % FCS medium and cells were incubated for another 48 h before analysis.

#### **2.2.1.7 siRNA Electroporation of 3T3 L1 Adipocytes**

siRNA knock-down of EFR3a in 3T3 L1 adipocytes was carried out by electroporation. Cells were cultured in 10 cm dishes and differentiated as described in 2.2.1.2 and 2.2.1.3. Electroporation was carried out on day 5 of differentiation using the Bio-Rad Gene Pulser<sup>®</sup> II. All solutions were prewarmed to 37 °C. Cells were washed twice with DPBS and detached by adding a detaching solution made up of equal parts trypsin-EDTA and 2 mg·ml<sup>-1</sup> collagenase type I. The detaching solution was neutralised with complete medium and cells centrifuged for 2 min at 500 x g. The resulting cell pellet was washed 3x with DPBS and resuspended in DPBS (0.5 ml per 10 cm dish). 3 nmol of siRNA and 400  $\mu$ l of this cell suspension were added in an electroporation cuvette and electroporation was carried out at 0.25 kV and 950  $\mu$ F. Dead cells that had floated to the top were discarded and remaining cells were re-plated on glass cover slips for dSTORM.

### **2.2.2 IF Staining**

IF staining was carried out using antibodies described in 2.1.3.1 and 2.1.3.3.

#### **2.2.2.1 IF Staining for Permeabilised Cells**

Cells were cultured on cover glasses as described in 2.2.1.5 or on 96 well plates with glass bottom. For cells expressing a GFP construct the following incubations were carried out in the dark. Prior to staining, cells were washed 3x with PBS

and fixed with PFA for 20 min at room temperature. Cover glasses were washed 3x with PBS and any residual PFA activity was removed by incubation in quenching buffer for 10 min. Cover glasses were washed again 3x with PBS and incubated in permeabilisation buffer for 4 min. Cover glasses were washed 3x with PBS and blocked in IF buffer for 30 min. Staining was then carried out by incubating the cover glasses with the primary antibody in IF buffer for 60 min. Cover glasses were washed 3x with IF buffer and incubated with the secondary antibody in IF buffer. Cover glasses were washed 3x with IF buffer and if nucleus staining was required, they were incubated in  $1 \mu\text{g}\cdot\text{ml}^{-1}$  DAPI in IF buffer for 5 min. Cover glasses were then washed again 3x with IF buffer and mounted onto microscope slides using Immu-Mount mounting medium. Cover glasses were left to dry at room temperature for at least 12 h prior to imaging.

#### **2.2.2.2 IF Surface Staining for Confocal Microscopy**

Cells were cultured on cover glasses as described in 2.2.1.5. For cells expressing a GFP construct the following incubations were carried out in the dark. Prior to staining, cover glasses were washed 3x with ice-cold PBS and fixed with PFA for 20 min on ice. Cover glasses were washed 3x with PBS and PFA activity was quenched by incubating in Gly for 10 min. Cover glasses were washed 3x with Gly and blocked by incubating in Gly with 2 % BSA and 5 % goat serum for 30 min. Staining was then carried out by incubating the cover glasses with the primary antibody in the blocking solution for 45 min. Cover glasses were washed 3x in the blocking solution and incubated with the secondary antibody in the blocking solution for 30 min. Cover glasses were then washed again 3x with blocking solution and mounted onto microscope slides using Immu-Mount mounting medium. Cover glasses were left to dry at room temperature for at least 12 h prior to imaging.

#### **2.2.2.3 IF Surface Staining for dSTORM**

Cells were cultured on high performance cover glasses as described in 2.2.1.5. Prior to staining, cover glasses were washed 3x with ice-cold PBS and fixed with PFA at  $4^\circ\text{C}$  for at least 12 h. Cover glasses were washed 3x with PBS and PFA activity was quenched by incubating in Gly for 10 min. Cover glasses were washed 3x with Gly and blocked by incubating in Gly with 2 % BSA and 5 % goat

serum for 30 min. Staining was then carried out by incubating the cover glasses with the Alexa Fluor 647 tagged HA antibody in the blocking solution for 45 min. Cover glasses were washed 3x with PBS, returned to a fresh 12 well dish in PBS, and stored in the dark at 4 °C. On the day of imaging, cover glasses were mounted on cavity microscope slides containing MEA buffer and sealed using Picodent Twinsil®.

## **2.2.3 Lentivirus**

### **2.2.3.1 Lentivirus Production**

Lentivirus was produced using HEK 293TN cells and the pPACKH1 Lentiviral packaging kit according to the manufacturer's instructions.  $7 \times 10^6$  HEK 293TN cells were seeded per T150 cell culture flask one day prior to transfection. 45  $\mu$ l of the commercially provided pPACKH1 and 4.5  $\mu$ g of plasmid DNA were incubated in serum-free DMEM for 15 min at room temperature. 55  $\mu$ l PureFection transfection reagent was added and incubated for another 15 min before being added to the cell culture flask. Supernatant containing lentivirus was collected at 48 h and 72 h after transfection and presence of lentiviral particles was confirmed with Lenti-X GoStix. Supernatants were stored at -80 °C prior to further use.

Custom-made lentivirus was purchased from VectorBuilder and stored at -80 °C.

### **2.2.3.2 Lentiviral Infection**

HeLa cells were infected with lentivirus at 70 % confluence. 3T3 L1 adipocytes were infected on day 6 of differentiation. 0.5 ml untreated lentiviral supernatant from 2.2.3.1 was used per ml of serum-free DMEM. 5  $\mu$ g·ml<sup>-1</sup> polybrene was included to increase infection efficiency. After 5-6 h, the medium was diluted 2:1 with FCS containing DMEM. Medium was replaced with fresh DMEM after 24 h and incubated for an additional 48-96 h before analysis.

### **2.2.3.3 Generation of a Stable Cell Line Using Lentivirus.**

A 3T3 L1 cell line stably expressing HA-GLUT4-eGFP was generated using custom-made lentivirus. Undifferentiated cells of a low passage number were infected

with the virus at a multiplicity of infection (MOI) of 100-200 as described in 2.2.3.2. Selection pressure was applied by adding selection medium containing  $1.5 \mu\text{g}\cdot\text{ml}^{-1}$  puromycin. This concentration had previously been determined to kill cells not expressing the lentiviral plasmid. Selection medium was added every other day until all cells in a negative control well (not infected) had died. The stable cell line was maintained by continual addition of  $0.15 \mu\text{g}\cdot\text{ml}^{-1}$  puromycin.

## 2.2.4 Molecular Biology Methods

### 2.2.4.1 Transformation

Transformation was carried out under semi-sterile conditions in the vicinity of a Bunsen burner flame.

50  $\mu\text{mol}$  of One Shot<sup>®</sup> Stbl3<sup>™</sup> or XLO-1 (generated by Alexandra Kaupisch or Laura Stirrat) chemically competent *E. coli* was used per transformation. Depending on the DNA concentration, 1-50 ng of plasmid was added to the cells and incubated on ice for 30 min. DNA was then taken up by cells during a heat-shock at 42 °C for 30 sec and cells were returned on ice for another 2 min. 450  $\mu\text{l}$  of prewarmed SOC medium was added to the cells and incubated at 37 °C in a shaking incubator for at least 30 min. 1-100  $\mu\text{l}$  of the cell suspension was then streaked out onto agar plates containing 2YT medium and  $1 \mu\text{g}\cdot\text{ml}^{-1}$  ampicillin and colonies grew at 37 °C overnight.

### 2.2.4.2 Plasmid DNA Purification

Bacterial cultures were grown in 2YT medium supplemented with  $1 \mu\text{g}\cdot\text{ml}^{-1}$  ampicillin. Cultures were inoculated with single colonies from agar plates and grown at 37 °C in a shaking incubator.

Depending on the growth culture volume, plasmids were purified either by Miniprep (Promega, A1330) or Maxiprep (Quiagen, 12163) according to the manufacturer's instructions. DNA concentration was determined by NanoDrop 1000 spectrophotometry.

### 2.2.4.3 Agarose Gel Electrophoresis

Agarose gels were made up of 1 % (w/v) agarose in TAE buffer. SYBR™ safe DNA stain was added at a dilution of 1:10,000 to enable visualisation of DNA bands. DNA 6x sample buffer was added to the samples and run on the gel alongside the 1 kb DNA marker at a constant voltage of 100 V. Gels were visualised under UV light with the Bio-Rad Gel Doc™ System.

### 2.2.4.4 Restriction Endonuclease Digest

Restriction endonuclease digest was carried out using enzymes and the corresponding buffers from New England Biolabs in 50 µl reaction volume, using 1 µl plasmid DNA. The components of the reaction mix were mixed by pipetting and incubated for at least 60 min at the enzyme-specific temperature.

### 2.2.4.5 Cloning

Vector and insert plasmids were both digested as described in 2.2.4.4 in a “big” reaction, using at least 2 µg of DNA and leaving the reaction overnight. The reaction mix was run by agarose gel electrophoresis as described in 2.2.4.3 and bands visualised under UV. The bands containing the cut vector and insert were cut out and purified using the Wizard® SV Gel and PCR Clean-Up System according to the manufacturer’s instructions.

The vector was dephosphorylated to prevent re-ligation using shrimp alkaline phosphatase at 37 °C for 30 min and the reaction was subsequently heat-inactivated at 65 °C for 5 min. Vector and insert were combined at a 1:1 and 1:2 molar ratio and ligated using T4 DNA ligase at room temperature for 15 min. The ligation mix was used to transform XLO-1 cells as described in 2.2.4.1 and the complete reaction was streaked out onto a 2YT agar plate containing ampicillin.

Single colonies were picked and grown in liquid cultures. Plasmids were then purified by Miniprep and successful clones were determined by restriction endonuclease digest and agarose gel electrophoresis as described in 2.2.4.4 and 2.2.4.3.



## 2.2.5 Gel Electrophoresis and Western Blotting

### 2.2.5.1 Cell Lysates

Cells in cell culture dishes were placed on ice and washed 3x with ice-cold PBS. Lysis buffer was added and the cells were scraped off the surface of the well. The cell suspension was passed through a 26G needle 10x, incubated on ice for 20 min and passed through the needle 10x again. Cell debris was removed by centrifugation at 14,000 rpm for 10 min at 4 °C and lysates were stored at -20 °C prior to further use.

### 2.2.5.2 SDS-PAGE

**Table 2.10 SDS-PAGE Gel Components**

Gel	Components (For 10 ml)
5 % polyacrylamide stacking gel	6.8 ml H <sub>2</sub> O 1.7 ml 30 % acrylamide 1.25 ml 1 M Tris (pH 6.8) 100 µl 10 % SDS 100 µl 10 % APS 10 µl TEMED
12 % polyacrylamide resolving gel	3.3 ml H <sub>2</sub> O 4 ml 30 % acrylamide 2.5 ml 1.5 M Tris (pH 8.8) 100 µl 10 % SDS 100 µl 10 % APS 4 µl TEMED

Polyacrylamide mini gels were cast on the Bio-Rad mini-Protean III equipment and consisted of 12 % resolving gels and 5 % stacking gels, as described in Table 2.10. Cell lysates (see 2.2.5.1) were combined with LSB in a ratio of 1:1 and samples were boiled at 95 °C (GLUT4 at 65 °C) for 10 min. Samples were then run alongside a protein marker at a constant voltage of 120 V until the blue dye had run off the gel.

### 2.2.5.3 Immunoblotting

Protein bands were transferred from SDS-PAGE gels onto nitrocellulose membranes by wet transfer. The gel and the membrane were sandwiched together with sponges and 3 mm filter paper in a transfer cassette and placed

into a tank filled with transfer buffer. Transfer was then carried out at a constant current of 200 mA for 2 h or at 30 mA overnight.

After transfer, the nitrocellulose membrane was stained with Ponceau S to verify that transfer had worked. Ponceau S was washed off with PBS and the membrane was blocked with 5 % milk in PBS for 30 min while constantly moving on a roller. The membrane was then incubated with the primary antibody at 4 °C overnight. The next day, the antibody was removed and frozen at -20 °C for the next use. The membrane was washed 3x with PBST and incubated with the secondary antibody for 1 h at room temperature in the dark. The antibody was removed and refrozen, while the membrane was again washed 3x with PBST. Blots were then visualised with the Odyssey infra-red LICOR imaging system.

## **2.2.6 BN-PAGE**

### **2.2.6.1 BN-PAGE Sample Preparation**

3T3 L1 cells were differentiated into adipocytes and cultured on 10 cm dishes and lysed for BN-PAGE immediately before loading on the gel. Every step was carried out at 4 °C to avoid sample denaturation. Cell lysates were prepared by scraping the cells into HES buffer containing protease inhibitor (1 tablet per 50 ml). They were lysed mechanically with a dounce glass homogeniser and by passing through a 26G needle. The cell lysate was then mixed with either triton or digitonin in varying concentrations and incubated on a vortex for 30 min at 4 °C before mixing with BN-PAGE sample buffer and loading on the gel.

## 2.2.6.2 BN-PAGE

Table 2.11 BN-PAGE Gel Components

Gel	Components (For 10 ml)
4 % polyacrylamide stacking gel	4.15 ml H <sub>2</sub> O 5 ml Gel Buffer 800 µl BN-PAGE polyacrylamide solution 80 µl APS 8 µl TEMED
6 % polyacrylamide resolving gel	3.7 ml H <sub>2</sub> O 5 ml Gel Buffer 1.25 ml BN-PAGE polyacrylamide solution 80 µl APS 8 µl TEMED
16 % polyacrylamide resolving gel	5 ml Gel Buffer 3.3 ml BN-PAGE polyacrylamide solution 1.7 ml 87 % Glycerol 80 µl APS 8 µl TEMED

6-16 % gradient mini polyacrylamide gels were cast with the help of a gradient mixer and the Bio-Rad mini-Protean III equipment. The gradient mixer was placed on a stirrer above the gel cast and both chambers filled with the gel solutions. The 16 % gel solution poured into the cast by gravity flow. Once the bottom of the gel had poured, the valve on the gradient mixer was opened to allow mixing of the two gel solutions. The gradient gel was left to polymerise for one hour covered with isopropanol before the stacking gel was added.

Every step after preparing the gels was carried out at 4 °C to avoid denaturation of the samples.

Gels were run in a dedicated gel tank for BN-PAGE to avoid Coomassie contamination of SDS-PAGE gels. The cathode compartment between the gels was filled with blue cathode buffer and the anode compartment around the gels was filled with anode buffer. Samples were mixed with BN-PAGE 10x sample buffer and loaded in the dry gel wells before they were topped up with blue cathode buffer. Samples were run alongside a BN-PAGE protein marker at 100 V for 90 min. Then the blue cathode buffer was replaced with the colourless cathode buffer and the run continued for 60 min at 300 V.

### **2.2.6.3 BN-PAGE Immunoblotting**

BN-PAGE gels were transferred onto PVDF membranes by semi-dry transfer. PVDF membranes were soaked in methanol prior to transfer and gels were destained using BN-PAGE destain solution for 10 min. Semi-dry transfer was carried out using the Bio-Rad Trans-Blot® SD Semi-Dry Transfer Cell and semi-dry transfer buffer. The gel and PVDF membrane were wedged between moistened filter papers and transfer was carried out at a constant voltage of 15 V for 50 min.

Antibody incubation was carried out as in 2.2.5.3, except the secondary antibody was HRP-tagged and blots were visualised via ECL.

## **2.2.7 Microscopy**

The microscopy-based techniques are described in more detail in the corresponding chapters of this thesis.

### **2.2.7.1 Confocal Microscopy**

Live and fixed cells were imaged by confocal microscopy using a 63x plan apochromat oil-immersion objective lens with a numerical aperture of 1.4 fitted to a Zeiss LSM 5 Pascal Exciter laser scanning head coupled to a Zeiss Axiovert 200M inverted microscope and the corresponding software.

### **2.2.7.2 TIRF Microscopy**

TIRFM was carried out using an objective based TIRFM system constructed by Niall Geoghegan (Geoghegan, 2015). The light from a Horiba 481 nm diode laser was directed to the far aperture of a Zeiss objective lens with a numerical aperture of 1.45 using a Till Photonics TIRF condenser. The condenser contained a micrometre screw gauge for lateral manipulation of the beam relative to the optical axis. The resultant fluorescence light was collected by the same objective and focussed to an Andor Ixon EMCCD using a C-mount 1.6x expansion lens.

### 2.2.7.3 dSTORM

dSTORM experiments were performed on an Olympus IX-81 microscope equipped with Olympus Cell<sup>^</sup>R acquisition software, an ImageEM EM-CCD 512 × 512 camera (Hamamatsu) and an Olympus × 150 UAPO oil lens with a numerical aperture of 1.45 and a resulting pixel size of 106 nm.

## 2.2.8 Image Analysis

Images acquired by confocal and TIRF microscopy were analysed and processed using ImageJ/Fiji.

### 2.2.8.1 HA/GLUT4 Ratio

HA/GLUT4 ratios of cells expressing HA-GLUT4-GFP were determined by dividing the fluorescence intensity of the blue channel (HA signal, plasma membrane located GLUT4) by the fluorescence intensity of the green channel (GFP signal, intracellular GLUT4).

### 2.2.8.2 Spatial Intensity Distribution Analysis

For Spatial Intensity Distribution Analysis (SpIDA), the stand-alone MATLAB Graphical User Interface program, available at the Neurophotronics Web site (Godin et al., 2011) was used. The pixel size was 0.09 μm and the beam size was set to 0.2215 μm. These values had previously been determined by John Pediani.

### 2.2.8.3 Colocalisation Analysis

Colocalisation analysis was carried out using the JaCoP plugin in ImageJ (Bolte & Cordelières, 2006). Each image was recorded twice and the Pearson's coefficient, which relates to colocalisation, was determined for the two images of the green and the red channel respectively ( $P_{\text{green}}$  and  $P_{\text{red}}$ ). These values were used to determine the correction factor  $C$ :

$$C = \frac{1}{\sqrt{P_{\text{green}} \cdot P_{\text{red}}}} \quad (2-1)$$

Then the Pearson's coefficients for all four combinations of red and green channels were calculated. The colocalisation value was the average of all four coefficients multiplied by the correction factor C.

#### **2.2.8.4 dSTORM Analysis**

dSTORM images were processed using the ThunderSTORM plugin in ImageJ (Ovesný et al., 2014). The base level A/D counts was 1693, as determined by recording an image with the camera cap on. The EM gain for all images was 300. Default values of the software were used for all other input values.

Localisation density was determined using the Plugin LocFileVisualizer\_v1.1 (van de Linde, 2019). Cluster analysis was carried out using Bayesian cluster analysis (Griffié et al., 2016) and Ripley's K-function analysis (Levet et al., 2015).

#### **2.2.9 Statistical Analysis**

Statistical analysis was carried out using GraphPad Prism (version 5). Depending on the data, unpaired t-test, 2-way ANOVA, or Chi Square test was performed, all with 95 % confidence levels. Details are given in the respective figure legends. The values reported are mean  $\pm$  standard error unless stated otherwise.

## Chapter 3 Comparison of HeLa Cells and 3T3 L1 Adipocytes Using TIRFM

### 3.1 Introduction

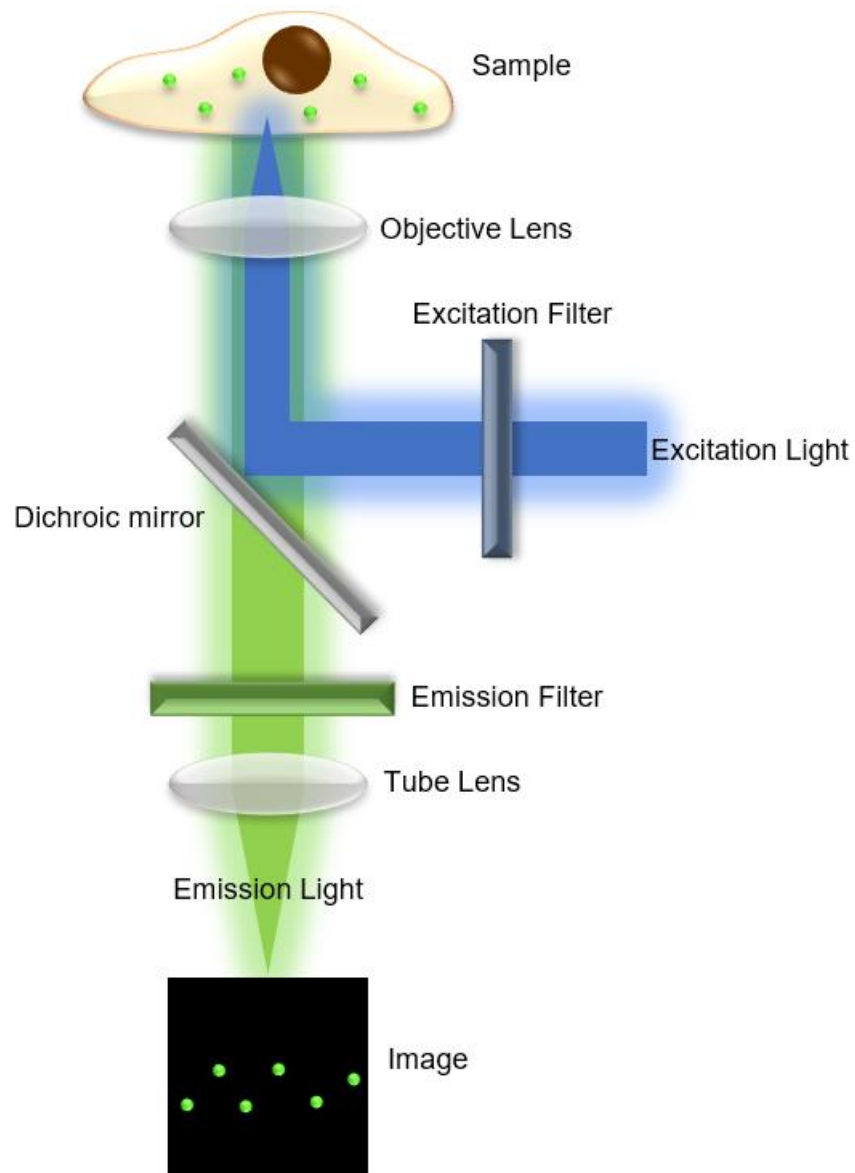
#### 3.1.1 Principles of Fluorescence Microscopy

Fluorescence microscopy is a very common technique that has been used for many years to visualise biological mechanisms on a cellular and even molecular level. Cells can be either genetically modified to express a fluorescent protein such as GFP or stained with an external fluorophore, which can be essentially any fluorescent molecule (Combs, 2010). A fluorescent molecule absorbs light of a certain wavelength and in response, emits light of a slightly longer wavelength. The shift between the absorption and emission spectrum is known as the Stokes shift and is characteristic for each fluorophore (Coling & Kachar, 1997). The absorption maximum of GFP, for example, is 489 nm and its emission peaks at 508 nm (Patterson et al., 2001). This characteristic is used in fluorescence microscopy.

Figure 3.1 shows a schematic of an epifluorescence widefield microscope. The excitation light is passed through a filter that only permits a specific wavelength. The light is reflected off a dichroic mirror and directed to the sample through an objective lens. The light excites the fluorophores in the sample, which upon return from their excited state emit light of a longer wavelength than the excitation light. This light passes through the dichroic mirror and an emission filter and is collected in a tube lens before the image is generated either digitally or in the eyepiece. In epifluorescence microscopy, both, the excitation and the emission light are passed through the same objective lens (Webb & Brown, 2013).

Widefield microscopy provides good temporal and spatial resolution in XY. It does not require high laser power and is therefore less phototoxic for live cell imaging. Another advantage is its relatively low cost. The biggest disadvantage in widefield microscopy is the poor resolution in Z. Since the excitation light passes through the entire sample every fluorophore gets excited and emits light (Combs, 2010). This is particularly problematic for cells with high expression

levels of fluorescent proteins, as this leads to a very high background from fluorescence from outside the focal plane and blurred images.



**Figure 3.1 Schematic of an Epifluorescence Widefield Microscope**

Excitation light passes through a filter and reflects off a dichroic mirror through the objective lens onto the sample. Emission light from the excited fluorophores then passes through the same lens and mirror and through another filter and the tube lens to the eyepiece or a camera to generate the image.

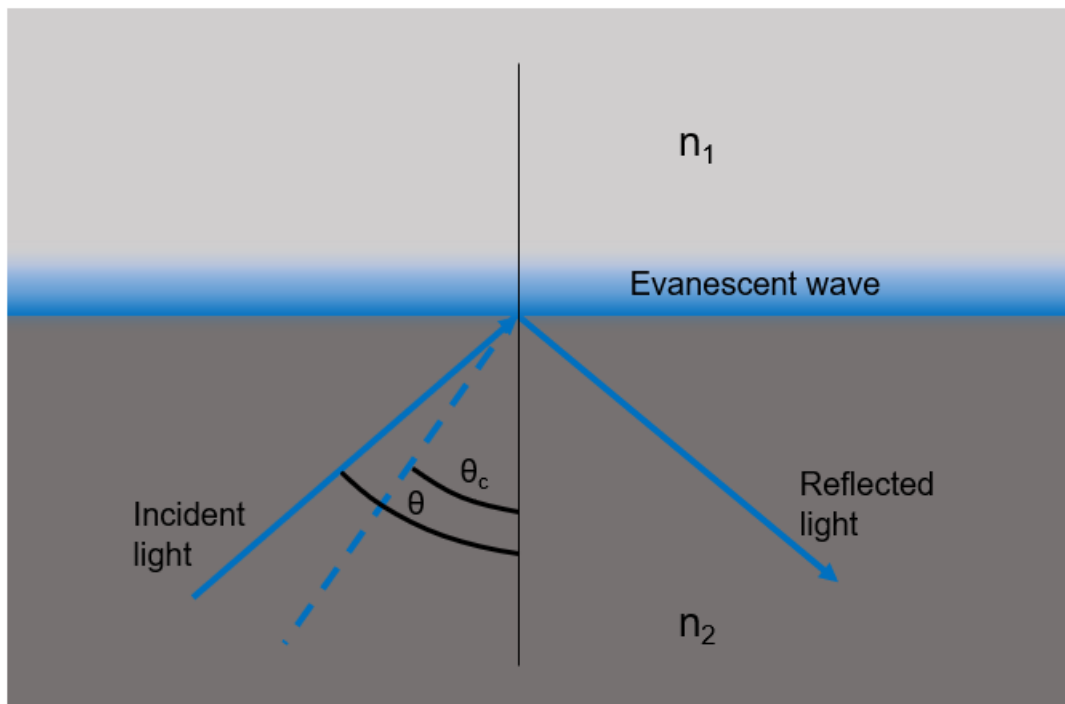


With the development of the confocal microscope, this problem was circumvented (Paddock, 1999). In this technique, a small pinhole is placed between the tube lens and the detector, which excludes light that originates from outside the focal plane. This allows the user to take images of optical sections with much better resolution along the Z-axis, which is typically between 600 nm and 1  $\mu\text{m}$  (Combs, 2010). Although this is a significant improvement compared to widefield microscopy, this axial resolution is not good enough to resolve processes inside or close to the plasma membrane. For such applications, Daniel Axelrod developed TIRFM in 1981 (Axelrod, 1981).

### 3.1.2 Principles of Total Internal Reflection Fluorescence Microscopy

The first imaging technique using total internal reflection (TIR) was already described in 1961 as “Surface Contact Microscopy”. It was used to study the movements of fibroblasts (E. J. Ambrose, 1961).

The principle of TIR is demonstrated in Figure 3.2.



**Figure 3.2 Principle of TIR**

Incident light arrives at the interface of two media with refractive indices  $n_1$  and  $n_2$ , with  $n_1 < n_2$ , at an angle  $\theta$  that is equal to or greater than the critical angle  $\theta_c$  and is totally internally reflected, which generates an exponentially decaying evanescent wave.

Two factors are crucial for TIR: the refractive indices  $n_1$  and  $n_2$  of the liquid and the solid medium and the incidence angle  $\theta$  at which the light arrives at the surface between the two media. The incident light beam propagates through the solid medium, e.g. glass, which has a high refractive index  $n_2$  at an incident angle  $\theta$  that exceeds the critical angle  $\theta_c$ . The refractive index  $n_1$  of the liquid medium, e.g. water, is lower, which means the light beam will undergo TIR (Axelrod, 2001b). The critical angle  $\theta_c$  depends on  $n_1$  and  $n_2$  and is given by

$$\theta_c = \sin^{-1}(n_1/n_2) \quad (3-1)$$

If  $n_1 < n_2$  and  $\theta > \theta_c$ , the incident light beam is totally reflected back into the solid medium except for a small amount of light which propagates perpendicularly to the interface between the two media as a so-called evanescent wave.

The evanescent wave is an electromagnetic field that decays exponentially (Axelrod, 2001b). The intensity  $I$  at a given distance  $z$  from the interface is defined by

$$I(z) = I_0 e^{-z/d} \quad (3-2)$$

Where  $I_0$  is the intensity at the interface and  $d$  is the penetration depth, which depends on the wavelength  $\lambda$  of the incidence light beam as well as  $n_1$ ,  $n_2$ , and  $\theta$

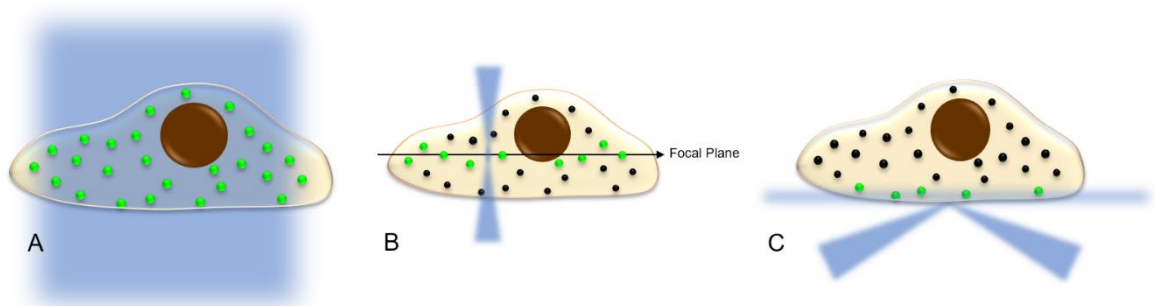
$$d = \frac{\lambda}{4\pi} \cdot \frac{1}{\sqrt{n_1^2 \sin^2 \theta - n_2^2}} \quad (3-3)$$

It is incurred from equation 3-3 that the penetration depth decreases with increasing incidence angle. Practically, this means that the evanescent wave can illuminate an area of less than 100 nm (Martin-Fernandez et al., 2013).

With Ambrose's technique, cells were imaged in brightfield and the contrast was very low. 20 years later, the technique was therefore developed further by changing the light source to a laser beam, which allowed imaging of fluorescently labelled targets near the plasma membrane and also increased the accuracy of the penetration depth  $d$ , as a laser beam with a defined wavelength was used rather than the whole range of visible light (Axelrod, 1981).

TIR can be achieved by two different means: in prism based TIRFM, the evanescent wave is generated on top of the sample through a prism, while the objective is placed underneath. This allows for a large incidence angle of the laser beam, which results in a very small penetration depth (see equation 3-3). The other advantage is that the reflected light is directed away from the objective and is not collected (W. P. Ambrose et al., 1999). This set-up, however, can only be used for very thin samples and is unsuitable for thick cell lines such as adipocytes. An easier and more versatile set-up is objective based TIRFM. Here, excitation and emission light are both passing through the objective lens, which makes the system easier to manipulate and suitable for thick cell types or even tissue samples. The obvious disadvantage is that the angle of the incidence light beam is limited and penetration depth is therefore higher (Martin-Fernandez et al., 2013).

Figure 3.3 summarises the difference between widefield, confocal, and TIRF illumination. In widefield, the laser beam penetrates the entire cell and all fluorophores are equally excited, which leads to a high background and very poor axial resolution. This is less of an issue in confocal microscopy, where out-of-focus light is eliminated by a pinhole in front of the detector and only fluorophores along the focal plane are imaged. TIRF illumination allows imaging of a very thin area adjacent to the coverslip and is ideal for imaging of membrane proteins.



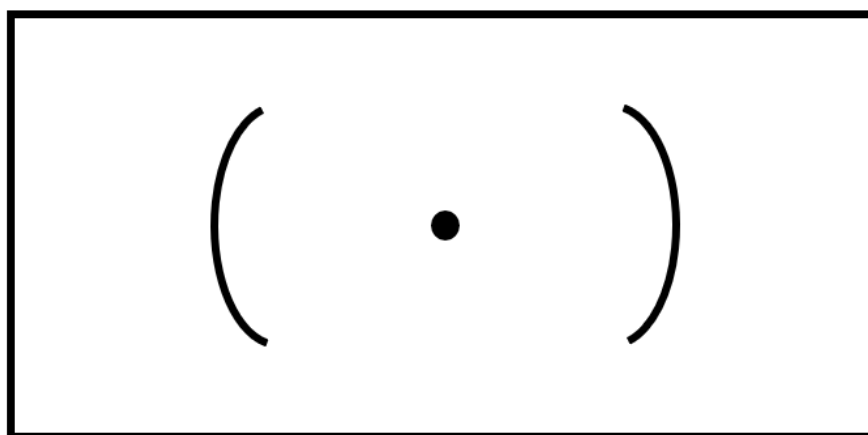
**Figure 3.3 Widefield vs Confocal vs TIRF**

A: Widefield illumination, the laser penetrates the entire sample and excites all fluorophores. B: Confocal illumination, the sample is rastered through along the focal plane. C: TIRF illumination, the laser beam is totally reflected, and the surface is illuminated by an evanescent wave.

Since its first implementation (Axelrod, 1981), TIRFM has been used in many studies. An obvious application is the spatial and temporal imaging of processes near the plasma membrane that would otherwise be dominated by a high background signal from the cytosol (Mattheyses et al., 2010). Examples are vesicle trafficking along the cytoskeleton (Schmoranzler & Simon, 2003) and clathrin-mediated endocytosis (Rappoport, 2008). The intensity decay of the evanescent wave also allows improved axial resolution; fluorescence is more intense closer to the membrane, which has thus allowed the characterisation of exocytotic events (Schmoranzler et al., 2000), paving the way for the analysis of GSVs, which has been discussed in detail in section 1.7.

### 3.1.3 The Built In-House TIRFM System

The TIRF microscope used in this work was the one built by Dr Niall Geoghegan in the context of his PhD Thesis (Geoghegan, 2015). A 481 nm pulsed laser diode was used for illumination, which was attached to a TIRF condenser. This instrument allowed the alignment of the laser and manipulation of the TIR angle. The laser beam was directed to a mask in the condenser that consisted of two side slits and a pinhole in the middle, as shown in Figure 3.4. Alignment of the laser was achieved by directing the laser beam through the central pinhole. A micrometre at the bottom of the condenser enabled the manipulation of the angle at which the laser beam met the substrate, and therefore TIR. With this set-up, a penetration depth of as little as 118 nm could be achieved (Geoghegan, 2015)



**Figure 3.4 TIR Alignment Mask**

The laser beam is directed through the central pinhole for alignment of the laser. When focused through the slits, the TIR angle can be manipulated.

It is important to emphasize that this is a home-built set-up that comes with certain limitations. Most importantly, the TIR angle had to be adjusted manually by turning the micrometre, which was located in the back of instrument, while simultaneously observing the sample through the eyepiece at the front of the instrument. This was not only physically challenging, but also meant that settings from previous experiments could not be adopted. Consequently, the TIR angle was not precisely the same for each experiment. Another limitation was the lack of a suitable stage-top incubator, which made imaging of live cells more challenging.

### 3.1.4 Hypothesis and Aims

TIRFM has been a valuable tool and 3T3 L1 adipocytes are a well characterised model cell line to study GLUT4 trafficking (Bai et al., 2007; S. Huang et al., 2007; Jiang et al., 2008; C. H. Li et al., 2004; Y. Xu et al., 2011). 3T3 L1 cells are a murine fibroblasts line that can differentiate into adipocytes *in vitro* by differentiation (Green & Kehinde, 1974; Green & Meuth, 1974). Compared to primary cells, they are much easier and cheaper to use, differentiation into adipocytes is relatively simple and experiments are relatively robust (Ruiz-Ojeda et al., 2016). A major shortcoming of the cell line is that it is very difficult to transfect (Carlotti et al., 2004; Ross et al., 2003) and although the cell line is not too difficult to maintain, differentiation into adipocytes is time-consuming (see section 2.2.1.3) and requires a certain level of expertise to avoid contamination of the culture when being grown over such a long period.

The HeLa cell line is the oldest and most frequently used human cell line (Lucey et al., 2009). The cells are very easy to culture and to genetically modify. The cell line does not express endogenous GLUT4, but when transfected with HA-GLUT4-GFP, cells show the characteristic intracellular retention of GLUT4 in the absence of insulin and translocation to the cell membrane after insulin stimulation (Haga et al., 2011; Kioumourtzoglou et al., 2015). This observation raises the question whether HA-GLUT4-GFP HeLa cells could be a valid model for GLUT4 trafficking. Another advantage of HeLa is that this is a human cell line, whereas 3T3 L1 is of murine origin. A human model cell line may be a more valid model for the study of a disease that is common in humans. In a recent study,

Camus *et al.* (2020) have indeed found that the formation of the GSC differs in human cells compared to rodents (see Chapter 6).

The aim of this chapter was to compare HeLa cells to 3T3 L1 adipocytes with regards to GSV translocation to the plasma membrane in response to insulin. For this, we used the built in-house TIRFM system described in section 3.1.3.

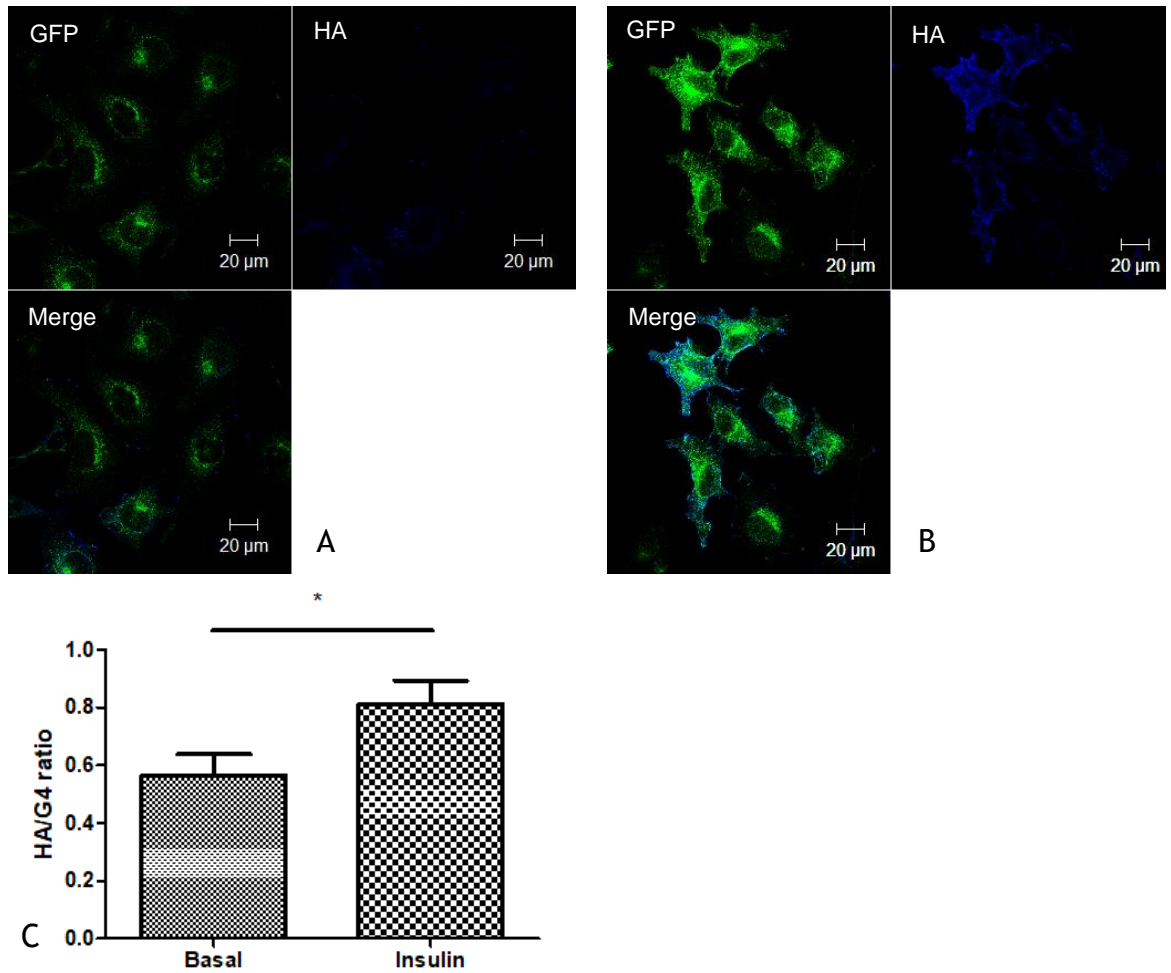
## 3.2 Results

### 3.2.1 HA-GLUT4-GFP Expression in HeLa Cells and 3T3 L1 Adipocytes

The cell lines that were used in this study were HeLa cells and 3T3 L1 adipocytes stably expressing HA-GLUT4-GFP. Expression of the glucose transporter as HA-GLUT4-GFP allows imaging of the molecule via green fluorescence in both, live and fixed cells. Translocation in response to insulin stimulation can be visualised by surface HA-staining in fixed cells as outlined in 1.7 and 2.2.2. This is shown in Figure 3.5 for HeLa cells and in Figure 3.6 for 3T3 L1 adipocytes.

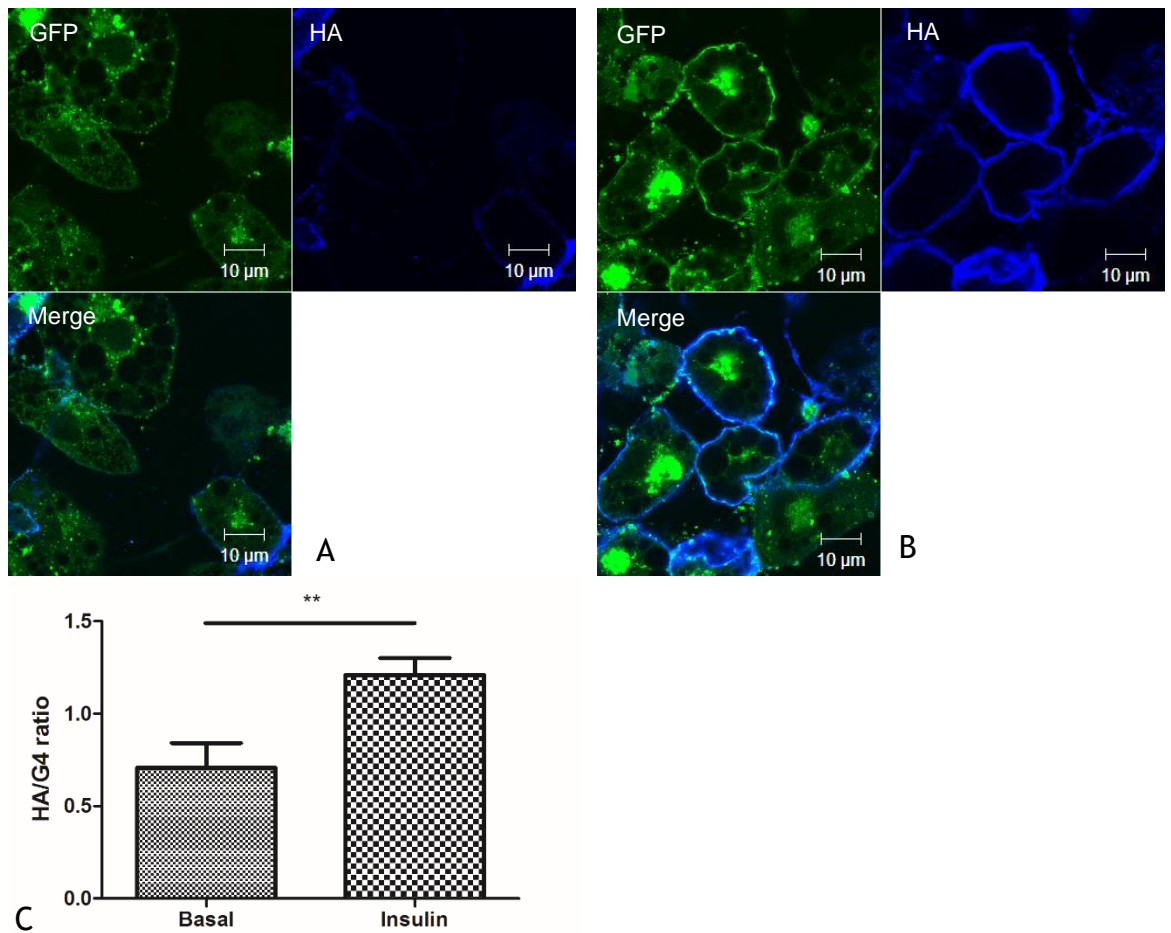
The two figures outline the differences and similarities between the two cell lines. In the basal state, GLUT4 is located intracellularly mostly near the nucleus, and there is only a weak HA signal on the cell surface. In response to insulin, the GFP signal is more dispersed in the cytoplasm and the characteristic blue HA-ring can be seen, which signifies GLUT4 translocation and subsequent exocytosis. This is also reflected in the HA/GLUT4 ratio, which significantly increases after insulin stimulation in both cell types.

HeLa cells clearly respond to insulin, even though they require longer stimulation (60 min vs 20 min in 3T3 L1). The translocation of GLUT4 is, however, visually not as clear as in 3T3 L1 adipocytes.



**Figure 3.5 HA Surface Staining of HA-GLUT4-GFP HeLa Cells in Response to Insulin**

HA-GLUT4-GFP HeLa cells were incubated in serum-free medium for 2 h prior to the experiment and stimulated with 100 nM insulin for 60 min or left untreated. Cells were then fixed and stained for surface HA as described in section 2.2.2. The HA/G4 ratio was determined as described in 2.2.8.1 A: Representative image of basal cells B: Representative image of cells after stimulation with insulin C: HA/G4 ratio, Basal:  $0.57 \pm 0.07$  (n = 14) Insulin:  $0.81 \pm 0.08$  (n = 14). Mean  $\pm$  SE. Unpaired two-tailed t-test 95 % confidence intervals p = 0.0329



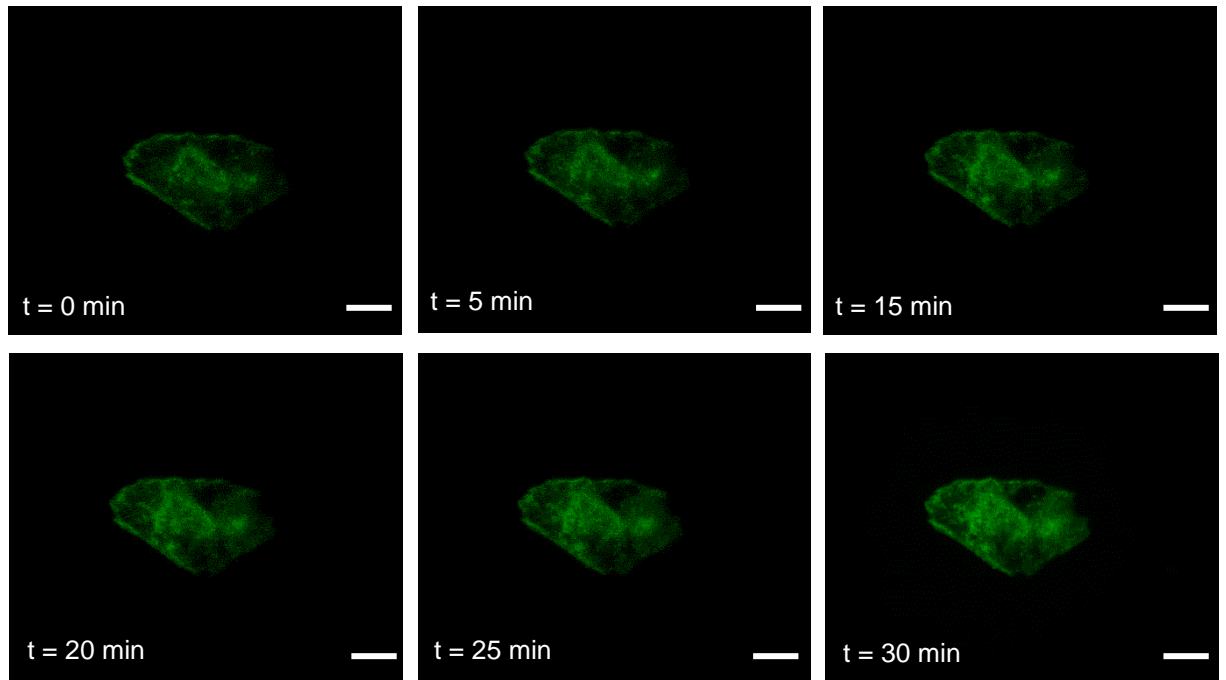
**Figure 3.6 HA Surface Staining of HA-GLUT4-GFP 3T3 L1 Adipocytes in Response to Insulin**  
 HA-GLUT4-GFP 3T3 L1 adipocytes were incubated in serum-free medium for 2 h prior to the experiment and stimulated with 100 nM insulin for 20 min or left untreated. Cells were then fixed and stained for surface HA as described in section 2.2.2. The HA/G4 ratio was determined as described in 2.2.8.1 A: Representative image of basal cells B: Representative image of cells after stimulation with insulin C: HA/G4 ratio, Basal:  $0.71 \pm 0.14$  (n = 11) Insulin:  $1.21 \pm 0.09$  (n = 19). Mean  $\pm$  SE. Unpaired two-tailed t-test 95 % confidence intervals p = 0.0037

### 3.2.2 Fluorescence Intensity in the TIRF Zone

Building up on the results from section 3.2.1, we studied the translocation of HA-GLUT4-GFP upon insulin stimulation in the TIRF zone via the GFP tag of the protein. For this, cells were grown and differentiated if applicable on Ibidi  $\mu$ -dishes and imaged live. As imaging took place over a period of at least 30 min, appropriate cell culture conditions had to be maintained. Cell culture medium was therefore supplemented with 25 mM HEPES to avoid pH dropping and the dish was placed in a heated microscope stage insert to sustain a temperature of 37 °C within the culture dish. Figure 3.7 shows representative images of a single HeLa cell just before insulin administration (t = 0 min) and at different time points thereafter. The rise in fluorescence intensity in the TIRF zone over time is evident, which suggests that HeLa cells indeed respond to an insulin stimulus with the translocation of exogenous HA-GUT4-GFP. This was quantified by

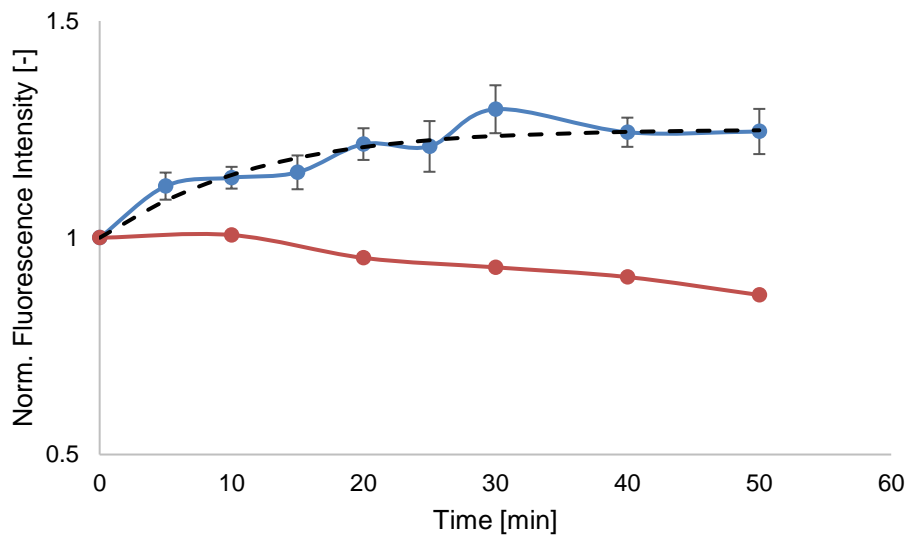


measuring the fluorescence intensity within the footprint of the cell and normalising the result to the intensity at  $t = 0$  min. The result of this experiment is depicted in Figure 3.8.



**Figure 3.7 Time Course of Insulin Stimulated HeLa Cells in TIRFM**

HeLa cells were grown on Ibidi  $\mu$ -dishes and imaged live in TIRFM after stimulation with 100 nM insulin. Images were acquired in 5 min intervals with an exposure time of 500 ms and a frame rate of 2 Hz. Shown are representative images of a single HeLa cell at  $t = 0$  min (immediately before insulin administration),  $t = 5$  min,  $t = 15$  min,  $t = 20$  min,  $t = 25$  min, and  $t = 30$  min. Scalebar: 50  $\mu$ m.



**Figure 3.8 Normalised Fluorescence Intensity in HeLa Cells in TIRFM**

HeLa cells were grown on Ibidi  $\mu$ -dishes and imaged live in TIRFM after stimulation with 100 nM insulin (blue) or remained in the basal state (red). Images were acquired in 5 min intervals for insulin stimulated cells and 10 min intervals for control cells with an exposure time of 500 ms and a frame rate of 2 Hz. Fluorescence intensity of the cell footprint was measured in each image and normalised to the value at  $t = 0$  min, immediately before insulin stimulation. Blue line: Insulin stimulated ( $n = 7$ ). Red line: Basal ( $n = 1$ ). Data points are Mean  $\pm$  SE. Black dashed line: mathematical modelling of the fluorescence intensity increase according to equation (3-4) with  $F_{\max} = 1.25$  and  $r = 0.1$ .

Insulin stimulation lead to an increase of fluorescence intensity due to GSV translocation to the plasma membrane by about 25 % after 30 min.

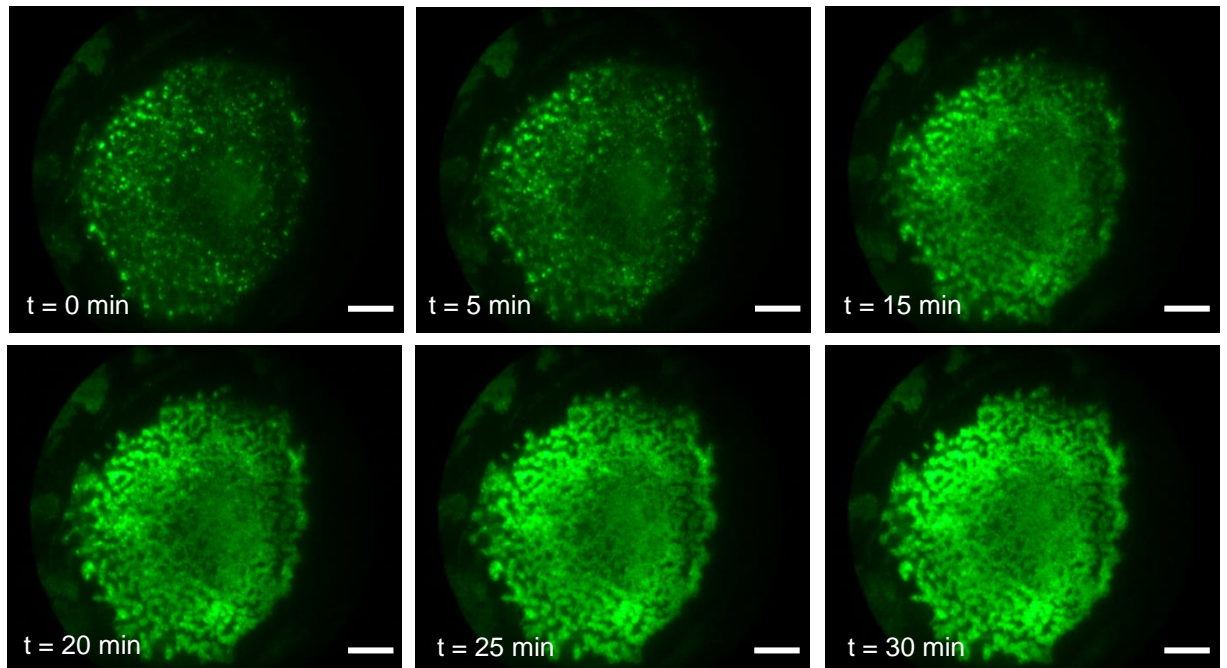
Mathematically, this increase appears to obey a logistic function (see equation (3-4)), which means, there is a steep increase at first, then it slows down and converges to a maximum. In this case 1.25, which is the maximal normalised fluorescence intensity after stimulation with 100 nm insulin in this cell type. In

$$F(t) = \frac{F_{\max}}{1 + \left( \frac{F_{\max} - F(t_0)}{F(t_0)} \right) e^{-rt}} \quad (3-4)$$

$F(t_0)$  is the fluorescence intensity at  $t = 0$  min, which is 1 for normalised values, and  $F_{\max}$  is the maximal fluorescence intensity, in this case 1.25. The growth rate  $r$  corresponds to the initial steepness of the curve and is the only parameter in this equation that remains to be determined. When  $r$  is assumed to be 0.1, the graph follows the black dashed line in Figure 3.8.

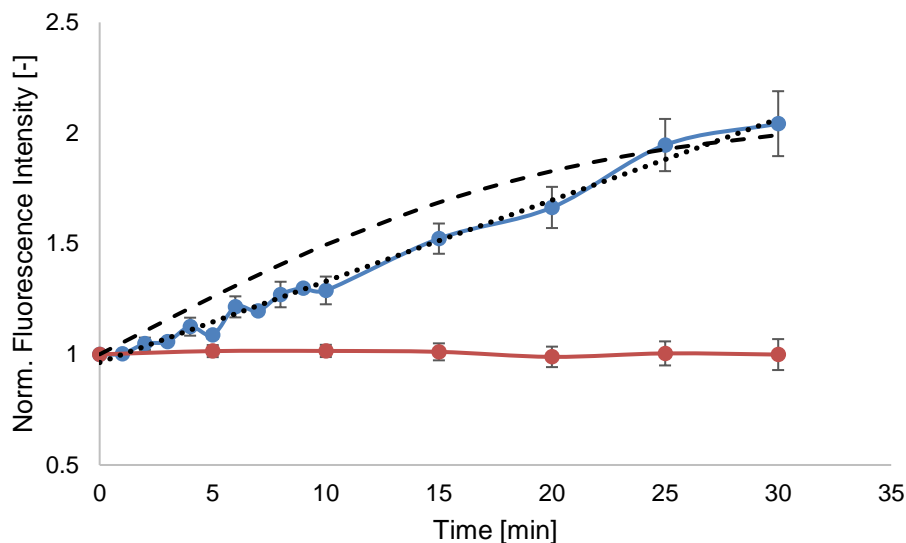
A control experiment was carried out, in which cell culture medium instead of insulin was added to the cells. As expected, the fluorescence intensity did not increase in the basal state, which means that the increase in insulin stimulated cells was solely due to insulin-induced HA-GLUT4-GFP translocation. In fact, the fluorescence intensity in the basal control decreased by approximately 13 %, which was probably a result of photobleaching.

The same experiment was carried out in 3T3 L1 adipocytes. Representative images of a single cell over the course of 30 min are shown in Figure 3.9. After the administration of insulin, the fluorescence intensity increased considerably, which was unmistakably obvious by eye. Immediately before insulin stimulation, clearly defined green fluorescent spots were visible in the TIRF zone. These were likely GSVs near the plasma membrane. With the addition of insulin, more spots emerged in the TIRF zone and those already present seemed to increase in size, until an almost ‘cauliflower-like’ appearance was achieved. This phenomenon was likely due to the limited resolution of the system, when the number of GSVs got so high that single vesicles could not be resolved anymore. This is likely also a result of increased dispersal of GLUT4 in the plasma membrane.



**Figure 3.9 Time Course of Insulin Stimulated 3T3 L1 Adipocytes in TIRFM**

3T3 L1 fibroblasts were grown and differentiated into adipocytes as described in 2.2.1.3 on Ibidi  $\mu$ -dishes and imaged live in TIRFM after stimulation with 100 nM insulin. Images were acquired in 5 min intervals with an exposure time of 500 ms and a frame rate of 2 Hz. Shown are representative images of a single cell at  $t = 0$  min (immediately before insulin administration),  $t = 5$  min,  $t = 15$  min,  $t = 20$  min,  $t = 25$  min, and  $t = 30$  min. Scalebar: 50  $\mu$ m.



**Figure 3.10 Normalised Fluorescence Intensity in 3T3 L1 Adipocytes in TIRFM**

3T3 L1 fibroblasts were grown and differentiated into adipocytes as described in 2.2.1.3 on Ibidi  $\mu$ -dishes and imaged live in TIRFM after stimulation with 100 nM insulin (blue) or remained in the basal state (red). Images were acquired in 5 min intervals with an exposure time of 500 ms and a frame rate of 2 Hz. Fluorescence intensity of the cell footprint was measured in each image and normalised to the value at  $t = 0$  min, immediately before insulin stimulation. Blue line: Insulin stimulated ( $n = 12$ ). Red line: Basal ( $n = 8$ ). Data points are Mean  $\pm$  SE. Black dashed line: mathematical modelling of the fluorescence intensity increase according to equation (3-4) with  $F_{\max} = 2.1$  and  $r = 0.1$ . Black dotted line: Linear regression.

As for HeLa cells, the fluorescence intensity was quantified within the footprint of the cell and normalised to the fluorescence intensity immediately prior to insulin administration. In control experiments, cell culture medium without insulin was added to the cell culture dish. This is shown in Figure 3.10.

As expected, the fluorescence intensity increased over time during insulin stimulation and more than doubled after 30 min of stimulation with 100 nM insulin. However, it is not clear whether the maximum had been reached at the end of the experiment, since images were only taken for 30 min. Interestingly, the fluorescence intensity decreased by less than 1 % in the control experiment. Different from the time course depicted in Figure 3.8, the data cannot be approximated by a logistic function with the same parameters (dashed line), in fact, a linear regression (dotted line) fits the data set almost perfectly. This is contradictory to the fluorescence intensity time courses in 3T3 L1 adipocytes reported by others, where the curve indeed follows a logistic function and the fluorescence intensity increases by 2-3 fold after 20-30 minutes of insulin stimulation (Dawicki-McKenna et al., 2012; S. Huang et al., 2007). Furthermore, the time courses for both cell lines are slower than that of 3T3 L1 adipocytes reported by others (Holman et al., 1994; Muretta et al., 2008) These differences are likely due to the home-built microscope set-up that did not allow for exact regulation of parameters such as temperature or CO<sub>2</sub> content.

### **3.2.3 Mobile and Static Vesicles in the TIRF Zone**

The results presented in this section were generated in collaboration with Dr Niall Geoghegan in the context of his PhD Thesis (Geoghegan, 2015).

In time-lapse images of the TIRF experiments conducted during this study, single vesicles were clearly visible in the TIRF zone. The majority of them appeared static, while a smaller portion were moving around the field of vision, either approaching the cell surface, or moving along the xy plane. We were interested in the fraction of static and mobile GSVs and whether this changed in a time-dependent manner in the presence of insulin. Further, we used this data as another reference point in the comparison of 3T3 L1 adipocytes and the potential cell model HeLa.

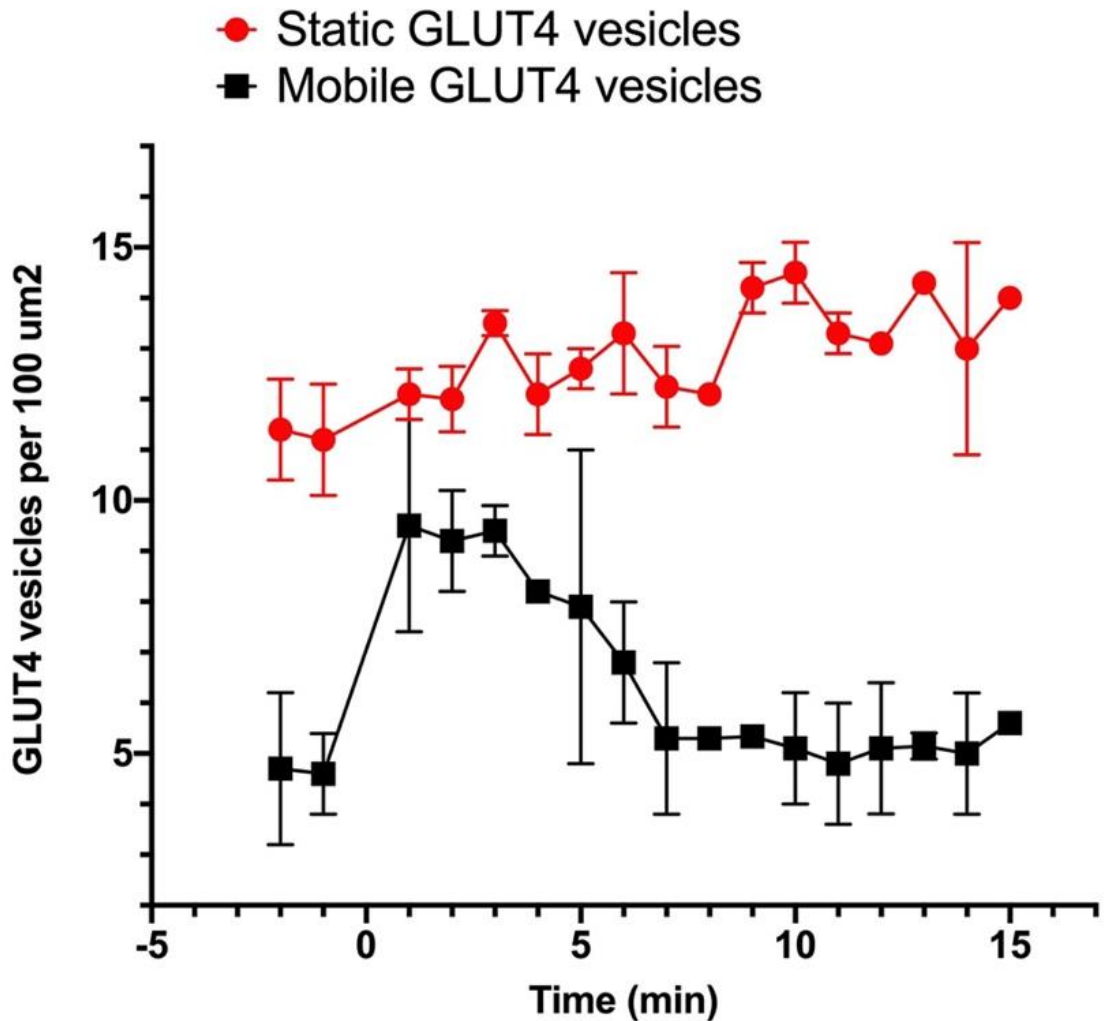
GSVs were identified using algorithms of the ImageJ/Fiji platform. First, background fluorescence was removed by applying a rolling ball algorithm: for each pixel, the signal intensity of the pixels surrounding it was averaged and subtracted from the signal, which results in a smoother background (Sternberg, 1983). The ball radius we used was 5 pixels. The image was processed further by

removing single pixel noise with the plugin “despeckle”. GSVs were defined by three criteria: (1) the particle contained a local intensity maximum (2) 75 % of the signal was contained within a radius of 5 pixels (3) the minimum size of the particle was 2 pixels. Particles that did not belong in these categories were treated as outliers and were excluded from the analysis with the help of the FindFoci algorithm (A. D. Herbert et al., 2014). Static and mobile GSVs were then identified in time lapse image stacks, where each frame had been treated as described. Stationary signals were filtered out from the image stack by subtracting an average projection of the stack pixel by pixel. The resulting stack contained only moving vesicles. This secondary stack was subtracted from the original image stack frame by frame, which yielded images of only stationary vesicles. GSVs could then be counted in different regions of interest (ROIs) in single images of each stack. The results are shown for three individual cells and ten  $100 \mu\text{m}^2$  ROIs in Figure 3.11 for 3T3 L1 adipocytes and in Figure 3.12 for HeLa cells. Images were recorded for 2 min before and 15 min after stimulation with 100 nM insulin. Addition of insulin occurred at  $t = 0$  min.

Figure 3.11 demonstrates impressively the translocation of GLUT4 vesicles to the cell surface in response to insulin in 3T3 L1 adipocytes. With the addition of insulin to the cell culture medium, the number of mobile vesicles increased dramatically within the first minute and stayed elevated for about 5 minutes. During this time, the majority of GSV translocation appeared to be taking place, before the number of mobile vesicles dropped back down to levels from the basal state ( $t < 0$  min). The number of static vesicles on the other hand was steadily increasing, reflecting the arrival of new GSVs in the TIRF zone and tethering to the membrane. This data is consistent with observations by Stenkula *et al.* (2010), who found a sharp increase in fusion events within the first five minutes of insulin stimulation.

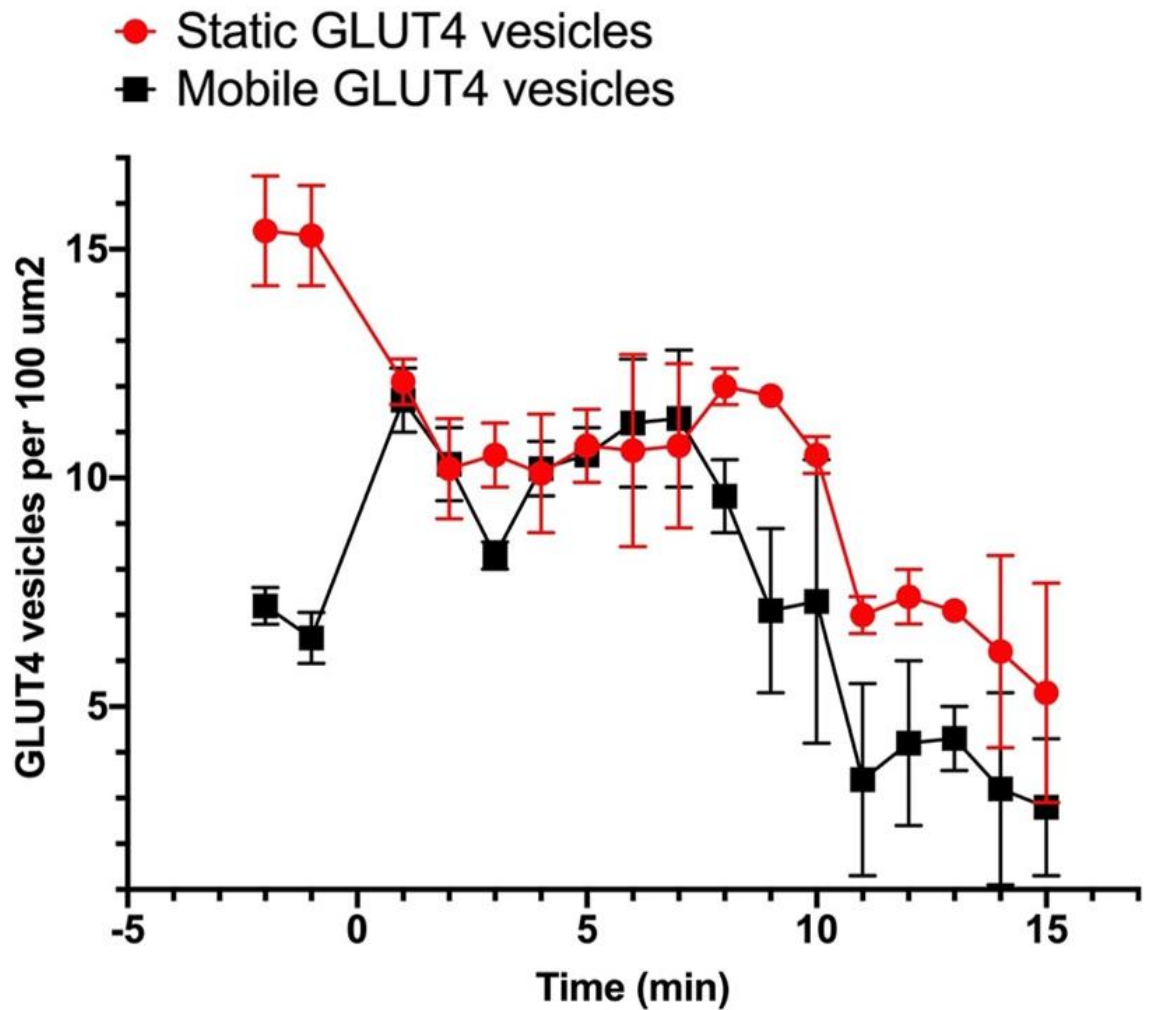
Figure 3.12 shows the same experiment in HeLa cells. Similar to the data collected for 3T3 L1 adipocytes, the number of mobile vesicles increased considerably immediately after the addition of insulin. However, the increased activity lasted closer to 8 minutes in this cell type. Interestingly, the number of both, static and mobile GSVs then dropped to levels below those prior to insulin

stimulation. This may be the reason for the reduced increase in fluorescence intensity after addition of insulin compared to 3T3 L1 adipocytes.



**Figure 3.11 Static and Mobile GLUT4 Vesicles in 3T3 L1 Adipocytes**

3T3 L1 fibroblasts were grown and differentiated into adipocytes as described in 2.2.1.3 on ibidi  $\mu$ -dishes and imaged live in TIRFM before and after stimulation with 100 nM insulin at  $t = 0$  min. Images were acquired in 1 min intervals with an exposure time of 500 ms and a frame rate of 2 Hz. Counts of mobile and static vesicles were determined as described. Static vesicles are shown in red, mobile vesicles in black.  $N = 3$  cells, 10 ROIs ( $100 \mu\text{m}^2$ ) per cell were analysed. Data points are Mean  $\pm$  SD.



**Figure 3.12 Static and Mobile GLUT4 Vesicles in HeLa Cells**

HeLa cells were grown on Ibidi  $\mu$ -dishes and imaged live in TIRFM before and after stimulation with 100 nM insulin at  $t = 0$  min. Images were acquired in 1 min intervals with an exposure time of 500 ms and a frame rate of 2 Hz. Counts of mobile and static vesicles were determined as described. Static vesicles are shown in red, mobile vesicles in black.  $N = 3$  cells, 10 ROIs ( $100 \mu\text{m}^2$ ) per cell were analysed. Data points are Mean  $\pm$  SD.

### 3.3 Discussion

The aim of this chapter was the characterisation of HeLa cells with respect to their ability to translocate HA-GLUT4-GFP in response to insulin and compare the cell line to the frequently used model cell line 3T3 L1.

Overall, HA-GLUT4-GFP HeLa cells responded to an insulin stimulus in a similar manner as HA-GLUT4-GFP 3T3 adipocytes with respect to their ability to translocate the protein to the TIRF zone. In adipocytes the membrane associated fluorescence more than doubled, in HeLa cells, the increase was less prominent and averaged out at about 25%. In unstimulated HeLa cells, fluorescence decreased strongly over time due to photobleaching. This appeared to be less of

an issue in 3T3 L1 adipocyte, where fluorescence intensity remained constant. This may be due to a combination of higher expression levels of HA-GLUT4-GFP, higher levels of the protein in the vicinity of the membrane, and higher recycling rates, meaning that photobleached molecules are cleared from the cell surface more rapidly than in HeLa cells. One or a combination of these factors may have resulted in the fluorescence intensity remaining almost constant in the absence of insulin. An important aspect to consider in this observation is that there was only one successful HeLa control experiment, making it difficult to draw conclusions with regards to photobleaching, as another cell may have behaved differently. Similarly, it is important to mention that out of the 3T3 L1 control experiments, some single cells exhibited a fluorescence decrease of about 20 % in the absence of insulin, while others remained unchanged.

One significant problem we came across when working with HeLa cells was that these cells were more prone to detaching off the culture dish during imaging than adipocytes, resulting in more failed experiments, which is also the reason for the lower number of data points for this cell line.

Our TIRFM setup was not powerful enough to give more insight into the dynamics of GLUT4 in the plasma membrane. Single fusion events could occasionally be observed but the majority of time-lapse images showed GSVs that appeared mostly static. After 15 - 20 min of insulin stimulation in 3T3 L1 adipocytes the signal increased to an extent where single vesicles could not be identified anymore. In HeLa cells single vesicles were even less frequently observed. This may be due to differences in the GSV translocation machinery in this cell type. HeLa cells do not express endogenous GLUT4 or the insulin receptor and other, crucial components of the insulin signalling pathway may be missing too, resulting in different composition and structure of GSVs. The consequence may well be smaller vesicles that are below the detection limit of our TIRFM setup. Fusion of GSVs with the plasma membrane appeared unaffected, as HA-surface staining delivered results comparable to those of 3T3 L1 adipocytes. HeLa cells clearly respond to insulin stimulation with the translocation of HA-GLUT4-GFP containing vesicles to the surface and insertion of the protein in the plasma membrane as shown in section 3.2.1.



Image manipulation in ImageJ allowed a clearer display of single vesicles and the comparison of mobile versus static GSVs. This analysis showed again that HeLa cells were reacting in a similar way to an insulin stimulus with regards to their GSVs dynamics in the TIRF zone. The number of mobile GSVs near the membrane increased noticeably with insulin stimulation for a similar length of time and then dropped again.

Overall, the results suggest that HeLa cells are indeed comparable to 3T3 L1 adipocytes to some extent and may be a suitable model for preliminary screens in the study of GSV translocation. HeLa cells are easy to maintain, and genetic manipulation is straightforward and reproducible. Indeed, other groups have used the cell line in published studies (Camus et al., 2020; Haga et al., 2011; Sadler et al., 2013; Trefely et al., 2015). In addition, it is known that HeLa cells react to insulin stimulation with the phosphorylation of Akt and AS160 (Bogan, 2012) and that they express sortilin (Camus et al., 2020).

Overall, the comparison of HeLa cells and 3T3 L1 adipocytes could be expanded by an almost infinite amount of experiments. Recycling kinetics of GLUT4 in HeLa cells, as carried out by Muretta *et al.* (2008) in 3T3 L1 adipocytes, would be particularly interesting. In a similar experiment, FACS analysis has been carried out by our group after completion of this work and added further evidence towards the comparability of the two cell lines. (S. Morris et al., 2020).

The cell line can be used to deliver preliminary results. However, too little is known about the insulin signalling pathway and whether or not its components are present in HeLa cells to consider them a suitable substitute for adipocytes.

A limitation of TIRFM itself is that despite its improved background elimination, it still does not differentiate between a fluorescent signal inside and outside the plasma membrane. The evanescent wave illuminates a region that is over 100 nm deep. The thickness of the plasma membrane itself, however, is only about 10 nm (Freedman, 2012). This means that the vast majority of the illuminated field contains fluorescence that originates from molecules outside the plasma membrane. This complicates our experiments significantly, since insulin stimulation of HA-GLUT4-GFP 3T3 L1 adipocytes and HeLa cells leads to translocation of the fluorescent fusion protein to the plasma membrane. The

signal in the TIRF zone increased dramatically, but it is unclear which portion was derived from GSVs approaching the membrane and which from actually fused vesicles. Events in the plasma membrane are therefore still overlaid with a substantial amount of background fluorescence, even though TIRF eliminates signals from fluorescent molecules deeper inside the cell. This problem can be circumvented by using a different probe, such as IRAP-pHluorin (Jiang et al., 2008; Stenkula et al., 2010) or VAMP2-pHluorin (Y. Xu et al., 2011). As described in section 1.7.3, pHluorin is a pH-sensitive fluorophore and only emits light when exposed to the neutral pH of the cell culture medium, but not in the acidic environment inside the GSVs. We have indeed developed a construct expressing IRAP-pHluorin that also translocated to the cell surface in response to insulin in HeLa cells. However, this probe was not used for TIRFM experiments, as it could not be expressed in high enough levels in 3T3 L1 adipocytes.

Another way to overcome the issues surrounding background fluorescence is to label the HA-tag of HA-GLUT4-GFP on the surface of cells, as demonstrated in section 3.2.1. This excludes proteins that are not integrated in the plasma membrane and is an experiment that is routinely carried out in our laboratory to visualise and quantify GLUT4 exocytosis. Using surface labelling in TIRFM could lead to a better resolution of membrane integrated GLUT4, however this technique can only be used for fixed cells and does not allow for live imaging. In addition, this technique cannot be applied to the existing TIRFM setup, since the instrument only has a 481 nm laser available, but a different wavelength would be needed to excite the surface labelling.

In conclusion, the TIRFM setup used in this work had some shortcomings that prevented us from carrying out further experiments concerning the dynamics of plasma membrane GLUT4. To find out more about the organisation of the transporter in the plasma membrane, we employed two different fluorescence microscopy-based techniques (see Chapter 4 and Chapter 5). In terms of the comparability of HeLa cells and 3T3 L1 adipocytes, we used these results as a basis for a study of SNARE proteins that affect intracellular GLUT4 trafficking, which is presented and discussed in Chapter 6.

## Chapter 4 The Oligomeric State of GLUT4 in the Plasma Membrane

### 4.1 Introduction

#### 4.1.1 Oligomerisation of Proteins


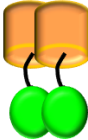
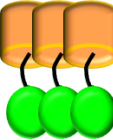
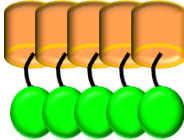
Cell signalling pathways are largely depending on protein-protein interactions. In many cases, the same proteins interact with each other, forming dimers, trimers, tetramers or oligomers of even higher order (Cornish-Bowden & Koshland Jr, 1971). So called homooligomers are involved in different processes including gene expression, control of receptor, enzyme, or ion channel activity, and cell-cell interactions (Hashimoto & Panchenko, 2010). There are cases where the oligomeric state of a protein has a profound influence on its function. For example, the regulatory protein 14-3-3 $\zeta$  binds to phosphoserine motifs in its dimeric form and phosphorylation of a serine residue domain prevents oligomerisation and subsequently the binding of its substrate (Woodcock et al., 2003). G-protein coupled receptors (GPCRs) are another family of proteins that exist in different oligomeric states, which affects their function and in some cases even their location within the cell (Fotiadis et al., 2006; Gurevich & Gurevich, 2008).

According to protein structure databases, most proteins can form oligomers with themselves (Henrick & Thornton, 1998), but experimental investigation of the oligomeric state of proteins has been challenging. Energy transfer methods like fluorescence resonance energy transfer (FRET) or bioluminescence resonance energy transfer (BRET) have been employed to argue that proteins are in very close proximity to each other (Floyd et al., 2003; Issafras et al., 2002). However, these methods are limited as they cannot differentiate between true oligomers and molecules that are only very close to each other (Gurevich & Gurevich, 2008). Other microscopy based techniques, determine the oligomeric state of a protein by analysing the temporal fluctuation of fluorescence intensity of a fluorescent protein of interest (Yan Chen et al., 1999; Kask et al., 1999). These methods, however, are time-dependent and can only be carried out in live samples.

Disulphide trapping by chemical crosslinking has been used to investigate the oligomeric state of GPCRs (Klco et al., 2003), but this method has the disadvantage that temporary interactions as opposed to true oligomerisations are crosslinked as well. BN-PAGE is a gel electrophoresis method that separates proteins and protein complexes in their native state, allowing the analysis of protein complexes and oligomers (Schägger et al., 1994). This method has been used for instance to determine the native oligomeric state of the plasma membrane based enzymes NTPDase1 and 2 (Failer et al., 2003) but it is an intricate and complicated technique that requires a lot of expertise.

### 4.1.2 Spatial Intensity Distribution Analysis

Spatial Intensity Distribution Analysis (SpIDA) was designed by Godin *et al.* to overcome the shortcomings of the aforementioned techniques. The protein of interest is expressed as a chimera with a fluorescent protein. Images are acquired using standard confocal laser scanning microscopy (CLSM) in either live cells or fixed samples and the fluorescence intensity is measured. On CLSMs this is usually done with an analogue photomultiplier tube that counts the number of collected photoelectrons (Paddock, 1999). The intensity of all pixels in an ROI is then plotted in an intensity histogram over which a Poissonian distribution is fitted. This distribution will look different for monomeric, oligomeric, or mixed populations and is used to calculate the quantal brightness  $\epsilon$  of the fluorophore (Godin et al., 2011).  $\epsilon$  is defined as the mean intensity in the point spread function (see Chapter 5.1) of a fluorescent unit (Godin et al., 2015). For SpIDA to work, it is crucial that the used fluorescent protein cannot form oligomers with itself, as regular GFP does. This is the case for monomeric eGFP, which has an Ala<sup>206</sup>Lys point mutation (von Stetten et al., 2012). If this is fused to the protein of interest, the intensity histogram and therefore  $\epsilon$  will reflect the oligomeric state of the protein. First, it is therefore necessary to acquire images of monomeric eGFP and determine the monomeric quantal brightness  $\epsilon_0$  (Godin et al., 2011). This in turn is dependent on the laser power of the instrumental setup (Marsango et al., 2017). The oligomeric state of the protein of interest is determined by the measured quantal brightness, which will be a multimer of  $\epsilon_0$  as demonstrated in Figure 4.1.

Monomer	Dimer	Trimer	n-mer
			
$\varepsilon = \varepsilon_0$	$\varepsilon = 2\varepsilon_0$	$\varepsilon = 3\varepsilon_0$	$\varepsilon = n\varepsilon_0$

**Figure 4.1 The Quantal Brightness  $\varepsilon$  Depends on the Oligomeric State of the Protein.**

The quantal brightness  $\varepsilon$  of a population of monomeric eGFP-tagged proteins is a multimer of the quantal brightness of the monomeric eGFP  $\varepsilon_0$ .

The quantal brightness  $\varepsilon$  of a primarily monomeric population will be equal to  $\varepsilon_0$ , a dimeric population will be  $2 \cdot \varepsilon_0$ , a trimeric population  $3 \cdot \varepsilon_0$  and so on.

Since the development of SpIDA by Godin *et al.* the technique has been used in a number of published studies by the Milligan group in our institute to determine the quaternary structure of different GPCRs (Marsango *et al.*, 2017; Pediani *et al.*, 2016; Ward *et al.*, 2015; Zakrys *et al.*, 2014). In one study investigating  $M_1$  muscarinic acetylcholine receptors it was found that about 75 % of these receptors in the plasma membrane are monomers in the basal state. Upon treatment with the antagonist pirenzepine the receptor oligomerises and the majority of receptors now exist as dimers or higher order oligomeric complexes (Pediani *et al.*, 2016). Using simulated data, Godin *et al.* (2011) showed that the technique delivers reliable results for densities of up to 10,000 fluorophores per laser beam area. This means, SpIDA can be employed for the analysis of high-density populations, as would be expected to be the case for GLUT4 in the plasma membrane.

### 4.1.3 Hypothesis and Aims

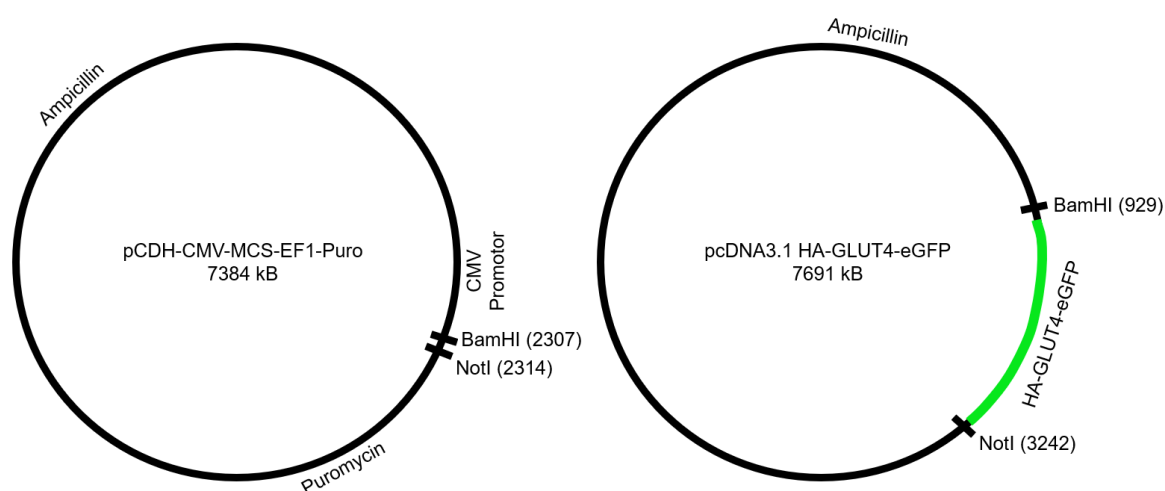
It has been shown that some GPCRs are delivered to their place in the plasma membrane in the form of oligomers (Prinster *et al.*, 2006). We hypothesised that this may be the case for GLUT4 in GSVs and the clusters reported by Lizunov *et al.* and Gao *et al.* are in fact GLUT4 oligomers that break up into monomers upon insulin stimulation.

We used SpIDA to determine the oligomeric state of GLUT4 in HeLa cells and 3T3 L1 adipocytes in the basal state and after insulin stimulation. For this, we transfected HeLa cells with a HA-GLUT4-eGFP construct and established a 3T3 L1 cell line stably expressing HA-GLUT4-eGFP. Since SpIDA is still a relatively new method and not widely used, we validated the method by repeating the published work by Padiani *et al.* who investigated the change in oligomeric state of the  $M_1$  muscarinic receptor in response to the antagonist drug pirenzepine (Padiani *et al.*, 2016). To confirm our results acquired by SpIDA, we carried out BN-PAGE of lysates from wild type 3T3 L1 adipocytes.

## 4.2 Results

### 4.2.1 Construction of a HA-GLUT4-eGFP Lentiviral Plasmid

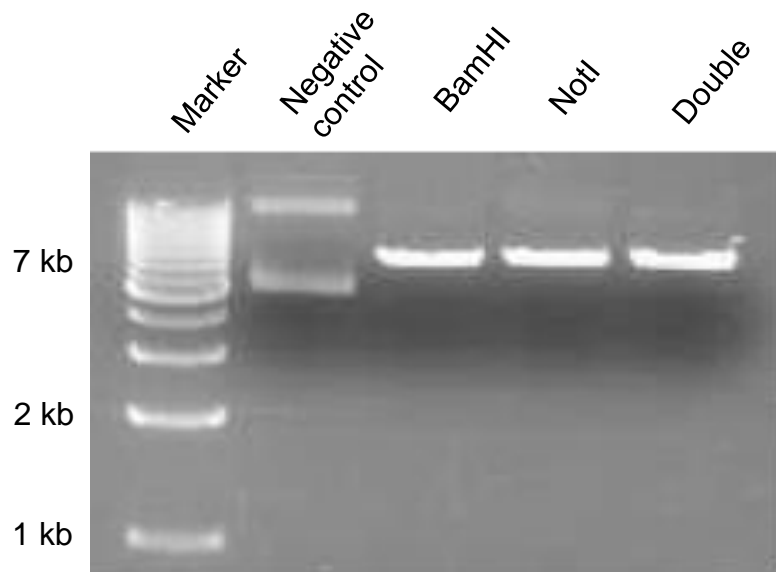
Our laboratory routinely uses HeLa and 3T3 L1 cell lines expressing HA-GLUT4-GFP. However, the construct expressed in these cells contains standard GFP which is capable of forming oligomers with itself (von Stetten *et al.*, 2012) and is therefore unsuitable for SpIDA. Hence, the first step was to construct a plasmid that contains HA-GLUT4 tagged with the monomeric eGFP described by von Stetten *et al.* However, 3T3 L1 cells are known to be difficult to transfect by traditional means (Ross *et al.*, 2003) and introduction of DNA via a viral vector has been more successful (Carlotti *et al.*, 2004).



**Figure 4.2 Maps of pCDH-CMV-MCS-EF1-Puro and pcDNA3.1 HA-GLUT4-eGFP**

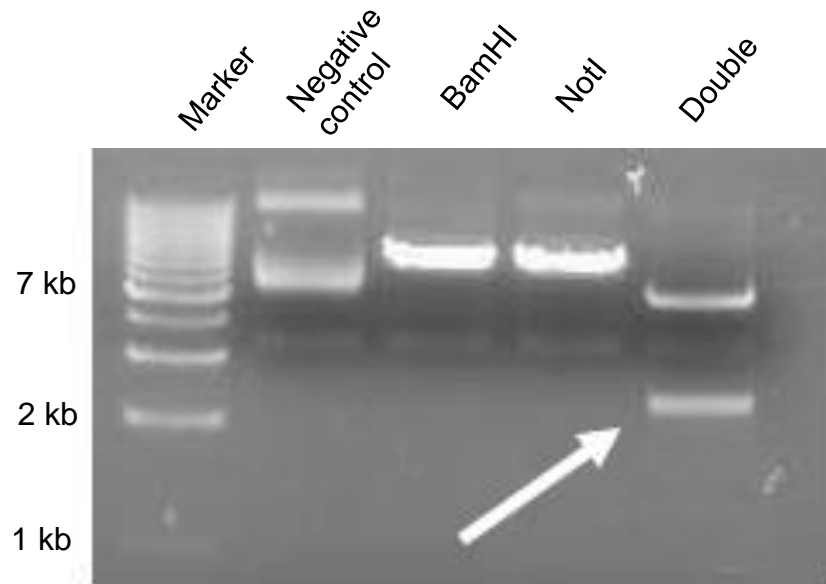
Schematic map of the vector and insert plasmids with positions of used restriction sites (BamHI and NotI), antibiotic resistances and promoter)

For this reason, we decided to construct a lentiviral plasmid containing HA-GLUT4-eGFP. As shown in Figure 4.2, we used the lentiviral vector pCDH with the CMV promoter and a puromycin resistance gene. In its multiple cloning site, this plasmid contains both a BamHI and a NotI restriction site. HA-GLUT4-eGFP was generated synthetically and introduced into the pcDNA3.1 vector flanked by the same restriction sites BamHI and NotI. Figure 4.3 and Figure 4.4 show the digested pCDH-CMV-MCS-EF1-Puro and the pcDNA3.1 HA-GLUT4-eGFP plasmid respectively. The negative control sample did not contain any endonucleases in the reaction mix and shows the typical band pattern of uncut, supercoiled plasmids, which run lower in the gel than their size would suggest. The single digests with BamHI and NotI lead to a single band the size of the linear plasmid at around 7 kb, demonstrating that the restriction sites were unique in both plasmids. When digested with both restriction endonucleases, pcDNA3.1 dropped out the HA-GLUT4-eGFP insert, which has a size of 2313 bp. The drop out in the pCDH plasmid is only 7 bp, which cannot be resolved in a 1 % agarose gel. This is why the double digested pCDH plasmid shows only a single band at around 7 kb.



**Figure 4.3 pCDH-CMV-MCS-EF1-Puro Digested with BamHI and NotI**

Representative restriction digests of pCDH-CMV-MCS-EF1-Puro using the enzymes shown on the figure performed as described in 2.2.4.4. Samples were analysed on 1 % agarose gels as described in section 2.2.4.3. The marker used was a 1 kb DNA ladder and the negative control was the reaction mix minus enzymes.

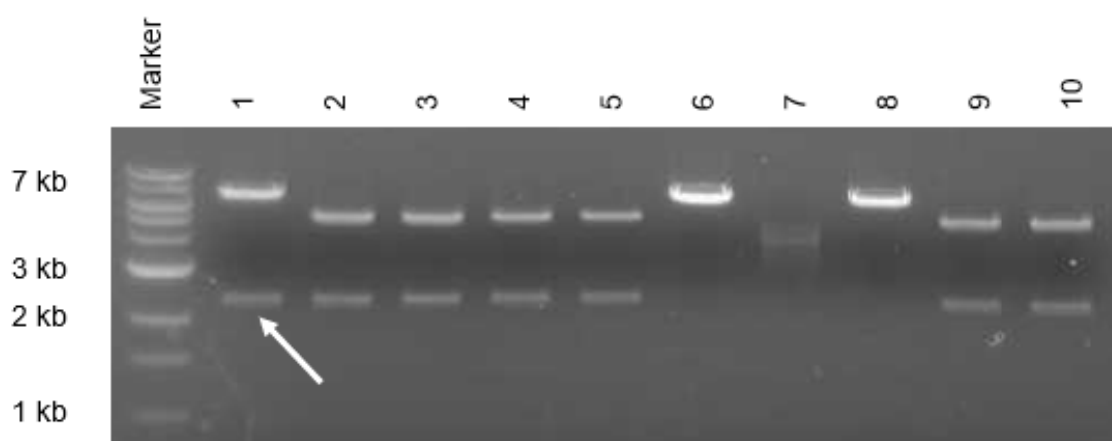


**Figure 4.4 pcDNA3.1 HA-GLUT4-eGFP Digested with BamHI and NotI**

Representative restriction digests of pcDNA3.1 HA-GLUT4-eGFP using the enzymes shown on the figure performed as described in 2.2.4.4. Samples were analysed on 1 % agarose gels as described in section 2.2.4.3. The marker used was a 1 kb DNA ladder and the negative control was the reaction mix minus enzymes. Double digestion was expected to release the 2.3 kb GLUT4-GFP cDNA insert, as indicated by the arrow.

The digested pCDH vector was combined with the HA-GLUT4-eGFP insert by molecular cloning as described in 2.2.4.5 and ten clones were picked for further analysis. The plasmid DNA was purified by Miniprep and digested with BamHI and NotI. Successful cloning should yield two bands: One at about 7 kb, which is the linearised pCDH vector, and the 2.3 kb HA-GLUT4-eGFP insert. Figure 4.5 shows the outcome of this experiment. Only sample 1 showed the desired band pattern. Sample 6 and 8 only showed one band at 7 kb, which is probably the empty pCDH vector, the single band in sample 7 is likely an empty pcDNA3.1 plasmid. Samples 2-5, 9, and 10 have the band at 2.3 kb, but the vector only has a size of about 5 kb, which corresponds to an empty pcDNA3.1 plasmid. Sample 1 was used for the generation of lentivirus.





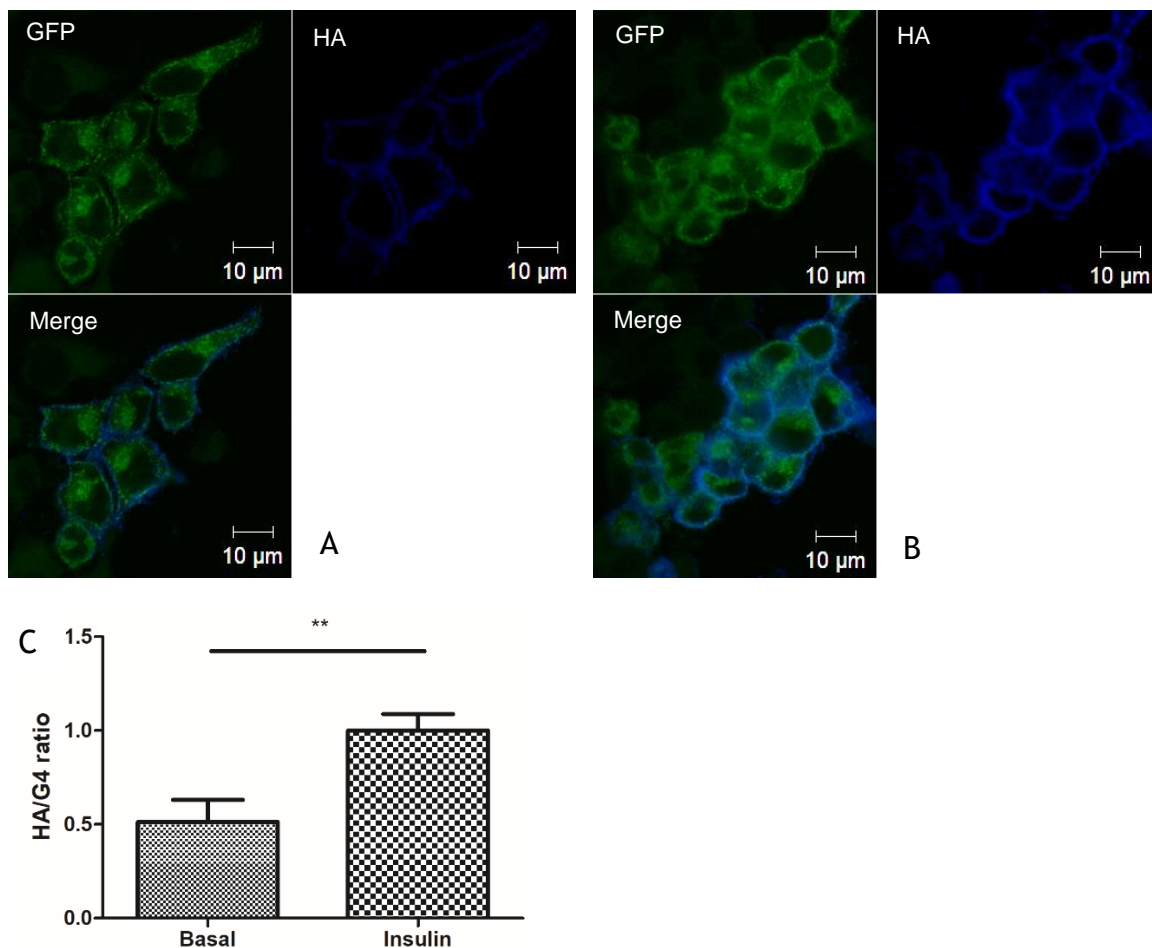
**Figure 4.5 pCDH HA-GLUT4-eGFP Clones**

Restriction digests of 10 Miniprep purified clones. Plasmids were digested with BamHI and NotI as described in 2.2.4.4 and analysed on a 1 % agarose gel as described in section 2.2.4.3. successful clones were expected to release the 2.3 kb GLUT4-GFP cDNA insert as indicated by the arrow and show the linearised pCDH plasmid at 7 kb.

### 4.2.2 Production and Testing of Lentivirus

Lentivirus was produced as described in 2.2.3. The presence of lentiviral particles in the packaging cell supernatants was confirmed using the Lenti-X GoStix tests. However, these tests only recognise the capsid protein p24 which would also be present in unfunctional viruses that do not contain the genetic information for HA-GLUT4-eGFP. In order to determine the functionality of the virus, HeLa cells were infected with the packaging cell supernatant, HA-surface stained and examined by confocal microscopy in the basal state and after insulin stimulation. Representative images of the infected cells are shown in Figure 4.6.

Transfection efficiency was low and ranged between 5 % and 20 %, this was determined by microscopy as western blotting did not yield any results, suggesting that levels of HA-GLUT4-eGFP were too low for immunoblotting. Cells expressing the construct were usually found in clusters as seen in Figure 4.6, which are probably derived from single cells that were successfully transfected. The cells showed the typical perinuclear distribution of GLUT4 in the basal state and a more dispersed pattern with a bright blue HA-ring after insulin stimulation and the HA/G4 ratio in the basal state vs insulin stimulation confirms effective GLUT4 translocation in response to insulin.



#### Figure 4.6 HeLa Cells Infected with HA-GLUT4-eGFP Lentivirus

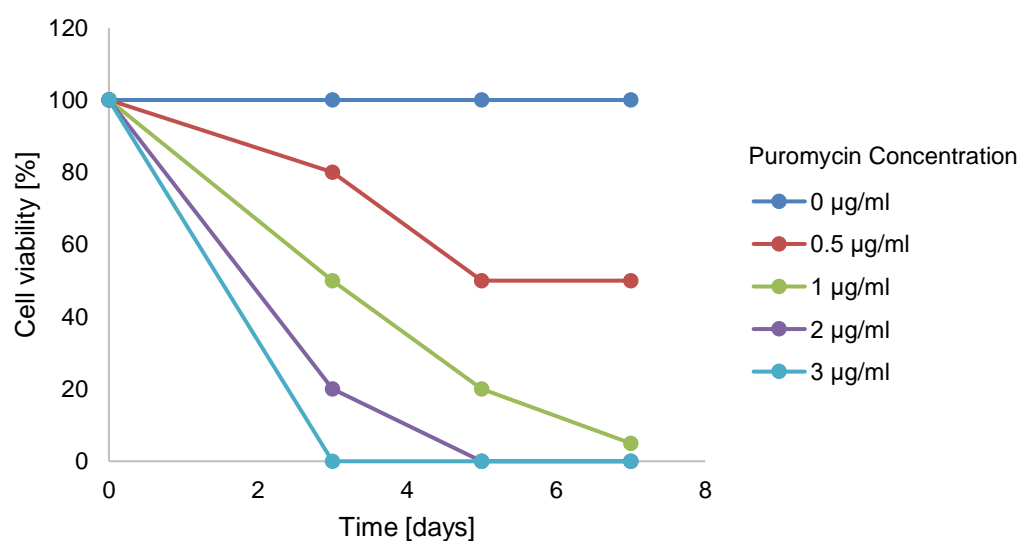
HeLa cells were infected with lentiviral supernatant as described in 2.2.3.2. Cells were incubated in serum-free medium for 2 h prior to the experiment and stimulated with 100 nM insulin for 60 min or left untreated. Cells were then fixed and stained for surface HA as described in section 2.2.2.2. A: Representative image of basal cells B: Representative image of cells after stimulation with insulin C: HA/G4 ratio, Basal:  $0.51 \pm 0.12$  (n = 30) Insulin:  $1.00 \pm 0.09$  (n = 21). Mean  $\pm$  SE. Unpaired two-tailed t-test 95 % confidence intervals p = 0.0037

Infection of 3T3 L1 cells could not be achieved with this lentivirus. Because the transfection efficiency was also very low in HeLa cells, we hypothesised that this may be due to a low virus titer. Attempts to increase this by ultracentrifugation or PEGylation failed, which is why we purchased a highly concentrated lentivirus from VectorBuilder made from the here described HA-GLUT4-eGFP construct. This custom-made lentivirus achieved a transfection efficiency of about 50 % in differentiated 3T3 L1 adipocytes at MOI = 200 (not shown) and we used this for the generation of a 3T3 L1 cell line stably expressing HA-GLUT4-eGFP, which was then used for SpIDA experiments.

### 4.2.3 Generation of a 3T3 L1 Cell Line Expressing HA-GLUT4-eGFP

The lentiviral HA-GLUT4-eGFP construct contains a puromycin resistance gene, which was used to apply selection pressure on the infected cells. The appropriate concentration of puromycin was determined by creating a kill curve. Varying concentrations of puromycin were added to confluent cultures of undifferentiated 3T3 L1 cells and cell viability was estimated by evaluating the cultures under a conventional light microscope after 3, 5, and 7 days of culture in the presence of the drug. The resulting kill curve is shown in Figure 4.7.

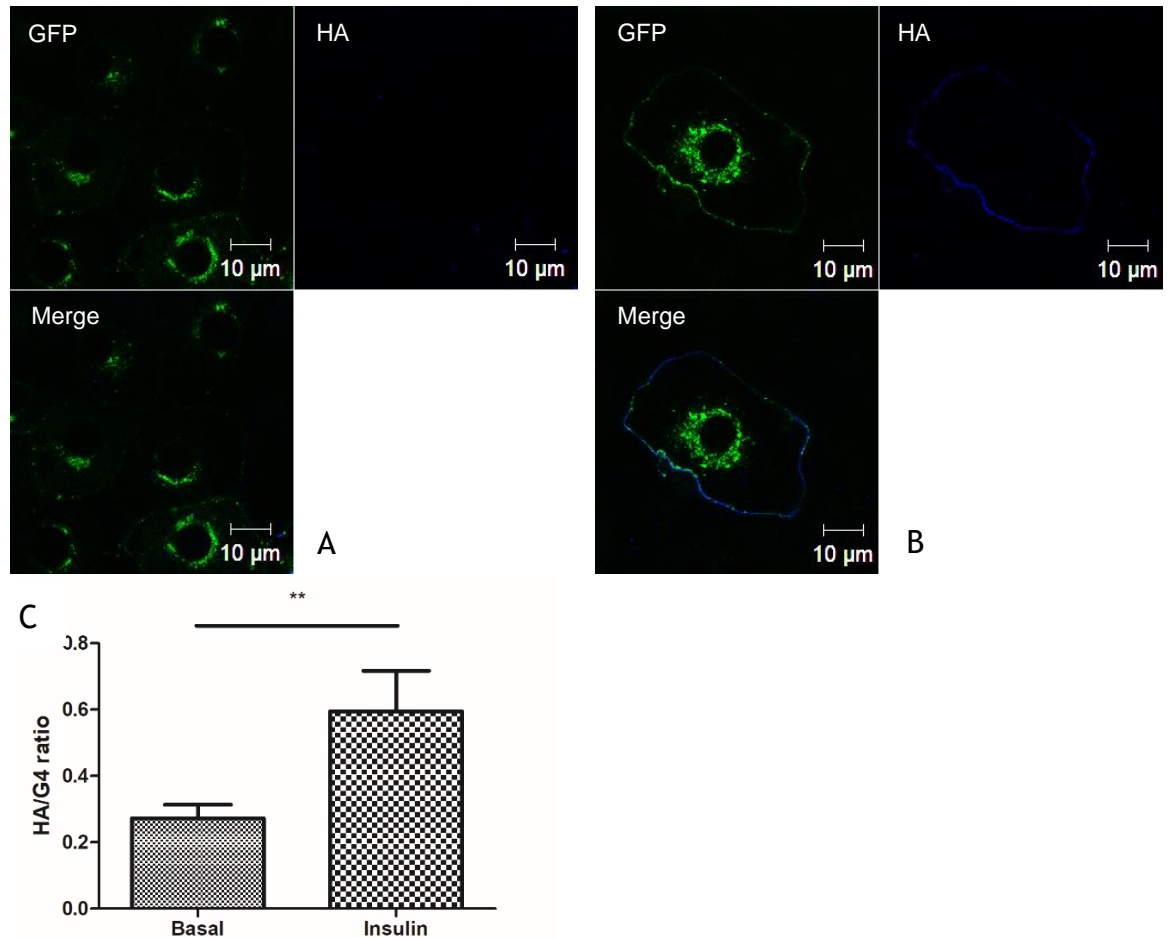
Puromycin concentrations higher than  $3 \mu\text{g}\cdot\text{ml}^{-1}$  resulted in complete cell death after 3 days of culture.  $2 \mu\text{g}\cdot\text{ml}^{-1}$  puromycin killed the entire culture after 7 days and with  $1 \mu\text{g}\cdot\text{ml}^{-1}$  puromycin about 5 % of the culture survived after 7 days. The ideal concentration for applied selection pressure was therefore decided to be  $1.5 \mu\text{g}\cdot\text{ml}^{-1}$  puromycin.



**Figure 4.7 Kill Curve of 3T3 L1 Cells Treated with Puromycin**

3T3 L1 fibroblasts were seeded in a 24 well plate and cultured until confluent. Confluent 3T3 L1 cells were then treated with 0 -  $6 \mu\text{g}\cdot\text{ml}^{-1}$  puromycin, 3 wells for each concentration and cell viability was estimated by examination under a light microscope after 3, 5, and 7 days of culture. Puromycin containing medium was changed every other day. Puromycin concentrations higher than  $3 \mu\text{g}\cdot\text{ml}^{-1}$  resulted in complete cell death after 3 days, these data points are therefore not shown. The experiment was only carried out once.

The 3T3 L1 cell line stably expressing HA-GLUT4-eGFP was generated as described in 2.2.3.3 and analysed by confocal microscopy as previously described in 4.2.2. Results are shown in Figure 4.8. Expression levels were very low and could only be picked up by confocal microscopy but not by immunoblotting. Single cells that expressed higher levels of HA-GLUT4-eGFP showed the typical perinuclear distribution and the blue HA ring after insulin stimulation. These cells were used for SpIDA.



**Figure 4.8 3T3 L1 Adipocytes Stably Expressing HA-GLUT4-eGFP**

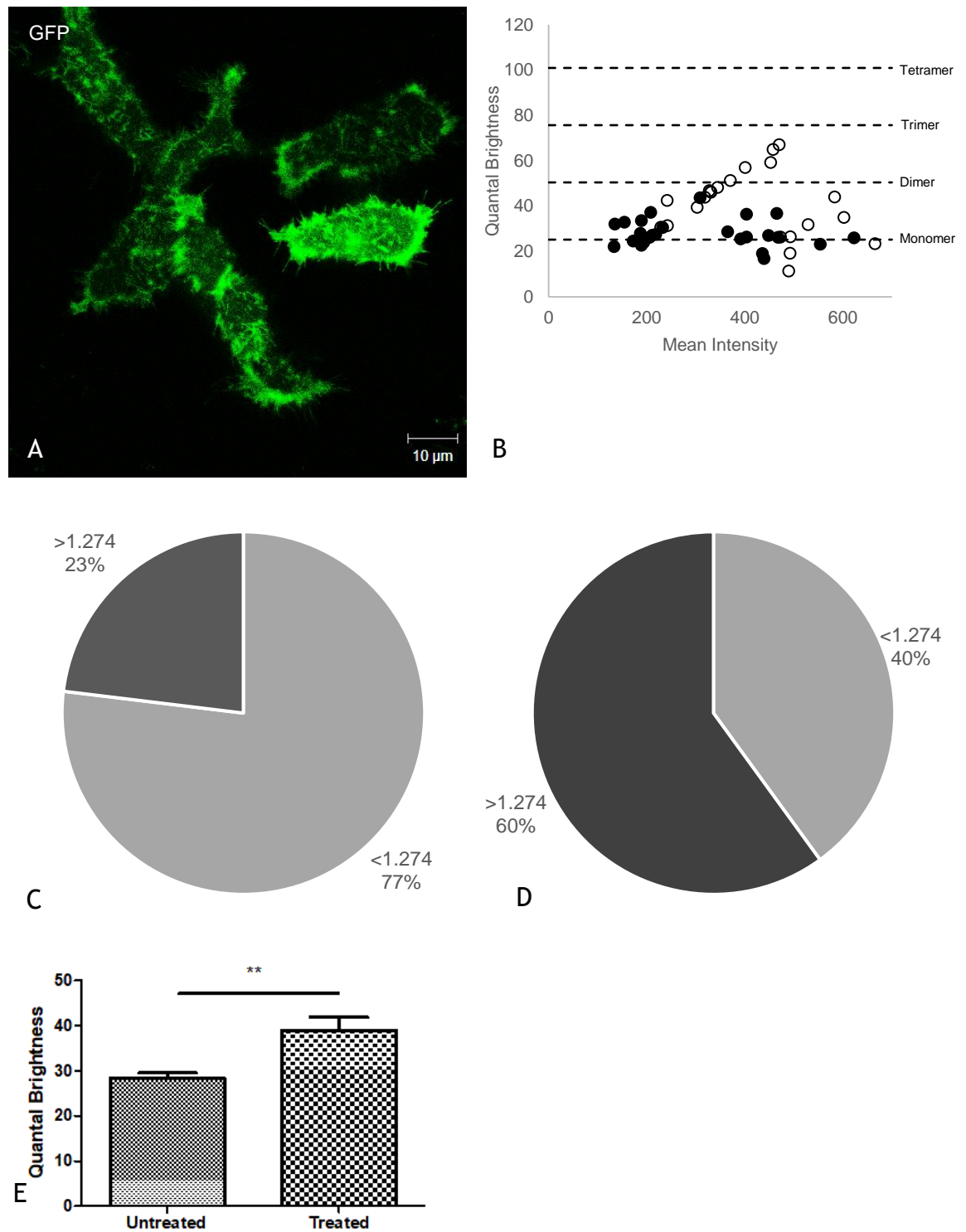
The cell line was generated as previously described in this section. Cells were incubated in serum-free medium for 2 h prior to the experiment and treated with 100 nM insulin for 20 min or left untreated. Cells were then fixed and stained for surface HA as described in section 2.2.2.2. A: Representative image of basal cells B: Representative image of cells after stimulation with insulin C: HA/GLUT4 ratio, Basal:  $0.27 \pm 0.04$  (n = 12) Insulin:  $0.60 \pm 0.10$  (n = 4). Mean  $\pm$  SE. Unpaired two-tailed t-test 95 % confidence intervals p = 0.0053

#### 4.2.4 Validation of the Method – Oligomeric State of the M<sub>1</sub> Muscarinic Receptor

Pediani *et al.* used SpIDA to study the oligomeric state of the M<sub>1</sub> muscarinic receptor. They generated a Flp-In T-REx 293 cell line stably expressing eGFP-tagged human M<sub>1</sub> after induction with doxycycline and performed SpIDA. They found that the majority of the receptor (69.1 %) in the basolateral membrane is monomeric and the remaining 30.9 % either dimeric or of higher oligomeric organisation. Treatment with the antagonistic M<sub>1</sub> ligand pirenzepine then reversed this distribution and only 26.5 % of the receptor was monomeric (Pediani *et al.*, 2016). We repeated this experiment with the same cell line that was used in this study, kindly provided by Dr Richard Ward and we found similar results that are shown in Figure 4.9.

The quantal brightness of monomeric eGFP in this experimental setup with the laser power at 6 % had previously been determined and was  $\epsilon_0 = 25.24$  (Pediani *et al.*, 2016). By normalising the values of the single  $\epsilon$  measurements of monomeric eGFP to  $\epsilon_0$ , the monomeric equivalent unit (MEU) of each measurement was obtained. Pediani *et al.* found that 75 % of all monomeric eGFP MEUs were below 1.274. Populations were therefore considered to be monomeric if their  $\epsilon$  was less than  $1.274 \cdot \epsilon_0$ . After induction of M<sub>1</sub>-eGFP expression with doxycycline, green fluorescent cells could be observed under the confocal microscope. The mean quantal brightness  $\epsilon$  of these untreated cells was  $28.24 \pm 1.21$  (Mean  $\pm$  SE,  $n = 26$ ). This value is very close to the quantal brightness of monomeric eGFP. The monomeric M<sub>1</sub> population in untreated cells was 77 %. After treatment with the M<sub>1</sub> antagonist pirenzepine, this decreased to 40 % and the mean  $\epsilon$  was  $39.03 \pm 2.88$  (Mean  $\pm$  SE,  $n = 25$ ), significantly greater than in untreated cells as seen in Figure 4.9.

With these results mirroring the published study by Pediani *et al.* we felt confident that the SpIDA experiments were carried out correctly.

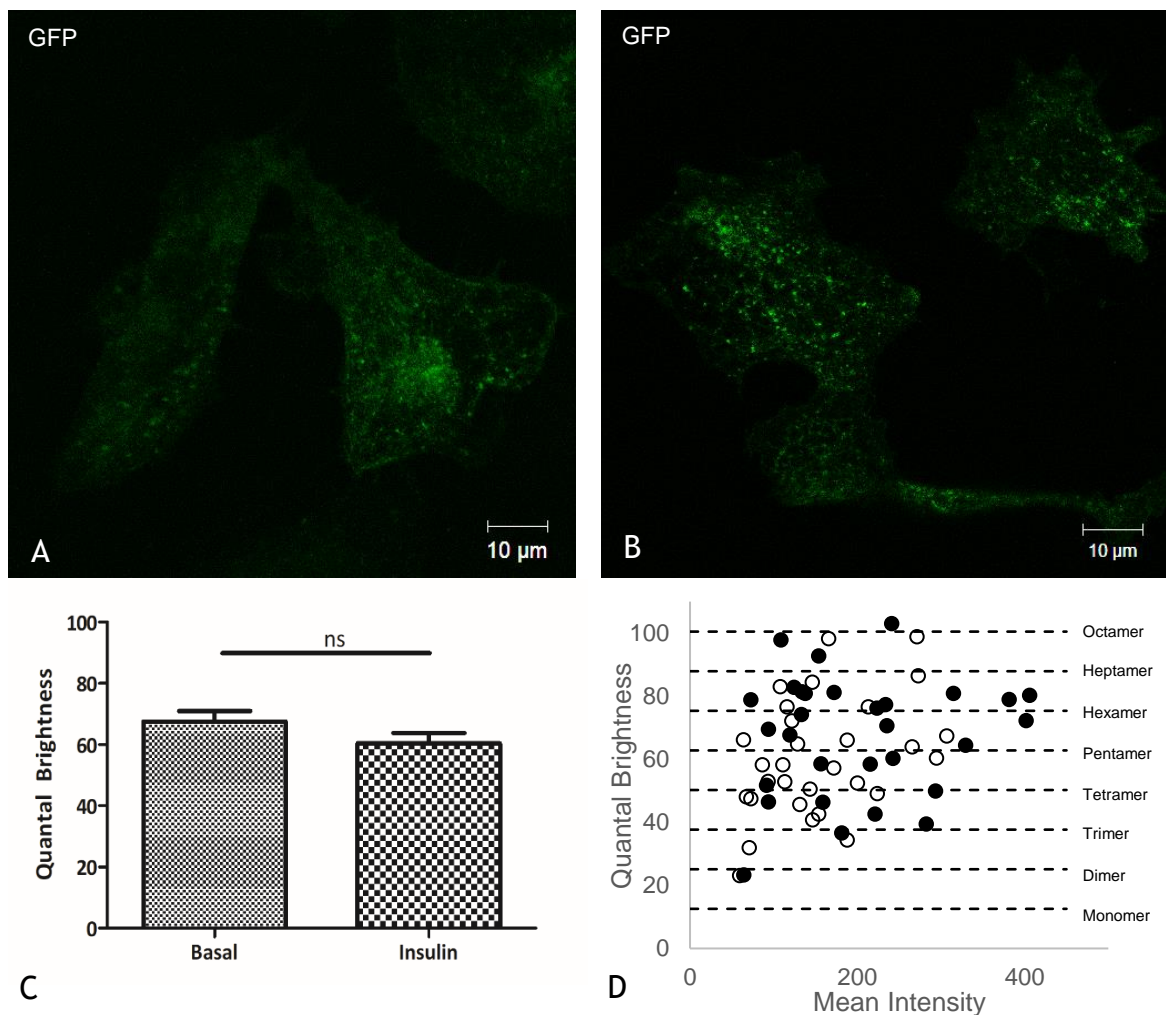


### Figure 4.9 Oligomeric State of the M<sub>1</sub> Muscarinic Receptor

Flp-In T-REx 293 cell line stably expressing eGFP-tagged human M<sub>1</sub> were induced with 100 ng·ml<sup>-1</sup> doxycycline for 24 h and treated with 10 μM pirenzepine for 24 h or left untreated. Cells were imaged live. SpIDA was carried out as described in 2.2.8.2 A: Representative image of basolateral membrane of treated cells. B: Quantal brightness and mean fluorescence intensity of single ROIs. Filled symbols: untreated, open symbols: treated with 10 μM pirenzepine C: Distribution of monomeric (< 1.274) and higher oligomeric state (> 1.274) M<sub>1</sub> in untreated cells. D: Distribution of monomeric (< 1.274) and higher oligomeric state (> 1.274) M<sub>1</sub> in cells treated with 10 μM pirenzepine. E: Mean quantal brightness of untreated cells and cells treated with 10 μM pirenzepine. Untreated: 28.24 ± 1.21 (n = 26) Treated: 39.03 ± 2.88 (n = 25). Mean ± SE. Unpaired two-tailed t-test, 95 % confidence intervals p = 0.0011.

### 4.2.5 Oligomeric State of GLUT4 as by SpIDA

SpIDA was carried out in both HeLa and 3T3 L1 cells to add to the comparison of the two cell types in Chapter 3. HeLa cells were infected with the lentivirus, and the previously described HA-GLUT4-eGFP 3T3 L1 cell line was used for SpIDA in adipocytes. The quantal brightness of monomeric eGFP in this experimental setup with the laser power at 2 % had previously been determined and was  $\epsilon_0 = 12.56$  (Zakrys et al., 2014).



**Figure 4.10 Oligomeric State of GLUT4 in HeLa Cells**

HeLa cells were infected with lentiviral supernatant as described in 2.2.3.2. Cells were incubated in serum-free medium for 2 h prior to the experiment and treated with 100 nM insulin for 60 min or left untreated. Cells were imaged live. SpIDA was carried out as described in 2.2.8.2 A: Representative image of basolateral membrane of HeLa cells expressing HA-GLUT4-eGFP in the basal state. B: Representative image of basolateral membrane of HeLa cells expressing HA-GLUT4-eGFP after insulin stimulation. C: Mean quantal brightness in the basal state and after insulin stimulation. Basal:  $67.50 \pm 3.47$  ( $n = 30$ ) Insulin:  $60.36 \pm 3.40$  ( $n = 30$ ). Mean  $\pm$  SE. Unpaired two-tailed t-test, 95 % confidence intervals  $p = 0.1463$ . D: Quantal Brightness and mean fluorescence intensity of single ROIs. Filled symbols: Basal, open symbols: Insulin

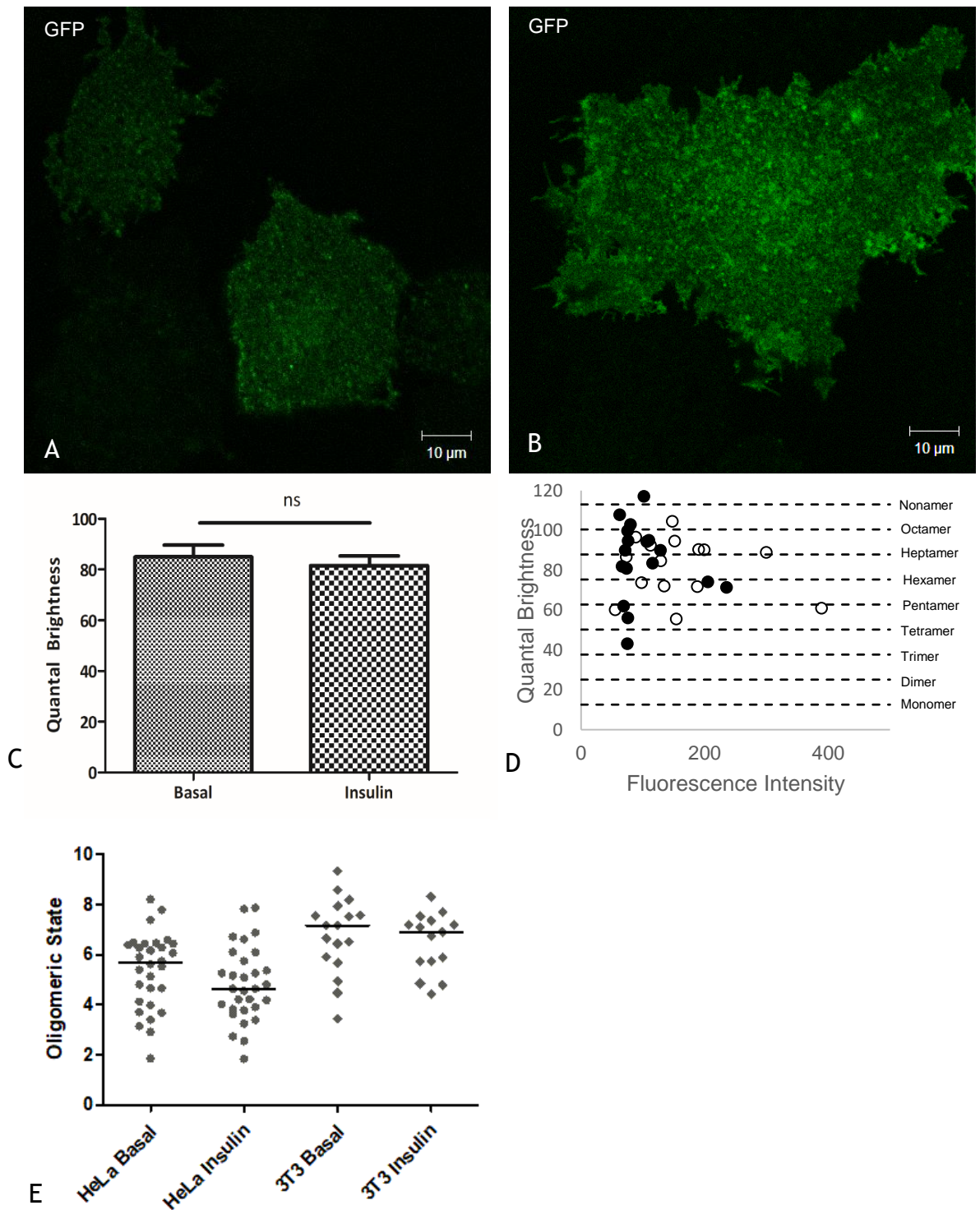
Figure 4.10 shows the basolateral membrane of HeLa cells expressing the construct in the basal state (A) and after insulin stimulation (B). It is difficult to judge the effect of insulin on this cell type as these cells are less insulin sensitive, which has been discussed in Chapter 3. The mean fluorescence intensity in the analysed ROIs was not affected in this experiment (Figure 4.10 D, x-axis) but HA-GLUT4-eGFP translocated to the cell surface in response to insulin in these cells as has been shown in Figure 4.6.

The mean quantal brightness of HA-GLUT4-eGFP in this cell type was 67.50 in the basal state and 60.36 after insulin stimulation, which is not a significant difference. It is however substantially higher than  $\epsilon_0$  and most ROIs indeed had values for  $\epsilon$  that suggest that GLUT4 is expressed in complexes of high oligomeric order. According to Figure 4.10 D, complexes consisted of at least two and up to eight GLUT4 molecules and there was no difference between basal cells and cells that had been stimulated with insulin.

HeLa cells do not express endogenous GLUT4 (Sadler et al., 2013) and it is conceivable that they lack other proteins that are part of the insulin signalling pathways. It is possible that our hypothesis that the oligomeric state of GLUT4 is influenced by insulin is still valid in adipocytes, but not in HeLa cells if the oligomerisation or de-oligomerisation requires other proteins that are not present in this cell type. We therefore conducted the same experiment in 3T3 L1 adipocytes. The results are shown in Figure 4.11.

Successful translocation of HA-GLUT4-eGFP in 3T3 L1 adipocytes was demonstrated in Figure 4.8 and the fluorescence intensity increased more visibly in this cell type than in HeLa cells. The mean quantal brightness was higher than in HeLa cells, with 84.99 in basal cells, but also remained the same after insulin stimulation, when the mean quantal brightness was 81.56. Similar to HeLa cells, the data suggests that GLUT4 is not monomeric in the cell membrane of adipocytes but exists as an oligomer. The size ranges from trimers to nonamers, which is larger than that observed in HeLa cells. The majority of ROIs measured a quantal brightness that corresponds to the size of a Heptamer, which is reflected in the data's median shown in Figure 4.11 E.





### Figure 4.11 Oligomeric State of GLUT4 in 3T3 L1 Adipocytes

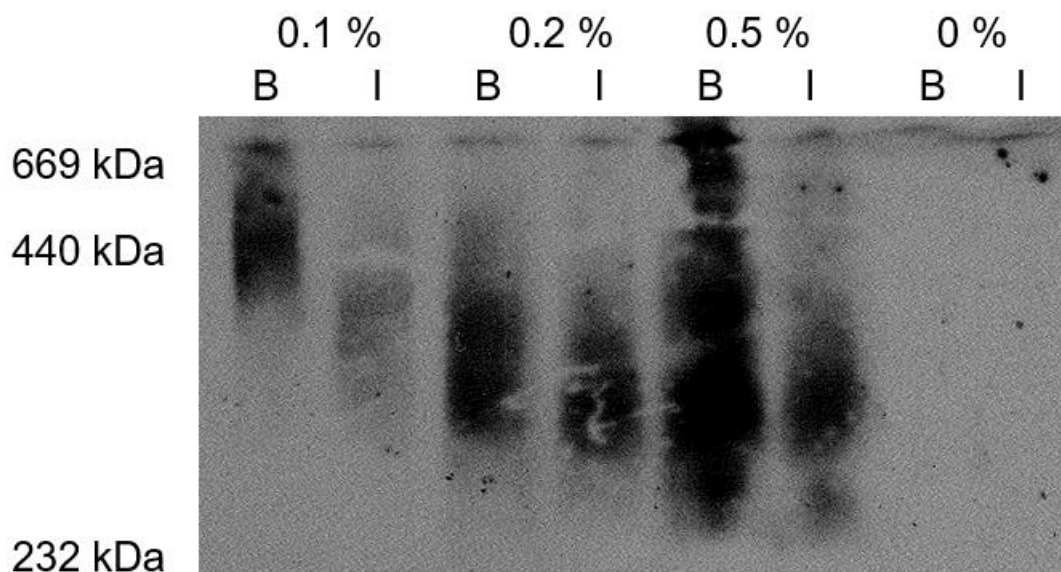
The 3T3 L1 cell line described in section 4.2.3 was used for this experiment. Cells were incubated in serum-free medium for 2 h prior to the experiment and treated with 100 nM insulin for 20 min or left untreated. Cells were imaged live. SpIDA was carried out as described in 2.2.8.2.

**A:** Representative image of basolateral membrane of 3T3 L1 adipocytes expressing HA-GLUT4-eGFP in the basal state. **B:** Representative image of basolateral membrane of 3T3 L1 adipocytes expressing HA-GLUT4-eGFP after insulin stimulation (100 nM, 20 min). **C:** Mean quantal brightness in the basal state and after insulin stimulation. Basal:  $84.99 \pm 4.65$  ( $n = 17$ ) Insulin:  $81.56 \pm 3.84$  ( $n = 15$ ). Mean  $\pm$  SE. Unpaired two-tailed t-test, 95 % confidence intervals  $p = 0.5800$ .

**D:** Quantal Brightness and mean fluorescence intensity of single ROIs. Filled symbols: Basal, open symbols: Insulin. **E:** Comparison of oligomeric states in HeLa cells and in 3T3 L1 adipocytes. Shown are single data points as the oligomeric state, as well as the median. HeLa Basal: 5.69 ( $n = 30$ ) HeLa Insulin: 4.63 ( $n = 30$ ) 3T3 L1 Basal: 7.16 ( $n = 17$ ) 3T3 L1 Insulin: 6.90 ( $n = 15$ )

### 4.2.6 Oligomeric State of GLUT4 as by BN-PAGE

Proteins subjected to BN-PAGE maintain their native conformation and stay in complexes. BN-PAGE does not allow the use of SDS as this would denature the proteins and protein complexes. However, GLUT4 is a membrane protein and therefore has to be solubilised by adding a mild detergent. For successful BN-PAGE the choice of an appropriate detergent is crucial. This is particularly true for membrane proteins. The detergent has to be powerful enough to solubilise the membrane, but at the same time it has to be mild enough to leave the protein or protein complex of interest intact. The non-ionic detergents digitonin, Triton X-100, and *n*-dodecyl- $\beta$ -D-maltoside are the most frequently used detergents for the separation of membrane proteins by BN-PAGE (Reisinger & Eichacker, 2008). We therefore decided to test two of these detergents, Triton X-100 (subsequently referred to as Triton) and digitonin, for the solubilisation of GLUT4 and following BN-PAGE.



**Figure 4.12 BN-PAGE of 3T3 L1 Lysates**

Lysates of 3T3 L1 adipocytes were prepared from cells in the basal state (B) and after stimulation with insulin (100 nM, 20min) (I) and incubated with 0.1 %, 0.2 %, 0.5 %, and 0 % Triton on ice as outlined in 2.2.6.1. Equal volumes of samples were run on a blue native gel (see section 2.2.6.2) alongside the BN-PAGE Marker (see 2.1.1) and immunoblotted for GLUT4 (see section 2.2.6.3). Protein concentrations in the samples were considered equal due to identical sample preparation. The marker was not visible on the x-ray film and was denoted manually after comparison with the nitrocellulose membrane. The immunoblot shown is a representative image from 3 repeats.

Samples were incubated with either digitonin or Triton at concentrations ranging from 0 % to 0.5 %. BN-PAGE and western blotting was carried out as described in 2.2.6. Figure 4.12 shows a representative blot for Triton incubated samples, incubation with digitonin did not lead to a clean blot and is therefore not shown. The negative control sample with 0 % Triton did not show a signal, indicating that solubilisation with the detergent was successful. With increasing Triton concentration, a band of about 300-350 kDa became visible, indicating that this band was indeed a GLUT4 complex consisting of 6 to 7 monomers, since monomeric GLUT4 has a size of about 54 kDa (Fukumoto et al., 1989).

### 4.3 Discussion

SpIDA requires the expression of the protein of interest as a chimera with a fluorescent protein that does not form oligomers with itself, such as eGFP (von Stetten et al., 2012). Part of this project was therefore to generate an HA-GLUT4-eGFP construct that can be expressed in HeLa cells and 3T3 L1 adipocytes. This was complicated by the fact that 3T3 L1 adipocytes are notoriously difficult to transfect (Ross et al., 2003), which is why the construct had to be delivered by a lentivirus (Carlotti et al., 2004). We generated such a virus and successfully transfected both HeLa cells and 3T3 L1 cells with HA-GLUT4-eGFP, however, expression levels in adipocytes were very low, which made carrying out SpIDA difficult. The reason for this appears to be the promoter in the host plasmid. Differentiated 3T3 L1 adipocytes suppress the CMV promoter, which makes it very difficult to obtain good expression levels (Brewer et al., 2014). While low expression levels complicate the detection of the protein by immunoblotting or even by microscopy, it also means that the cell trafficking systems are unlikely to be saturated with the HA-GLUT4-eGFP fusion protein. This means that the protein is more likely to be folded and undergo posttranslational modifications correctly, which makes experimental artefacts less probable (Tate, 2001). This is particularly advantageous in a study such as this one, as oligomerisation could be influenced by an altered quaternary structure of GLUT4, thus possibly leading to oligomerisation of the protein, when this would not be the case in correctly folded and glycosylated GLUT4 or vice versa.

Results from SpIDA and BN-PAGE both suggest that GLUT4 exists as a complex of high oligomeric order in the basolateral membrane of 3T3 L1 adipocytes and HeLa cells. Adipocytes contain predominantly hexamers, heptamers, and octamers, while most complexes in HeLa cells are slightly smaller, with more tetramers and pentamers being detected in this cell type. With regards to the comparison of the two cell types in the previous chapter, the data adds more depth. The HeLa cell line behaves similarly to 3T3 L1 adipocytes with respect to GLUT4 translocation as previously discussed. In addition, the protein also oligomerises, although to a lesser extent than in adipocytes. This may be due to other GLUT4 translocation machinery being missing in this cell type, which makes it tempting to assume that the oligomeric state of GLUT4 does play a role in GLUT4 trafficking.

The results obtained by SpIDA are to be considered carefully, as the technique is not without limitations. For one, cells were imaged on a confocal microscope with the focal plane focused on what we considered to be the plasma membrane. As discussed in 3.1.1, the axial resolution in confocal microscopy is severely limited, which means that the obtained signal is not only from HA-GLUT4-eGFP molecules located in the plasma membrane, but there will be a considerable amount of background fluorescence from GSVs approaching the membrane. This background signal may mask the dispersal of monomers in the plasma membrane. For this reason, a TIRF microscope may be more suitable for the analysis. However, this would have meant that we could not use the monomeric quantal brightness value  $\epsilon_0$  previously obtained by Zakrys *et al.* who used the same instrument and experimental parameters for their study. The experiments necessary to determine all these parameters for a different experimental set-up would have gone beyond the scope of this study. In past publications, SpIDA has mostly been used to investigate monomers or dimers (Barbeau, Godin, et al., 2013; Pediani et al., 2016; Ward et al., 2015; Zakrys et al., 2014). Although the method is theoretically capable of dissolving higher oligomeric structures, it is limited in that respect (Barbeau, Swift, et al., 2013). Especially when the cell line is expressing the protein endogenously as is the case for 3T3 L1 adipocytes and GLUT4, oligomers could be made up of eGFP-tagged GLUT4 and endogenous GLUT4, but only the fluorescently labelled molecules are taken into consideration. Heterooligomers pose a similar problem,

as non-labelled complex components are not detected. With regards to our findings that GLUT4 forms greater complexes in 3T3 L1 adipocytes than in HeLa cells this could mean that the complexes are actually even bigger in reality, either due to additional untagged GLUT4 or other proteins that are part of the complex.

For the BN-PAGE experiments we used whole cell lysates instead of membrane fractions for practical reasons; protein complexes are often very sensitive and must be handled carefully. This experiment had to be carried out exclusively in the cold room at 4 °C and without stopping points, as freeze/thawing or sample preparation at room temperature led to breakup of the complexes and no signal was obtained on the resulting immunoblot. The fact that we used whole cell lysates essentially means that BN-PAGE has the same limitation as SpIDA on the CLSM, namely that the analysis is not restricted to the plasma membrane and potential dispersal effects may be masked. However, a subcellular fractionation in addition to the already very extensive process was considered too impractical. The sensitive nature of many protein complexes is what limits the technique the most. Proteins and protein complexes are very prone to denaturation. We experienced this problem when carrying out steps of the sample preparation outside the cold room at more than 4 °C. In this case we could not detect any bands in the immunoblot, suggesting that the GLUT4 complex is extremely unstable at higher temperatures. Another important parameter is the detergent that is used to solubilise membrane proteins. Often, a mild detergent such as digitonin is used to avoid protein denaturation. At the same time, the detergent has to be potent enough to sufficiently solubilise the hydrophobic membrane proteins. In the case of ATP synthase for example, the apparent oligomeric state depends on the concentration of Triton (Wittig et al., 2006).

We have experienced all of these issues during our BN-PAGE experiments and even when finally successful, the resulting immunoblots only showed smeared, blotchy bands different from conventional SDS-PAGE immunoblots (as seen in Figure 4.12). Another shortcoming of this experiment is that we could not run a suitable control sample. We can therefore only assume that the observed bands are indeed GLUT4 complexes. The fact that the SpIDA experiments yielded the

same result makes this more plausible and SpIDA was carried out correctly as the method had been validated by duplicating the experiment from Pediani *et al.*

The question remains why GLUT4 forms an oligomer of such high order. It is not a very surprising discovery, since about 35 % of cellular proteins are thought to be oligomeric with the average oligomeric state being tetrameric (Ali & Imperiali, 2005). Little research has been undertaken in the investigation of the quaternary structure of GLUT4, but homology modelling based on the crystal structure of GLUT1 has shown that GLUT4 is likely to form a pore through which glucose can travel, furthermore ATP- and cytochalasin B binding sites were identified (Mohan et al., 2009). This makes it unlikely that oligomerisation is needed for the functionality of the transporter. It is however plausible that GLUT4 molecules have a tendency to attract each other based on their tertiary structure and that the conditions in the membrane thermodynamically favour the association to oligomers. This would also explain the broad range of oligomer sizes and the oligomers may be smaller in HeLa cells due to the different membrane phospholipid composition.

Indeed, GLUT1 has long been known to exist as an oligomer and its function is controlled by its oligomeric state (D. N. Herbert & Carruthers, 1991, 1992). Performing size exclusion chromatography, Herbert and Carruthers found that purified GLUT1 from erythrocytes exists as a mixture of homodimers and homotetramers. The native structure *in vivo* is understood to be tetrameric, stabilised by intramolecular, extracellular disulphide bonds (Zottola et al., 1995), while purification in the presence of an alkaline reductant produces dimers. The ability of GLUT1 to transport glucose is indeed dependent on its oligomeric structure. While the GLUT1 dimer only exhibits one glucose binding site, the tetramer presents multiple binding sites. Interestingly, the dimer also presents more binding sites for the glucose transport inhibitor cytochalasin B than the tetrameric form (D. N. Herbert & Carruthers, 1992). Based on the fact that GLUT4 is structurally very similar to GLUT1, it is conceivable that it forms oligomers in a similar manner.

This discovery in itself is interesting; however, insulin does not appear to have any influence on the size of the oligomers, which contradicts our hypothesis that GLUT4 clusters are in fact highly oligomerised GLUT4 complexes that break up

into monomers under the influence of insulin. Based on the limitations of SpIDA and BN-PAGE, it is important to note that the hypothesis cannot be rejected entirely. It is possible that particularly SpIDA is simply not powerful enough to detect the dispersal of GLUT4 complexes into monomers and monomeric GLUT4 is too small to be detected by BN-PAGE, so this technique cannot be used as a dispersal assay and only served in this section as validation of the GLUT4 oligomer size.

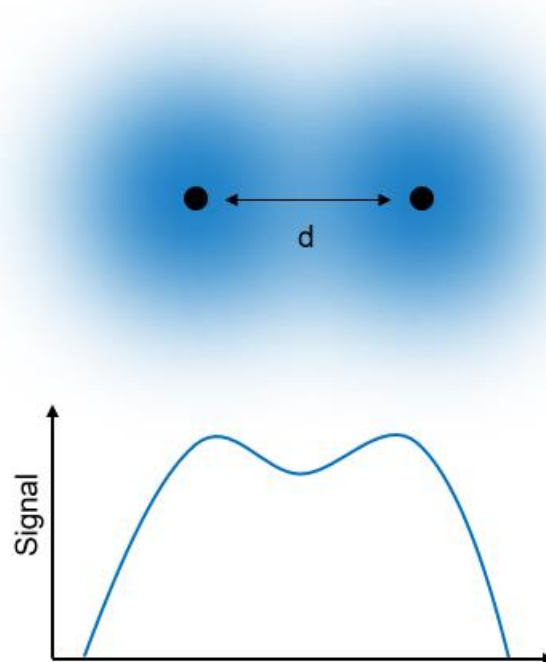
Either way, SpIDA could not be used as a tool to visualise and quantify GLUT4 dispersal. We therefore decided to attempt to do this with a much more potent microscopy technique and ventured into the for us unknown territories of super-resolution microscopy.

## Chapter 5 Clustering and Dispersal of GLUT4 in the Plasma Membrane

### 5.1 Introduction

#### 5.1.1 Super Resolution Microscopy

Chapter 3.1 has introduced the principles of fluorescence microscopy. Instruments such as confocal or TIRF microscopes enable advanced image acquisition with a small signal to noise ratio and little background fluorescence. However, the resolution is limited even in state-of-the-art light microscopes. Resolution is defined as the smallest distance between two points that can be resolved, which is illustrated in Figure 5.1. This is known as the diffraction limit. The signal coming from a fluorophore is visible as a blur around the source. Translated into the image plane, this is known as the point spread function (PSF). When the signal intensity is plotted along the xy plane, the PSF is visualised as a three-dimensional peak (Rottenfusser et al., 2019). Two points can be distinguished from each other if their PSFs are clearly distinguishable. When the peaks merge, it is not clear anymore whether the signal comes from one or more sources.



**Figure 5.1 Principle of Resolution**

Point sources emit light as circular intensity profiles. When the signal is plotted over the xy plane, this is visualised as peaks. The resolution is defined as the smallest distance  $d$  between two point sources that still results in separate peaks in the signal plot.



The diffraction limit is dependent on the wavelength  $\lambda$  of the light used as well as the numerical aperture (NA) of the objective. It was defined by Ernst Karl Abbe in 1873 (Abbe, 1873). According to the diffraction limit, the smallest resolvable distance  $d$  between two points is

$$d = \frac{\lambda}{2NA} \quad (5-1)$$

The value for NA typically lies between 1.4 and 1.6, the wavelength of the laser depends on the fluorophore that is excited. The excitation maximum for GFP for example is 488 nm (Patterson et al., 2001). For this example and a NA of 1.6, the resolution would be approximately 150 nm according to equation (5-1). However, this theoretical value does not take into consideration slight imperfections in the instrumental setup and background fluorescence. 180 - 200 nm is a much more realistic value for most applications (Heintzmann & Ficz, 2006). Even with a perfect instrument and a high signal to noise ratio, the diffraction limit is a physical boundary that cannot be breached. The only way to accurately image structures that are below the resolution limit by light microscopy is therefore to circumvent the Abbe diffraction limit. This is done in super resolution microscopy.

Super resolution microscopy techniques can be divided into two categories, depending on how the diffraction limit is evaded (B. Huang et al., 2010). In the first category, fluorescent properties are modulated by means of patterned illumination, which results in not all fluorophores emitting at the same time. Structured Illumination Microscopy (SIM) and Stimulated Emission Depletion (STED) Microscopy belong in this category. In SIM a grid pattern is superposed on the sample, which results in the interference of the signals and subsequently the occurrence of Moiré fringes. By rotating the grid pattern, a series of images is recorded, which can be reconstructed to an image with a resolution of about half the diffraction limit (Gustafsson, 2000). In STED, a depletion laser is used in addition to the excitation laser. This depletion laser is donut shaped and negatively interferes with the signal outside the focal point of the excitation laser, which effectively narrows the PSF (Hell & Wichmann, 1994). The second category of super resolution microscopy is also known as single molecule

localisation microscopy (SMLM), which has been briefly mentioned in section 1.7.5. SMLM avoids the Abbe diffraction limit altogether by focusing on localisation of single molecules whose PSFs do not overlap with those of neighbouring molecules. Once light is emitted by isolated molecules, the resolution is only limited by the localisation precision, which can be in the nanometre scale (Ober et al., 2004). The key difference is that the obtained data is not a true image of the sample but only a set of coordinates of detected localisations. Stochastic Optical Reconstruction Microscopy (STORM) (Rust et al., 2006) and Fluorescence Photoactivation Localisation Microscopy (FPALM) (Betzig et al., 2006) belong in this category.

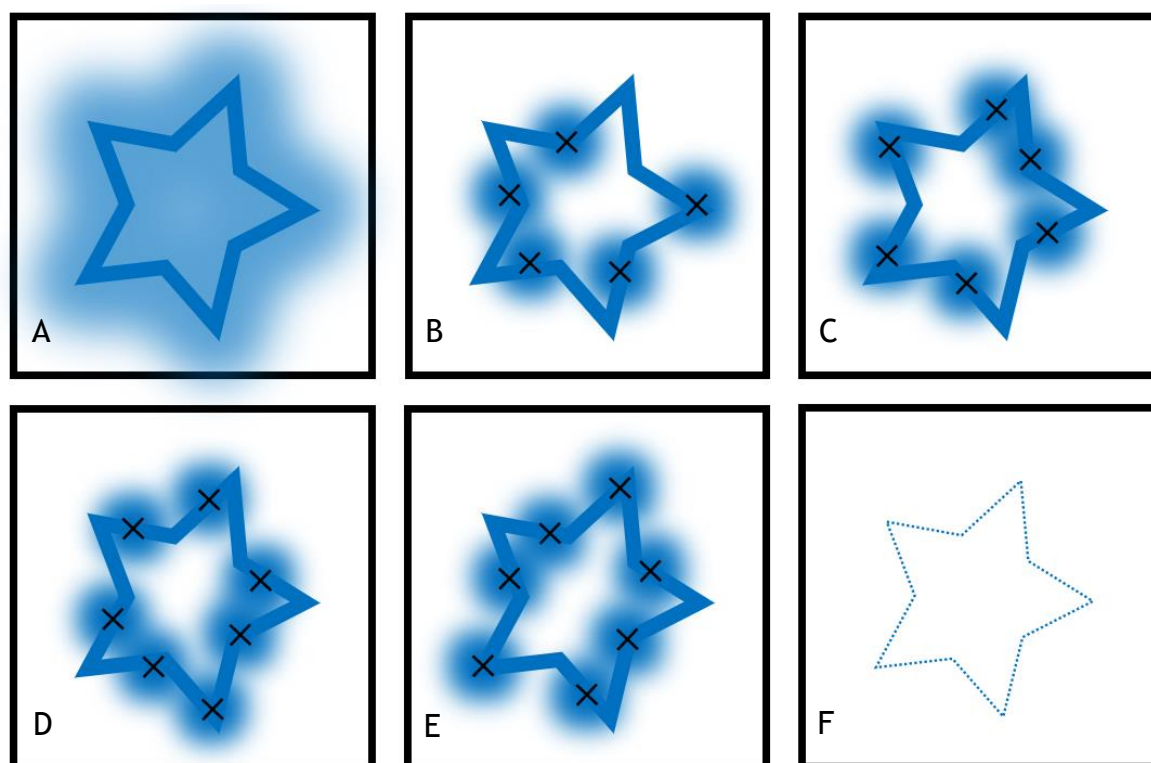
### 5.1.2 Stochastic Optical Reconstruction Microscopy

The position of a fluorophore could be determined at very high precision for a long time by fitting a Gaussian function over its PSF (Gelles et al., 1988). The localisation precision  $\Delta x$  can be approximated by

$$\Delta x = \frac{\sigma}{\sqrt{n}} \quad (5-2)$$

with  $\sigma$  being the standard deviation of the PSF and  $n$  being the number of photons collected (Thompson et al., 2002).

The localisation accuracy, however, does not directly translate to a high resolution, since the density of fluorophores in stained biological samples is usually too high and PSFs overlap, making it impossible to localise single molecules. SMLM techniques such as STORM circumvent this problem by using fluorophores that can switch on and off, which appears as blinking during imaging. Figure 5.2 illustrates the principle of the technique. When imaging the specimen over a long time, only a fraction of fluorophores is switched on in each frame, which can be localised with high precision. Stochastically, each frame contains a different subset of fluorophores. Combining the localisations of all frames allows reconstruction of the image with a resolution of up to 20 nm (Rust et al., 2006). The resolution is not restricted by the diffraction limit of light anymore, but only by how accurately the position of a single fluorophore can be determined (B. Huang et al., 2010).



**Figure 5.2 Principle of STORM and other SMLM Techniques**

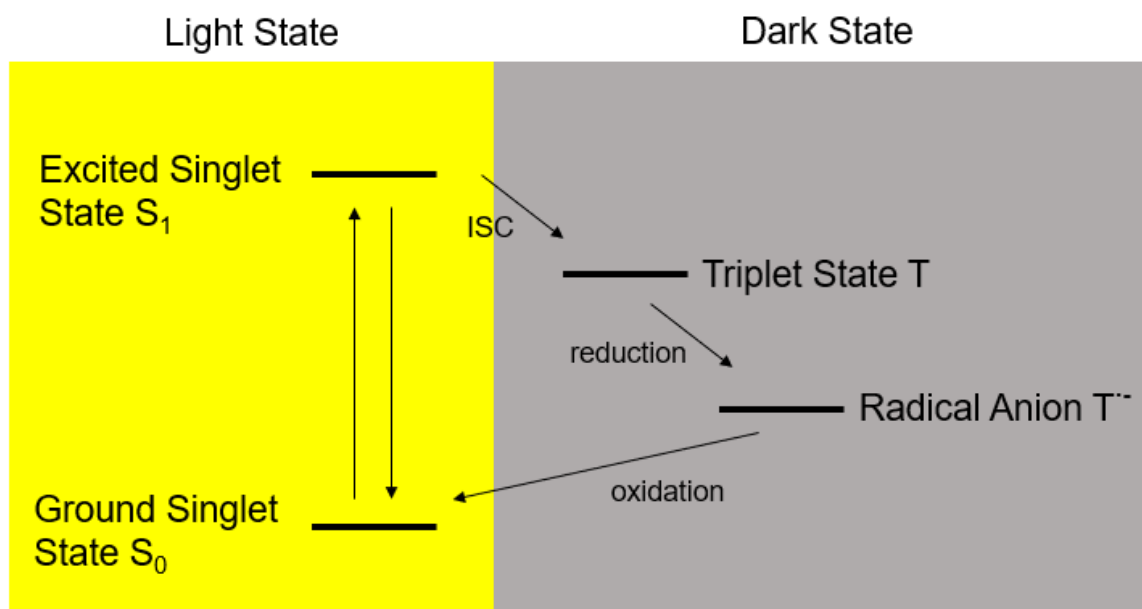
A: High density of fluorophores means that their PSFs overlap and the resolution is limited by the Abbe diffraction limit. B-E: Selective activation of isolated fluorophores over a number of frames F: Localisations of single molecules represented in a scatterplot

STORM was first described by Rust *et al.* in 2006. The group employed a pair of cyanine dyes, Cy5 and Cy3 that can act as a photoswitch (Bates *et al.*, 2005; Heilemann *et al.*, 2005). Cy5 fluoresces in response to 633 nm red laser light and can also be transferred to a stable dark state at high laser power. In the presence of Cy3, 532 nm green laser light brings Cy5 back into the excited state, but at much lower density, allowing the localisation of isolated molecules. The photoswitch can cycle between the dark and the excited state several hundred times before photobleaching and a resolution of up to 20 nm could be achieved (Rust *et al.*, 2006).

Albeit a remarkable discovery, the technique could not be applied easily to biological samples due to the necessity of both dyes being in close proximity to each other, making labelling complicated (Bates *et al.*, 2007). The group around Markus Sauer found that conventional cyanine dyes, such as Alexa Fluor 647, had in fact the ability to switch between the dark and the excited state in the absence of an activator fluorophore, provided the laser light that returns the fluorophore to the excited state is sufficiently powerful, namely about 200 times higher than that reported by Rust *et al.* They termed their improved technique

direct STORM (dSTORM) (Heilemann et al., 2008). In fact, most publications that refer to STORM in their experimental section, have in fact carried out dSTORM experiments.

The cycling between the fluorescent light state and the dark state is enabled by the principle of electrons being transferred between what is called the ground, the singlet and the triplet state. The principle is illustrated in Figure 5.3. When an electron is excited by taking up energy, it leaves the ground state and enters the singlet state. During de-excitation, when the electron returns to the ground state, the energy is released by fluorescence. Alternatively, if the laser power is high enough, the electron can undergo intersystem crossing (ISC) and enter the so-called triplet state. Returning from the triplet to the ground state results in phosphorescence, which is also visible as emitted light and cannot be distinguished from fluorescence by eye (Jameson, 2014; Noomnarm & Clegg, 2009). Heilemann *et al.* found that adding a reducing agent with thiol groups, such as MEA, quenches the triplet state and therefore phosphorescence, which retains the electron in the dark state. Subsequent oxidation relocates the electron into the ground state, from where the cycle starts again (Heilemann et al., 2009; van de Linde, Krstić, et al., 2011).



**Figure 5.3 Principle of Photoswitching**

Excitation of the fluorophore promotes an electron from the singlet ground state  $S_0$  into the excited singlet state  $S_1$ . From there, it can either return to the ground state, resulting in fluorescence, or undergo intersystem crossing (ISC) into the triplet state  $T$ . A thiol group reduces the fluorophore to a radical anion  $T^{\cdot-}$ , which quenches phosphorescence. Molecular oxygen oxidises the anion and it can return to the ground singlet state  $S_0$ , from where it can be excited again (Heilemann et al., 2009).

The optimal blinking rate, at which the activated fluorophores in each frame are further apart than the diffraction limit was found by varying the laser intensity, thiol, and oxygen concentration (van de Linde, Löschberger, et al., 2011).

Compared with FPALM and other super resolution microscopy techniques, dSTORM offers many advantages. The instrumental setup is relatively simple and cheap, requiring only a standard fluorescence microscope with lasers of sufficient power (5 - 30 kW cm<sup>-2</sup>). The execution of the experiment itself is very straightforward as well, as illustrated in 2.2.2.3 and 2.2.7.3 (van de Linde, Löschberger, et al., 2011). Antibodies tagged with conventional fluorescent dyes such as Alexa Fluor 647, can be used for the staining of virtually any intracellular target, whereas FPALM requires the expression of a photoswitchable fusion protein (Hess et al., 2006). This is an immense advantage for cells such as 3T3 L1 adipocytes, which are very difficult to genetically manipulate (Ross et al., 2003). Furthermore, photoswitchable fluorophores used for dSTORM are brighter than fluorescent proteins and can cycle between the dark and the light state hundreds of times, while photoswitchable proteins bleach quickly (Jensen & Crossmann, 2014).

Since the development of SMLM, and more specifically, STORM and dSTORM, the technique has allowed exciting insights into cellular processes that have not been possible to image by light microscopy before. The imaging of nuclear pore complexes (Löschberger et al., 2014), HIV-1 envelope proteins at the plasma membrane of infected T-cells (Muranyi et al., 2013), and chromatin structures at different stages of mitosis (J. Xu et al., 2018) are only a few examples of the successful implementation of dSTORM. Furthermore, the method has been used to gain insights into the clustering of the glucose transporters GLUT1 (Yan et al., 2018) and GLUT4 (Gao et al., 2017), which has been described in more detail in section 1.7.5.

### 5.1.3 Cluster Analysis

Super resolution microscopy, particularly SMLM has allowed visualisation of cluster-forming proteins, of which some were previously unknown to exhibit this characteristic (Lang & Rizzoli, 2010). While large clusters are often apparent in the reconstructed images, small clusters can be difficult to distinguish from

randomly distributed points. It is therefore necessary to mathematically analyse and quantify the spatial point pattern that is obtained in SMLM. In this study, this was achieved using two different methods: Ripley's K function analysis and Bayesian cluster analysis.

### 5.1.3.1 Ripley's K Function Analysis

Ripley's K function analysis was first published by Brian Ripley in 1976 (Ripley, 1976) and is described as

$$K(r) = \frac{1}{n} \sum_{i=1}^n N_{pi}(r)/A \quad (5-3)$$

$n$  is the number of points,  $N_{pi}$  is the number of points within a distance  $r$  of another point and  $A$  is the area. When a number of points  $n$  is distributed in an area  $A$ , it can be determined with the help of equation (5-3) whether these points are either randomly distributed, or comparatively scattered or clustered (Kiskowski et al., 2009). A circle with the radius  $r$  is drawn around each point and the points that lie within this circle are counted. The  $K$  values are plotted against  $r$  and the resulting graph indicates the type of distribution. For a random distribution, this graph is a parabola, for more clustered points it becomes steeper and for more scattered points it becomes flatter. The  $L$  value is the normalised  $K$  value and is derived from equation (5-3) by

$$L(r) = \sqrt{K(r)/\pi} \quad (5-4)$$

The  $L$  value plotted over  $r$  produces a straight line if the points follow a random distribution. In case of clustering, the graph is bent (Kiskowski et al., 2009). Ripley's K function analysis is very easy to realise, and data can be obtained rapidly. It is the method of choice when it comes to cluster analysis and is very commonly used in many fields of biology (Gao et al., 2017; Hess et al., 2005; Prior et al., 2003).

### 5.1.3.2 Bayesian Cluster Analysis

SMLM data points come with a value that describes their precision, which is called uncertainty (Ovesný et al., 2014; Thompson et al., 2002). This value is not considered for Ripley's and other popular types of cluster analysis. The group of Dylan Owen therefore developed an approach based on Bayesian cluster analysis to analyse SMLM data (Griffié et al., 2016). Based on the K function, their program generates several thousand of cluster proposals, which are evaluated against the original data set. The cluster model that approximates the data best is chosen to represent it (Rubin-Delanchy et al., 2015). While this approach delivers more precise results than Ripley's K function analysis, it is also very time consuming and requires much more computing power.

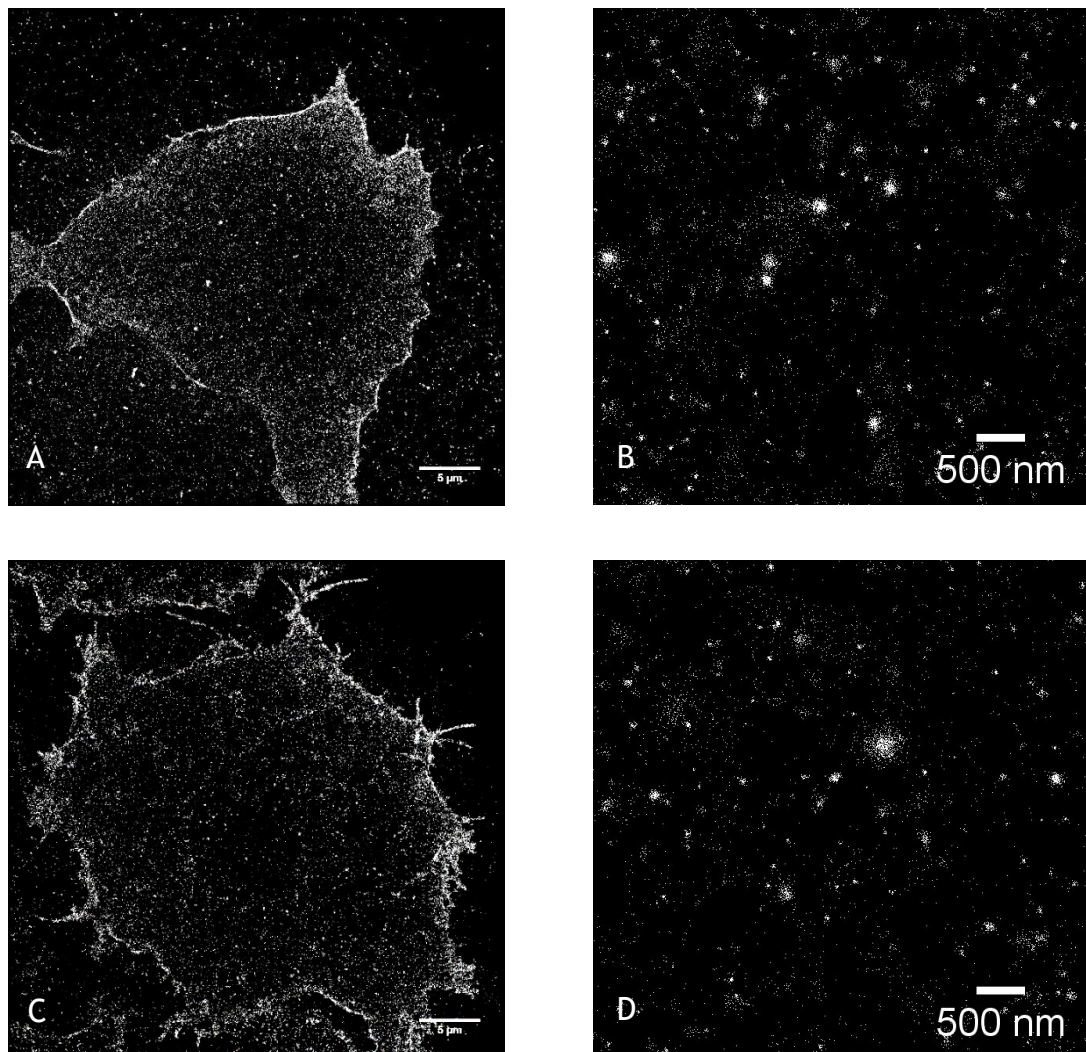
### 5.1.4 Hypothesis and Aims

One key aim of this work was to find an assay that allows light microscopic visualisation and quantification of GLUT4 clusters in basal 3T3 L1 adipocytes and dispersal of the transporter in response to insulin. Conventional TIRFM was not powerful enough to resolve the clusters in the membrane and SpIDA showed that the clustering is not dependant on the oligomeric state of GLUT4. By going beyond the diffraction limit using STORM, we hoped to achieve a resolution low enough to resolve GLUT4 clusters in the plasma membrane and use this as an assay for the quantification of their dispersal. Subsequently, we made further inquiries into the molecular mechanisms behind the dispersal. For this, we investigated the role of EFR3 in the clustering mechanism as outlined in sections 1.7.7 and 1.8. Once STORM was established as a suitable assay, we knocked down EFR3 in 3T3 L1 adipocytes and analysed the altered clustering characteristics of the transporter. We also carried out experiments with the lectin Galectin-3. It has been shown that this protein directly binds to the insulin receptor and causes insulin resistance in mice as well as in cell models (P. Li et al., 2016). With the help of STORM, we investigated, whether Galectin-3 also has an influence on the clustering behaviour, which would give further insights into the nature of GLUT4 clustering.

## 5.2 Results

### 5.2.1 Insulin Regulates GLUT4 Dispersal

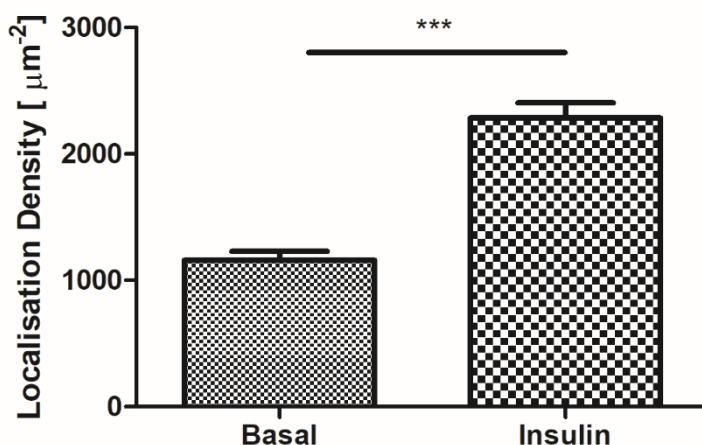
The cell line used in this chapter was the same HA-GLUT4-GFP 3T3 L1 cell line that was used in Chapter 3. In section 3.2.1, specifically Figure 3.6 the cells' response to insulin was outlined. HA-GLUT4-GFP translocated to the cell surface and integrated itself in the plasma membrane as expected. This could be visualised by HA surface staining and quantified by measuring the fluorescence intensity of the blue HA ring around the cells.



**Figure 5.4 STORM Images of Surface GLUT4 in Basal and Insulin Stimulated 3T3 L1 Adipocytes**

HA-GLUT4-GFP 3T3s were incubated in serum-free medium for 2 h prior to the experiment and stimulated with 100 nM insulin for 20 min or left untreated. Cells were then fixed and stained for surface HA as described in section 2.2.2.3. dSTORM image acquisition and analysis was carried out as described in section 2.2.7.3. Raw datasets were processed using the ImageJ plugin ThunderSTORM (see 2.2.8.4) to obtain scatterplots showing single molecules. A: Representative scatterplot of a basal cell. Scalebar: 5 µm. B: Magnified section of image A. C: Representative scatterplot of an insulin stimulated cell. Scalebar: 5 µm D: Magnified section of image C.





**Figure 5.5 STORM Localisation Density in Basal and Insulin Stimulated 3T3 L1 Adipocytes**

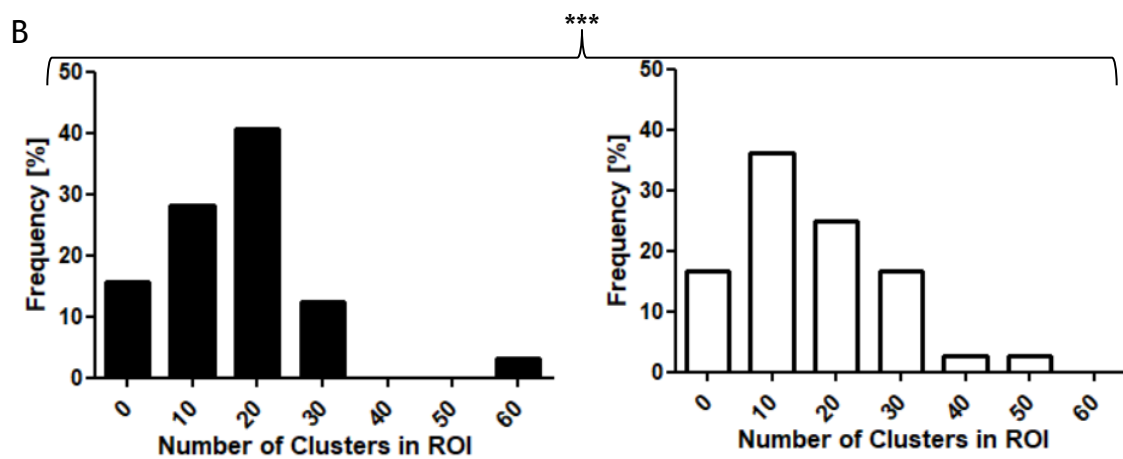
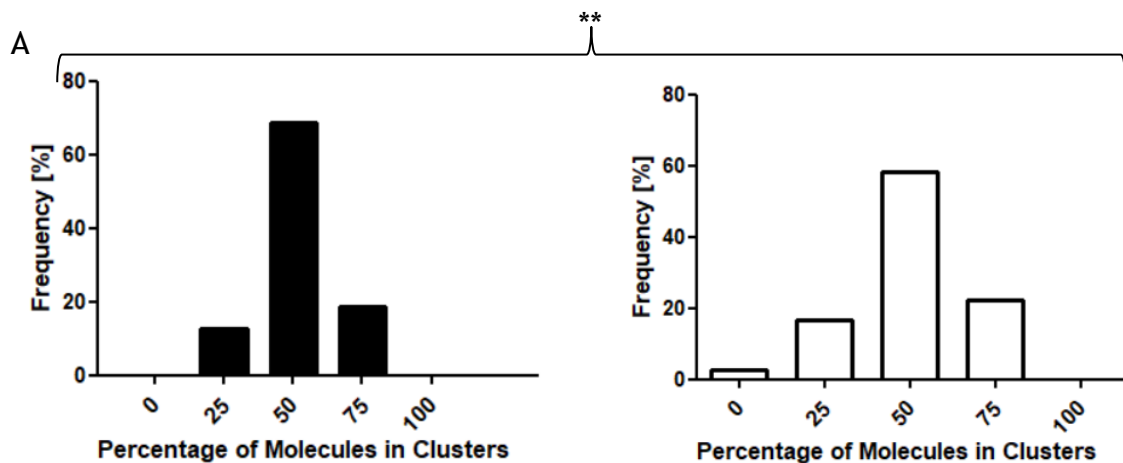
HA-GLUT4-GFP 3T3s were incubated in serum-free medium for 2 h prior to the experiment and stimulated with 100 nM insulin for 20 min or left untreated. Cells were then fixed and stained for surface HA as described in section 2.2.2.3. dSTORM image acquisition and analysis was carried out as described in section 2.2.7.3. Raw datasets were processed using the ImageJ plugin ThunderSTORM and the localisation density was determined using the ImageJ plugin LocFileVisualizer (see 2.2.8.4). 10 ROIs where the localisations appeared homogenous were chosen per cell to carry out this analysis. Basal: 1158  $\pm$  70 (n = 80) Insulin: 2283  $\pm$  120 (n = 80). Mean  $\pm$  SE. Unpaired two-tailed t-test 95 % confidence intervals  $p < 0.0001$ . This experiment was repeated four times with similar results.

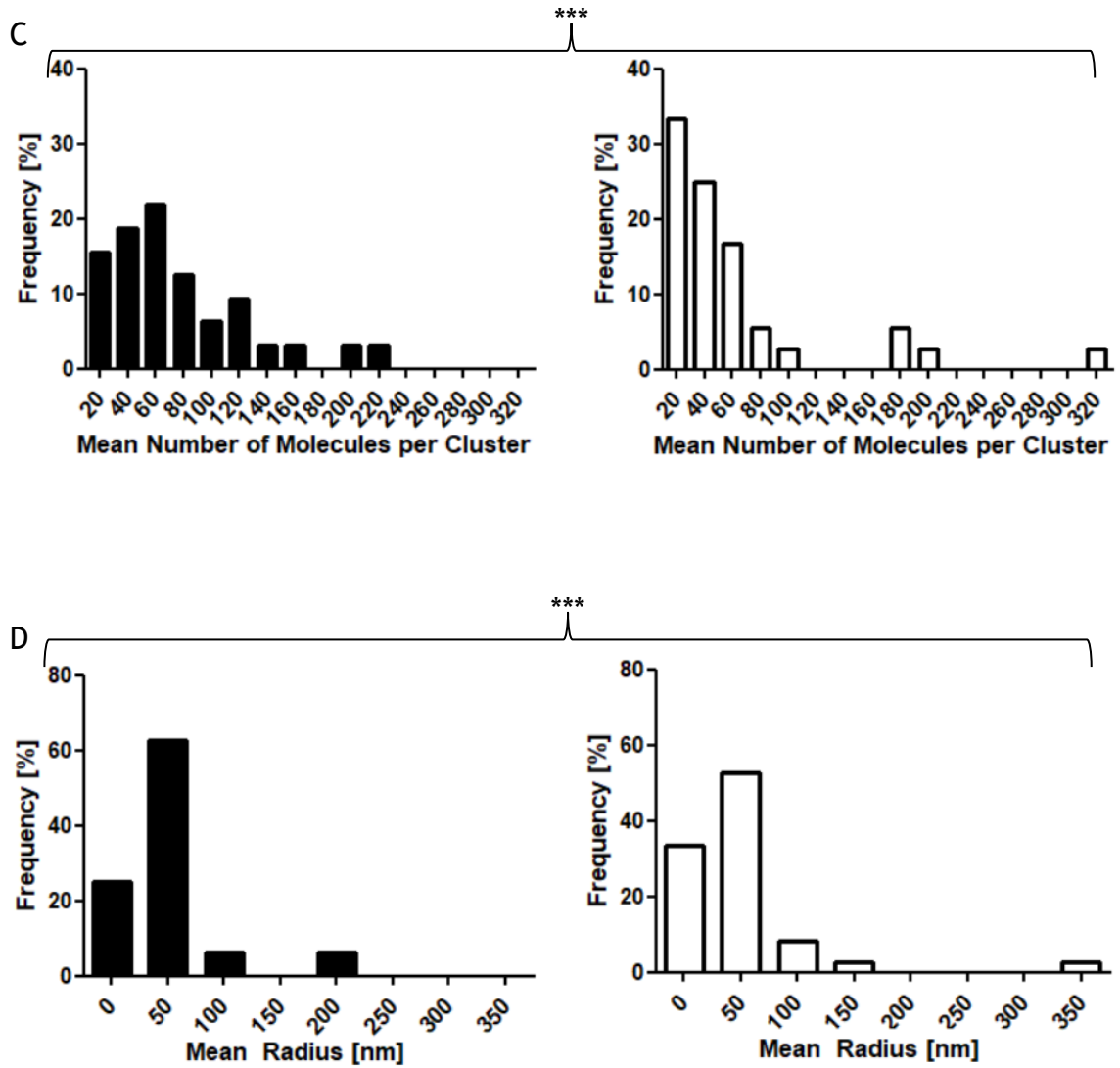
Essentially the same experiment was carried out for STORM and the obtained data was subjected to cluster analysis. Under STORM conditions, the footprint of the cells was well defined and initial background blinking could be mostly eliminated by simultaneously turning on the 405 nm laser at low power together with the 640 nm excitation laser. Figure 5.4 shows the spatial pattern of a HA-GLUT4-GFP 3T3 L1 adipocyte in the basal state and another cell after insulin stimulation as well as a zoomed in image of each cell. The reconstructed images show single molecules as well as clusters of HA-GLUT4-GFP. Under basal conditions, there were notably more clusters and denser clusters, whereas the insulin stimulated cells showed a more dispersed pattern and more single molecules.

As insulin stimulation leads to GLUT4 translocation in adipocytes, the signal density was expected to be higher in stimulated cells. This was confirmed by determination of the localisation density in  $\mu\text{m}^{-2}$  and the result is shown in Figure 5.5. The localisation density almost doubled from 1158 localisations per  $\mu\text{m}^2$  in the basal state to 2283 per  $\mu\text{m}^2$  after insulin stimulation. It is important to note that the localisation density is not an accurate measurement of antigen concentration, which is explained in more detail in section 5.3.

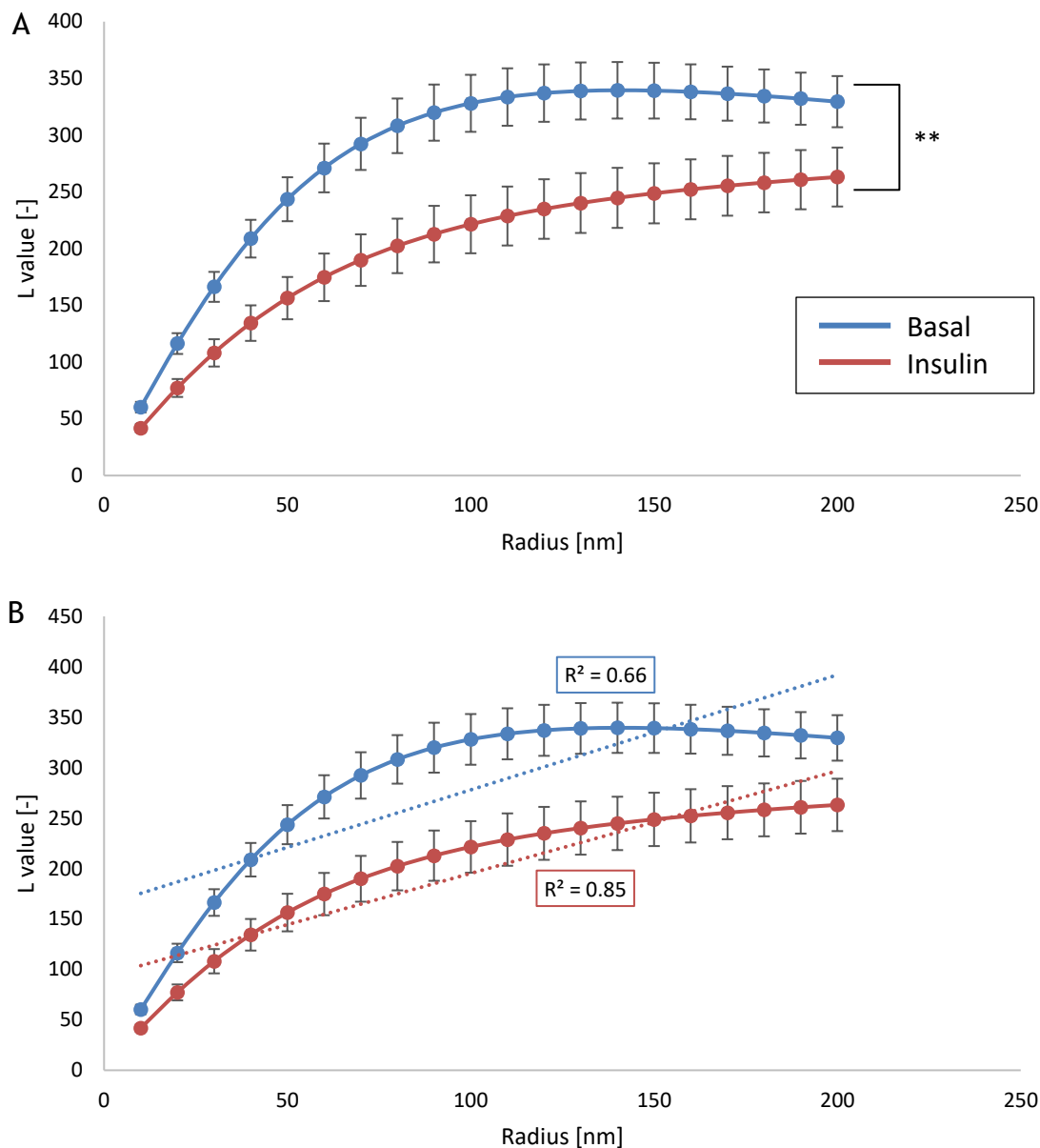
The STORM data underwent Bayesian cluster analysis. For this,  $3 \times 3 \mu\text{m}$  sized ROIs of STORM images were analysed to determine the percentage of molecules in clusters, the number of clusters per ROI, the mean number of molecules per cluster, and the mean radius of clusters in nm. The frequency distributions of the obtained results are shown in Figure 5.6. In the vast majority of ROIs in basal cells, 50 % of molecules were found in clusters, with fewer ROIs showing 25 % and 75 % of molecules in clusters. After insulin stimulation, only slightly more than half of the ROIs showed 50 % of molecules in clusters and some ROIs did not include any clusters at all, indicating that more molecules were dispersed in the insulin stimulated state. Similarly, the frequency distribution for the number of clusters per ROI shifted towards the right after insulin stimulation, which shows that more ROIs contained indeed fewer clusters in the insulin stimulated state than under basal conditions. The clusters themselves exhibited less molecules per cluster after insulin treatment, indicating that they decreased in size. A result which was also reflected in the frequency distribution of the mean cluster radius. More clusters were smaller than 50 nm after insulin stimulation than in the basal state. A few ROIs showed large clusters, some of them of more than 350 nm radius. These clusters could either be artefacts of the Bayesian approach, or signify dispersing clusters, which would be less compact and therefore appear larger.

Bayesian cluster analysis such as that shown in Figure 5.6 delivered interesting results and compelling evidence that insulin stimulation indeed leads to dispersal of GLUT4 out of clusters in the plasma membrane. However, the approach based on the protocol provided by Griffié *et al.* (2016) was immensely time-consuming and not practicable for large data sets. For this reason, we decided to rely on Ripley's K function analysis for further investigations.





**Figure 5.6 Bayesian Cluster Analysis of Basal and Insulin Stimulated 3T3 L1 Adipocytes**  
 HA-GLUT4-GFP 3T3s were incubated in serum-free medium for 2 h prior to the experiment and stimulated with 100 nM insulin for 20 min or left untreated. Cells were then fixed and stained for surface HA as described in section 2.2.2.3. dSTORM image acquisition and analysis was carried out as described in section 2.2.7.3. Raw datasets were processed using the ImageJ plugin ThunderSTORM (see 2.2.8.4) and the raw data was subjected to Bayesian cluster analysis. Basal cells: Black, left,  $n = 8$ ; Insulin stimulated: White, right,  $n = 9$ . 4 ROIs of  $3 \times 3 \mu\text{m}$  size per cell were analysed. The bar graphs shown here are frequency distributions, the values shown on the x-axes are the bin centres of these frequency distributions. Chi Square tests with 95 % confidence intervals were carried out to determine whether differences between the distributions were significant A: Percentage of molecules in clusters, bin width: 25 %,  $p = 0.002$ . B: Number of clusters per ROI, bin width: 10,  $p < 0.0001$ . C: Mean number of molecules per cluster, bin width: 20,  $p = 0.0001$ . D: Mean radius of clusters in nm, bin width: 50 nm,  $p < 0.0001$ . This experiment was repeated twice with similar results.



**Figure 5.7 Ripley's K-Function Analysis of Basal and Insulin Stimulated 3T3 L1 Adipocytes** HA-GLUT4-GFP 3T3s were incubated in serum-free medium for 2 h prior to the experiment and stimulated with 100 nM insulin for 20 min or left untreated. Cells were then fixed and stained for surface HA as described in section 2.2.2.3. dSTORM image acquisition and analysis was carried out as described in section 2.2.7.3. Raw datasets were processed using the ImageJ plugin ThunderSTORM (see 2.2.8.4) and the obtained data was subjected to Ripley's K-function analysis with the minimum radius 10 nm, step radius 10 nm, and maximum radius 200 nm. Displayed is the L value Basal cells: Blue,  $n = 8$ ; Insulin stimulated: Red,  $n = 9$ . Data Points are Mean  $\pm$  SE. This experiment was repeated four times with similar results. A: L values. The curves were compared by an unpaired two-tailed t-test with 95 % confidence intervals  $p = 0.0011$  B: L values with linear trendline and corresponding  $R^2$ .

The results obtained by Ripley's K function analysis for basal and insulin stimulated 3T3 L1 adipocytes are summarised in Figure 5.7. As described in section 5.1.3.1, the obtained L value plotted over the radius results in a straight line for randomly distributed points. A clustered distribution, on the other hand,

delivers a curved graph. For simplicity, the degree of curvature of the two graphs was approximated by calculating a linear trendline and its  $R^2$  value.  $R^2$  is an indicator of how well a trendline fits the data set: The closer  $R^2$  is to 1, the better the fit. In our case, this means that the curvature of the graph is stronger when  $R^2 \ll 1$ . The blue graph in Figure 5.7 represents the L value obtained from basal cells and is strongly curved, with  $R^2 = 0.66$  suggesting a clustered distribution of GLUT4 in the cell membrane. Results for insulin stimulated cells are shown in red. This graph is also curved, however, less so than the basal (blue) one, signified by its greater  $R^2 = 0.85$ , indicating a less clustered distribution of molecules. The curves were compared by an unpaired two-tailed t-test and showed a significant difference, confirming this observation. As the K value, and therefore the L value, is a function of the reciprocal number of points (see equation (5-3)), the apparent maximum of the plotted L value is higher for a smaller number of localisations. The difference in maxima in Figure 5.7 is therefore due to the increased number of HA-GLUT4-GFP molecules and subsequently the increased number of localisations.

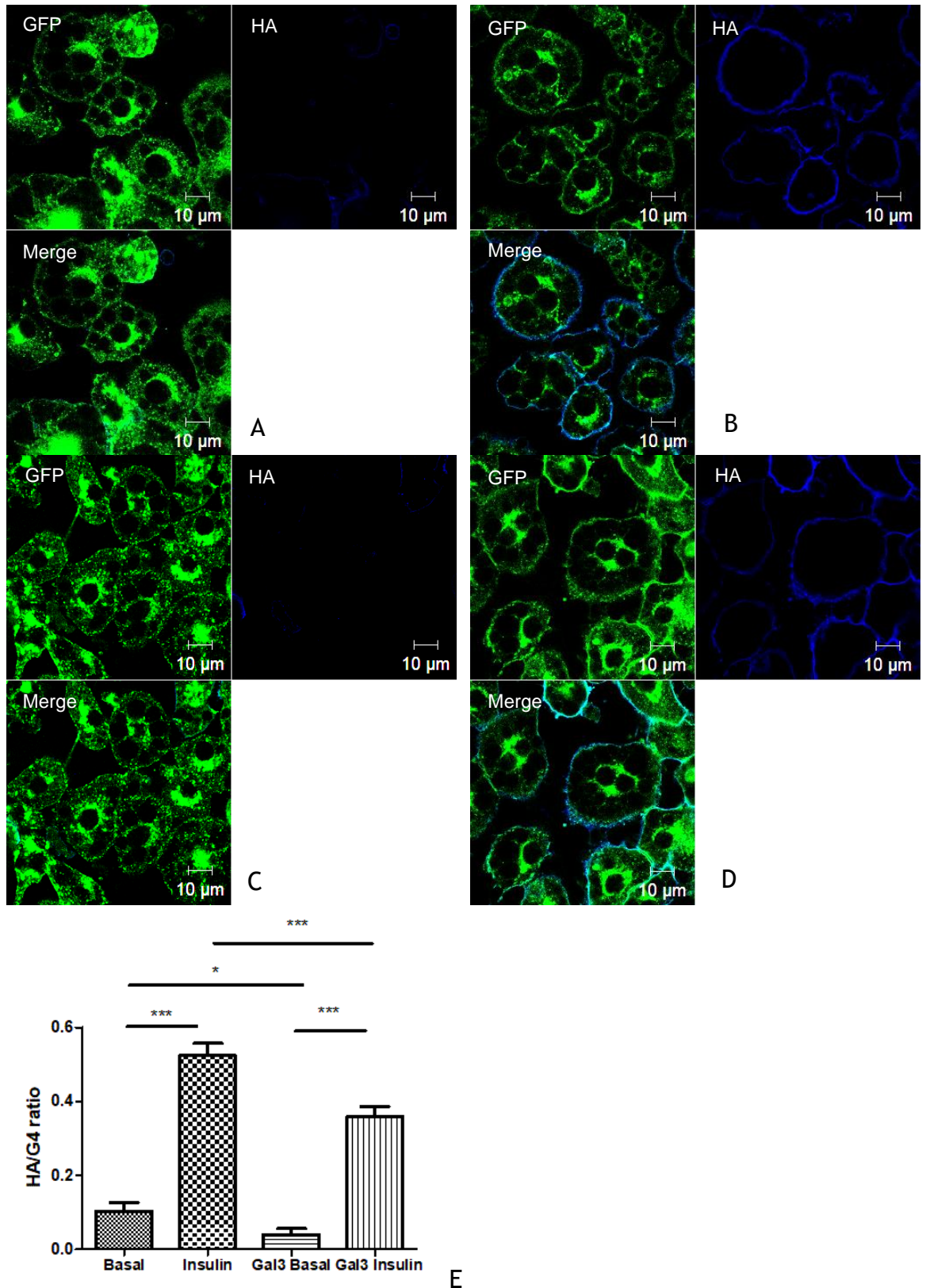
### 5.2.2 Galectin-3 Inhibits GLUT4 Clustering

Lectins are proteins that bind to specific carbohydrates, in the case of Galectins, these are  $\beta$ -galactoside sugars. Galectins are expressed by many tissues, but even though there are many glycoconjugates containing a  $\beta$ -galactoside sugar, *in vitro* binding assays have shown that the interactions of galectins with their targets are more specific (Barondes et al., 1994). Galectin-3 is highly expressed in and secreted by macrophages, which are known to be elevated in adipose tissue of obese and insulin resistant individuals (Weisberg et al., 2003). The presence of macrophages in this tissue is linked to inflammation, which is related to obesity-induced insulin resistance (Patsouris et al., 2008).

Based on these findings, Galectin-3 was investigated with regards to its ability to bind the insulin receptor and it was found that this interaction can induce insulin-resistance in 3T3 L1 adipocytes (P. Li et al., 2016). Quantification of this data is shown in Figure 5.8 E. Although a reduction in basal HA-staining is apparent from this graph, it is important to note that the very low HA-staining intensity in the absence of insulin means the HA/GFP ratio is skewed by small alterations in a small signal. Nevertheless, our data confirms that Galectin-3

reduces the magnitude of insulin-stimulated GLUT4 translocation, consistent with an effect on glucose transport published by others (P. Li et al., 2016). We therefore investigated whether Galectin-3 also has an influence on the clustering of GLUT4 in the plasma membrane. From section 5.2.1, it is known that GLUT4 dispersal in the membrane is controlled by insulin. Galectin-3 may reduce this dispersal, which could result in re-endocytosis of the clustered transporter. This would explain the results in Figure 5.8. We carried out STORM, followed by ThunderSTORM image processing and Ripley's K function analysis. The result is depicted in Figure 5.9. Similar to Figure 5.7, the L values for the control basal cells show the typical curvature of clustered points, whereas the graph for insulin stimulated cells is less curved and approximates more a straight line, which indicates dispersal. Again, this was verified by  $R^2$  values, which was much larger for the insulin stimulated cells than for the basal data set.

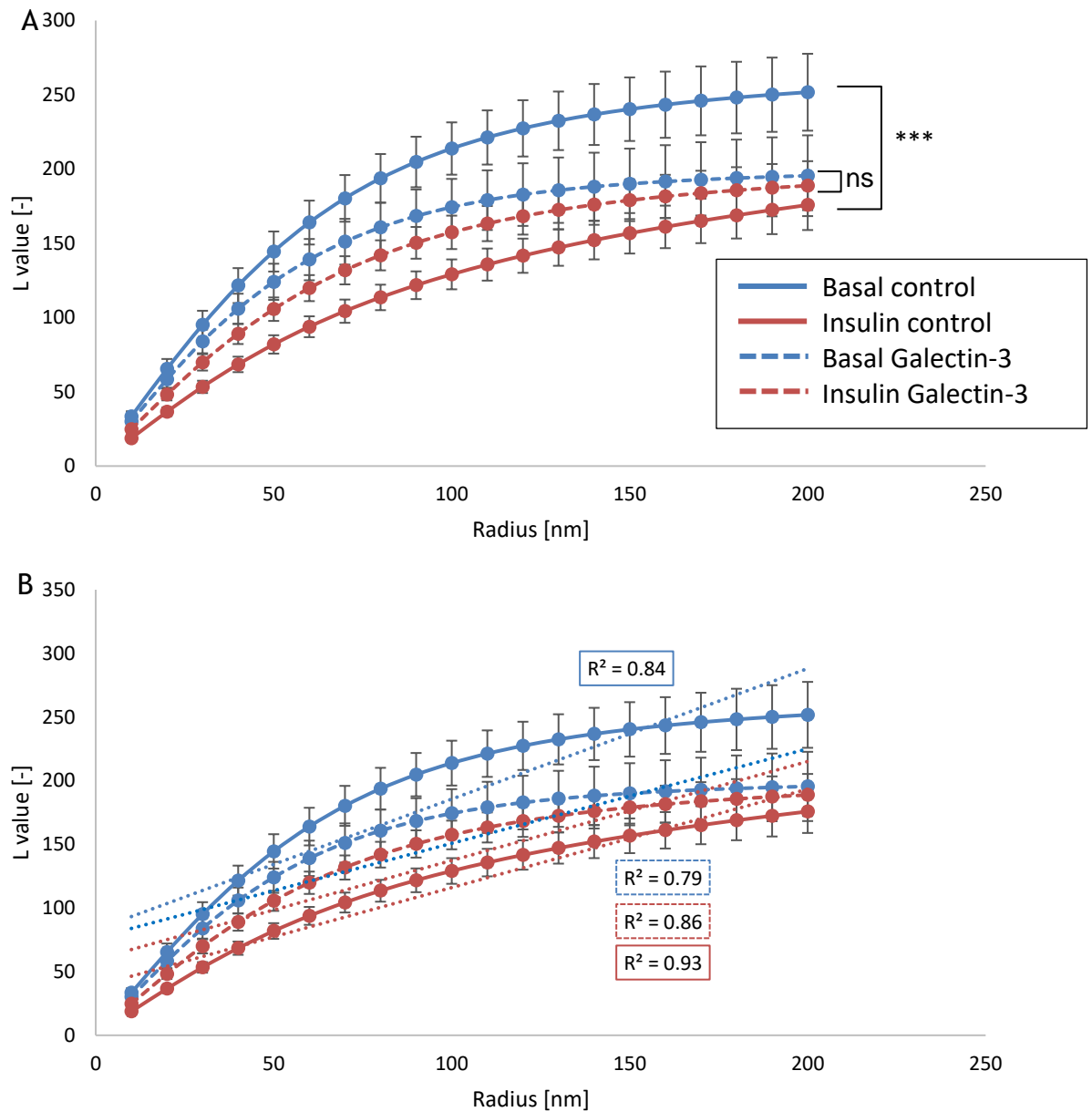
The graphs for Galectin-3 treated cells both show a similar progression. Both data sets have a similar number of localisations, which is reflected in the maxima and both show a similar dispersal pattern, which is related to the curvature of the graphs and hence the  $R^2$  value of the linear regression. Carrying out t-test on the curves confirmed this observation. According to these graphs, Galectin-3 treatment lead to inhibited GLUT4 translocation, which was already apparent from Figure 5.8. In addition, the dispersal in the plasma membrane appeared to be disrupted. Galectin was found to inhibit insulin-stimulated glucose uptake in 3T3 L1 adipocytes (P. Li et al., 2016). To confirm this result, we focused on the effect of Galectin-3 on the translocation of HA-GLUT4-GFP to the plasma membrane of 3T3 L1 adipocytes. Figure 5.8 A-D shows confocal images of HA-surface stained 3T3 L1 adipocytes in the basal and insulin stimulated state with and without Galectin-3 treatment. Comparing the HA/GLUT4 ratios clearly shows that Galectin-3 treated adipocytes exhibited reduced insulin-stimulated HA-GLUT4-GFP translocation.



**Figure 5.8 HA-Surface Staining in Galectin-3 Treated 3T3 L1 Adipocytes**

HA-GLUT4-GFP 3T3 L1 adipocytes were serum starved in the presence of  $1.25 \mu\text{g}\cdot\text{ml}^{-1}$  Galectin-3 for 4 h or without Galectin-3 (control) and then stimulated with 100 nM insulin for 20 min or left untreated. Cells were then fixed and stained for surface HA as described in section 2.2.2.2. A: Representative image of control basal cells B: Representative image of control cells stimulated with insulin C: Representative image of Galectin-3 treated basal cells D: Representative image of Galectin-3 and insulin treated cells E: HA/G4 ratio, Basal:  $0.10 \pm 0.02$  (n = 15) Insulin:  $0.52 \pm 0.03$  (n = 15). Gal3 Basal:  $0.04 \pm 0.02$  (n = 15) Gal3 Insulin:  $0.36 \pm 0.03$  (n = 15) Mean  $\pm$  SE. Unpaired two-tailed t-test 95 % confidence intervals: Basal vs Insulin  $p < 0.0001$ , Gal3 Basal vs Gal3 Insulin  $p < 0.0001$ , Basal vs Gal3 Basal  $p = 0.0413$ , Insulin vs Gal3 Insulin  $p = 0.0006$ .





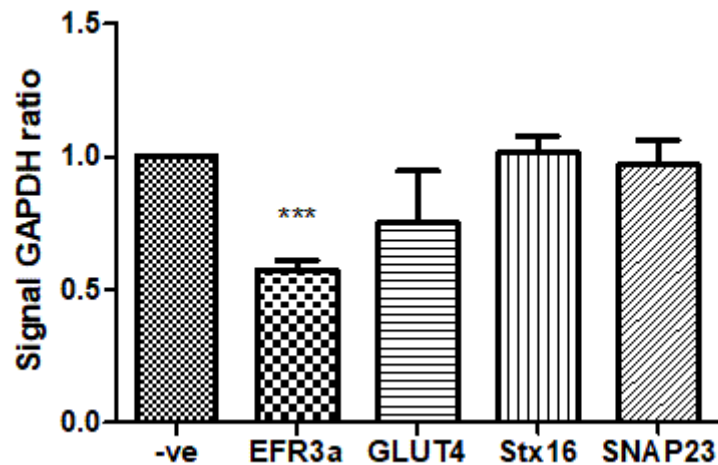
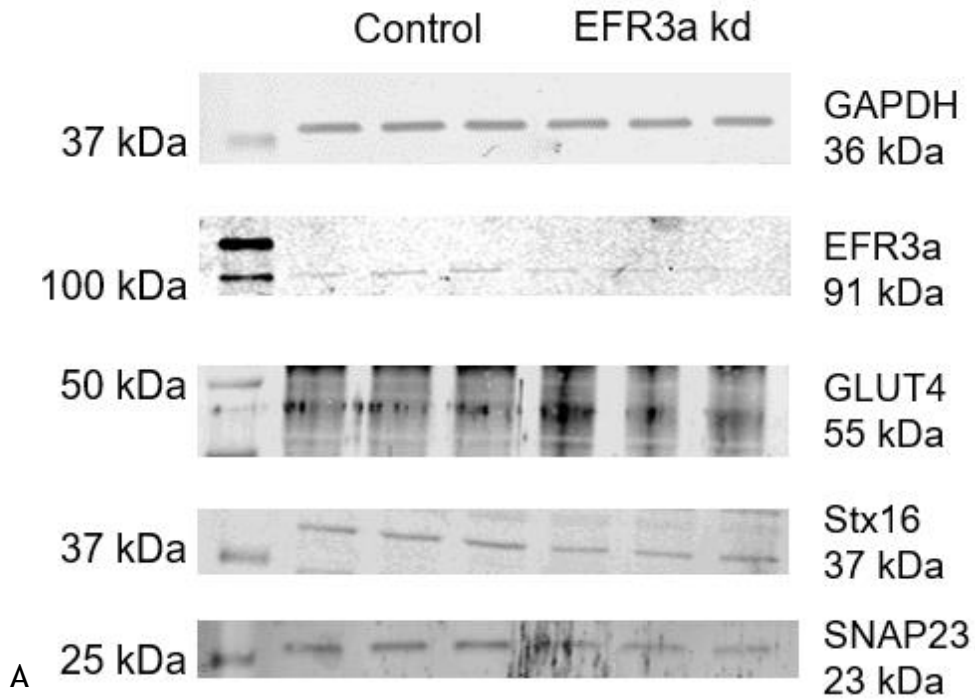
**Figure 5.9 Ripley's K-Function Analysis of Galectin-3 Treated Basal and Insulin Stimulated 3T3 L1 Adipocytes**

HA-GLUT4-GFP 3T3 L1 adipocytes were serum starved in the presence of  $1.25 \mu\text{g}\cdot\text{ml}^{-1}$  Galectin-3 for 4 h or without Galectin-3 (control) and then stimulated with 100 nM insulin for 20 min or left untreated. Cells were then fixed and stained for surface HA as described in section 2.2.2.3. dSTORM image acquisition and analysis was carried out as described in section 2.2.7.3. Raw datasets were processed using the ImageJ plugin ThunderSTORM (see 2.2.8.4) and the data was subjected to Ripley's K-function analysis with the minimum radius 10 nm, step radius 10 nm, and maximum radius 200 nm. Displayed is the L value. Basal: Blue, Insulin stimulated: Red, Control: Solid line, Galectin-3 treated: Dashed line,  $n = 8$ . Data Points are Mean  $\pm$  SE. This experiment was repeated twice with similar results. A: L values. The curves were compared by unpaired two-tailed t-tests with 95 % confidence intervals. Basal control vs Insulin control:  $p = 0.0004$ , Basal Galectin-3 vs Insulin Galectin-3:  $p = 0.4022$  (not significant). B: L values with linear trendline and corresponding  $R^2$ .

### 5.2.3 EFR3a Knock-Down in 3T3 L1 Adipocytes

Previously, a robust electroporation method had been established in our group, with which EFR3a could be efficiently knocked down in differentiated 3T3 L1 adipocytes (Laidlaw, 2018). The protocol was used in this section. The knock-down efficiency and a potential effect on levels of other GSV components GLUT4, Syntaxin16 (Stx16), and SNAP23 were determined via immunoblotting. In a negative control experiment, electroporation was carried out with water instead of siRNA to account for possible effects of the procedure on protein concentrations. A representative immunoblot as well as levels of the proteins of interest normalised to the level of the housekeeping protein GAPDH are shown in Figure 5.10.

Consistent with Laidlaw (2018) a 50 % knock-down of EFR3a could be achieved by electroporation. As expected, levels of GAPDH remained constant, so this protein could be used to normalise and quantify levels of the GSV proteins and EFR3a. GLUT4, Stx16, and SNAP23 did not change and levels of these proteins remained constant.



B

### Figure 5.10 EFR3a Knock-Down in 3T3 L1 Adipocytes

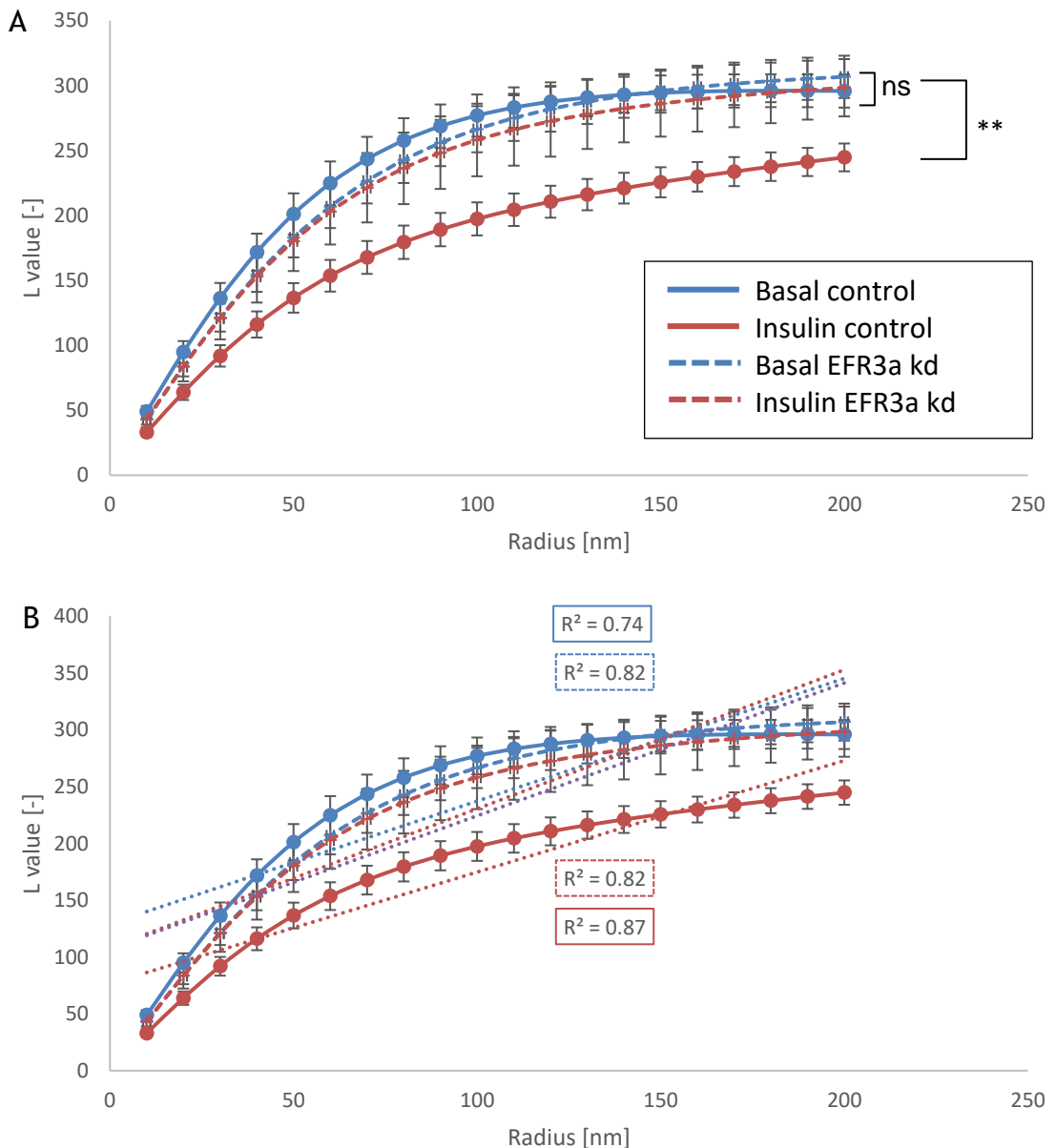
EFR3a knock-down was carried out as described in section 2.2.1.7 in HA-GLUT4-GFP 3T3 L1 adipocytes. In a control experiment water was used instead of siRNA. 72 h later, knock-down efficiency was determined by immunoblotting for EFR3a as described in 2.2.5. Immunoblots for Stx16, SNAP23, and GLUT4 were carried out to examine the effect of EFR3a knock-down on other GSV components. GAPDH was used as a housekeeping protein. A: Representative Immunoblots. Marker, three replicates of the control sample, three replicates of EFR3a knock-down. Complete immunoblots can be found in the Appendix B: Signal ratio of each protein of interest to the housekeeping protein GAPDH and normalised to the negative control experiment. The experiment was carried out four times with similar results. Signal GAPDH ratio: EFR3a:  $0.58 \pm 0.03$   $p < 0.0001$ , GLUT4:  $0.75 \pm 0.20$   $p = 0.2506$ , Stx16:  $1.01 \pm 0.06$   $p = 0.8021$ , SNAP23:  $0.97 \pm 0.09$   $p = 0.7429$ . Unpaired two-tailed t-test 95 % confidence intervals.

### 5.2.4 EFR3a Controls Insulin Regulated GLUT4 Dispersal

The clustering behaviour of GLUT4 in EFR3a knock-down cells was investigated via STORM. Electroporation is a very aggressive transfection technique that kills a fraction of the cells and can have other adverse effects. For example, electroporated cells are often smaller than untreated cells, whether this is due to electroporation or if electroporation kills predominantly big cells, is unknown. To rule out possible effects of electroporation on the dispersal behaviour, the negative control cells in this experiment also underwent electroporation. In this case, purified water was added instead of siRNA and the rest of the treatment was unaltered.

The result of the cluster analysis is summarised in Figure 5.11. The control cells behaved as expected from Figure 5.7. The L value for basal cells was strongly curved which is reflected in the low  $R^2$  value, indicating a clustered distribution. Insulin stimulated cells on the other hand, showed a more linear graph with a lower maximum, which is the result of a more dispersed distribution of a higher number of points.

Knock-down of EFR3a did not affect the basal L values, which still curved strongly. Interestingly, L values for insulin stimulated cells showed an almost identical distribution, suggesting that insulin stimulated dispersal of GLUT4 was completely inhibited by EFR3a knock-down. Statistical analysis of the curves via t-tests confirmed the observation.



**Figure 5.11 Ripley's K-Function Analysis of EFR3a Knock-Down Basal and Insulin Stimulated 3T3 L1 Adipocytes**

EFR3a knock-down was carried out as described in section 2.2.1.7 in HA-GLUT4-GFP 3T3 L1 adipocytes. In a control experiment water was used instead of siRNA. After 72 h, cells were incubated in serum-free medium for 2 h prior to the experiment and stimulated with 100 nM insulin for 20 min or left untreated. Cells were then fixed and stained for surface HA as described in section 2.2.2.3. dSTORM image acquisition and analysis was carried out as described in section 2.2.7.3. Raw datasets were processed using the ImageJ plugin ThunderSTORM (see 2.2.8.4) and the data was subjected to Ripley's K-function analysis with the minimum radius 10 nm, step radius 10 nm, and maximum radius 200 nm. Displayed is the L value. Basal: Blue, Insulin stimulated: Red, Control: Solid line, EFR3a knock-down: Dashed line,  $n = 10$ . Data Points are Mean  $\pm$  SE. This experiment was repeated three times with similar results. A: L values. The curves were compared by unpaired two-tailed t-test with 95 % confidence intervals. Basal control vs Insulin control:  $p = 0.0061$ , Basal Efr3a kd vs Insulin Efr3a kd:  $p = 0.7955$  (not significant). B: L values with linear trendline and corresponding  $R^2$ .

## 5.3 Discussion

Using STORM to go beyond the diffraction limit allowed us to visualise and analyse clusters of GLUT4 in the plasma membrane of 3T3 L1 adipocytes for the first time in our laboratory. With the techniques discussed in 2.2.2.3, 2.2.7.3, and 2.2.8.4, a robust assay was established in our group that offers the possibility to assay the dispersal of GLUT4 in the membrane in response to insulin.

The method, however, is not without flaws and artefacts are common in STORM imaging. Depending on the sample preparation, different clustering behaviours can be witnessed (Whelan & Bell, 2015), which is why careful and consistent sample preparation was especially important during this work. The quantified results reported in this chapter, especially cluster sizes obtained by Bayesian cluster analysis and localisation densities, are to be viewed critically.

The nature of antibody staining provides another basis for false clustering. More than one antibody can bind to a protein, in addition, each antibody can be tagged with more than one fluorophore, which is often desirable in conventional fluorescence microscopy, as it amplifies the signal. When primary and secondary antibodies are used as in conventional fluorescence microscopy, the clustering effect of the antibody binding is magnified immensely. An additional problem is faced when the structures of interest are very dense and large antibodies sterically hinder themselves, so that labelling cannot be carried out efficiently (Kamiyama & Huang, 2012). These issues can be partially circumvented by using fab fragments or nanobodies for labelling (Ries et al., 2012), but these smaller probes are only available for a small number of targets at the moment, HA not being one of them. Another source of clustering artefacts is the blinking behaviour of the fluorophores as this allows for multiple localisations of one and the same fluorophore (Annibale et al., 2011). The localisation density is also subject to imaging parameters, such as laser power and number of frames. However, all these parameters were kept consistent throughout each data set.

Since this work focused on the changing clustering behaviour between two states, basal and insulin stimulated, issues around clustering artefacts were less critical as long as sample preparation was carried out simultaneously for all

samples of each data set. It is, however, important to note that the reported results of this work are always considered in a comparative manner and never as absolute values. This is particularly vital for localisation densities and cluster sizes.

Confirming the published results from Gao *et al.* (2017), we found that GLUT4 is predominantly located in clusters in the plasma membrane of 3T3 L1 adipocytes, which disperse upon insulin stimulation. By applying the technique to Galectin-3 treated and EFR3a knock-down cells, we hoped to gain further insights into the molecular mechanisms behind the dispersal.

With their discovery that Galectin-3 causes insulin resistance in mice and also in cell models such as 3T3 L1 adipocytes, Li *et al.* (2016) provided a link between inflammatory diseases and insulin resistance. They showed that Galectin-3 knockout in mice led to decreased levels of inflammation as well as improved insulin sensitivity. In 3T3 L1 adipocytes and L6 myocytes, they found that insulin stimulated glucose uptake is significantly diminished after Galectin-3 treatment in a dose-dependent manner. Our results indicate that this is due to both corrupted GLUT4 translocation and impaired dispersal in the membrane, since both mechanisms are disrupted following Galectin-3 treatment. Galectin-3 binds directly to the insulin receptor and thus inhibits its autophosphorylation as well as the stimulation and phosphorylation of the downstream targets PDK1 and Akt respectively (P. Li *et al.*, 2016). Our findings substantiate the hypothesis that insulin regulates glucose uptake by dispersal of GLUT4 in the membrane and dispersal appears to be directly enabled by the signalling cascade initiated by insulin binding to its receptor.

EFR3 is a protein that has been characterised in adipocytes and extensively studied in our laboratory in the context of insulin mediated glucose uptake by Laidlaw (2018). There are two homologues, EFR3a and b (Bojjireddy *et al.*, 2014), and 3T3 L1 adipocytes express predominantly EFR3a (Laidlaw, 2018). Laidlaw found the protein localised in the plasma membrane of this cell type and there was no redistribution following insulin stimulation, indicating that whatever role EFR3a plays in GLUT4 trafficking, is limited to the plasma membrane and EFR3a does not translocate to the plasma membrane as GSV or other vesicle cargo. Overexpression of EFR3a lead to increased GLUT4

translocation in HeLa cells and 3T3 L1 adipocytes, overexpression of a dominant negative mutant, on the other hand, inhibited insulin-stimulated GLUT4 translocation. In addition, the knock-down of EFR3a in 3T3 L1 adipocytes lead to significantly diminished glucose uptake in response to insulin.

The work discussed in this chapter adds to these results. EFR3a knock-down by electroporation delivered a similar extend of knock-down as reported by Laidlaw (50 - 60 %, Laidlaw 2018). In addition, levels of the GSV proteins GLUT4, Syntaxin16, IRAP, and SNAP23 after EFR3a knock-down were determined in order to study the effect EFR3a has on the expression of these proteins and by inference GSV formation. EFR3a knock-down did not have a significant effect on the levels of either of these proteins in whole cell lysates. This suggests that EFR3a acts independently from the GSV machinery and that none of these proteins compensate for the lack of EFR3a. It is important to note that the level of the plasma membrane SNARE SNAP23, known to be important for fusion of GSVs with the plasma membrane was also unaffected by EFR3a knock-down, indicating that a generalised defect in the plasma membrane is unlikely to be in evidence. However, to exclude a role for any of these proteins entirely, further tests would be necessary. Subcellular fractionation and visualisation of the protein distribution by microscopy are two experiments that would add more depth to this result.

We investigated the dispersal behaviour of GLUT4 in EFR3a knock-down cells and found that there was virtually no difference between basal and insulin stimulated cells. This was an exciting result, showing that EFR3a plays an important role in the clustering of GLUT4 in the cell membrane. Control experiments in which electroporation was carried out without the addition of siRNA had the same outcome as untreated cells, demonstrating that electroporation alone did not have an effect on GLUT4 clustering and dispersal in the membrane. The inhibition of dispersal is therefore very likely to be an effect of the EFR3a knock-down and it makes sense that the clustering is controlled by a membrane localised protein such as EFR3a. The fact that EFR3a knock-down also leads to inhibited glucose uptake makes it tempting to suggest that insulin sensitivity and therefore glucose uptake are controlled by clustering of GLUT4 in the plasma membrane of adipocytes. It appears as if the ability of



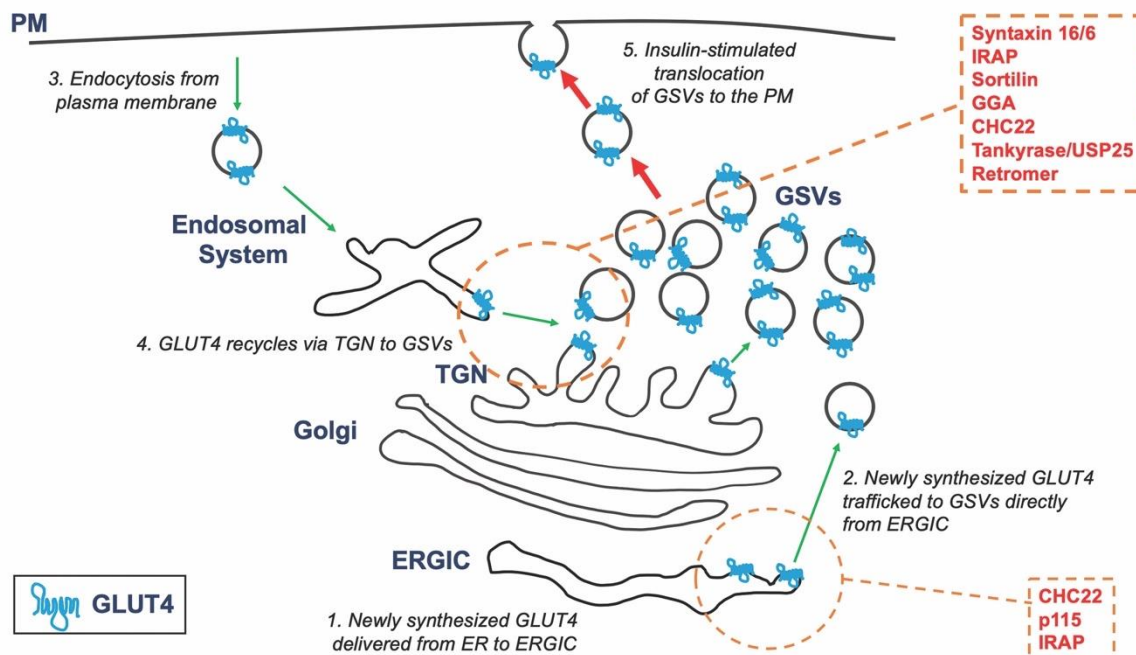
GLUT4 to transport glucose into the cell is diminished when the transporter is located in clusters, this may be due to a sterical hindrance of clustered GLUT4 preventing the inward-outward conformational changes known to accompany transport (Barrett et al., 1999), but it could also be simply the fact that clustered GLUT4 is less evenly distributed, which allows for less contact with extracellular glucose molecules. Further experiments are necessary to answer these questions. The results presented in this chapter support our working hypothesis outlined in section 1.8: Knock-down of EFR3a inhibits GLUT4 dispersal. This suggests that EFR3a is in fact the key component in the machinery involved in PI4P production, allowing PI4KIII $\alpha$  to be active at the plasma membrane.

## Chapter 6 SNARE Proteins Regulating Intracellular GLUT4 Trafficking

### 6.1 Introduction

#### 6.1.1 The ERGIC is Involved in the GSC formation in Human Cells

Chapter 1.4 described the cycling of GLUT4 between the GSC, the Golgi and endosomes, which is well characterised. Less is known about the initial formation of the GSC, which has been the subject of a recent study from this group, the Bryant group and the group of Frances Brodsky (Camus *et al.*, 2020). Camus *et al.* found a link between GLUT4 cycling, GSC formation, and different clathrin isoforms. The isoform CHC17 is known to be involved in the re-endocytosis of GLUT4 and protein sorting at the TGN in all mammals (Brodsky, 2012). The clathrin isoform CHC22, however, is not as universally expressed. It is found at high levels in human myocytes and at lower levels in adipocytes, but it is not expressed in mouse cells, including 3T3 L1 adipocytes, a widely-used cell model for studying GLUT4 trafficking (Wakeham *et al.*, 2005). Brodsky and colleagues showed that CHC22 colocalises with GLUT4 and other GSV proteins, such as GGA, VAMP2, and IRAP in HeLa cells. Furthermore, knock-down of CHC22 in human myocytes results in reduced GLUT4 levels, a lower insulin-response, and apparent loss of the GSC (Vassilopoulos *et al.*, 2009). These findings lead to the proposal that CHC22 plays a role in GLUT4 trafficking towards the GSC in human, but not in rodent, cells. In a recent study, Brodsky's group found that CHC22 also interacts and/or colocalises with markers of the ERGIC, specifically p115, but there is no interaction or colocalisation with the Golgi marker GM130. Furthermore, CHC22 colocalised with newly synthesised GLUT4 in the perinuclear region, but was not observed in the GSC (Camus *et al.*, 2020). These studies revealed that trafficking of GLUT4 requires CHC22 acting early in the secretory pathway at the ERGIC to deliver newly synthesised GLUT4 into GSVs. In these studies, it was observed that ERGIC membranes containing CHC22 were in close proximity to internalised GLUT4 after insulin-mediated release and compartments marked by Syntaxin 6. Hence, we believe that the pathway for delivery of newly synthesised GLUT4 (involving the ERGIC and CHC22) connects with GLUT4 re-internalised from endosomes in close proximity within the cell.



**Figure 6.1 Model of Intracellular GLUT4 Trafficking in Human Cells**

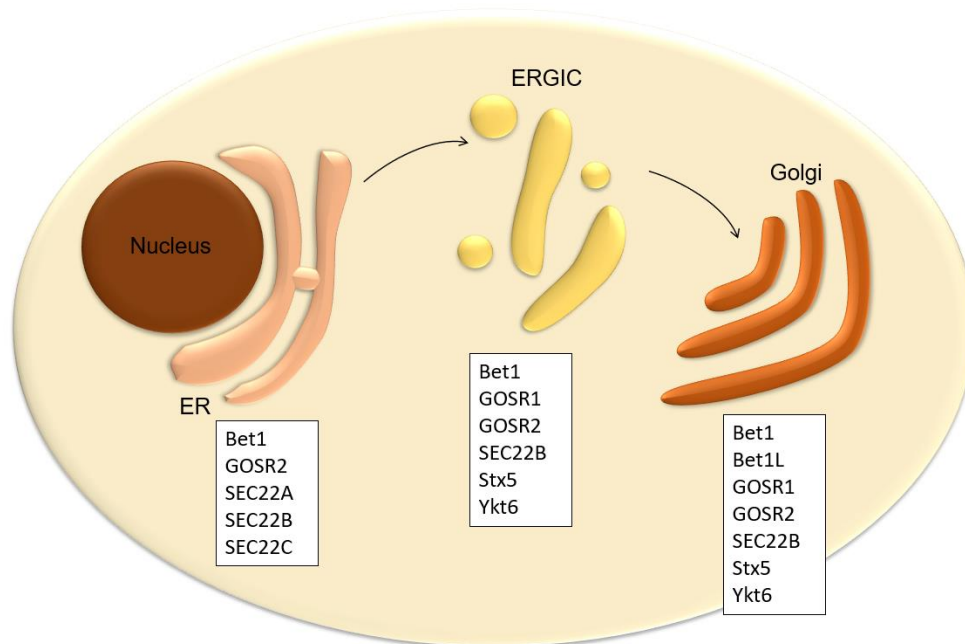
1: GLUT4 is synthesised in the ER and traffics to the ERGIC. 2: Direct trafficking of GLUT4 into GSVs bypassing the Golgi and utilising CHC22, p115, and IRAP (orange box). 3: Endocytosis of GLUT4 4: intracellular GLUT4 recycling (see Figure 1.3), with multiple proteins being involved including IRAP, GGA etc, see orange box 5: GSVs translocate to the plasma membrane upon insulin stimulation. Figure provided by Gwyn Gould.

Based on biochemical analysis, Camus *et al.* developed the model schematised in Figure 6.1: GLUT4 is newly synthesised in the ER and traffics together with IRAP and sortilin to the ERGIC. CHC22 then mediates the formation of the GSC, from where GSVs can translocate to the plasma membrane upon insulin stimulation. Re-endocytosis is then facilitated by the clathrin isoform CHC17 and GLUT4 cycles between endosomes, the Golgi, the GSC, and the plasma membrane as previously discussed, involving a range of molecules including GGA, sortilin, IRAP and tankyrase (Sadler *et al.*, 2019).

### 6.1.2 SNAREs Involved in Intracellular Trafficking

GLUT4 synthesis begins with the transcription of its gene, *SLC2A4*, to mRNA, which is then translated into an amino acid sequence by ribosomes bound to the ER. Subsequently, the protein is folded and glycosylated at its highly conserved exofacial glycosylation site in the ER and undergoes further post-translational modifications in the Golgi, which affect its function and trafficking in response to insulin (Sadler *et al.*, 2013). In their recent study, Camus *et al.* (2020) have introduced the ERGIC as another organelle that is involved in GLUT4 synthesis.

SNARE proteins are employed when trafficking between these three organelles, the ER, the Golgi, and the ERGIC. Section 1.6.2 introduced SNARE proteins as key regulators of membrane fusion. SNARE proteins involved in the fusion of GSVs with the plasma membrane are clearly a crucial component of insulin signalling. However, SNARE proteins facilitating intracellular fusion of vesicle and target membranes must not be underestimated. Syntaxin 6 and 16 have been identified to play a critical role in intracellular GLUT4 trafficking. By overexpressing a dominant negative inhibitor of endogenous Syntaxin 6, it could be shown that this SNARE is involved in a step that sequesters GLUT4 away from the recycling pool with the plasma membrane (Perera et al., 2003). A similar study found that GLUT4 travels through a domain of the TGN enriched with Syntaxin 6 and Syntaxin 16, suggesting that these two SNAREs are involved in an intracellular sorting step of the glucose transporter (Shewan et al., 2003). Other SNAREs that are involved in these processes remain to be discovered.



**Figure 6.2 Intracellular Localisation of ERGIC-related SNARE proteins**

The SNARE proteins Bet1, Bet1L, GOSR1, GOSR2, SEC22A, SEC22B, SEC22C, Stx5, and Ykt6 and their intracellular localisation with regards to the ER, ERGIC, and Golgi.

The SNARE proteins BET1, BET1L, GOSR1, GOSR2, SEC22A, SEC22B, SEC22C, Stx5, and Ykt6 are known to be involved in ERGIC trafficking (Adnan et al., 2019; Appenzeller-Herzog & Hauri, 2006; Inoue et al., 2016; Linders et al., 2019; Zhang & Hong, 2001). Their intracellular location is outlined in Figure 6.2.

### 6.1.3 Hypothesis and Aims

This chapter seeks to evaluate the possible role of the previously mentioned SNARE proteins in GLUT4 sorting, extending the study of Camus *et al.* (2020) The involvement of the syntaxins Stx6 and Stx16 in GLUT4 trafficking is well characterised (Bryant & Gould, 2011; Hamilton, 2011; Perera et al., 2003; Shewan et al., 2003) hence they are also included in this analysis by way of comparison.

Since GSC formation appears to be different in murine and human cells, this investigation could not be carried out in 3T3 L1 adipocytes but rather was undertaken in a human cell line. Additionally, 3T3 L1 adipocytes or other models for GLUT4 trafficking are difficult to genetically manipulate and were therefore deemed unsuitable for a larger scale screening as carried out in this study. Based on the results in Chapter 3 and the study by Camus *et al.*, we used a stably expressing HA-GLUT4-GFP HeLa cell line for our investigations. Knock-down of aforementioned SNARE proteins was performed via lipofectamine transfection of siRNA duplexes and the degree of colocalisation of the GFP tagged GLUT4 with markers of the ER, the Golgi, and the ERGIC was determined using microscopy. In addition, the total GLUT4 content and intracellular dispersal patterns were compared. We used siRNA duplexes provided by Jeremy Simpson; the Simpson group have employed and validated this siRNA library for a genome-wide screening to identify proteins of the early secretory pathway (J. C. Simpson et al., 2012).

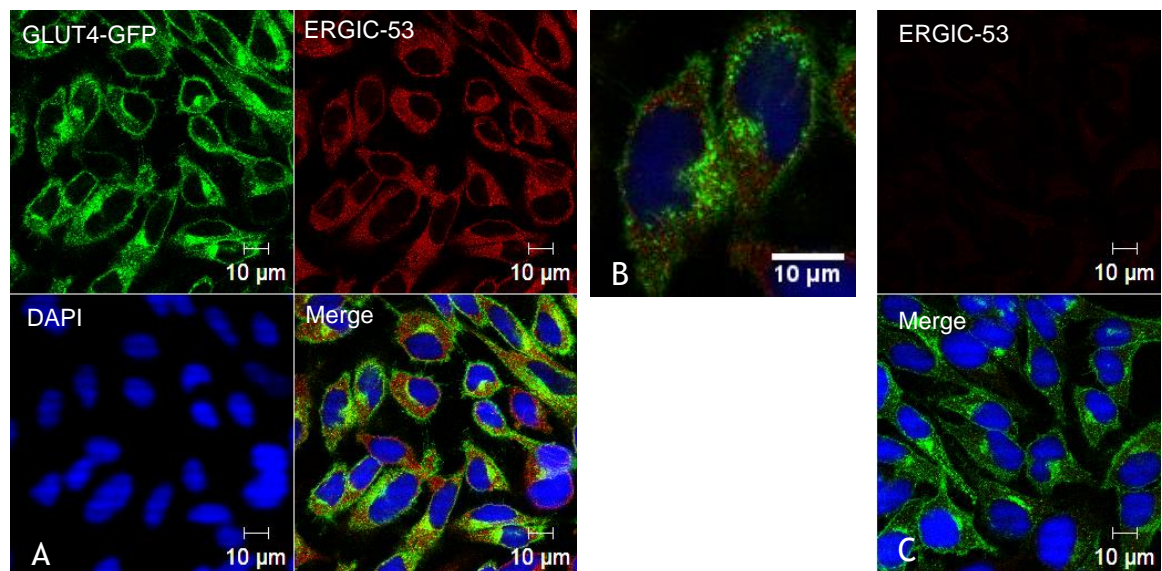
## 6.2 Results

### 6.2.1 GLUT4 Colocalisation

Knock-down of a SNARE protein that is involved in intracellular GLUT4 trafficking might be expected to result in an altered distribution of GLUT4 between the intracellular organelles. The following sections concentrate on the colocalisation of GFP-tagged GLUT4 with markers of the ERGIC (ERGIC-53), the ER (ID3), and the Golgi (GM130). These experiments were carried out employing conventional CLSM.

#### 6.2.1.1 GLUT4 Colocalisation with the ERGIC

Using the ImageJ plugin JaCoP (Bolte & Cordelières, 2006), colocalisation between GLUT4 and the ERGIC marker ERGIC-53 was determined. For each experiment, 5 to 10 images were recorded that contained approximately 10 to 20 cells each. Each experiment was carried out in 4 biological replicates. Representative images for ERGIC staining in the negative control experiment and the block control are shown in Figure 6.3.



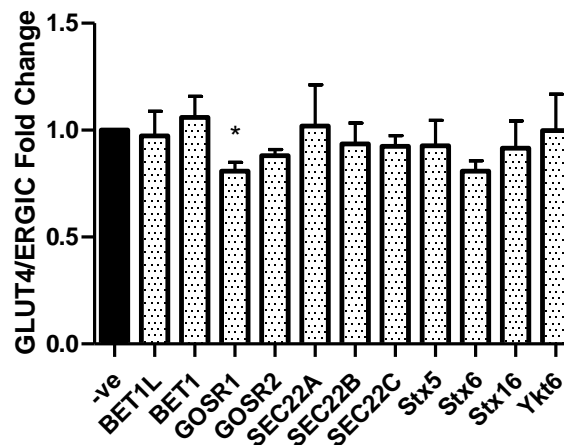
**Figure 6.3 ERGIC and DAPI Staining of HA-GLUT4-GFP HeLa Cells (negative control)**

HA-GLUT4-GFP HeLa cells were cultured on a 96 well plate with glass bottom as outlined in section 2.2.1.1. siRNA knock-down was carried out as described in 2.2.1.6, shown here is an image of the negative control cells, where siRNA was replaced by water. Cells were fixed and stained with an antibody for the ERGIC marker ERGIC-53 and the nucleus was stained with DAPI as described in 2.2.2.1. Images were acquired on a confocal microscope and show GLUT4-GFP, the ERGIC staining, the nucleus staining (DAPI) and a merge of all three channels.

A: Representative image of ERGIC staining B: Zoomed in image from A to show colocalisation C: Representative image of block control without primary antibody.

Figure 6.3 A shows the ERGIC-53 staining we typically observed in HeLa cells. DAPI was used for the staining of the nuclei. Similar to the ER, the ERGIC is broadly distributed within the entire cell. This is in fact atypical; typically, the ERGIC staining is more prominent in the perinuclear region. The atypical staining here may be attributed to lower antibody concentrations. The green channel shows the distribution of GFP-tagged GLUT4, which is also present throughout the cell and predominantly expressed in the perinuclear region. Figure 6.3 B shows a representative control experiment, in which the cells were not incubated with the primary antibody. This experiment was carried out to control that blocking of the sample was sufficient to prevent any staining derived from non-specific binding of the secondary antibody.

The data from all four separate experiments were pooled and normalised to the average of the negative control and 2-way ANOVA was carried out to determine statistical significance. The result is summarised in Figure 6.4. If values are significantly higher than the negative control after SNARE knock-down, this indicates an accumulation of GLUT4 in the ERGIC possibly due to the respective SNARE enabling downstream trafficking of GLUT4.



**Figure 6.4 GLUT4/ERGIC Colocalisation**

HA-GLUT4-GFP HeLa cells were cultured on a 96 well plate with glass bottom as outlined in section 2.2.1.1. siRNA knock-down was carried out as described in 2.2.1.6. Cells were fixed and stained with an antibody for the ERGIC marker ERGIC-53 and two consecutive images were acquired by confocal microscopy. Colocalisation of GLUT4-GFP and ERGIC-53 was determined using the ImageJ plugin JaCoP (see 2.2.8.3). Between 5 and 10 sets of images were analysed per knock-down and each experiment was carried out in four biological replicates. The data of all four experiments was pooled and normalised to the average value of the negative control experiment and 2-way ANOVA with 95 % confidence intervals was carried out for statistical analysis. GOSR1:  $p = 0.0115$

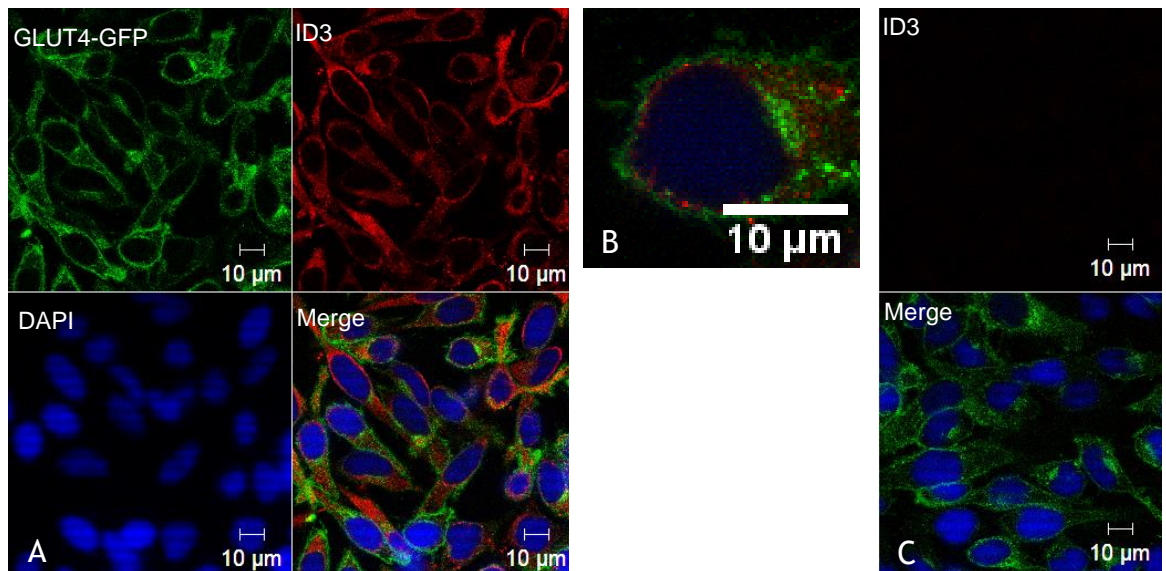
Similarly, lower colocalisation values suggest that GLUT4 is accumulating upstream of the ERGIC with the respective SNARE protein being involved in this part of GLUT4 trafficking. According to Figure 6.4, only the knock-down of GOSR1 lead to significant decrease of colocalisation of GLUT4 and ERGIC-53, suggesting that this SNARE protein is involved in GLUT4 trafficking upstream of the ERGIC. The knock-down of Stx6 also lead to a notable decrease in colocalisation, however, with  $p = 0.07$ , this did not reach statistical significance.

#### **6.2.1.2 GLUT4 Colocalisation with the ER**

Similar to the ERGIC staining, Figure 6.5 A shows HA-GLUT4-GFP HeLa cells stained with the ER marker ID3. As expected, the staining is broadly dispersed within the cells and the control experiment in panel B shows that there is no non-specific binding of the secondary antibody.

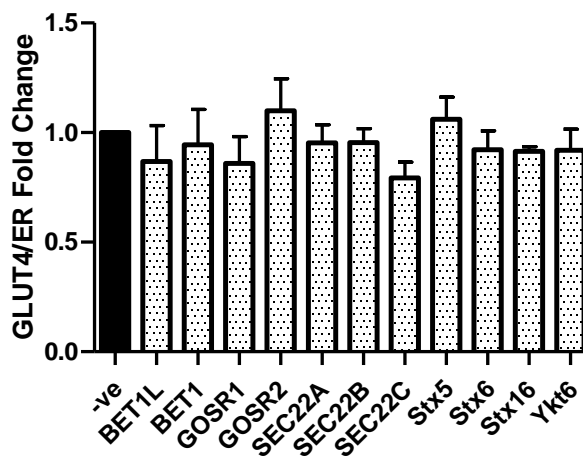
Similar to the experiment shown in Figure 6.4, colocalisation of GLUT4 with the ER was determined. The results are summarised in Figure 6.6. Decreased colocalisation values, compared to the negative control, would suggest that the respective SNARE is involved in GLUT4 trafficking upstream of the ER, whereas increased colocalisation is an indicator for a role downstream between the ER and the ERGIC. The raw data of all four experiments were pooled and depicted as fold change compared to the negative control experiment. Statistical analysis using 2-way ANOVA did not show any significant changes of the colocalisation of GLUT4 and the ER-marker ID3 after knock-down of the investigated SNAREs.





**Figure 6.5 ER and DAPI Staining of HA-GLUT4-GFP HeLa Cells (negative control)**

HA-GLUT4-GFP HeLa cells were cultured on a 96 well plate with glass bottom as outlined in section 2.2.1.1. siRNA knock-down was carried out as described in 2.2.1.6, shown here is an image of the negative control cells, where siRNA was replaced by water. Cells were fixed and stained with an antibody for the ER marker ID3 and the nucleus was stained with DAPI as described in 2.2.2.1. Images were acquired on a confocal microscope and show GLUT4-GFP, the ER staining, the nucleus staining (DAPI) and a merge of all three channels. A: Representative image of ER staining B: Zoomed in image from A to show colocalisation C: Representative image of block control without primary antibody.

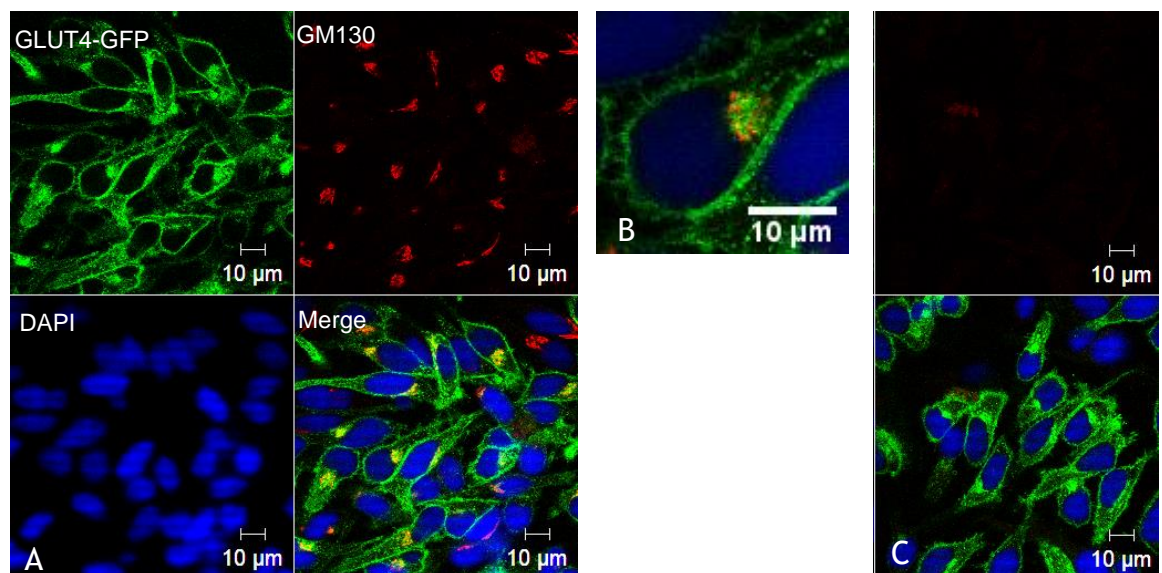


**Figure 6.6 GLUT4/ER Colocalisation**

HA-GLUT4-GFP HeLa cells were cultured on a 96 well plate with glass bottom as outlined in section 2.2.1.1. siRNA knock-down was carried out as described in 2.2.1.6. Cells were fixed and stained with an antibody for the ER marker ID3 and two consecutive images were acquired by confocal microscopy. Colocalisation of GLUT4-GFP and ID3 was determined using the ImageJ plugin JaCoP (see 2.2.8.3). Between 5 and 10 sets of images were analysed per knock-down and each experiment was carried out in four biological replicates. The data of all four experiments was pooled and normalised to the average value of the negative control experiment and 2-way ANOVA with 95 % confidence intervals was carried out for statistical analysis. There were no significant changes compared to the negative control.

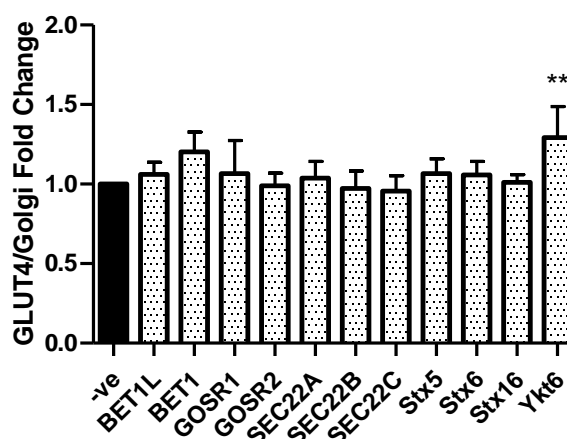
### 6.2.1.3 GLUT4 Colocalisation with the Golgi

Finally, colocalisation of GFP-tagged GLUT4 with GM130, a marker of the Golgi, was investigated in a third set of experiments. Figure 6.7 shows the Golgi staining, which is notably different from the ERGIC and ER staining in Figure 6.3 and Figure 6.5, respectively. As expected, the Golgi is localised in a perinuclear region and is not as widely distributed as other organelles. The control experiment in panel B showed once again that there was very limited non-specific binding of the secondary antibody. Colocalisation data was obtained as previously described and is summarised in Figure 6.8. Decreased colocalisation compared to the negative control after knock-down would argue for an accumulation of GLUT4 upstream of the Golgi, while an increase would signify an involvement of the respective SNARE downstream of the Golgi. The experiment was carried out in four biological replicates and the data was pooled and normalised to the average colocalisation value of the negative control. Statistical analysis was conducted by 2-way ANOVA and the result is depicted in Figure 6.8. According to this data, the knock-down of Ykt6 lead to a significant increase in colocalisation of GLUT4 and the Golgi, indicating that the SNARE protein is involved in GLUT4 trafficking downstream of the Golgi.



**Figure 6.7 Golgi and DAPI Staining of HA-GLUT4-GFP HeLa Cells (negative control)**

HA-GLUT4-GFP HeLa cells were cultured on a 96 well plate with glass bottom as outlined in section 2.2.1.1. siRNA knock-down was carried out as described in 2.2.1.6, shown here is an image of the negative control cells, where siRNA was replaced by water. Cells were fixed and stained with an antibody for the Golgi marker GM130 and the nucleus was stained with DAPI as described in 2.2.2.1. Images were acquired on a confocal microscope and show GLUT4-GFP, the Golgi staining, the nucleus staining (DAPI) and a merge of all three channels. A: Representative image of Golgi staining B: Zoomed in image from A to show colocalisation C: Representative image of block control without primary antibody.

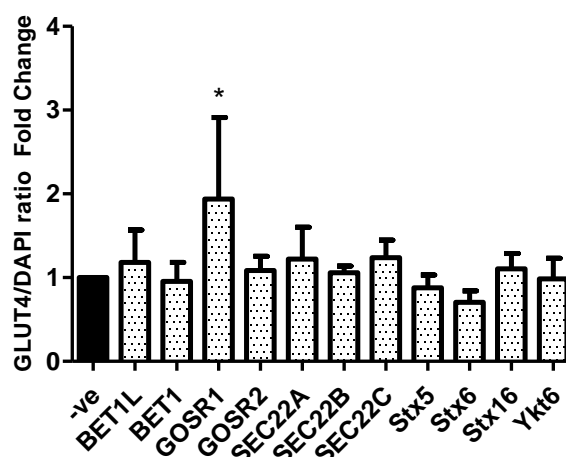


**Figure 6.8 GLUT4/Golgi Colocalisation**

HA-GLUT4-GFP HeLa cells were cultured on a 96 well plate with glass bottom as outlined in section 2.2.1.1. siRNA knock-down was carried out as described in 2.2.1.6. Cells were fixed and stained with an antibody for the Golgi marker GM130 and two consecutive images were acquired by confocal microscopy. Colocalisation of GLUT4-GFP and GM130 was determined using the ImageJ plugin JaCoP (see 2.2.8.3). Between 5 and 10 sets of images were analysed per knock-down and each experiment was carried out in four biological replicates. The data of all four experiments was pooled and normalised to the average value of the negative control experiment and 2-way ANOVA with 95 % confidence intervals was carried out for statistical analysis. Ykt6:  $p = 0.0036$ .

## 6.2.2 Total GLUT4 Levels after SNARE Knock-Down

We were interested in the total levels of GLUT4 after the knock-down of the aforementioned SNAREs. Traditionally, levels would be determined via western blot analysis. However, we chose to remain true to the central microscopy theme of this thesis and calculated the total GLUT4 levels as a ratio of the GLUT4-GFP fluorescence over DAPI signal (nucleus staining). The results of four separate experiments are shown in Figure 6.9. An augmented GLUT4/DAPI ratio signify increased GLUT4 expression, possibly as a compensation mechanism for disturbed intracellular GLUT4 trafficking. Reduced values on the other hand, indicate diminished GLUT4 levels, which could be due to impaired GLUT4 synthesis.



### Figure 6.9 Total GLUT4 Levels after siRNA Knock-Down

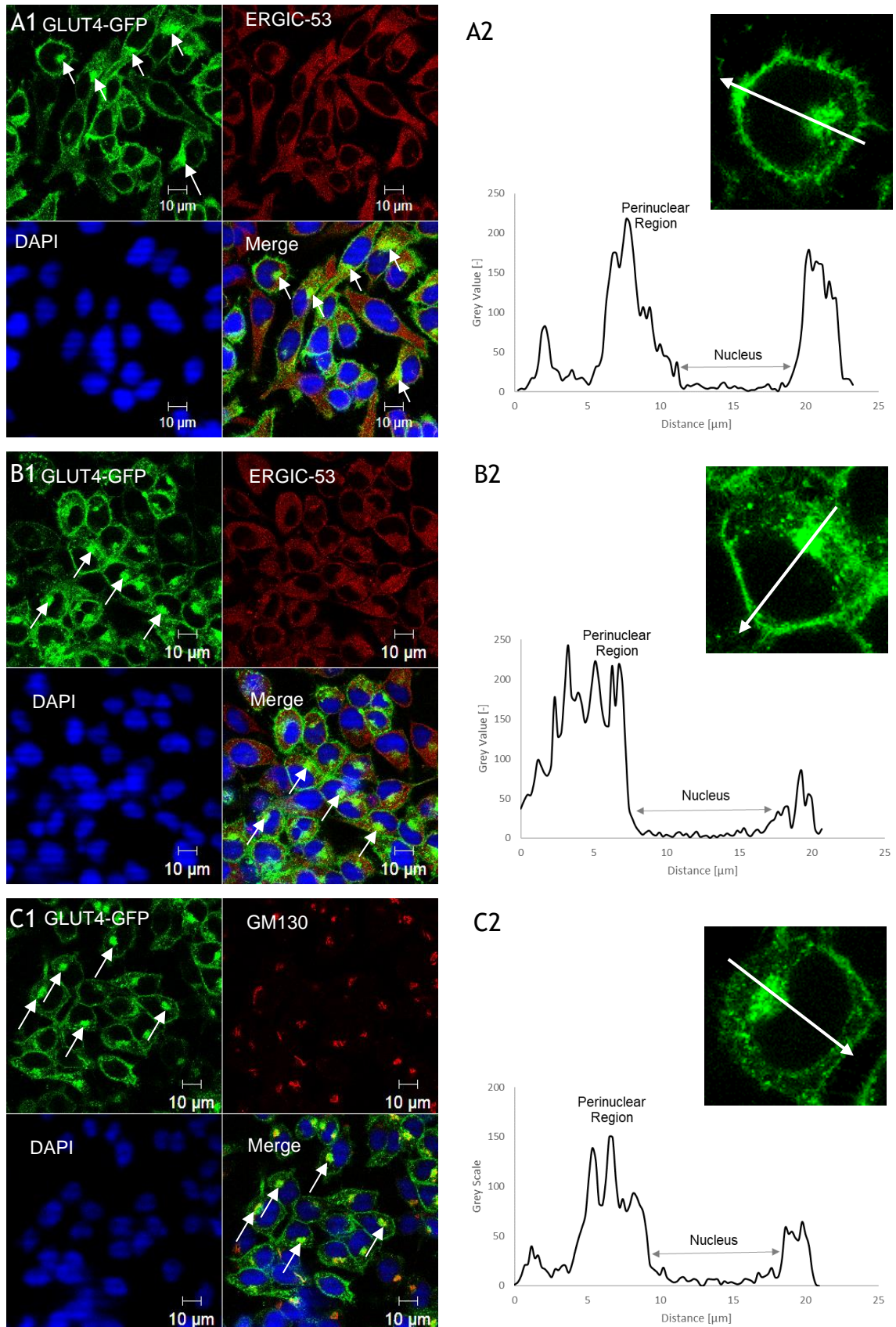
HA-GLUT4-GFP HeLa cells were cultured on a 96 well plate with glass bottom as outlined in section 2.2.1.1. siRNA knock-down was carried out as described in 2.2.1.6. Cells were fixed and the nucleus stained with DAPI. Total GLUT4 levels were compared by determining the ratio of DAPI signal over GLUT4-GFP signal. Between 5 and 10 sets of images were analysed per knock-down. Data of all four experiments was pooled and normalised to the average value of the negative control experiment. 2-way ANOVA with 95 % confidence intervals was carried out for statistical analysis. GOSR1:  $p = 0.0115$ .

The experiment was repeated four times and the data points were normalised to the average negative control GLUT4/DAPI ratio, which is shown in Figure 6.9.

Statistical analysis by 2-way ANOVA revealed a significant increase of GLUT4/DAPI ratio, and hence an increase in GLUT4 expression, after knock-down of GOSR1.

### 6.2.3 Intracellular GLUT4 Distribution After SNARE Knock-Down

The intracellular distribution of GLUT4 was examined visually after knock-down of those SNARE proteins that had been identified in 6.2.1 and 6.2.2, namely GOSR1 and Ykt6. Images of negative control cells as well as knock-down cells are depicted in Figure 6.10. Additionally, single cells were selected from each knock-down as well as from the negative control and an intensity profile of the GLUT4-GFP signal of each cell was generated in ImageJ, which is also shown.



**Figure 6.10 Intracellular GLUT4 Distribution**

HA-GLUT4-GFP HeLa cells were cultured on a 96 well plate with glass bottom as outlined in section 2.2.1.1. siRNA knock-down and staining was carried out as described in 2.2.1.6 and 2.2.2.1. Images show GLUT4-GFP, the ERGIC or Golgi staining, the nucleus staining (DAPI) and a merge of all three channels. Perinuclear GLUT4 concentration is highlighted by white arrows. Single cells were randomly selected and intensity profiles of the GLUT4 signal was generated along the white arrow using ImageJ. A: negative control B: GOSR1 knock-down C: Ykt6 knock-down.



Figure 6.10 A1 shows the typical intracellular distribution of GLUT4 in the basal state. A large fraction of the protein is located in the perinuclear region, which is depicted by white arrows. The fluorescence intensity profile through the cross section of a single cell shows the same, with a strong intensity peak in the perinuclear region and smaller peaks closer to the plasma membrane. Consistent with studies in other cell types, including adipocytes (Dawson et al., 2001; O. J. Martin et al., 2006; Powell et al., 1999), GLUT4 is also widely dispersed throughout the cell in punctae, likely corresponding to small vesicles.

Knock-down of involved SNARE proteins was suspected to have an effect on GLUT4 distribution within the cell. Representative images of cells after knock-down of GOSR1 and Ykt6 are shown in panels B and C. The knock-down of GOSR1, which was characterised by decreased colocalisation of GLUT4 and the ERGIC appeared to have little visual effect on the intracellular distribution of GLUT4, although it could be argued that the perinuclear GLUT4 cluster is somewhat denser than in the negative control. An impression that is deepened by the intensity profile that shows a much wider perinuclear region GLUT4-GFP intensity peak. GOSR1 knock-down also resulted in increased total GLUT4 levels, which is also evident in Figure 6.10 B, where the GFP signal is visibly more pronounced than in the negative control image in panel A, even though acquisition parameters were not changed between the two data sets.

Knock-down of Ykt6 had a similar effect and GLUT4 appears to be more concentrated in the periphery of the nucleus than in the control. This observation is in accordance with the finding that GLUT4/Golgi colocalisation is increased after Ykt6 knock-down.

### **6.3 Discussion**

In Chapter 3, the suitability of HeLa cells as a cell model for GLUT4 trafficking was investigated. Here, the cell line was used as a model for an initial screen of SNARE proteins potentially affecting intracellular GLUT4 trafficking.

Out of the eleven SNARE proteins that were investigated, knock-down of GOSR1 and Ykt6 showed altered characteristics in HeLa cells. Knocking down GOSR1 resulted in decreased colocalisation of GLUT4 with the ERGIC and increased

levels of total GLUT4, Stx6 also showed lower colocalisation, although this did not reach statistical significance. Ykt6 knock-down lead to increased GLUT4 colocalisation with the Golgi.

Total GLUT4 levels were measured as GLUT4-GFP signal in relation to the DAPI-nucleus staining, which was presumed to be unaffected by siRNA knock-down. This was also the reason why we did not carry out HA staining, as this requires the same channel as needed for DAPI staining. It has to be kept in mind that this type of analysis method for measuring total GLUT4 levels is at best semi-quantitative and for more reliable results western blotting of whole cell lysates or qPCR should be carried out, which could also be employed to verify the result presented here. Alternatively, FACS analysis would likely be more accurate by analysing larger numbers of cells in each experiment. These caveats notwithstanding, the data presented here, is a good primary indication of which SNARE proteins might affect the expression levels of GLUT4 and could direct future research endeavours.

The colocalisation experiments highlighted GOSR1, Stx6 and Ykt6 as potential participants in intracellular GLUT4 trafficking. After knock-down of GOSR1 and Stx6, GLUT4 content is reduced in the ERGIC. Images of GOSR1 knock-down cells suggest that GLUT4 is more concentrated in the perinuclear region. However, there is no increased colocalisation with the Golgi, which is located in the same position. These results suggest that GOSR1 is involved in the trafficking upstream of the ERGIC, however, since the Golgi colocalisation is not affected, this would imply that GOSR1 is not part of the GSC Golgi recycling pathway. GOSR1 is located in the *cis*-Golgi and involved in ER to Golgi trafficking (Subramaniam et al., 1996; Zhang & Hong, 2001), which we now know includes the ERGIC. It is plausible that GLUT4 traffics between the ER and the ERGIC with the help of a SNARE complex including GOSR1. Our results are in accordance with the findings presented by Camus *et al.*, which suggest a role of the ERGIC in the formation of the GSC in human cells. Since GSC formation is not affected by depletion of GM130, Camus *et al.* also suggest a bypass of the Golgi in line with our observations, and hypothesise that this may be due to a delayed maturation of carbohydrate side chains, which had previously been observed (Camus et al., 2020; Hudson et al., 1992). Knock-down of the SNARE protein not only leads to

an accumulation of GLUT4 in the ERGIC, but also results in increased levels of total GLUT4. This may be a compensation mechanism of the cells to increase GLUT4 expression when trafficking between the ER and the ERGIC and therefore translocation of the transporter to the GSC is impaired. However, there are other possible explanations for the increased GLUT4-GFP fluorescence intensity. GLUT4 may be accumulating in a different compartment as a result of the GOSR1 knock-down, leading to an accumulated fluorescence signal that is falsely interpreted. Alternatively, it is possible that degradation of GLUT4 is decreased due to reduced de-novo synthesis of GLUT4.

Our data, albeit not statistically significant, support the role of Stx6 in intracellular GLUT4 trafficking proposed by previous studies from our group, consistent with Stx6 localisation to the TGN region (Perera et al., 2003).

The knock-down of Ykt6 demonstrated an increase in Golgi colocalisation. This suggests an involvement of the SNARE protein in GLUT4 trafficking downstream of the Golgi. Previous studies have shown that Ykt6 is associated with the Golgi. Zhang and Hong (2001) found Ykt6 predominantly in the *cis*-Golgi, where they attributed a role in ER-Golgi trafficking to the protein, and found it forming a SNARE complex with Stx5, GOSR1, and BET1. Tai *et al.* (2004) on the other hand, argued its involvement in transport between the TGN and early/recycling endosomes, where they suggested Ykt6 forms part of a SNARE complex consisting of Stx5, GOSR1 and GS15. Our data supports Tai *et al.*'s findings and it is possible that GLUT4 is trafficked between the TGN and the endosomal system with the help of Ykt6.

The results reported in this chapter must be viewed critically. Only initial experiments could be carried out due to time constraints. For the future, however it is important to repeat these experiments using stricter controls. For one, knock-down of the proteins of interest should be verified by means of western blotting. Lack of reliable respective antibodies lead to the decision to forgo this important test. However, the oligonucleotide pairs used for siRNA knock-down were the same used by Simpson *et al.* (2012) and we strictly followed their protocol for knock-down experiments.



For siRNA knock-down, short oligonucleotide sequences are used to induce interference with the target mRNA, this is often associated with off-target effects, in which parts of the relatively short sequences bind to other, irrelevant mRNA. Such off-target effects are called microRNA-like off-target effects and were first described when a screening of siRNAs that meant to interfere with one certain mRNA lead to multiple different phenotypes because of unspecific binding to other sequences (Jackson & Linsley, 2010). To avoid this type of off-target effects, it is important to carry out the knock-down with more than one siRNA sequence. In this study, two sequences were used for each knock-down, but a higher number is advantageous. Further important control experiments include rescue experiment controls, in which the knocked-down SNARE is reintroduced by transfection.

With regards to the colocalisation data, it is important to note that there cannot be “true colocalisation”, as this would mean that two proteins are located in the same position at the same time, which is impossible. When two signals colocalise, it is in fact their PSFs that are overlapping. Colocalisation therefore depends on spatial resolution of the microscope. For LSM, this means two “colocalised” molecules are within ~200 nm of each other, which is in biological terms a significant distance.

The data collected for this chapter is by no means conclusive for GLUT4 trafficking, because HeLa cells do not express endogenous GLUT4 and may exhibit distinct subtle differences to muscle and adipocytes, the normal sites of GLUT4 expression. However, since the genetically modified HA-GLUT4-GFP HeLa cell line behaves similarly to the preferred cell model 3T3 L1 and also in light of the findings by Camus *et al.*, who argue for distinct trafficking mechanisms in human cells, it can be used as a tool for pre-screening of an siRNA library as reported here. Narrowing down the siRNA library previously consisting of eleven SNARE proteins potentially involved in intracellular GLUT4 trafficking to a smaller number provides a significant advantage for subsequent studies in more relevant models, which can focus on a smaller number of targets and thus save resources and time. With regards to the findings reported in this chapter, the SNARE proteins GOSR1, Stx6, and Ykt6 are suggested to be investigated further. Knock-down or knock-out of those three, as opposed to eleven, proteins can be

carried out preferably in a human adipocyte or myocyte cell line and effects on GLUT4 trafficking, translocation and total levels can be investigated by means of microscopy or more traditional biochemistry techniques.

## Chapter 7 Discussion

### 7.1 Summary of Results

The objective of this work can be split into two main branches. Firstly, the dynamics of GLUT4 in the plasma membrane upon insulin stimulation were investigated by means of different microscopy approaches. The second aim of this work was to compare the human HeLa cell line with 3T3 L1 adipocytes and determine whether this could be used as a suitable model for GLUT4 trafficking.

With regards to plasma membrane dynamics, we had established the working hypothesis that GLUT4 clusters in the plasma membrane are maintained by unphosphorylated PI. Insulin stimulation leads to activation of PI4KIII $\alpha$  through mobilisation of EFR3a and subsequent phosphorylation of PI to PI4P, which releases GLUT4 from the clusters (see Figure 1.9). To test this hypothesis, we sought to develop a microscopy-based assay that would allow us to quantify the clustering and dispersal of GLUT4 in the plasma membrane. Using SpIDA and BN-PAGE, we tested whether the clustering behaviour is related to the oligomeric state of the transporter. We found that GLUT4 is indeed highly oligomeric, however, the degree of oligomerisation did not change upon insulin stimulation. TIRFM offered exciting insights into the dynamics of GLUT4 in the vicinity of the plasma membrane but the method was not powerful enough to resolve single clusters of GLUT4 after insulin stimulation.

Using dSTORM, we managed to visualise clusters of GLUT4 and quantification by Bayesian cluster analysis and Ripley's K function analysis indeed showed that insulin stimulation induces dispersal of GLUT4 from clusters. The hypothesis that EFR3 is involved in the dynamics of GLUT4 in the plasma membrane was first derived from the finding that  *$\Delta hxt fgy1-1 fgy4X$*  mutant strains of *Saccharomyces cerevisiae* depleted of all endogenous GLUTs could translocate GLUT4 to the cell surface and grow on glucose medium (Wieczorke et al., 2003). The mammalian homologue to *fgy1-1* is EFR3 and this protein had been investigated extensively by Laidlaw (2018) in the context of insulin stimulated glucose uptake and GLUT4 translocation to the plasma membrane. Laidlaw found that EFR3a knock-down has an inhibitory effect on glucose uptake in 3T3 L1 adipocytes and overexpression of the protein leads to increased plasma membrane located

GLUT4. We built on this research by knocking down EFR3a in 3T3 L1 adipocytes and subjected these modified cells to dSTORM. The exciting result was that EFR3a knock-down indeed resulted in disturbed GLUT4 dispersal, suggesting that our hypothesis that EFR3a facilitates GLUT4 dispersal in response to insulin (see section 1.8) was correct. In addition to this, we found that Galectin-3 inhibits not only GLUT4 translocation but also dispersal in the plasma membrane.

Finally, we investigated the suitability of HeLa cells as a model for GLUT4 trafficking by means of confocal and TIRF microscopy and found that the cell line does behave similarly to the commonly used cell line 3T3 L1 with regards to insulin induced GLUT4 translocation to the plasma membrane. The results presented in Chapter 4 add to these findings, since GLUT4 forms highly oligomerised complexes in both cell types. Based on these findings, we carried out a preliminary screening of SNARE proteins that may be involved in intracellular GLUT4 trafficking between the ER, the ERGIC, and the Golgi in HeLa cells and found a potential role for the SNAREs GOSR1 and Ykt6 as knock-down of these proteins affected intracellular distribution of GLUT4.

For this work, a number of different microscopes were used. CLSM was employed to carry out SpIDA and for acquiring HA surface stained images of HA-GLUT4-GFP expressing cells. With the help of TIRFM we investigated the dynamics of GLUT4 in the vicinity of the plasma membrane. dSTORM, a powerful SMLM technique, finally allowed us to visualise single GLUT4 molecules in the plasma membrane of 3T3 L1 adipocytes and characterise the clustering behaviour of the transporter. Each technique came with its own advantages and disadvantages. CLSM is a standard microscopy technique that is easy to carry out and most laboratories (including ours) have access to such an instrument. Its resolution is diffraction limited, which means it cannot resolve GLUT4 clusters and even though its resolution in the z plane is improved compared to standard epifluorescence microscopy, there is still a significant amount of background signal, which makes it difficult to focus on the plasma membrane. This issue is improved in TIRFM, where only a thin layer adjacent to the coverslip is illuminated by the evanescent wave created by TIR. This allows elimination of background fluorescence but does not limit the signal to the plasma membrane. Our homebuilt TIRFM setup came with its own unique challenges that were

mostly of an engineering nature, e.g. the manipulation of the critical angle was difficult due to the position of the screw gauge. dSTORM was clearly the method of choice to resolve single molecules of plasma membrane GLUT4. Sample preparation and the technique itself was relatively straightforward, however, it did require travelling to an external imaging facility. As opposed to CLSM and TIRFM, dSTORM had to be carried out in fixed cells, which meant that the dynamics of cluster dispersal in response to insulin eluded us.

## 7.2 Results in the Context of Existing Literature

Type 2 Diabetes belongs to the world's most common diseases and its prevalence is on the rise (Tareque et al., 2016). Current medication for type 2 diabetes treats the main symptom of the illness, which is to lower blood glucose levels, often by increasing insulin sensitivity, or failing that, insulin has to be administered externally (Maruthur et al., 2016). There is no cure and since the molecular reasons for the outbreak of the disease are still unknown, there is no medication to treat the cause of type 2 diabetes.

Intracellular GLUT4 trafficking as well as insulin induced GLUT4 translocation are well characterised (Bryant et al., 2002; S. Huang & Czech, 2007; Leto & Saltiel, 2012; Saltiel & Kahn, 2001; Tavaré et al., 2001) but only few studies shed light on the dynamics of GLUT4 in the plasma membrane itself (Bai et al., 2007; Gao et al., 2017; S. Huang et al., 2007; Jiang et al., 2008; C. H. Li et al., 2004; Lizunov et al., 2005; Lizunov, Lee, et al., 2013; Lizunov, Stenkula, et al., 2013; Stenkula et al., 2010; Y. Xu et al., 2011). Lizunov *et al.* (2013) were the first to propose clustering of the transporter in the membrane and dispersal upon insulin stimulation. Using dSTORM, we confirmed these findings and while this work was carried out, Gao *et al.* (2017) published similar findings, also using dSTORM.

A lot of basic research is still to be conducted to unravel the complexities of GLUT4 trafficking and basic research is the foundation of drug development. Without understanding the molecular mechanisms of a disease, it is not possible to develop a directed approach to alleviate it. In this work, HA-GLUT4-GFP expressing HeLa cells were studied as a potential cell model and deemed suitable to carry out preliminary screening tests. Using a cell line that is as easy

to maintain and genetically manipulate as HeLa cells has the great advantage that a substantial number of experiments can be carried out relatively easily.

Previously, VAMP2 and VAMP4 have been found to play important roles in the delivery of GSVs to the plasma membrane and to the GSC, respectively, in 3T3 L1 adipocytes (Sadler, 2014). Knocking down VAMP2 in HeLa cells results in significantly reduced GLUT4 translocation to the plasma membrane, while VAMP4 knock-down also leads to impairment, albeit not significantly (S. Morris et al., 2020). This example shows that knock-down experiments in HeLa cells can give conclusive results with regards to GLUT4 trafficking. Screening of HA-GLUT4-GFP HeLa cells that are depleted of different VAMP isoforms would have focussed on VAMP2 and VAMP4 in simple experiments quickly and without the difficulties that come with genetic manipulation of cell lines such as 3T3 L1.

## 7.3 Future Directions

### 7.3.1 GLUT4 Clustering and EFR3a

Our hypothesis is that the insulin-induced dispersal of GLUT4 in the plasma membrane of adipocytes is defective in individuals with type 2 diabetes and we propose this mechanism as a potential new drug target. The finding that knock-down of EFR3a inhibits GLUT4 dispersal is the first step in this direction. We showed that dSTORM can be used as an effective and reproducible tool to visualise the clustering of GLUT4 in the plasma membrane and quantify its dispersal upon insulin stimulation with the means of cluster analysis. This assay opens up an immense variety of possible research approaches. Gao *et al.* (2017) used it to carry out a number of interesting experiments. They investigated GLUT4 clustering in insulin resistant 3T3 L1 adipocytes and found that clustering is enhanced in those cells. They found the same for F<sup>5</sup>QQI mutated cells. In order to investigate whether GLUT4 clusters are related to lipid rafts, they treated basal F<sup>5</sup>QQA-GLUT4 mutant 3T3 L1 adipocytes with methyl- $\beta$ -cyclodextrin and found that this led to a reduction of clustering to levels similar to those in wild-type adipocytes.

To define the role of EFR3a further, it would be of great interest to investigate the effect of EFR3a overexpression, which would be expected to result in

decreased clustering. Another obvious experiment is the knock-down or overexpression of PI4KIII $\alpha$  and its effect on GLUT4 clusters. Our hypothesis suggested that GLUT4 clusters are maintained by pools of PI. This offers another interesting approach. As part of her work, Laidlaw implemented a pseudojanin system, which allows the targeted manipulation of PI, by dephosphorylating the 4' and/or 5' phosphate. The proteins FKBP (FK506 Binding Protein 12) and FRB (FKBP rapamycin binding protein) can bind to each other in the presence of rapamycin. In the system, the FKBP component is fused to the pseudojanin phosphatase, which can dephosphorylate the 4' and/or 5' phosphate of PI. By fusing the second component, FRB, with a membrane anchor, such as LYN11, the pseudojanin is directed to the plasma membrane after induction with rapamycin, allowing the direct manipulation of PI patches (Hammond et al., 2014; Laidlaw, 2018). In combination with the dSTORM assay presented here, this could be an interesting experiment to further test our hypothesis. 4' phosphorylation of PI should result in dispersal of GLUT4 even in the absence of insulin or after knock-down of PI4KIII $\alpha$ .

We showed that the knock-down of EFR3a in 3T3 L1 adipocytes results in impaired GLUT4 dispersal after insulin stimulation and Gao *et al* (2017) showed that insulin resistance is related to deficient GLUT4 dispersal. It would be interesting to explore GLUT4 dispersal and the role of EFR3a in other cell types. An obvious one would be muscle cells, such as C<sub>2</sub>C<sub>12</sub>, where GLUT4 is also expressed. Interestingly this myocyte cell line lacks an insulin-responsive GSC (Tortorella & Pilch, 2002) and muscle cells respond with GLUT4 translocation to exercise (Z. Li et al., 2018). It would be interesting to investigate whether GLUT4 also clusters in the plasma membrane of C<sub>2</sub>C<sub>12</sub> myotubes and whether it disperses in response to exercise. This could be investigated in combination with optoelectric stimulation. For this approach, C<sub>2</sub>C<sub>12</sub> cells are transfected with a light-sensitive variant of channelrhodopsin, which allows induction of contractility by stimulation with light pulses (Ambrosi et al., 2014; Asano et al., 2015).

Other obvious models are primary cells and tissue samples of healthy humans and type 2 diabetics. Is GLUT4 dispersal defective in diabetics? Is EFR3a expressed in adipose tissue of diabetics at lower levels than in healthy test

subjects? If the answer to both these questions is yes, EFR3a could be investigated as a potential new drug target. An active component that rescues the phenotype of impaired GLUT4 dispersal would need to be investigated in terms of its ability to rescue insulin stimulated glucose uptake for example in EFR3a knock-down 3T3 L1 adipocytes.

### **7.3.2 HeLa Cells as Model for GLUT4 Trafficking**

In Chapter 6 a preliminary screening was carried out to find SNARE proteins involved in intracellular GLUT4 trafficking. GOSR1 and Ykt6 were found to be involved in the trafficking between the ER, the ERGIC, and the Golgi. These results can build the basis for more detailed research that concentrates on the exact role of GOSR1 and Ykt6. As discussed in section 6.3, the results have to be verified in larger-scale screenings, e.g. FACS or plate reader analysis and a similar study in a more relevant cell model, such as 3T3 L1 adipocytes, would be advisable too, to confirm the involvement of these SNAREs in GLUT4 trafficking. Yeasts offer another interesting platform, GOSR1 and Ykt6 can be knocked out and effects on cell growth (is knock-out lethal?) and glucose metabolism can be investigated. Furthermore, it would be interesting to study which other SNAREs are associated with GOSR1 and Ykt6 in SNARE complexes and what effect the disturbance of these complexes has on intracellular GLUT4 trafficking as well as GLUT4 translocation to and dispersal in the plasma membrane in response to insulin.

GSV kinetics near the plasma membrane may not be completely comparable in HeLa cells and 3T3 L1 adipocytes, but insulin stimulation clearly leads to translocation of GLUT4 in both cell types, which makes them a valuable model for screenings such as the one carried out in this work. Recent findings suggest that GLUT4 trafficking indeed differs in human and in murine cells (Camus et al., 2020), arguing that a human cell line such as HeLa may be even more suitable for some investigations.

As a next step, and to bring the two strands of this work together, dSTORM experiments should be carried out in HA-GLUT4-GFP HeLa cells to determine whether GLUT4 clusters and disperses in the same way as in 3T3 L1 adipocytes. Laidlaw (2018) found that HeLa cells express EFR3a, so this is indeed plausible.



It would be easy to establish a stable EFR3a knock-out HeLa cell line, on which potential active ingredients could be tested as discussed previously.

## 7.4 Conclusions

The main objective of this work was to develop a microscopy-based assay to visualise and quantify the clustering and dispersal of GLUT4 in the plasma membrane. Using dSTORM, this aim has been met. Additionally, advances have been made in uncovering the molecular mechanisms behind these dynamics and EFR3a was identified as potential key component.

The second aim of this work was to establish a HeLa cells expressing HA-GLUT4-GFP as a model cell line to study GLUT4. HA-GLUT4-GFP HeLa cells have been characterised with regards GLUT4 dynamics near the plasma membrane and deemed suitable as a model cell line for preliminary screenings, of which we carried out one to identify SNARE proteins involved in intracellular GLUT4 trafficking.

## **Chapter 8 Appendices**



Figure 8.1 Full GAPDH Blot from Figure 5.10

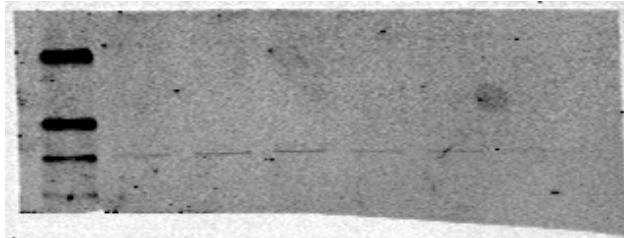


Figure 8.2 Full EFR3a Blot from Figure 5.10

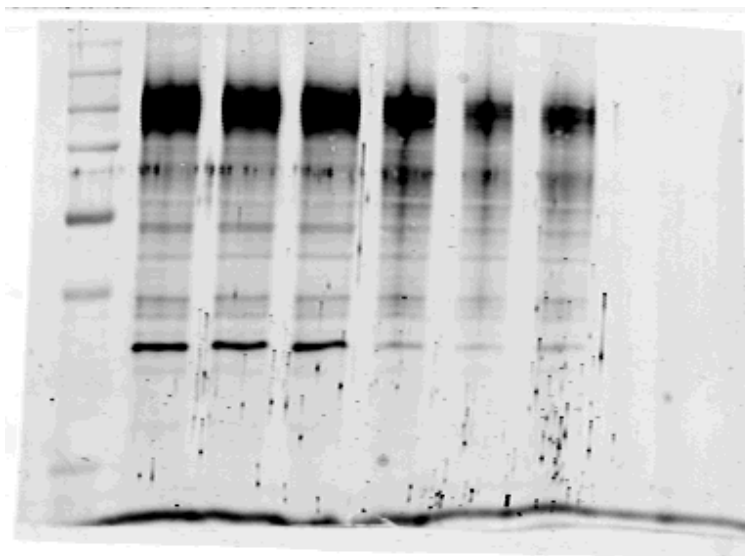


Figure 8.3 Full GLUT4 Blot from Figure 5.10

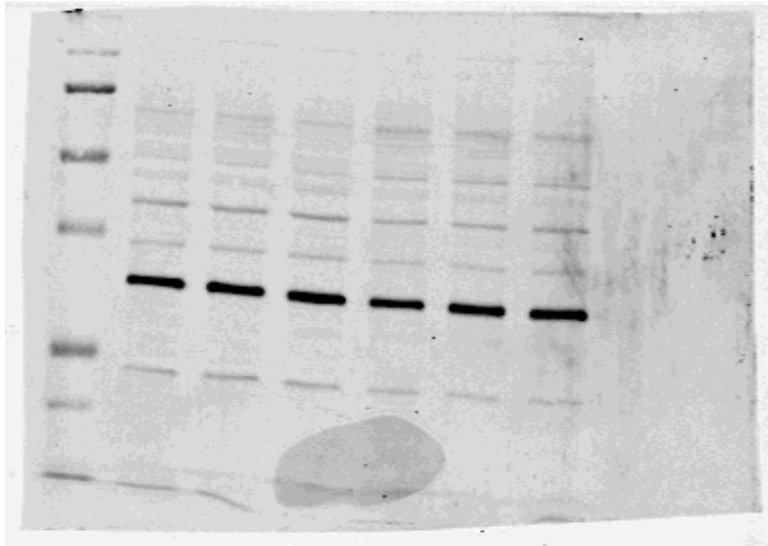


Figure 8.4 Full Stx16 Blot from Figure 5.10



Figure 8.5 Full SNAP23 Blot from Figure 5.10

## List of References

- Abbe, E. (1873). Beiträge zur Theorie des Mikroskops und der mikroskopischen Wahrnehmung. *Archiv Für Mikroskopische Anatomie*, 9, 413-418.
- Abel, E. D., Peroni, O., Kim, J. K. K. Y., Boss, O., Hadro, E., Minnemann, T., et al. (2001). Adipose-selective targeting of the GLUT4 gene impairs insulin action in muscle and liver. *Nature*, 409(6821), 729-733.
- Adnan, M., Islam, W., Zhang, J., Zheng, W., & Lu, G.-D. (2019). Diverse Role of SNARE Protein Sec22 in Vesicle Trafficking, Membrane Fusion, and Autophagy. *Cells*, 8(337), 1-15. <https://doi.org/10.3390/cells8040337>
- Al-hasani, H., Sanders Hinck, C., & Cushman, S. W. (1998). Endocytosis of the Glucose Transporter GLUT4 Is Mediated by the GTPase Dynamin. *The Journal of Biological Chemistry*, 273(28), 17504-17510.
- Albiston, A. L., McDowall, S. G., Matsacos, D., Sim, P., Clune, E., Mustafa, T., et al. (2001). Evidence That the Angiotensin IV (AT 4) Receptor Is the Enzyme Insulin-regulated Aminopeptidase. *The Journal of Biological Chemistry*, 276(52), 48623-48626. <https://doi.org/10.1074/jbc.C100512200>
- Ali, M. H., & Imperiali, B. (2005). Protein oligomerization : How and why. *Bioorganic and Medicinal Chemistry*, 13, 5013-5020. <https://doi.org/10.1016/j.bmc.2005.05.037>
- Ambrose, E. J. (1961). The Movements of Fibrocytes. *Experimental Cell Research, Suppl 8*, 54-73.
- Ambrose, W. P., Goodwin, P. M., & Nolan, J. P. (1999). Single-Molecule Detection With Total Internal Reflection Excitation: Comparing Signal-to-Background and Total Signals in Different Geometries. *Cytometry*, 36, 224-231.
- Ambrosi, C. M., Klimas, A., Yu, J., & Entcheva, E. (2014). Cardiac applications of optogenetics. *Progress in Biophysics and Molecular Biology*, 115(2-3), 294-

304. <https://doi.org/10.1016/j.pbiomolbio.2014.07.001>

- Annibale, P., Vanni, S., Scarselli, M., Rothlisberger, U., & Radenovic, A. (2011). Identification of clustering artifacts in photoactivated localization microscopy. *Nature*, *8*(7), 527-528. <https://doi.org/10.1038/nmeth.1627>
- Appenzeller-Herzog, C., & Hauri, H.-P. (2006). The ER-Golgi intermediate compartment (ERGIC): in search of its identity and function. *Journal of Cell Science*, *119*(11), 2173-2183. <https://doi.org/10.1242/jcs.03019>
- Asano, T., Ishizuka, T., Morishima, K., & Yawo, H. (2015). Optogenetic induction of contractile ability in immature C2C12 myotubes. *Scientific Reports*, *5*, 8317. <https://doi.org/10.1038/srep08317>
- Ashby, M. C., Ibaraki, K., & Henley, J. M. (2004). It's green outside: tracking cell surface proteins with pH-sensitive GFP. *TRENDS in Neurosciences*, *27*(5), 257-261. <https://doi.org/10.1016/j.tins.2004.03.010>
- Atkinson, M. A., Eisenbarth, G. S., & Michels, A. W. (2014). Type 1 diabetes. *The Lancet*, *383*(9911), 69-82. [https://doi.org/10.1016/S0140-6736\(13\)60591-7](https://doi.org/10.1016/S0140-6736(13)60591-7)
- Axelrod, D. (1981). Cell-Substrate Contacts Illuminated by Total Internal Reflection Fluorescence. *The Journal of Cell Biology*, *89*, 141-145.
- Axelrod, D. (2001a). Total Internal Reflection Fluorescence Microscopy in Cell Biology. *Traffic*, *2*, 764-774.
- Axelrod, D. (2001b). Total Internal Reflection Fluorescence Microscopy in Cell Biology. In *Methods in enzymology* (Vol. 361).
- Bai, L., Wang, Y., Fan, J., Chen, Y., Ji, W., Qu, A., et al. (2007). Dissecting Multiple Steps of GLUT4 Trafficking and Identifying the Sites of Insulin Action. *Cell Metabolism*, *5*(1), 47-57. <https://doi.org/10.1016/j.cmet.2006.11.013>
- Baird, D., Stefan, C., Audhya, A., Weys, S., & Emr, S. D. (2008). Assembly of the PtdIns 4-kinase Stt4 complex at the plasma membrane requires Ypp1 and

Efr3. *The Journal of Cell Biology*, 183(6), 1061-1074.

<https://doi.org/10.1083/jcb.200804003>

Barbeau, A., Godin, A. G., Swift, J. L., De Koninck, Y., Wiseman, P. W., & Beaulieu, J. M. (2013). *Quantification of receptor tyrosine kinase activation and transactivation by G-protein-coupled receptors using spatial intensity distribution analysis (SpIDA)*. *Methods in Enzymology* (1st ed., Vol. 522). Elsevier Inc. <https://doi.org/10.1016/B978-0-12-407865-9.00007-8>

Barbeau, A., Swift, J. L., Godin, A. G., Koninck, Y. De, Wiseman, P. W., & Beaulieu, J.-M. (2013). *Spatial Intensity Distribution Analysis (SpIDA): A New Tool for Receptor Tyrosine Kinase Activation and Transactivation Quantification*. *Methods in Cell Biology* (1st ed., Vol. 117). Elsevier Inc. <https://doi.org/10.1016/B978-0-12-408143-7.00001-3>

Barondes, S. H., Cooper, D. N. W., Gitt, M. A., & Leffler, H. (1994). Galectins. *The Journal of Biological Chemistry*, 269(33), 20807-20810.

Barrett, M. P., Walmsley, A. R., & Gould, G. W. (1999). Structure and function of facilitative sugar transporters. *Current Opinion in Cell Biology*, 11(4), 496-502.

Baskin, J. M., Wu, X., Christiano, R., Oh, M. S., Schauder, M., Gazzero, E., et al. (2016). The leukodystrophy protein FAM126A/Hyccin regulates PI4P synthesis at the plasma membrane. *Nat Cell Biol*, 18(5), 132-138. <https://doi.org/10.1038/ncb3271>.The

Bates, M., Blosser, T. R., & Zhuang, X. (2005). Short-Range Spectroscopic Ruler Based on a Single-Molecule Optical Switch. *Physical Review Letters*, 94(10), 108101-1-108101-4. <https://doi.org/10.1103/PhysRevLett.94.108101>

Bates, M., Huang, B., Dempsey, G. T., & Zhuang, X. (2007). Multicolor Super-Resolution Imaging with Photo-Switchable Fluorescent Probes. *Science*, 317, 1749-1753. <https://doi.org/10.1126/science.1146598>

Bellve, K. D., Leonard, D., Standley, C., Lifshitz, L. M., Tuft, R. A., Hayakawa,

- A., et al. (2006). Plasma Membrane Domains Specialized for Clathrin-mediated Endocytosis in Primary Cells. *The Journal of Biological Chemistry*, 281(23), 16139-16146. <https://doi.org/10.1074/jbc.M511370200>
- Bernhardt, U., Carlotti, F., Hoeben, R. C., Joost, H.-G., & Al-hasani, H. (2009). A dual role of the N-terminal FQQL motif in GLUT4 trafficking. *Biological Chemistry*, 390(9), 883-892. <https://doi.org/10.1515/BC.2009.095>
- Betzig, E., Patterson, G. H., Sougrat, R., Lindwasser, O. W., Olenych, S., Bonifacino, J. S., et al. (2006). Imaging Intracellular Fluorescent Proteins at Nanometer Resolution. *Science*, 313(September), 1642-1646.
- Blot, V., & McGraw, T. E. (2006). GLUT4 is internalized by a cholesterol-dependent nystatin-sensitive mechanism inhibited by insulin. *The EMBO Journal*, 25, 5648-5658. <https://doi.org/10.1038/sj.emboj.7601462>
- Bogan, J. S. (2012). Regulation of Glucose Transporter Translocation in Health and Diabetes. *Annual Review of Biochemistry*, 81(March), 507-532. <https://doi.org/10.1146/annurev-biochem-060109-094246>
- Bojjireddy, N., Guzman-Hernandez, M. L., Reinhard, N. R., Jovic, M., & Balla, T. (2014). EFR3s are palmitoylated plasma membrane proteins that control responsiveness to G protein-coupled receptors. *Journal of Cell Science*, 128(1), 118-128.
- Bolte, S., & Cordelières, F. P. (2006). A guided tour into subcellular colocalization analysis in light microscopy. *Journal of Microscopy*, 224(April), 213-232.
- Bracher, A., & Weissenhorn, W. (2002). Structural basis for the Golgi membrane recruitment of Sly1p by Sed5p. *The EMBO Journal*, 21(22), 6114-6124.
- Brewer, P. D., Habtemichael, E. N., Romenskaia, I., Mastick, C. C., & Coster, A. C. F. (2014). Insulin-regulated Glut4 translocation: Membrane protein trafficking with six distinctive steps. *Journal of Biological Chemistry*, 289(25), 17280-17298. <https://doi.org/10.1074/jbc.M114.555714>



- Brodsky, F. M. (2012). Diversity of Clathrin Function: New Tricks for an Old Protein. *Annual Review of Cell and Developmental Biology*, 28(1), 17.1-17.28. <https://doi.org/10.1146/annurev-cellbio-101011-155716>
- Bryant, N. J., & Gould, G. W. (2011). SNARE Proteins Underpin Insulin-Regulated GLUT4 Traffic. *Traffic*, 12(6), 657-664. <https://doi.org/10.1111/j.1600-0854.2011.01163.x>
- Bryant, N. J., Govers, R., & James, D. E. (2002). Regulated transport of the glucose transporter GLUT4. *Nature Reviews Molecular Cell Biology*, 3(4), 267-277. <https://doi.org/10.1038/nrm782>
- Campbell, N. A., & Reece, J. B. (2006). *Biologie*. Pearson Studium.
- Camus, S. M., Camus, M. D., Figueras-Novoa, G. B., Sadacca, L. A., Esk, C., Bigot, A., et al. (2020). CHC22 Clathrin Mediates Traffic from Early Secretory Compartments for Human GLUT4 Pathway Biogenesis. *Journal of Cell Biology*, 219(1), 1-21.
- Carlotti, F., Bazuine, M., Kekarainen, T., Seppen, J., Pognonec, P., Maassen, J. A., & Hoeben, R. C. (2004). Lentiviral vectors efficiently transduce quiescent mature 3T3-L1 adipocytes. *Molecular Therapy*, 9(2), 209-217. <https://doi.org/10.1016/j.ymthe.2003.11.021>
- Chakrabarti, R., Buxton, J., Joly, M., & Corvera, S. (1994). Insulin-sensitive Association of GLUT-4 with Endocytic Clathrin-coated Vesicles Revealed with the Use of Brefeldin A. *The Journal of Biological Chemistry*, 269(11), 7926-7933.
- Chang, L., Adams, R. D., & Saltiel, A. R. (2002). The TC10-interacting protein CIP4/2 is required for insulin-stimulated Glut4 translocation in 3T3L1 adipocytes. *Proceedings of the National Academy of Sciences of the United States of America*, 99(20), 12835-12840.
- Charron, M. J., Brosius III, F. C., Alper, S. L., & Lodish, H. F. (1989). A glucose transport protein expressed predominately in insulin-responsive tissues.

*Proceedings of the National Academy of Sciences of the United States of America*, 86(April), 2535-2539.

- Chatterjee, S., Khunti, K., & Davies, M. J. (2017). Type 2 diabetes. *The Lancet*, 389(10085), 2239-2251. [https://doi.org/10.1016/S0140-6736\(17\)30058-2](https://doi.org/10.1016/S0140-6736(17)30058-2)
- Cheatham, B., Volchuk, A., Kahn, C. R., Wang, L., Rhodes, C., & Klip, A. (1996). Insulin-stimulated translocation of GLUT4 glucose transporters requires SNARE-complex proteins. *Proceedings of the National Academy of Sciences of the United States of America*, 93(December), 15169-15173.
- Chen, Y. A., & Scheller, R. H. (2001). SNARE-Mediated Membrane Fusion. *Nature Reviews Molecular Cell Biology*, 2(February), 98-106.
- Chen, Yan, Müller, J. D., So, P. T. C., & Gratton, E. (1999). The Photon Counting Histogram in Fluorescence Fluctuation Spectroscopy. *Biophysical Journal*, 77(July), 553-567.
- Chen, Yu, & Lippincott-Schwartz, J. (2015). Selective Visualization of GLUT4 Storage Vesicles and Associated Rab Proteins Using IRAP-pHlourin. In *Rab GTPases: Methods and Protocols* (Vol. 1298, pp. 181-186). <https://doi.org/10.1007/978-1-4939-2569-8>
- Chen, Yu, Wang, Y., Zhang, J., Deng, Y., Jiang, L., Song, E., et al. (2012). Rab10 and myosin-va mediate insulin-stimulated GLUT4 storage vesicle translocation in adipocytes. *Journal of Cell Biology*, 198(4), 545-560. <https://doi.org/10.1083/jcb.201111091>
- Coling, D., & Kachar, B. (1997). Theory and Application of Fluorescence. *Current Protocols in Neuroscience*, 00(1), 2.1.1-2.1.11.
- Combs, C. (2010). Fluorescence Microscopy: A Concise Guide to Current Imaging Methods. *Current Protocols in Neuroscience Author Manuscript*, 1-19. <https://doi.org/10.1002/0471142301.ns0201s50.Fluorescence>
- Cormack, B. P., Valdivia, R. H., & Falkow, S. (1996). FACS-optimized mutants of

the green fluorescent protein (GFP). *Gene*, 173(1), 33-38.

- Cornish-Bowden, A. J., & Koshland Jr, D. E. (1971). The Quaternary Structure of Proteins Composed of Identical Subunits. *The Journal of Biological Chemistry*, 246(10), 3092-3102.
- Corvera, S., Graver, D. F., & Smith, R. M. (1989). Insulin Increases the Cell Surface Concentration of  $\alpha$ 2-Macroglobulin Receptors in 3T3-L1 Adipocytes. *The Journal of Biological Chemistry*, 264(June), 10133-10138.
- Corvera, S., Chawla, A., Chakrabarti, R., Joly, M., Buxton, J., & Czech, M. P. (1994). A Double Leucine within the GLUT4 Glucose Transporter COOH-Terminal Domain Functions as an Endocytosis Signal. *Journal of Cell Biology*, 126(4), 979-989.
- Coster, A. C. F., Govers, R., & James, D. E. (2004). Insulin Stimulates the Entry of GLUT4 into the Endosomal Recycling Pathway by a Quantal Mechanism. *Traffic*, 5, 763-771. <https://doi.org/10.1111/j.1600-0854.2004.00218.x>
- Cushman, S. W., & Wardzala, L. J. (1980). Potential Mechanism of Insulin Action on Glucose Transport in the Isolated Rat Adipose Cell. *The Journal of Biological Chemistry*, 255(10), 4758-4762.
- Davis, R. J., Corvera, S., & Czech, M. P. (1986). Insulin Stimulates Cellular Iron Uptake and Causes the Redistribution of Intracellular Transferrin Receptors to the Plasma Membrane. *The Journal of Biological Chemistry*, 261(19), 8708-8711.
- Dawicki-McKenna, J. M., Goldman, Y. E., & Ostap, E. M. (2012). Sites of glucose transporter-4 vesicle fusion with the plasma membrane correlate spatially with microtubules. *PLoS ONE*, 7(8), 1-12. <https://doi.org/10.1371/journal.pone.0043662>
- Dawson, K., Aviles-Hernandez, A., Cushman, S. W., & Malide, D. (2001). Insulin-regulated trafficking of dual-labeled glucose transporter 4 in primary rat adipose cells. *Biochemical and Biophysical Research Communications*,

287(2), 445-454. <https://doi.org/10.1006/bbrc.2001.5620>

DelVecchio, R. L., & Pilch, F. (1991). Phosphatidylinositol 4-Kinase Is a Component of Glucose Transporter (GLUT 4)-containing Vesicles. *The Journal of Biological Chemistry*, 266(20), 13278-13283.

Diabetes UK. (2016). Diabetes UK Facts and Stats.  
<https://doi.org/10.1007/s11245-009-9073-4>

Dobson, S. P., Livingstone, C., Gould, G. W., & Tavaré, J. M. (1996). Dynamics of insulin-stimulated translocation of GLUT4 in single living cells visualised using green fluorescent protein. *FEBS Letters*, 393(2-3), 179-184.  
[https://doi.org/10.1016/0014-5793\(96\)00879-4](https://doi.org/10.1016/0014-5793(96)00879-4)

Duelli, R., & Kuschinsky, W. (2001). Brain Glucose Transporters: Relationship to Local Energy Demand. *American Physiological Society*, 16(April 2001), 71-76.

Ehtisham, S., Barrett, T., & Shaw, N. (2000). Type 2 diabetes mellitus in UK children - an emerging problem. *Diabetic Medicine*, 17(12), 867-871.

El-Jack, A. K., Kandror, K. V., & Pilch, P. F. (1999). The formation of an insulin-responsive vesicular cargo compartment is an early event in 3T3-L1 adipocyte differentiation. *Molecular Biology of the Cell*, 10(5), 1581-1594.

Failer, B. U., Aschrafi, A., Schmalzing, G., & Zimmermann, H. (2003). Determination of native oligomeric state and substrate specificity of rat NTPDase1 and NTPDase2 after heterologous expression in *Xenopus* oocytes. *European Journal of Biochemistry*, 270, 1802-1809.  
<https://doi.org/10.1046/j.1432-1033.2003.03542.x>

Falkenburger, B. H., Jensen, J. B., Dickson, E. J., Suh, B., & Hille, B. (2010). Phosphoinositides: lipid regulators of membrane proteins. *Journal of Physiology*, 588(17), 3179-3185.  
<https://doi.org/10.1113/jphysiol.2010.192153>

Floyd, D. H., Geva, A., Bruinsma, S. P., Overton, M. C., Blumer, K. J., &

Baranski, T. J. (2003). C5a Receptor Oligomerization. *The Journal of Biological Chemistry*, 278(37), 35354-35361.

<https://doi.org/10.1074/jbc.M305607200>

Fotiadis, D., Jastrzebska, B., Philippsen, A., Müller, D. J., Palczewski, K., & Engel, A. (2006). Structure of the rhodopsin dimer: a working model for G-protein-coupled receptors. *Current Opinion in Structural Biology*, 16, 252-259. <https://doi.org/10.1016/j.sbi.2006.03.013>

Freedman, J. C. (2012). Cell Membranes. In *Cell Physiology Sourcebook* (Fourth Edi, pp. 49-59). Elsevier Inc. <https://doi.org/10.1016/B978-0-12-387738-3.00003-2>

Fujita, H., Hatakeyama, H., Watanabe, T. M., Sato, M., Higuchi, H., & Kanzaki, M. (2010). Identification of Three Distinct Functional Sites of Insulin-mediated GLUT4 Trafficking in Adipocytes Using Quantitative Single Molecule Imaging. *Molecular Biology of the Cell*, 21(August 1), 2721-2731. <https://doi.org/10.1091/mbc.E10>

Fujiwara, T., Ritchie, K., Murakoshi, H., Jacobson, K., & Kusumi, A. (2002). Phospholipids undergo hop diffusion in compartmentalized cell membrane. *The Journal of Cell Biology*, 157(6), 1071-1081. <https://doi.org/10.1083/jcb.200202050>

Fukumoto, H., Kayano, T., Buse, J. B., Edwards, Y., Pilch, P. F., Bell, G. I., & Seino, S. (1989). Cloning and Characterization of the Major Insulin-responsive Glucose Transporter Expressed in Human Skeletal Muscle and Other Insulin-responsive Tissues. *The Journal of Biological Chemistry*, 264(14), 7776-7779.

Funaki, M., Randhawa, P., & Janmey, P. A. (2004). Separation of Insulin Signaling into Distinct GLUT4 Translocation and Activation Steps. *Molecular and Cellular Biology*, 24(17), 7567-7577. <https://doi.org/10.1128/MCB.24.17.7567>

Gao, L., Chen, J., Gao, J., Wang, H., & Xiong, W. (2017). Super-resolution

microscopy reveals the insulin-resistance-regulated reorganization of GLUT4 on plasma membranes. *Journal of Cell Science*, 130(November), 396-405. <https://doi.org/10.1242/jcs.192450>

Garvey, W. T., Matthaei, S., & Olefsky, J. M. (1988). Role of glucose transporters in the cellular insulin resistance of type II non-insulin-dependent diabetes mellitus. *Journal of Clinical Investigation*, 81(5), 1528-1536.

Gelles, J., Schnapp, B. J., & Sheetz, M. P. (1988). Tracking kinesin-driven movements with nanometre-scale precision. *Nature*, 331(4), 450-453.

Geoghegan, N. D. (2015). *Advanced Fluorescence Methods for the Investigation of Biological Membranes*. University of Glasgow.

Gerich, J. E. (1981). Somatostatin and Diabetes. *The American Journal of Medicine*, 70(3), 619-626.

Godin, A. G., Costantino, S., Lorenzo, L.-E., Swift, J. L., Sergeev, M., Ribeiro-da-Silva, A., et al. (2011). Revealing protein oligomerization and densities in situ using spatial intensity distribution analysis. *Proceedings of the National Academy of Sciences of the United States of America*, 108(17), 7010-7015. <https://doi.org/10.1073/pnas.1018658108>

Godin, A. G., Rappaz, B., Potvin-Trottier, L., Kennedy, T. E., De Koninck, Y., & Wiseman, P. W. (2015). Spatial Intensity Distribution Analysis Reveals Abnormal Oligomerization of Proteins in Single Cells. *Biophysical Journal*, 109, 710-721. <https://doi.org/10.1016/j.bpj.2015.06.068>

Gould, G. W., Thomas, H. M., Jess, T. J., & Belli, G. I. (1991). Expression of Human Glucose Transporters in *Xenopus* Oocytes: Kinetic Characterization and Substrate Specificities of the Erythrocyte, Liver, and Brain Isoforms. *Biochemistry*, 30, 5139-5145.

Govers, R., Coster, A. C. F., & James, D. E. (2004). Insulin increases cell surface GLUT4 levels by dose dependently discharging GLUT4 into a cell surface recycling pathway. *Molecular and Cellular Biology*, 24(14), 6456-66.

<https://doi.org/10.1128/MCB.24.14.6456-6466.2004>

Green, H., & Kehinde, O. (1974). Sublines of Mouse 3T3 Cells That Sublines of Mouse 3T3 Cells That Accumulate Lipid. *Cell*, 1(3), 113-116.

Green, H., & Meuth, M. (1974). An Established Pre-Adipose Cell Line and its Differentiation in Culture. *Cell*, 3, 127-133.

Griffié, J., Shannon, M., Bromley, C. L., Boelen, L., Burn, G. L., Williamson, D. J., et al. (2016). A Bayesian cluster analysis method for single-molecule localization microscopy data. *Nature Protocols*, 11(12), 2499-2514.  
<https://doi.org/10.1038/nprot.2016.149>

Gurevich, V. V, & Gurevich, E. V. (2008). GPCR monomers and oligomers: it takes all kinds. *TRENDS in Neurosciences*, 31(2), 74-81.  
<https://doi.org/10.1016/j.tins.2007.11.007.GPCR>

Gustafsson, M. G. L. (2000). Surpassing the lateral resolution limit by a factor of two using structured illumination microscopy. *Journal of Microscopy*, 198(May 2000), 82-87.

Haga, Y., Ishii, K., & Suzuki, T. (2011). N-Glycosylation Is Critical for the Stability and Intracellular Trafficking of Glucose Transporter GLUT4. *The Journal of Biological Chemistry*, 286(36), 31320-31327.  
<https://doi.org/10.1074/jbc.M111.253955>

Hamilton, N. S. (2011). *An investigation into the role of syntaxin 16 in GLUT4 trafficking.*

Hammond, G. R. V, Machner, M. P., & Balla, T. (2014). A novel probe for phosphatidylinositol 4-phosphate reveals multiple pools beyond the Golgi. *The Journal of Cell Biology*, 205(1), 113-126.  
<https://doi.org/10.1083/jcb.201312072>

Haney, P. M., Slot, J. W., Piper, R. C., James, D. E., & Mueckler, M. (1991). Intracellular Targeting of the Insulin-regulatable Glucose Transporter

(GLUT4) Is Isoform Specific and Independent of Cell Type. *The Journal of Cell Biology*, 114(4), 689-699.

- Hashimoto, K., & Panchenko, A. R. (2010). Mechanisms of protein oligomerization, the critical role of insertions and deletions in maintaining different oligomeric states. *Proceedings of the National Academy of Sciences of the United States of America*, 107(47), 20352-20357. <https://doi.org/10.1073/pnas.1012999107/-/DCSupplemental.www.pnas.org/cgi/doi/10.1073/pnas.1012999107>
- Hashiramoto, M., & James, D. E. (2000). Characterization of Insulin-Responsive GLUT4 Storage Vesicles Isolated from 3T3-L1 Adipocytes. *Molecular and Cellular Biology*, 20(1), 416-427.
- Hatakeyama, H., & Kanzaki, M. (2011). Molecular Basis of Insulin-Responsive GLUT4 Trafficking Systems Revealed by Single Molecule Imaging. *Traffic*, 1805-1820. <https://doi.org/10.1111/j.1600-0854.2011.01279.x>
- Heilemann, M., Margeat, E., Kasper, R., Sauer, M., & Tinnefeld, P. (2005). Carbocyanine Dyes as Efficient Reversible Single-Molecule Optical Switch. *Journal of the American Chemical Society*, 127(12), 3801-3806.
- Heilemann, M., van de Linde, S., Schüttpehlz, M., Kasper, R., Seefeldt, B., Mukherjee, A., et al. (2008). Subdiffraction-Resolution Fluorescence Imaging with Conventional Fluorescent Probes. *Angewandte Chemie*, 47, 6172-6176. <https://doi.org/10.1002/anie.200802376>
- Heilemann, M., van de Linde, S., Mukherjee, A., & Sauer, M. (2009). Super-Resolution Imaging with Small Organic Fluorophores. *Angewandte Chemie*, 48, 6903-6908. <https://doi.org/10.1002/anie.200902073>
- Heintzmann, R., & Ficz, G. (2006). Breaking the resolution limit in light microscopy. *Briefings in Functional Genomics and Proteomics*, 5(4), 289-301. <https://doi.org/10.1093/bfpg/ell036>
- Hell, S. W., & Wichmann, J. (1994). Breaking the diffraction resolution limit by



stimulated emission: stimulated-emission-depletion fluorescence microscopy. *Optics Letters*, 19(11), 780-782.

Henrick, K., & Thornton, J. M. (1998). PQS : a protein quaternary structure file server. *Trends in Biochemical Sciences*, 23(9), 358-361.

Herbert, A. D., Carr, A. M., & Hoffmann, E. (2014). FindFoci: A Focus Detection Algorithm with Automated Parameter Training That Closely Matches Human Assignments, Reduces Human Inconsistencies and Increases Speed of Analysis. *PLoS ONE*, 9(12), 1-33.  
<https://doi.org/10.1371/journal.pone.0114749>

Herbert, D. N., & Carruthers, A. (1991). Cholerae-solubilized erythrocyte glucose transporters exist as a mixture of homodimers and homotetramers. *Biochemistry*, 30(19), 4654-4658.

Herbert, D. N., & Carruthers, A. (1992). Glucose Transporter Oligomeric Structure Determines Transporter Function. *The Journal of Biological Chemistry*, 267(33), 23829-23838.

Herman, G. A., Bonzelius, F., Cieutat, A., & Kelly, R. B. (1994). A distinct class of intracellular storage vesicles , identified by expression of the glucose transporter GLUT4. *Proceedings of the National Academy of Sciences of the United States of America*, 91(December), 12750-12754.

de Herreros, A. G., & Birnbaum, M. J. (1989). The Acquisition of Increased Insulin-responsive Hexose Transport in 3T3-L1 Adipocytes Correlates with Expression of a Novel Transporter Gene. *The Journal of Biological Chemistry*, 264(33), 19994-19999.

Hess, S. T., Kumar, M., Verma, A., Farrington, J., Kenworthy, A., & Zimmerberg, J. (2005). Quantitative electron microscopy and fluorescence spectroscopy of the membrane distribution of influenza hemagglutinin. *Journal of Cell Biology*, 169(6), 965-976. <https://doi.org/10.1083/jcb.200412058>

Hess, S. T., Girirajan, T. P. K., & Mason, M. D. (2006). Ultra-High Resolution

Imaging by Fluorescence Photoactivation Localization Microscopy. *Biophysical Journal*, 91(11), 4258-4272.  
<https://doi.org/10.1529/biophysj.106.091116>

Hex, N., Bartlett, C., Wright, D., Taylor, M., & Varley, D. (2012). Estimating the current and future costs of Type1 and Type2 diabetes in the UK, including direct health costs and indirect societal and productivity costs. *Diabetic Medicine*, 29(7), 855-862. <https://doi.org/10.1111/j.1464-5491.2012.03698.x>

Holman, G. D., Leggio, L. Lo, & Cushman, S. W. (1994). Insulin-stimulated GLUT4 Glucose Transporter Recycling. *The Journal of Biological Chemistry*, 269(26), 17516-17524.

Huang, B., Babcock, H., & Zhuang, X. (2010). Breaking the Diffraction Barrier: Super-Resolution Imaging of Cells. *Cell*, 143(7), 1047-1058.  
<https://doi.org/10.1016/j.cell.2010.12.002>

Huang, J., Imamura, T., Babendure, J. L., Lu, J., & Olefsky, J. M. (2005). Disruption of Microtubules Ablates the Specificity of Insulin Signaling to GLUT4 Translocation in 3T3-L1 Adipocytes. *The Journal of Biological Chemistry*, 280(51), 42300-42306. <https://doi.org/10.1074/jbc.M510920200>

Huang, S., & Czech, M. P. (2007). The GLUT4 Glucose Transporter. *Cell Metabolism*, 5(4), 237-252. <https://doi.org/10.1016/j.cmet.2007.03.006>

Huang, S., Lifshitz, L. M., Jones, C., Bellve, K. D., Standley, C., Fonseca, S., et al. (2007). Insulin stimulates membrane fusion and GLUT4 accumulation in clathrin coats on adipocyte plasma membranes. *Molecular and Cellular Biology*, 27(9), 3456-3469. <https://doi.org/10.1128/MCB.01719-06>

Hudson, A. W., Ruiz, M. L., & Birnbaum, M. J. (1992). Isoform-specific subcellular targeting of glucose transporters in mouse fibroblasts. *Journal of Cell Biology*, 116(3), 785-797.  
<https://doi.org/https://doi.org/10.1083/jcb.116.3.785>

- Inoue, H., Tani, K., & Tagaya, M. (2016). SNARE-associated proteins and receptor trafficking. *Receptors & Clinical Investigation*, 3, 1-11.  
<https://doi.org/10.14800/rci.1377>
- Issafras, H., Angers, S., Bulenger, S., Blanpain, C., Parmentier, M., Labbé-Jullié, C., et al. (2002). Constitutive Agonist-independent CCR5 Oligomerization and Antibody-mediated Clustering Occurring at Physiological Levels. *The Journal of Biological Chemistry*, 277(38), 34666-34673.  
<https://doi.org/10.1074/jbc.M202386200>
- Jackson, A. L., & Linsley, P. S. (2010). Recognizing and avoiding siRNA off-target effects for target identification and therapeutic application. *Nature Reviews Drug Discovery*, 9(1), 57-67. <https://doi.org/10.1038/nrd3010>
- James, D. E., Brown, R., Navarro, J., & Pilch, P. F. (1988). Insulin-regulatable tissues express a unique insulin-sensitive glucose transport protein. *Nature*, 333(5), 183-185.
- James, D. E., Strube, M., & Mueckler, M. (1989). Molecular Cloning and Characterization of an Insulin-Regulatable Glucose Transporter. *Letters To Nature*, 338(6210), 83-87.
- Jameson, D. M. (2014). *Introduction to Fluorescence*.
- Jedrychowski, M. P., Gartner, C. A., Gygi, S. P., Zhou, L., Herz, J., Kandror, K. V., & Pilch, P. F. (2010). Proteomic Analysis of GLUT4 Storage Vesicles Reveals LRP1 to Be an Important Vesicle Component and Target of Insulin Signaling. *The Journal of Biological Chemistry*, 285(1), 104-114.  
<https://doi.org/10.1074/jbc.M109.040428>
- Jensen, E., & Crossmann, D. J. (2014). Technical Review: Types of Imaging – Direct STORM. *The Anatomical Record*, 297, 2227-2231.
- Jewell, J. L., Oh, E., Ramalingam, L., Kalwat, M. A., Tagliabracci, V. S., Tackett, L., et al. (2011). Munc18c phosphorylation by the insulin receptor links cell signaling directly to SNARE exocytosis. *Journal of Cell Biology*,

193(1), 185-199. <https://doi.org/10.1083/jcb.201007176>

- Jiang, L., Fan, J., Bai, L., Wang, Y., Chen, Y., Yang, L., et al. (2008). Direct quantification of fusion rate reveals a distal role for AS160 in insulin-stimulated fusion of GLUT4 storage vesicles. *Journal of Biological Chemistry*, 283(13), 8508-8516. <https://doi.org/10.1074/jbc.M708688200>
- Johnson, A. O., Subtil, A., Petrush, R., Kobylarz, K., Keller, S. R., & McGraw, T. E. (1998). Identification of an Insulin-responsive , Slow Endocytic Recycling Mechanism in Chinese Hamster Ovary Cells. *The Journal of Biological Chemistry*, 273(28), 17968-17977.
- Jordens, I., Molle, D., Xiong, W., Keller, S. R., & McGraw, T. E. (2010). Insulin-regulated Aminopeptidase Is a Key Regulator of GLUT4 Trafficking by Controlling the Sorting of GLUT4 from Endosomes to Specialized Insulin-regulated Vesicles. *Molecular Biology of the Cell*, 21(24), 4325-4337. <https://doi.org/10.1091/mbc.E10>
- Kaestner, K. H., Christy, R. J., McLenithan, J. C., Braiterman, L. T., Cornelius, P., Pekala, P. H., & Lane, M. D. (1989). Sequence, tissue distribution, and differential expression of mRNA for a putative insulin-responsive glucose transporter in mouse 3T3-L1 adipocytes. *Proceedings of the National Academy of Sciences of the United States of America*, 86(May), 3150-3154.
- Kahn, B. B. (1992). Facilitative Glucose Transporters: Regulatory Mechanisms and Dysregulation in Diabetes. *Journal of Clinical Investigation*, 89(May), 1367-1374.
- Kamiyama, D., & Huang, B. (2012). Development in the STORM. *Cell*, 23(6), 1103-1110. <https://doi.org/10.1016/j.devcel.2012.10.003>
- Kandror, K. V. (2018). The role of sortilin in the “Glut4 Pathway”. *Communicative & Integrative Biology*, 11(1), 1-3. <https://doi.org/10.1080/19420889.2017.1393592>
- Kandror, K. V., & Pilch, P. F. (1994). gpl60, a tissue-specific marker for insulin-

activated glucose transport. *Proceedings of the National Academy of Sciences of the United States of America*, 91(August), 8017-8021.

Kandror, K. V, & Pilch, P. F. (1996). Compartmentalization of protein traffic in insulin-sensitive cells. *The American Physiological Society*, 271, E1-E14.

Kandror, K. V, & Pilch, P. F. (2011). The Sugar Is sIRVed : Sorting Glut4 and Its Fellow Travelers. *Traffic*, 12(6), 665-671. <https://doi.org/10.1111/j.1600-0854.2011.01175.x>

Kane, S., Sano, H., Liu, S. C. H., Asara, J. M., Lane, W. S., Garner, C. C., & Lienhard, G. E. (2002). A method to identify serine kinase substrates. Akt phosphorylates a novel adipocyte protein with a Rab GTPase-activating protein (GAP) domain. *Journal of Biological Chemistry*, 277(25), 22115-22118. <https://doi.org/10.1074/jbc.C200198200>

Karylowski, O., Zeigerer, A., Cohen, A., & McGraw, T. E. (2004). GLUT4 Is Retained by an Intracellular Cycle of Vesicle Formation and Fusion with Endosomes. *Molecular Biology of the Cell*, 15(February), 870-882. <https://doi.org/10.1091/mbc.E03>

Kask, P., Palo, K., Ullmann, D., & Gall, K. (1999). Fluorescence-intensity distribution analysis and its application in biomolecular detection technology. *Proceedings of the National Academy of Sciences of the United States of America*, 96(24), 13756-13761.

Kasuga, M., Karlsson, F. A., & Kahn, C. R. (1982). Insulin Stimulates the Phosphorylation of the 95,000-Dalton Subunit of Its Own Receptor. *Science*, 215(4529), 185-216.

Kawaguchi, T., Tamori, Y., Kanda, H., Yoshikawa, M., Tateya, S., Nishino, N., & Kasuga, M. (2010). The t-SNAREs syntaxin4 and SNAP23 but not v-SNARE VAMP2 are indispensable to tether GLUT4 vesicles at the plasma membrane in adipocyte. *Biochemical and Biophysical Research Communications*, 391(3), 1336-1341. <https://doi.org/10.1016/j.bbrc.2009.12.045>

- Kayano, T., Fukumoto, H., Eddy, R. L., Fan, Y., Byers, M. G., Shows, T. B., & Bell, G. I. (1988). Evidence for a Family of Human Glucose Transporter-like Proteins. *The Journal of Biological Chemistry*, 263(25), 15245-15248.
- Keller, S. R. (2003). The insulin-regulated aminopeptidase: a companion and regulator of GLUT4. *Frontiers in Bioscience*, 8, 410-420.
- Keller, S. R., Scott, H. M., Mastick, C. C., Aebersold, R., & Lienhard, G. E. (1995). Cloning and Characterization of a Novel Insulin-regulated Membrane Aminopeptidase from Glut4 Vesicles. *The Journal of Biological Chemistry*, 270(40), 23612-23618.
- Kioumourtzoglou, D., Gould, G. W., & Bryant, N. J. (2014). Insulin Stimulates Syntaxin4 SNARE Complex Assembly via a Novel Regulatory Mechanism. *Molecular and Cellular Biology*, 34(7), 1271-1279.  
<https://doi.org/10.1128/MCB.01203-13>
- Kioumourtzoglou, D., Sadler, J. B. A., Black, H. L., Berends, R., Wellburn, C., Bryant, N. J., & Gould, G. W. (2014). Studies of the regulated assembly of SNARE complexes in adipocytes. *Biochemical Society Transactions*, 42(5), 1396-1400. <https://doi.org/10.1042/BST20140114>
- Kioumourtzoglou, D., Pryor, P. R., Gould, G. W., & Bryant, N. J. (2015). Alternative routes to the cell surface underpin insulin-regulated membrane trafficking of GLUT4. *Journal of Cell Science*, 128, 2423-2429.  
<https://doi.org/10.1242/jcs.166561>
- Kiskowski, M. A., Hancock, J. F., & Kenworthy, A. K. (2009). On the Use of Ripley's K-Function and Its Derivatives to Analyze Domain Size. *Biophysical Journal*, 97, 1095-1103. <https://doi.org/10.1016/j.bpj.2009.05.039>
- Klco, J. M., Lassere, T. B., & Baranski, T. J. (2003). C5a Receptor Oligomerization. *The Journal of Biological Chemistry*, 278(37), 35345-35353.  
<https://doi.org/10.1074/jbc.M305606200>
- Knip, M., Veijola, R., Virtanen, S. M., Hyöty, H., Vaarala, O., & Åkerblom, H. K.

(2005). Environmental Triggers and Determinants of Type 1 Diabetes. *Diabetes*, 54(11), S125-S136.

Kohn, A. D., Summers, S. A., Birnbaum, M. J., & Roth, R. A. (1996). Expression of a constitutively active Akt Ser/Thr kinase in 3T3-L1 adipocytes stimulates glucose uptake and glucose transporter 4 translocation. *Journal of Biological Chemistry*, 271(49), 31372-31378.  
<https://doi.org/10.1074/jbc.271.49.31372>

Koumanov, F., Pereira, V. J., Richardson, J. D., Sargent, S. L., Fazakerley, D. J., & Holman, G. D. (2015). Insulin regulates Rab3-Noc2 complex dissociation to promote GLUT4 translocation in rat adipocytes. *Diabetologia*, 58(8), 1877-1886. <https://doi.org/10.1007/s00125-015-3627-3>

Kraegen, E. W., James, D. E., Jenkins, A. B., & Chisholm, D. J. (1985). Dose-response curves for in vivo insulin sensitivity in individual tissues in rats. *The American Journal of Physiology*, 248(3 Pt 1), E353-E362.

Kupriyanova, T. A., Kandror, V., & Kandror, K. V. (2002). Isolation and characterization of the two major intracellular Glut4 storage compartments. *Journal of Biological Chemistry*, 277(11), 9133-9138.  
<https://doi.org/10.1074/jbc.M106999200>

Laidlaw, K. M. E. (2018). *A role for EFR3A during insulin stimulated dispersal of GLUT4 at the plasma membrane.*

Laidlaw, K. M. E., Livingstone, R., Al-Tobi, M., Bryant, N. J., & Gould, G. W. (2017). SNARE phosphorylation : a control mechanism for insulin-stimulated glucose transport and other regulated exocytic events. *Biochemical Society Transactions*, 45(6), 1271-1277.

Lampson, M. A., Racz, A., Cushman, S. W., & McGraw, T. E. (2000). Demonstration of insulin-responsive trafficking of GLUT4 and vpTR in fibroblasts. *Journal of Cell Science*, 113, 4065-4076.

Lang, T., & Rizzoli, S. O. (2010). Membrane Protein Clusters at Nanoscale

Resolution: More Than Pretty Pictures. *Physiology*, 25, 116-124.  
<https://doi.org/10.1152/physiol.00044.2009>

Larance, M., Ramm, G., Stöckli, J., Van Dam, E. M., Winata, S., Wasinger, V., et al. (2005). Characterization of the role of the Rab GTPase-activating protein AS160 in insulin-regulated GLUT4 trafficking. *Journal of Biological Chemistry*, 280(45), 37803-37813. <https://doi.org/10.1074/jbc.M503897200>

Leevers, S. J., Vanhaesebroeck, B., & Waterfield, M. D. (1999). Signalling through phosphoinositide 3-kinases: the lipids take centre stage. *Current Opinion in Cell Biology*, 11, 219-225.

Leto, D., & Saltiel, A. R. (2012). Regulation of glucose transport by insulin : traffic control of GLUT4. *Nature Reviews Molecular Cell Biology*, 13(6), 383-396. <https://doi.org/10.1038/nrm3351>

Levet, F., Hosy, E., Kechkar, A., Butler, C., Beghin, A., Choquet, D., & Sibarita, J. (2015). SR-Tesseler : a method to segment and quantify localization-based super-resolution microscopy data. *Nature Methods*, 12(11), 1065-1071. <https://doi.org/10.1038/nmeth.3579>

Li, C. H., Bai, L., Li, D. D., Xia, S., & Xu, T. (2004). Dynamic tracking and mobility analysis of single GLUT4 storage vesicle in live 3T3-L1 cells. *Cell Research*, 14(6), 480-6. <https://doi.org/10.1038/sj.cr.7290251>

Li, P., Liu, S., Lu, M., Bandyopadhyay, G., Oh, D., Imamura, T., et al. (2016). Hematopoietic-Derived Galectin-3 Causes Cellular and Systemic Insulin Resistance. *Cell*, 167(4), 973-984.e12. <https://doi.org/10.1016/j.cell.2016.10.025>

Li, Z., Yue, Y., Hu, F., Zhang, C., Ma, X., Li, N., et al. (2018). Electrical pulse stimulation induces GLUT4 translocation in C2C12 myotubes that depends on Rab8A , Rab13 , and Rab14. *American Journal of Physiology*, 314(5), 478-493. <https://doi.org/10.1152/ajpendo.00103.2017>

Lin, B.-Z., Pilch, P. F., & Kandror, K. V. (1997). Sortilin Is a Major Protein



Component of Glut4-containing Vesicles. *The Journal of Biological Chemistry*, 272(39), 24145-24148.

- van de Linde, S. (2019). Single-molecule localization microscopy analysis with ImageJ. *Journal of Physics D: Applied Physics*, 52, 1-12.  
<https://doi.org/10.1088/1361-6463/ab092f>
- van de Linde, S., Löschberger, A., Klein, T., Heidebreder, M., Wolter, S., Heilemann, M., & Sauer, M. (2011). Direct stochastic optical reconstruction microscopy with standard fluorescent probes. *Nature Protocols Protoc*, 6(7), 991-1009. <https://doi.org/10.1038/nprot.2011.336>
- van de Linde, S., Krstić, I., Prisner, T., Doose, S., Heilemann, M., & Sauer, M. (2011). Photoinduced formation of reversible dye radicals and their impact on super-resolution imaging. *Photochemical & Photobiological Sciences*, 10, 499-506. <https://doi.org/10.1039/c0pp00317d>
- Linders, P. T. A., van der Horst, C., ter Beest, M., & van den Bogaart, G. (2019). Stx5-Mediated ER-Golgi Transport in Mammals and Yeast. *Cells*, 8(780), 1-16. <https://doi.org/10.3390/cells8080780>
- Liu, J., Kimura, A., Baumann, C. A., & Saltiel, A. R. (2002). APS Facilitates c-Cbl Tyrosine Phosphorylation and GLUT4 Translocation in Response to Insulin in 3T3-L1 Adipocytes. *Molecular and Cellular Biology*, 22(11), 3599-3609.  
<https://doi.org/10.1128/MCB.22.11.3599>
- Livingstone, C., James, D. E., Rice, J. E., Hanpeter, D., & Gould, G. W. (1996). Compartment ablation analysis of the insulin-responsive glucose transporter (GLUT4) in 3T3-L1 adipocytes. *Biochemical Journal*, 315, 487-495.
- Lizunov, V. A., Matsumoto, H., Zimmerberg, J., Cushman, S. W., & Frolov, V. A. (2005). Insulin stimulates the halting, tethering, and fusion of mobile GLUT4 vesicles in rat adipose cells. *Journal of Cell Biology*, 169(3), 481-489.  
<https://doi.org/10.1083/jcb.200412069>
- Lizunov, V. A., Lee, J.-P., Skarulis, M. C., Zimmerberg, J., Cushman, S. W., &

- Stenkula, K. G. (2013). Impaired Tethering and Fusion of GLUT4 Vesicles in Insulin-Resistant Human Adipose Cells. *Diabetes*, 62(September), 3114-3119. <https://doi.org/10.2337/db12-1741>
- Lizunov, V. A., Stenkula, K., Troy, A., Cushman, S. W., & Zimmerberg, J. (2013). Insulin Regulates Glut4 Confinement in Plasma Membrane Clusters in Adipose Cells. *PLoS ONE*, 8(3). <https://doi.org/10.1371/journal.pone.0057559>
- Löschberger, A., Franke, C., Krohne, G., van de Linde, S., & Sauer, M. (2014). Correlative super-resolution fluorescence and electron microscopy of the nuclear pore complex with molecular resolution. *Journal of Cell Science*, (August 2014), 1-14.
- Lucey, B. P., Nelson-Rees, W. A., & Hutchins, G. M. (2009). Henrietta Lacks, HeLa Cells, and Cell Culture Contamination. *Archives of Pathology & Laboratory Medicine*, 133(9), 1463-1467.
- Maianu, L., Keller, S. R., & Garvey, W. T. (2001). Adipocytes Exhibit Abnormal Subcellular Distribution and Translocation of Vesicles Containing Glucose Transporter 4 and Insulin-Regulated Aminopeptidase in Type 2 Diabetes Mellitus: Implications Regarding Defects in Vesicle Trafficking. *The Journal of Clinical Endocrinology & Metabolism*, 86(11), 5450-5456.
- Malsam, J., Kreye, S., & Söllner, T. H. (2008). Membrane fusion: SNAREs and regulation. *Cellular and Molecular Life Sciences*, 65, 2814-2815. <https://doi.org/10.1007/s00018-008-8352-3>
- Manning, B. D., & Toker, A. (2007). AKT/PKB Signaling: Navigating the Network. *Cell*, 169(3), 381-405. <https://doi.org/10.1016/j.cell.2017.04.001>
- Marsango, S., Caltabiano, G., Jiménez-Rosés, M., Millan, M. J., Pediani, J. D., Ward, R. J., & Milligan, G. (2017). A Molecular Basis for Selective Antagonist Destabilization of Dopamine D3 Receptor Quaternary Organization. *Nature Scientific Reports*, 7, 1-17. <https://doi.org/10.1038/s41598-017-02249-3>

- Martin-Fernandez, M. L., Tynan, C. J., & Webb, S. E. D. (2013). A 'pocket guide' to total internal reflection fluorescence. *Journal of Microscopy*, 252(1), 16-22. <https://doi.org/10.1111/jmi.12070>
- Martin, C., Tu, Y., Euskirchen, G., Ward, W. W., & Prasher, D. C. (1994). Green fluorescent protein as a marker for gene expression. *Science*, 263(1988), 802-805.
- Martin, L. B., Shewan, A., Millar, C. A., Gould, G. W., & James, D. E. (1998). Vesicle-associated membrane protein 2 plays a specific role in the insulin-dependent trafficking of the facilitative glucose transporter GLUT4 in 3T3-L1 adipocytes. *Journal of Biological Chemistry*, 273, 1444-1452. <https://doi.org/10.1074/jbc.273.3.1444>
- Martin, O. J., Lee, A., & McGraw, T. E. (2006). GLUT4 distribution between the plasma membrane and the intracellular compartments is maintained by an insulin-modulated bipartite dynamic mechanism. *Journal of Biological Chemistry*, 281(1), 484-490. <https://doi.org/10.1074/jbc.M505944200>
- Martin, S., Tellam, J., Livingstone, C., Slot, J. W., Gould, G. W., & James, D. E. (1996). The glucose transporter (GLUT-4) and vesicle-associated membrane protein-2 (VAMP-2) are segregated from recycling endosomes in insulin-sensitive cells. *Journal of Cell Biology*, 134(3), 625-635. <https://doi.org/10.1083/jcb.134.3.625>
- Maruthur, N. M., Tseng, E., Hutflless, S., Wilson, L. M., Suarez-Cuervo, C., Berger, Z., et al. (2016). Diabetes Medications as Monotherapy or Metformin-Based Combination Therapy for Type 2 Diabetes. *Annals of Internal Medicine*, 164(11), 740-751. <https://doi.org/10.7326/M15-2650>
- Mastick, C. C., Aebersold, R., & Lienhard, G. E. (1994). Characterization of a Major Protein in GLUT4 Vesicles. *The Journal of Biological Chemistry*, 269(8), 6089-6092.
- Mathers, C. D., & Loncar, D. (2006). Projections of Global Mortality and Burden of Disease from 2002 to 2030. *PLOS Medicine*, 3(11), 2011-2030.

<https://doi.org/10.1371/journal.pmed.0030442>

Mattheyses, A. L., Simon, S. M., & Rappoport, J. Z. (2010). Imaging with total internal reflection fluorescence microscopy for the cell biologist. *Journal of Cell Science*, 123(Pt 21), 3621-8. <https://doi.org/10.1242/jcs.056218>

Mîinea, C. P., Sano, H., Kane, S., Sano, E., Fukuda, M., Peränen, J., et al. (2005). AS160, the Akt substrate regulating GLUT4 translocation, has a functional Rab GTPase-activating protein domain. *Biochemical Journal*, 391, 87-93. <https://doi.org/10.1042/BJ20050887>

Miller, S. (2006). *The Role of Synaptotagmins in insulin-stimulated glucose uptake in the 3T3-L1 Adipocyte*. University of Glasgow.

Mohan, S. S., Perry, J. J. P., Pouluse, N., Nair, B. G., & Anilkumar, G. (2009). Homology Modeling of GLUT4, an Insulin Regulated Facilitated Glucose Transporter and Docking Studies with ATP and its Inhibitors. *Journal of Biomolecular Structure and Dynamics*, 26(4), 455-464.

Molero, J. C., Whitehead, J. P., Meerloo, T., & James, D. E. (2001). Nocodazole Inhibits Insulin-stimulated Glucose Transport in 3T3-L1 Adipocytes via a Microtubule-independent Mechanism. *The Journal of Biological Chemistry*, 276(47), 43829-43835. <https://doi.org/10.1074/jbc.M105452200>

Morris, N. J., Ross, S. A., Lane, W. S., Moestrup, S. K., Petersen, C. M., Keller, S. R., & Lienhard, G. E. (1998). Sortilin Is the Major 110-kDa Protein in GLUT4 Vesicles from Adipocytes. *The Journal of Biological Chemistry*, 273(6), 3582-3587.

Morris, S., Geoghegan, N. D., Sadler, J. B. A., Koester, A. M., Black, H. L., Laub, M., et al. (2020). Characterisation of GLUT4 Trafficking in HeLa Cells: Comparable Kinetics and Orthologous Trafficking Mechanisms to 3T3-L1 Adipocytes. *PeerJ*, 8:e8751.  
<https://doi.org/https://doi.org/10.7717/peerj.8751>

Mueckler, M., Caruso, C., Baldwin, S. A., Panico, M., Blench, I., Morris, H. R., et

- al. (1985). Sequence and Structure of a Human Glucose Transporter. *Science*, 229(4717), 941-945.
- Muranyi, W., Malkusch, S., Müller, B., Heilemann, M., & Kräusslich, H.-G. (2013). Super-Resolution Microscopy Reveals Specific Recruitment of HIV-1 Envelope Proteins to Viral Assembly Sites Dependent on the Envelope C-Terminal Tail. *PLOS Pathogens*, 9(2), 1-13. <https://doi.org/10.1371/journal.ppat.1003198>
- Muretta, J. M., Romenskaia, I., & Mastick, C. C. (2008). Insulin releases Glut4 from static storage compartments into cycling endosomes and increases the rate constant for Glut4 exocytosis. *Journal of Biological Chemistry*, 283(1), 311-323. <https://doi.org/10.1074/jbc.M705756200>
- Nakatsu, F., Baskin, J. M., Chung, J., Tanner, L. B., Shui, G., Lee, S. Y., et al. (2012). PtdIns4P synthesis by PI4KIII $\alpha$  at the plasma membrane and its impact on plasma membrane identity. *Journal of Cell Biology*, 199(6), 1003-1016. <https://doi.org/10.1083/jcb.201206095>
- Nelson, D. L., & Cox, M. M. (2017). Principles of Biochemistry. In *Principles of Biochemistry* (7th ed.). Lehninger.
- Nikolaou, A., Stijlemans, B., Laoui, D., Schoupe, E., Tran, H. T. T., Tourwé, D., et al. (2014). Presence and regulation of insulin-regulated aminopeptidase in mouse macrophages. *Journal of the Renin-Angiotensin-Aldosterone System*, 15(4), 466-479. <https://doi.org/10.1177/1470320313507621>
- Noomnarm, U., & Clegg, R. M. (2009). Fluorescence lifetimes : fundamentals and interpretations. *Photosynthesis Research*, 101, 181-194. <https://doi.org/10.1007/s11120-009-9457-8>
- Ober, R. J., Ram, S., & Ward, E. S. (2004). Localization Accuracy in Single-Molecule Microscopy. *Biophysical Journal*, 86(2), 1185-1200. [https://doi.org/10.1016/S0006-3495\(04\)74193-4](https://doi.org/10.1016/S0006-3495(04)74193-4)
- Oka, Y., Mottola, C., Oppenheimer, C. L., & Czech, M. P. (1984). Insulin activates the appearance of insulin-like growth factor II receptors on the

adipocyte cell surface. *Proceedings of the National Academy of Sciences of the United States of America*, 81(July), 4028-4032.

- Ovesný, M., Křížek, P., Borkovec, J., Švindrych, Z., & Hagen, G. M. (2014). ThunderSTORM: a comprehensive ImageJ plug-in for PALM and STORM data analysis and super-resolution imaging. *Bioimage Informatics*, 30(16), 2389-2390. <https://doi.org/10.1093/bioinformatics/btu202>
- Paddock, S. W. (1999). Confocal Laser Scanning Microscopy. *BioTechniques*, 27, 992-1004.
- Pan, X., Zaarur, N., Singh, M., Morin, P., & Kandror, K. V. (2017). Sortilin and retromer mediate retrograde transport of Glut4 in 3T3-L1 adipocytes. *Molecular Biology of the Cell*, 28, 1667-1675. <https://doi.org/10.1091/mbc.E16-11-0777>
- Patki, V., Buxton, J., Chawla, A., Lifshitz, L., Fogarty, K., Carrington, W., et al. (2001). Insulin action on GLUT4 traffic visualized in single 3T3-L1 adipocytes by using ultra-fast microscopy. *Molecular Biology of the Cell*, 12(1), 129-141. <https://doi.org/10.1091/MBC.12.1.129>
- Patsouris, D., Li, P.-P., Thapar, D., Chapman, J., Olefsky, J. M., & Neels, J. G. (2008). Ablation of CD11c-positive cells normalizes insulin sensitivity in obese insulin resistant animals. *Cell Metabolism*, 8(4), 301-309. <https://doi.org/10.1016/j.cmet.2008.08.015>
- Patterson, G., Day, R. N., & Piston, D. (2001). Fluorescent Protein Spectra. *Journal of Cell Science*, 114(5), 837-838.
- Pearse, B. M. F. (1976). Clathrin: A unique protein associated with intracellular transfer of membrane by coated vesicles. *Proceedings of the National Academy of Sciences of the United States of America*, 73(4), 1255-1259.
- Pediani, J. D., Ward, R. J., Godin, A. G., Marsango, S., & Milligan, G. (2016). Dynamic regulation of quaternary organization of the M1 muscarinic receptor by subtype-selective antagonist drugs. *Journal of Biological*

*Chemistry*, 291(25), 13132-13146. <https://doi.org/10.1074/jbc.M115.712562>

- Perera, H. K. I., Clarke, M., Morris, N. J., Hong, W., Chamberlain, L. H., & Gould, G. W. (2003). Syntaxin 6 Regulates Glut4 Trafficking in 3T3-L1 Adipocytes. *Molecular Biology of the Cell*, 14(July), 2946-2958.  
<https://doi.org/10.1091/mbc.E02>
- Perley, M. J., & Kipnis, D. M. (1967). Plasma Insulin Responses to Oral and Intravenous Glucose : Studies in Normal and Diabetic Subjects. *The Journal of Clinical Investigation*, 46(12), 1954-1962.
- Piper, R. C., Hess, L. J., & James, D. E. (1991). Differential sorting of two glucose transporters expressed in insulin-sensitive cells. *American Journal of Physiology*, 260(3), C570-C580.
- Piper, R. C., Tai, C., Kulesza, P., Pang, S., Warnock, D., Baenziger, J., et al. (1993). GLUT-4 NH2 Terminus Contains a Phenylalanine-Based Targeting Motif that Regulates Intracellular Sequestration. *The Journal of Cell Biology*, 121(6), 1221-1232.
- Powell, K. A., Campbell, L. C., Tavare, J. M., Leader, D. P., A, W. J., & Gould, G. W. (1999). Trafficking of Glut4-Green Fluorescent Protein chimaeras in 3T3-L1 adipocytes suggests distinct internalization mechanisms regulating cell surface Glut4 levels. *Biochemical Journal*, 344, 535-543.
- Prinster, S. C., Holmqvist, T. G., & Hall, R. A. (2006).  $\alpha$ 2C -Adrenergic Receptors Exhibit Enhanced Surface Expression and Signaling upon Association with  $\beta$ 2 -Adrenergic Receptors. *The Journal of Pharmacology and Experimental Therapeutics*, 318(3), 974-981.  
<https://doi.org/10.1124/jpet.106.106526.surface>
- Prior, I. A., Muncke, C., Parton, R. G., & Hancock, J. F. (2003). Direct visualization of Ras proteins in spatially distinct cell surface microdomains. *Journal of Cell Biology*, 160(2), 165-170.  
<https://doi.org/10.1083/jcb.200209091>

- Proctor, K. M., Miller, S. C. M., Bryant, N. J., & Gould, G. W. (2006). Syntaxin 16 controls the intracellular sequestration of GLUT4 in 3T3-L1 adipocytes. *Biochemical and Biophysical Research Communications*, 347, 433-438. <https://doi.org/10.1016/j.bbrc.2006.06.135>
- Rappoport, J. Z. (2008). Focusing on clathrin-mediated endocytosis. *Biochemical Journal*, 412, 415-423. <https://doi.org/10.1042/BJ20080474>
- Rea, S., & James, D. E. (1997). Moving GLUT4 The Biogenesis and Trafficking of GLUT4 Storage Vesicles. *Diabetes*, 46(11), 1667-1677.
- Reisinger, V., & Eichacker, L. A. (2008). Solubilization of Membrane Protein Complexes for Blue Native PAGE. *Journal of Proteomics*, 71(31), 277-283. <https://doi.org/https://doi.org/10.1016/j.jprot.2008.05.004>
- Ribon, V., Hubbell, S., Herrera, R., & Saltiel, A. R. (1996). The Product of the cbl Oncogene Forms Stable Complexes In Vivo with Endogenous Crk in a Tyrosine Phosphorylation-Dependent Manner. *Molecular and Cellular Biology*, 16(1), 45-52.
- Richter, E. A., & Hargreaves, M. (2013). Exercise, GLUT4, and Skeletal Muscle Glucose Uptake. *Physiology Reviews*, 93, 993-1017. <https://doi.org/10.1152/physrev.00038.2012>
- Ries, J., Kaplan, C., Platonova, E., Eghlidi, H., & Ewers, H. (2012). A simple, versatile method for GFP-based super-resolution microscopy via nanobodies. *Nature Methods*, 9(6), 1-6. <https://doi.org/10.1038/nmeth.1991>
- Ripley, B. D. (1976). The second-order analysis of stationary point processes. *Journal of Applied Probability*, 13, 255-266. <https://doi.org/https://doi.org/10.2307%2F3212829>
- Robinson, L. J., & James, D. E. (1992). Insulin-regulated sorting in 3T3-L1 adipocytes of glucose transporters. *The American Physiological Society*, 263(2), 383-393.



- Robinson, L. J., Pang, S., Harris, D. S., Heuser, J., & James, D. E. (1992). Translocation of the Glucose Transporter (GLUT4) to the Cell Surface in Permeabilized 3T3-L1 Adipocytes: Effects of ATP, Insulin, and GTP $\gamma$ S and Localization of GLUT4 to Clathrin Lattices. *The Journal of Cell Biology*, 117(6), 1181-1196.
- Rogi, R., Tsujimoto, M., Nakazato, H., Mizutani, S., & Tomoda, Y. (1996). Human Placental Leucine Aminopeptidase / Oxytocinase. *The Journal of Biological Chemistry*, 271(1), 56-61.
- Ross, S. A., Song, X., Burney, M. W., Kasai, Y., & Orlicky, D. J. (2003). Efficient adenovirus transduction of 3T3-L1 adipocytes stably expressing coxsackie-adenovirus receptor. *Biochemical and Biophysical Research Communications*, 302, 354-358. [https://doi.org/10.1016/S0006-291X\(03\)00180-3](https://doi.org/10.1016/S0006-291X(03)00180-3)
- Rottenfusser, R., Wilson, E. E., & Davidson, M. W. (2019). The Point Spread Function.
- Rubin-Delanchy, P., Burn, G. L., Griffié, J., Williamson, D. J., Heard, N. A., Cope, A. P., & Owen, D. M. (2015). Bayesian cluster identification in single-molecule localization microscopy data. *Nature Methods*, 12(11), 1072-1076. <https://doi.org/10.1038/nmeth.3612>
- Ruiz-Ojeda, F. J., Rupérez, A. I., Gomez-llorente, C., Gil, A., & Aguilera, C. M. (2016). Cell Models and Their Application for Studying Adipogenic Differentiation in Relation to Obesity: A Review. *International Journal of Molecular Sciences*, 17(7), 1-26. <https://doi.org/10.3390/ijms17071040>
- Rust, M. J., Bates, M., & Zhuang, X. (2006). Sub-diffraction-limit imaging by stochastic optical reconstruction microscopy (STORM). *Nature Methods*, 3(10), 793-795. <https://doi.org/10.1038/NMETH929>
- Sadacca, L. A., Bruno, J., Wen, J., Xiong, W., & McGraw, T. E. (2013). Specialized sorting of GLUT4 and its recruitment to the cell surface are independently regulated by distinct Rabs. *Molecular Biology of the Cell*,

24(16), 2544-2557. <https://doi.org/10.1091/mbc.E13-02-0103>

Sadler, J. B. A. (2014). *Analysis of VAMP levels and function in 3T3 L1 adipocytes.*

Sadler, J. B. A., Bryant, N. J., Gould, G. W., & Welburn, C. R. (2013). Posttranslational Modifications of GLUT4 Affect Its Subcellular Localization and Translocation. *International Journal of Molecular Sciences*, *14*, 9963-9978. <https://doi.org/10.3390/ijms14059963>

Sadler, J. B. A., Bryant, N. J., & Gould, G. W. (2014). Characterisation of VAMP isoforms in 3T3-L1 adipocytes: Implications for GLUT4 trafficking. *Molecular Biology of the Cell*, *26*(3), 530-536.

Sadler, J. B. A., Lamb, C. A., Welburn, C. R., Adamson, I. S., Kioumourtzoglou, D., Chi, N.-W., et al. (2019). The deubiquitinating enzyme USP25 binds tankyrase and regulates trafficking of the facilitative glucose transporter GLUT4 in adipocytes. *Scientific Reports*, *9*(1), 1-7. <https://doi.org/10.1038/s41598-019-40596-5>

Saltiel, A. R., & Kahn, C. R. (2001). Insulin Signalling and The Regulation of Glucose and Lipid Metabolism. *Nature*, *414*(December), 799-806. <https://doi.org/10.1038/414799a>

Sano, H., Kane, S., Sano, E., Mîinea, C. P., Asara, J. M., Lane, W. S., et al. (2003). Insulin-stimulated Phosphorylation of a Rab GTPase-activating Protein Regulates GLUT4 Translocation. *The Journal of Biological Chemistry*, *278*(17), 14599-14603. <https://doi.org/10.1074/jbc.C300063200>

Sano, H., Egeuz, L., Teruel, M. N., Fukuda, M., Chuang, T. D., Chavez, J. A., et al. (2007). Rab10, a Target of the AS160 Rab GAP, Is Required for Insulin-Stimulated Translocation of GLUT4 to the Adipocyte Plasma Membrane. *Cell Metabolism*, *5*(April), 293-303. <https://doi.org/10.1016/j.cmet.2007.03.001>

Sano, H., Peck, G. R., Blachon, S., & Lienhard, G. E. (2015). A potential link between insulin signaling and GLUT4 translocation : Association of Rab10-

GTP with the exocyst subunit Exoc6 / 6b. *Biochemical and Biophysical Research Communications*, 465(3), 601-605.

<https://doi.org/10.1016/j.bbrc.2015.08.069>

Schägger, H., Cramer, W., & Jagow, G. von. (1994). Analysis of Molecular Masses and Oligomeric States of Protein Complexes by Blue Native Electrophoresis and Isolation of membrane Protein Complexes by Two-Dimensional Native Electrophoresis. *Analytical Biochemistry*, 217, 220-230.

Schmelzle, K., Kane, S., Gridley, S., Lienhard, G. E., & White, F. M. (2006). Temporal Dynamics of Tyrosine Phosphorylation in Insulin Signaling. *Diabetes*, 55(August), 2171-2179. <https://doi.org/10.2337/db06-0148>

Schmoranzer, J., & Simon, S. M. (2003). Role of Microtubules in Fusion of Post-Golgi Vesicles to the Plasma Membrane. *Molecular Biology of the Cell*, 14(April), 1558-1569. <https://doi.org/10.1091/mbc.E02>

Schmoranzer, J., Goulian, M., Axelrod, D., & Simon, S. M. (2000). Imaging Constitutive Exocytosis with Total Internal Reflection Fluorescence Microscopy. *The Journal of Cell Biology*, 149(1), 23-31.

Seuring, T., Archangelidi, O., & Suhrcke, M. (2015). The Economic Costs of Type 2 Diabetes : A Global Systematic Review. *Pharmacoeconomics*, 811-831. <https://doi.org/10.1007/s40273-015-0268-9>

Shaw, A. S. (2006). Lipid rafts: now you see them, now you don't. *Nature Immunology*, 7(11), 1139-1142. <https://doi.org/10.1038/ni1405>

Shepherd, P. R., & Kahn, B. B. (1999). Glucose Transporters and Insulin Action. *The New England Journal of Medicine*, 341, 248-257. <https://doi.org/10.1056/NEJM199907223410406>

Shewan, A. M., Marsh, B. J., Melvin, D. R., Martin, S., Gould, G. W., & James, D. E. (2000). The cytosolic C-terminus of the glucose transporter GLUT4 contains an acidic cluster endosomal targeting motif distal to the dileucine signal. *Biochemical Journal*, 350, 99-107.

- Shewan, A. M., van Dam, E. M., Martin, S., Luen, T. B., Hong, W., Bryant, N. J., & James, D. E. (2003). GLUT4 Recycles via a trans -Golgi Network (TGN) Subdomain Enriched in Syntaxins 6 and 16 But Not TGN38: Involvement of an Acidic Targeting Motif. *Molecular Biology of the Cell*, 14, 973-986. <https://doi.org/10.1091/mbc.E02>
- Shi, J., & Kandror, K. V. (2005). Sortilin is essential and sufficient for the formation of glut4 storage vesicles in 3T3-L1 adipocytes. *Developmental Cell*, 9(1), 99-108. <https://doi.org/10.1016/j.devcel.2005.04.004>
- Shi, J., Huang, G., & Kandror, K. V. (2008). Self-assembly of Glut4 Storage Vesicles during Differentiation of 3T3-L1 Adipocytes. *The Journal of Biological Chemistry*, 283(44), 30311-30321. <https://doi.org/10.1074/jbc.M805182200>
- Shia, M. A., & Pilch, P. F. (1983). The B Subunit of the Insulin Receptor Is an Insulin- Activated Protein Kinase. *Biochemistry*, 22(4), 717-721.
- Shimomura, O., Johnson, F. H., & Saiga, Y. (1962). Extraction, Purification and Properties of Aequorin, a Bioluminescent Protein from the Luminous Hydromedusan, Aequorea. *Journal of Cellular and Comparative Physiology*, 59(3), 223-239. <https://doi.org/10.1002/jcp.1030590302>
- Simpson, I. A., Yver, D. R., Hissin, P. J., Wardzala, L. J., Karnieli, E., Salans, L. B., & Cushman, S. W. (1983). Insulin-Stimulated Translocation of Glucose Transporters in the Isolated Rat Adipose Cells: Characterization of Subcellular Fractions. *Biochimica et Biophysica Acta*, 763, 393-407.
- Simpson, J. C., Joggerst, B., Laketa, V., Verissimo, F., Cetin, C., Erfle, H., et al. (2012). Genome-wide RNAi screening identifies human proteins with a regulatory function in the early secretory pathway. *Nature Cell Biology*, 14(7), 764-774. <https://doi.org/10.1038/ncb2510>
- Sinha, M. K., Raineri-Maldonado, C., Buchanan, C., Pories, W. J., Carter-Su, C., Pilch, P. F., & Caro, J. F. (1991). Adipose Tissue Glucose Transporters in NIDDM Decreased Levels of Muscle / Fat Isoform. *Diabetes*, 40(October),

472-477.

- Slot, J. W., Geuze, H. J., Gigengack, S., Lienhard, G. E., & James, D. E. (1991). Immuno-localization of the insulin regulatable glucose transporter in brown adipose tissue of the rat. *Journal of Cell Biology*, 113(1), 123-135. <https://doi.org/10.1083/jcb.113.1.123>
- Söllner, T., Bennett, M. K., Whiteheart, S. W., Scheller, R. H., & Rothman, J. E. (1993). A Protein Assembly-Disassembly Pathway In Vitro That May Correspond to Sequential Steps of Synaptic Vesicle Docking , Activation , and Fusion. *Cell*, 75, 409-418.
- Söllner, T., Whiteheart, S. W., Brunner, M., Erdjument-Bromage, H., Geromanos, S., Tempst, P., & Rothman, J. F. (1993). SNAP receptors implicated in vesicle targeting an fusion. *Nature*, 362, 318-362.
- Stenkula, K. G., Lizunov, V. A., Cushman, S. W., & Zimmerberg, J. (2010). Insulin controls the spatial distribution of GLUT4 on the cell surface through regulation of its postfusion dispersal. *Cell Metabolism*, 12(3), 250-259. <https://doi.org/10.1016/j.cmet.2010.08.005>
- Stephens, L., Anderson, K., Stokoe, D., Erdjument-Bromage, H., Painter, G. F., Holmes, A. B., et al. (1998). Protein Kinase B Kinases That Mediate Phosphatidylinositol 3,4,5-Trisphosphate-Dependent Activation of Protein Kinase B. *Science*, 279, 710-714.
- Sternberg, S. R. (1983). Biomedical Image Processing. *IEEE Computer*, 16(1), 22-34.
- von Stetten, D., Noirclerc-Savoye, M., Goedhart, J., Gadella Jr, T. W. J., & Royant, A. (2012). Structure of a fluorescent protein from *Aequorea victoria* bearing the obligate-monomer mutation A206K. *Acta Crystallographica, F68*, 878-882. <https://doi.org/10.1107/S1744309112028667>
- Subramaniam, V. N., Peter, F., Philp, R., Wong, S. H., & Hong, W. (1996). GS28, a 28-Kilodalton Golgi SNARE That Participates in ER-Golgi Transport.

*Science*, 272(5265), 1161-1163.

- Sun, X. J., Rothenberg, P., Kahn, C. R., Backer, J. M., Araki, E., Wilden, P. A., et al. (1991). Structure of the insulin receptor substrate IRS-1 defines a unique signal transduction protein. *Nature*, 352, 73-77.
- Sutton, R. B., Fasshauer, D., Jahn, R., & Brunger, A. T. (1998). Crystal structure of a SNARE complex involved in synaptic exocytosis at 2.4 Å resolution. *Nature*, 395(September), 347-353.
- Suzuki, K., & Kono, T. (1980). Evidence that insulin causes translocation of glucose transport activity to the plasma membrane from an intracellular storage site. *Proceedings of the National Academy of Sciences of the United States of America*, 77(5), 2542-2545.
- Tan, J., & Brill, J. A. (2014). Cinderella story: PI4P goes from precursor to key signaling molecule. *Critical Reviews in Biochemistry and Molecular Biology*, 49(1), 33-58. <https://doi.org/10.3109/10409238.2013.853024>
- Tareque, M. I., Koshio, A., Tiedt, A. D., Hasegawa, T., Obirikorang, Y., Obirikorang, C., et al. (2016). *WHO - Global Report on Diabetes* (Vol. 56). <https://doi.org/10.1371/journal.pone.0127954>
- Tate, C. G. (2001). Overexpression of mammalian integral membrane proteins for structural studies. *FEBS Letters*, 504, 94-98.
- Tavaré, J. M., Fletcher, L. M., Oatey, P. B., Tyas, L., Wakefield, J. G., & Welsh, G. I. (2001). Lighting up insulin action. *Diabetic Medicine*, 18, 253-260.
- Tellam, J. T., McIntosh, S., & James, D. E. (1995). Molecular Identification of Two Novel Munc-18 Isoforms Expressed in Non-neuronal Tissues. *Journal of Biological Chemistry*, 270, 5857-5863. <https://doi.org/10.1074/jcb.270.11.5857>
- Tellam, J. T., Macaulay, S. L., McIntosh, S., Hewish, D. R., Ward, C. W., & James, D. E. (1997). Characterization of Munc-18c and Syntaxin-4 in 3T3-L1

Adipocytes. *Journal of Biological Chemistry*, 272(10), 6179-6186.

- Thompson, R. E., Larson, D. R., & Webb, W. W. (2002). Precise Nanometer Localization Analysis for Individual Fluorescent Probes. *Biophysical Journal*, 82(5), 2775-2783. [https://doi.org/10.1016/S0006-3495\(02\)75618-X](https://doi.org/10.1016/S0006-3495(02)75618-X)
- Toonen, R. F. G., & Verhage, M. (2003). Vesicle trafficking: pleasure and pain from SM genes. *Trends in Cell Biology*, 13(4), 177-186. [https://doi.org/10.1016/S0962-8924\(03\)00031-X](https://doi.org/10.1016/S0962-8924(03)00031-X)
- Tortorella, L. L., & Pilch, P. F. (2002). C2C12 myocytes lack an insulin-responsive vesicular compartment despite dexamethasone-induced GLUT4 expression. *American Journal of Physiology*, 283(3), 514-524.
- Trefely, S., Khoo, P.-S., Krycer, J. R., Chaudhuri, R., Fazakerley, D. J., Parker, B. L., et al. (2015). Kinome Screen Identifies PFKFB3 and Glucose Metabolism as Important Regulators of the Insulin/Insulin-like Growth Factor (IGF)-1 Signaling Pathway. *The Journal of Biological Chemistry*, 290(43), 25834-25846. <https://doi.org/10.1074/jbc.M115.658815>
- Vassilopoulos, S., Esk, C., Hoshino, S., Funke, B. H., Chen, C.-Y., Plocik, A. M., et al. (2009). A Role for the CHC22 Clathrin Heavy-Chain Isoform in Human Glucose Metabolism. *Science*, 324(May), 1192-1197.
- Volchuk, A., Sargeant, R., Sumitani, S., Liu, Z., He, L., & Klip, A. (1995). Cellubrevin Is a Resident Protein of Insulin-sensitive GLUT4 Glucose Transporter Vesicles in 3T3-L1 Adipocytes. *The Journal of Biological Chemistry*, 270(14), 8233-8240.
- Wakeham, D. E., Abi-Rached, L., Towler, M. C., Wilbur, J. D., Parham, P., & Brodsky, F. M. (2005). Clathrin heavy and light chain isoforms originated by independent mechanisms of gene duplication during chordate evolution. *Proceedings of the National Academy of Sciences of the United States of America*, 102(20), 7209-7214.
- Ward, R. J., Pediani, J. D., Godin, A. G., & Milligan, G. (2015). Regulation of

oligomeric organization of the serotonin 5-hydroxytryptamine 2C (5-HT<sub>2C</sub>) receptor observed by spatial intensity distribution analysis. *Journal of Biological Chemistry*, 290(20), 12844-12857.  
<https://doi.org/10.1074/jbc.M115.644724>

Webb, D. J., & Brown, C. M. (2013). Epi-Fluorescence Microscopy. *Methods in Molecular Biology*, 931, 29-59. <https://doi.org/10.1007/978-1-62703-056-4>

Weber, T., Zemelman, B. V, McNew, J. A., Westermann, B., Gmachl, M., Parlati, F., et al. (1998). SNAREpins : Minimal Machinery for Membrane Fusion. *Cell*, 92, 759-772.

Weisberg, S. P., McCann, D., Desai, M., Rosenbaum, M., Leibel, R. L., & Ferrante, A. W. (2003). Obesity is associated with macrophage accumulation in adipose tissue. *The Journal of Clinical Investigation*, 112(12), 1796-1808.  
<https://doi.org/10.1172/JCI200319246>.Introduction

Whelan, D. R., & Bell, T. D. M. (2015). Image artifacts in Single Molecule Localization Microscopy: why optimization of sample preparation protocols matters. *Scientific Reports*, 5(7924), 1-10.  
<https://doi.org/10.1038/srep07924>

White, M. F. (2002). IRS proteins and the common path to diabetes. *American Journal of Physiology*, 283(3), E413-E422.

Wieczorke, R., Dlugai, S., Krampe, S., & Boles, E. (2003). Characterisation of mammalian GLUT glucose transporters in a heterologous yeast expression system. *Cellular Physiology and Biochemistry*, 13(3), 123-134.  
<https://doi.org/10.1159/000071863>

Wittig, I., Braun, H.-P., & Schägger, H. (2006). Blue native PAGE. *Nature Protocols*, 1(1), 418-428. <https://doi.org/10.1038/nprot.2006.62>

Wood, I. S., & Trayhurn, P. (2003). Horizons in Nutritional Science Glucose transporters ( GLUT and SGLT ): expanded families of sugar transport proteins. *British Journal of Nutrition*, (89), 3-9.



<https://doi.org/10.1079/BJN2002763>

- Woodcock, J. M., Murphy, J., Stomski, F. C., Berndt, M. C., & Lopez, A. F. (2003). The Dimeric Versus Monomeric Status of 14-3-3 $\zeta$  Is Controlled by Phosphorylation of Ser 58 at the Dimer Interface. *The Journal of Biological Chemistry*, 278(38), 36323-36327. <https://doi.org/10.1074/jbc.M304689200>
- Wu, X., Chi, R. J., Baskin, J. M., Lucast, L., Burd, C. G., Camilli, P. De, & Reinisch, K. M. (2014). Structural Insights into Assembly and Regulation of the Plasma Membrane Phosphatidylinositol 4-Kinase Complex. *Developmental Cell*, 28(1), 19-29. <https://doi.org/10.1016/j.devcel.2013.11.012>
- Xu, J., Ma, H., Jin, J., Uttam, S., Fu, R., Huang, Y., & Liu, Y. (2018). Super-Resolution Imaging of Higher-Order Chromatin Structures at Different Epigenomic States in Single Mammalian Cells. *Cell Reports*, 24, 873-882. <https://doi.org/10.1016/j.celrep.2018.06.085>
- Xu, Y., Rubin, B. R., Orme, C. M., Karpikov, A., Yu, C., Bogan, J. S., & Toomre, D. K. (2011). Dual-mode of insulin action controls GLUT4 vesicle exocytosis. *Journal of Cell Biology*, 193(4), 643-653. <https://doi.org/10.1083/jcb.201008135>
- Yan, Q., Lu, Y., Zhou, L., Chen, J., Xu, H., Cai, M., et al. (2018). Mechanistic insights into GLUT1 activation and clustering revealed by super-resolution imaging. *PNAS*, 115(27), 7033-7038. <https://doi.org/10.1073/pnas.1803859115>
- Yang, J., & Holman, G. D. (1993). Comparison of GLUT4 and GLUT 1 Subcellular Trafficking in Basal and Insulin-stimulated 3T3-L1 Cells. *The Journal of Biological Chemistry*, 268(7), 4600-4603.
- Yang, Z., Hong, L. K., Follett, J., Wabitsch, M., Hamilton, N. A., Collins, B. M., et al. (2016). Functional characterization of retromer in GLUT4 storage vesicle formation and adipocyte differentiation. *The FASEB Journal*, 30, 1037-1050. <https://doi.org/10.1096/fj.15-274704>

- Zakrys, L., Ward, R. J., Pediani, J. D., Godin, A. G., Graham, G. J., & Milligan, G. (2014). Roundabout 1 exists predominantly as a basal dimeric complex and this is unaffected by binding of the ligand Slit2. *The Biochemical Journal*, 461(1), 61-73. <https://doi.org/10.1042/BJ20140190>
- Zeigerer, A., Lampson, M. A., Karylowski, O., David, D., Adesnik, M., Ren, M., & McGraw, T. E. (2002). GLUT4 Retention in Adipocytes Requires Two Intracellular Insulin-regulated Transport Steps. *Molecular and Cellular Biology*, 13(July), 2421-2435. <https://doi.org/10.1091/mbc.E02>
- Zerial, M., & McBride, H. (2001). Rab Proteins as Membrane Organizers. *Nature Reviews Molecular Cell Biology*, 2(February), 107-119.
- Zhang, T., & Hong, W. (2001). Ykt6 Forms a SNARE Complex with Syntaxin 5, GS28, and Bet1 and Participates in a Late Stage in Endoplasmic Reticulum-Golgi Transport. *The Journal of Biological Chemistry*, 276(29), 27480-27487. <https://doi.org/10.1074/jbc.M102786200>
- Zhao, P., Yang, L., Lopez, J. A., Fan, J., Burchfield, J. G., Bai, L., et al. (2009). Variations in the requirement for v-SNAREs in GLUT4 trafficking in adipocytes. *Journal of Cell Science*, 122, 3472-3480. <https://doi.org/10.1242/jcs.047449>
- Zottola, R. J., Cloherty, E. K., Coderre, P. E., Hansen, A., Herbert, D. N., & Carruthers, A. (1995). Glucose Transporter Function is Controlled by Transporter Oligomeric Structure. A Single, Intramolecular Disulfide Promotes GLUT1 Tetramerization. *Biochemistry*, 34, 9734-9747.